Models of Non-Adiabatic Dynamics at Metal Surfaces

Ph.D. dissertation

Thomas Olsen

Center for Individual Nanoparticle Functionality
Department of Physics
Technical University of Denmark

July 29, 2010

Preface

This thesis is submitted in candidacy for the Ph.D. degree from the Technical University of Denmark (DTU). The presented work has been carried out in the period from April 2007 to July 2010 at the Danish National Research foundation's Center for Individual Nanoparticle Functionality (CINF) at the Department of Physics, under the supervision of associate professor Jakob Schiøtz.

Most of the research contained in this thesis has been published in the included papers. However, since the papers involve seemingly quite different subjects, it may not be obvious that the physics involved is intimately connected and can understood in a rather general and unifying framework of non-adiabatic dynamics. The primary aim of the present thesis is to give a lucid and coherent presentation of the subject, which hopefully can serve as a pedagogical introduction for anyone with an interest in the field.

I wish to thank my supervisor Jacob Schiøtz for providing inspiration, support and an indestructible good mood. I am also grateful to the many fellow Ph.D students at CAMd and CINF, who have provided a friendly and helpful atmosphere at the physics department. In particular, Peter C. K. Vesborg, Jakob L. Olsen, Anja Toftelund, Carsten Rostgaard, Anders B. Laursen, Simon H. Brodersen, and Najda B. Luciw with whom I have engaged in entertaining and enlightening discussions on every imaginable subject during our lunch breaks. Finally, I would like to thank Marie Kring for everlasting support, patience and for interesting discussions on whether or not physics do constitute the most fun you can have without laughing.

Abstract

This thesis presents a framework for modelling non-adiabatic dynamics at metal surfaces based on potential energy surfaces. A fast and efficient method to obtain *ab initio* excited state potential energy surfaces from Density Functional Theory is developed, and we construct a Hamiltonian, which incorporates the non-adiabatic coupling in terms of potential energy surfaces. The Hamiltonian is then analyzed from two fundamentally different perspectives, resulting in two complementary descriptions of non-adiabatic energy transfer at surfaces.

First, we consider hot electrons interacting with adsorbates in a framework of inelastic scattering. Approximating the vibrational modes of adsorbates with harmonic potentials, results in a model, which can be solved exactly when the coupling to hot electrons is either linear or quadratic. For diatomic molecules it turns out that the dominating channel for hot electron mediated energy transfer, is the internal vibrational mode, which is governed by linear coupling and we calculate the probability of transferring a given amount of energy to the adsorbate. When the adsorbate has its molecular axis perpendicular to the surface, the frustrated rotations and translations are quadratically coupled and we obtain the probability of exciting a particular rotational state. If the desorption coordinate is approximated by a Morse potential, we demonstrate how to calculate the velocity distribution of desorption induced by hot electrons within perturbation theory, and it is shown that highly excited initial vibrational states give rise to slow desorbates. Finally, we consider multiple inelastic scattering events within a quadratic model and derive a power law dependence of the reaction yield on the flux of hot electrons. The power law exponent is shown to represent the number of vibrational states contributing to the reaction.

Second, we study the reduced density matrix, which gives an effective description of the adsorbate under the influence of a thermal reservoir of metallic electrons. The result is a semiclassical Langevin equation, which is shown to give quantum mechanically exact results for quadratic potentials, provided the initial quantum state is properly included. We then investigate the Markov approximation and show that for reactions mediated by hot electrons, the approximation is usually well justified. However, the Markov approximation is typically not valid at temperatures relevant for reactions driven by thermal substrate phonons. Thus, non-Markovian effects become important when studying the impact of non-adiabatic coupling in surface reactions, which are not driven by hot electrons.

Resumé

Denne Ph.D afhandling præsenterer ikke-adiabatiske modeller for molekyledynamik på metaloverflader med udgangspunkt i potential overflader. En hurtig og effektiv metode til beregning af eksiterede potential overflader ved hjælp af tæthedsfunktional teori er blevet udviklet, og vi konstruerer en Hamiltonoperator der, via potential overflader, inkorporerer den ikke-adiabatiske kopling. Hamiltonoperatoren bliver derefter analyseret fra to vidt forskellige perspektiver, hvilket resulterer i to komplementære beskrivelser af ikke-adiabatisk overførsel af energy på overflader.

Først betragter vi varme elektroner der vekselvirker med adsorbater ved hjælp af inelastisk spredningsteori. Hvis potential overfladen der beskriver adsorbatet kan approksimeres med et harmonisk potential, fås en model der kan løses eksakt når koplingen er enten lineær eller kvadratisk. For diatomiske molekyler viser det sig, at den interne frihedsgrad dominerer energioverførslen fra varme elektroner, og vi beregner sansynligheden for at overføre en given mængde energy. Hvis den molekylære akse er ortogonal på overfladen, er de frustrærede rotationer kvadratisk koplede og vi beregner sansynligheden for at anslå en given rotationstilstand. Når desorptionskoordinaten er godt beskrevet ved et Morse potential, viser vi hvorledes hastighedsfordelingen af molekyler eller atomer desorberet af varme elektroner kan beregnes ved hjælp af perturbationsteori, og det bliver vist, at højt eksiterede vibrationstilstande i adsorbatet giver anledning til langsomme desorbater. Til sidst udvikler vi en metode, til at inkludere mange varme elektroner, der vekselvirker med adsorbatet på skift, og udleder en potentslov for reaktionsraten som funktion af fluxen af varme elektroner. Eksponenten vises at repræsentere antallet af vibrationstilstande der bidrager til reaktionen.

Derefter studerer vi den reducerede tæthedsmatrix, som giver en effektiv beskrivelse af adsorbatet under inflydelse af et termisk reservoir af metalliske elektroner. Dette resulterer i en semiklassik Langevin ligning der vises at være kvantemekanisk eksakt for kvadratiske potentialer, hvis den kvantemekaniske begyndelsestilstand inkluderes korrekt. Vi undersøger dernæst Markov approksimationen og viser at den som regel kan retfærdiggøres for reaktioner drevet af varme elektroner, men ikke for temperaturer der typisk er involveret i reaktioner drevet af termiske fononer. Tidskorreleret dynamik bliver derfor vigtigt hvis Langevin ligningen bruges til at undersøge effekten af ikke-adiabatisk kopling i reaktioner på overflader der ikke er drevet af varme elektroner.

List of Included Papers

Paper I
J. Gavnholt, T. Olsen, M. Engelund, and J. Schiøtz
Delta self-consistent field as a method to obtain potential energy surfaces of excited molecules on surfaces
Phys. Rev. B **78**, 075441 (2008).

Paper II
T. Olsen, J. Gavnholt, and J. Schiøtz
Hot-electron-mediated desorption rates calculated from excited state potential energy surfaces
Phys. Rev. B **79**, 035403 (2009).

Paper III
J. Gavnholt, A. Rubio, T. Olsen, K. S. Thygesen, and J. Schiøtz
Hot-electron-assisted femtochemistry at surfaces: A time-dependent density functional theory approach
Phys. Rev. B **79**, 195405 (2009).

Paper IV
T. Olsen
Inelastic scattering in a local polaron model with quadratic coupling to bosons
Phys. Rev. B **79**, 235414 (2009).

Paper V
T. Olsen and J. Schiøtz
Origin of Power Laws for Reactions at Metal Surfaces Mediated by Hot Electrons
Phys. Rev. Lett. **103**, 238301 (2009).

Paper VI
T. Olsen and J. Schiøtz
Vibrationally mediated control of single-electron transmission in weakly coupled molecule-metal junctions
Phys. Rev. B **81**, 115443 (2010).

Paper VII
R. Frigge, T. Hoger, B. Siemer, H. Witte, M. Silies, H. Zacharias, T. Olsen, and J. Schiøtz
Site Specificity in Femtosecond Laser Desorption of Neutral H Atoms from Graphite(0001)
Phys. Rev. Lett. **104**, 256102 (2010).

Paper VIII
B. Siemer, T. Olsen, T. Hoger, M. Rutkowski, C. Thewes, S. Düsterer, J. Schiøtz, and H. Zacharias
Desorption of H atoms from graphite(0001) using XUV free electron laser pulses
Submitted to Chem. Phys. Lett.

Paper IX
T. Olsen and J. Schiøtz
Quantum corrected Langevin dynamics for adsorbates on metal surfaces interacting with hot electrons
J. Chem. Phys. **133**, 034115 (2010).

Paper X
T. Olsen and J. Schiøtz
Memory effects in non-adiabatic molecular dynamics at metal surfaces
Submitted to J. Chem. Phys. arXiv:1006.2264.

Other Publications

J. S. Hummelshøj et al.
Density functional theory based screening of ternary alkali-transition metal borohydrides: A computational material design project
J. Chem. Phys. **131**, 014101 (2009).

J. Enkovaara et al.
Electronic structure calculations with GPAW: A real-space implementation of the projector-augmented wave method
J. Phys.: Condens. Matter **22**, 253202 (2010)

Contents

Chapter 1

Introduction

Theoretical models of chemical reactions at metal surfaces are usually formulated within the adiabatic approximation, where the dynamics of the nuclei are assumed to be governed by the instantaneous electronic ground state, and several surface reactions have been successfully modelled using the adiabatic approximation [20, 21]. However, non-adiabatic effects still seem to play an important role in some systems [76, 22, 63], but the quantitative impact on the dynamics is still debated due to the difficulty in performing molecular dynamics beyond the adiabatic approximation.

As an opposite extreme, reactions mediated by excited metallic electrons, are *only* understood in terms of non-adiabatic dynamics [113, 90]. Such reactions can be induced by applying an intense laser pulse to a metal surface with atoms or molecules adsorbed. The laser excites electrons in the metal, which may then migrate to the surface and transfer energy to the adsorbates. A different approach, has been proposed by Gadzuk [34], and involves a Metal-Insulator-Metal (MIM) device. With the MIM device it is possible to control the energy of the excited electrons, and the method could therefore, in principle, be used to induce surface reactions, which are otherwise suppressed. Whether the hot electrons are generated by means of a laser or an MIM device, the underlying physics is completely different from that involved in thermally driven reactions, and modelling the non-adiabatic dynamics remains a major challenge.

In this introductory chapter, we will start by reviewing the adiabatic approximation and the concept of potential energy surfaces. We then briefly discuss the conceptual picture of reactions induced by hot electrons, and illustrate how to think about electrons originating from an MIM device as well as from a laser.

1.1 The Adiabatic Approximation

The word adiabatic is derived from the ancient Greek ἀδιάβατος, which literally means impassable. To physicists, the term is probably most familiar from thermodynamics where an adiabatic process refers to a transition where a given system does not exchange heat with its environment. In quantum mechanics, the adiabatic theorem states that a physical system remains in its instantaneous eigenstate if a given perturbation is acting on it slowly enough. Hence, in quantum mechanics, adiabatic refers to the fact that a system does not make a transition from one Hamiltonian eigenstate to another. True adiabadicity is only obtained in the limit of infinitely slow perturbations, but in some cases it may be shown that an adiabatic approximation, will capture all the dominating effects and yield quantitatively reliable results.

In molecular and solid state physics, adiabatic processes is defined in terms of potential energy surfaces and is a special case of the adiabatic theorem in quantum mechanics. The derivation of the adiabatic approximation, which is often referred to as the Born-Oppenheimer approximation [5], is well known but we include it here for completeness since the result is so central to the analysis of molecular dynamics. The non-relativistic Hamiltonian for a system of N_e electrons and N_n nuclei is given by

$$\begin{aligned} H = &- \sum_{a=1}^{N_n} \frac{\hbar^2 \nabla_a^2}{2M_a} + \sum_{a>b}^{N_n} \sum_{b=1}^{N_n} \frac{e^2 Z_a Z_b}{|\mathbf{R}_a - \mathbf{R}_b|} - \sum_{a=1}^{N_n} \sum_{i=1}^{N_e} \frac{e^2 Z_a}{|\mathbf{R}_a - \mathbf{r}_i|} \\ &- \sum_{i=1}^{N_e} \frac{\hbar^2 \nabla_i^2}{2m_e} + \sum_{i>j}^{N_e} \sum_{j=1}^{N_e} \frac{e^2}{|\mathbf{r}_i - \mathbf{r}_j|}, \end{aligned} \tag{1.1}$$

where $\mathbf{R}_a$ and $\mathbf{r}_i$ denote the positions of the nuclei and electrons respectively, and Z_a is the number of protons in nuclei a. The eigenvalue equation for the Hamiltonian is

$$H\Psi(\mathbf{r}, \mathbf{R}) = E\Psi(\mathbf{r}, \mathbf{R}), \tag{1.2}$$

where the eigenfunction $\Psi(\mathbf{r}, \mathbf{R})$ depends on all electronic and nuclear degrees of freedom. However, the eigenvalue problem may be recast into a form, which can sometimes be convenient. Consider the adiabatic expansion

$$\Psi(\mathbf{r}, \mathbf{R}) = \sum_n \psi_n(\mathbf{r}, \mathbf{R}) \varphi_n(\mathbf{R}), \tag{1.3}$$

where ψ_n are eigenstates of the electronic Hamiltonian H_e

$$H_e\psi_n(\mathbf{r},\mathbf{R}) = E_n(\mathbf{R})\psi_n(\mathbf{r},\mathbf{R}), \qquad H_e = H - T_N, \tag{1.4}$$

and T_N is the first term in Eq. (1.1). Since there is no kinetic term for the nuclei in H_e, $\mathbf{R}$ only enters as a parameter in Eq. (1.4). Inserting the expansion (1.3) into Eq. (1.2), multiplying from the left with $\psi_n^*(\mathbf{r})$, and integrating over all electronic coordinates then gives

$$\Big(T_N + E_n(\mathbf{R})\Big)\varphi_n(\mathbf{R}) = E\varphi_n(\mathbf{R}) + F_n(\mathbf{R}), \tag{1.5}$$

where

$$\begin{aligned} F_n(\mathbf{R}) = &\sum_{n'} \int d\mathbf{r}\psi_n^*(\mathbf{r},\mathbf{R}) \sum_{a=1}^{N} \frac{\hbar^2}{2M_a}\Big(\nabla_a^2\psi_{n'}(\mathbf{r},\mathbf{R})\Big)\varphi_{n'}(\mathbf{R}) \\ &+ \sum_{n'} \int d\mathbf{r}\psi_n^*(\mathbf{r},\mathbf{R}) \sum_{a=1}^{N} \frac{\hbar^2}{M_a}\Big(\boldsymbol{\nabla}_a\psi_{n'}(\mathbf{r},\mathbf{R})\Big)\cdot\Big(\boldsymbol{\nabla}_a\varphi_{n'}(\mathbf{R})\Big). \end{aligned} \tag{1.6}$$

At this point, no approximation has been imposed. Equation (1.5) is just the eigenvalue equation for the full Hamiltonian (1.2) written in a particular basis. Neglecting the function $F_n(\mathbf{R})$ yields the Born-Oppenheimer approximation and the equations (1.5) simply become an infinite set of decoupled equations for the nuclei, one for each electronic eigenstate $\psi_n(\mathbf{r},\mathbf{R})$. Transitions between electronic eigenstates are then not possible and the dynamics in the electronic eigenstate n is governed by the function $E_n(\mathbf{R})$, which we will refer to as a potential energy surface. This is a huge simplification compared to the full problem, since one only needs to obtain the relevant potential energy surface, usually the ground state, to perform molecular dynamics. The Born-Oppenheimer approximation is typically expected to work well when the momenta of the nuclei are small and the potential energy surfaces are well separated.

1.2 Hot Electron Mediated Femtochemistry at Surfaces

A large class of chemical reactions are driven by heat and even with good catalysts, a high temperature and pressure may be necessary in order to obtain useful reaction yields. Very often, such reactions are well described in the adiabatic framework discussed above and a chemical reaction is the result of the

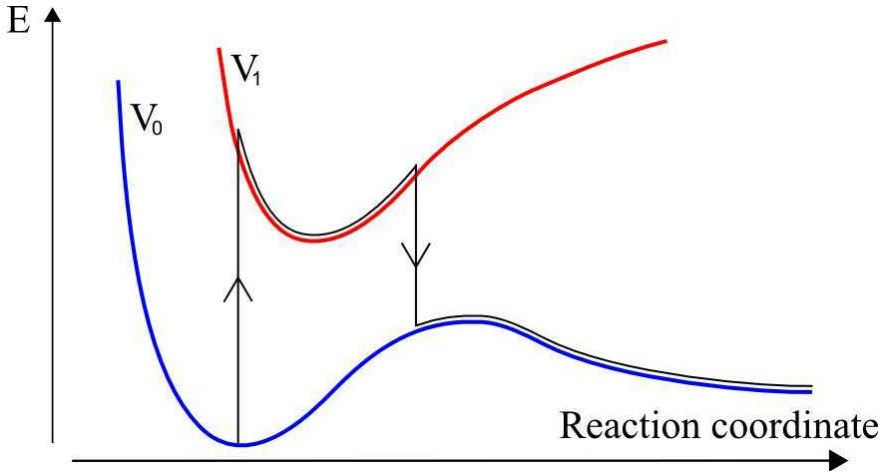

Figure 1.1: Model illustration of hot electron mediated energy transfer to an adsorbate at a metal surface. In an adiabatic process, the adsorbate never leaves the ground state potential energy surface V_0 and a reaction occurs when the adsorbate has acquired enough thermal energy to overcome the reaction barrier. A hot electron mediated reaction proceeds by excitation to a potential energy surface V_1 on which the adsorbate will propagate for a while before it decays to the ground state where it may have acquired enough energy to overcome the barrier.

reactants acquiring enough thermal energy to overcome a barrier on the ground state potential energy surface $E_0(\mathbf{R})$. Some reactions may, however, be driven by electronic transitions in the reactants induced by external means. Examples of such reactions are the photosynthesis of carbohydrates in plants and the ozone layer, which is the result of ultraviolet photons dissociating molecular oxygen in the stratosphere.

In the present thesis, we will be concerned with non-thermal chemistry at metal surfaces induced by excited metallic electrons. The idea is that a highly energetic electron may transiently occupy an empty orbital of an adsorbed atom or molecule and thereby transfer energy to the adsorbate. By highly energetic electrons we mean electrons, which exceed typical thermal excitations from the Fermi level such that $\varepsilon_i \gg \varepsilon_F + k_B T$, and such electrons will be referred to as hot electrons. We will discuss two methods to produce hot electrons in metals,

which give rise to very different distributions of hot electrons and thus require rather different models for the induced chemistry. Nevertheless, the conceptual picture of how energy transfer is mediated by hot electrons is common to all models and can be understood in terms of the potential energy surfaces $E_n(\mathbf{R})$ Eq. (1.4) [67, 87]. The principle is illustrated in Fig. 1.1, where it is assumed that the qualitative mechanism can be captured by considering two potential energy surfaces representing the electronic ground state $V_0(\mathbf{R}) \equiv E_0(\mathbf{R})$ and a state where an adsorbate orbital has been occupied by a hot electron $V_1(\mathbf{R}) \equiv E_1(\mathbf{R})$. Initially, the adsorbate is assumed at rest at the minimum of the adiabatic ground state $V_0(\mathbf{R})$. A transition to an excited state $V_1(\mathbf{R})$ is then induced by a hot electron and the adsorbate propagates according to the forces in this state. However, for chemisorbed species the excited electronic state is typically not an eigenstate of the electronic Hamiltonian and the state acquires a finite lifetime. Thus, the adsorbate will eventually decay to the ground state potential energy surface where it may have acquired enough energy to overcome a reaction barrier. It should be noted that the decay to the ground state is not due to the non-adiabatic coupling function Eq. (1.6), but simply because $V_1(\mathbf{R})$ does not represent an adiabatic state in the sense of (1.4).[1] We will return to the issue of lifetimes and spectral properties of non-adiabatic excited states within a simplified model in chapter 3.

1.2.1 Metal-Insulator-Metal devices

A very clever way of generating hot electrons is by means of a Metal-Insulator-Metal (MIM) device as proposed by Gadzuk [34, 35] in 1996. The device consists of a substrate metal covered by an ultra thin insulating layer, which has a thin metal film on top. The band structure of such a layered structure is shown in Fig. 1.2 and it is demonstrated that a bias voltage V_B can induce tunneling of electrons from the substrate metal through the oxide into the top layer, and thus result in hot electrons hitting the surface. Since, the hot electrons will primarily originate from the Fermi level of the substrate metal, the distribution of emerging hot electrons will be sharply peaked at $\varepsilon_F + eV_B$ in the top metal. This

[1] One can also derive an expression like Eq. (1.5) in a non-adiabatic basis of states $|k\rangle$. Neglecting coupling terms similar to Eq. (1.6) then yields

$$T_N\varphi_k(\mathbf{R}) + \sum_{k'} V_{kk'}(\mathbf{R})\varphi_{k'}(\mathbf{R}) = E\varphi_k(\mathbf{R}), \qquad V_{kk'}(\mathbf{R}) = \langle k(\mathbf{R})|H_e(\mathbf{R})|k'(\mathbf{R})\rangle.$$

The diagonal elements of $V_{kk'}(\mathbf{R})$ can be regarded as non-adiabatic potential energy surfaces, which are non-stationary due to coupling through the off-diagonal terms.

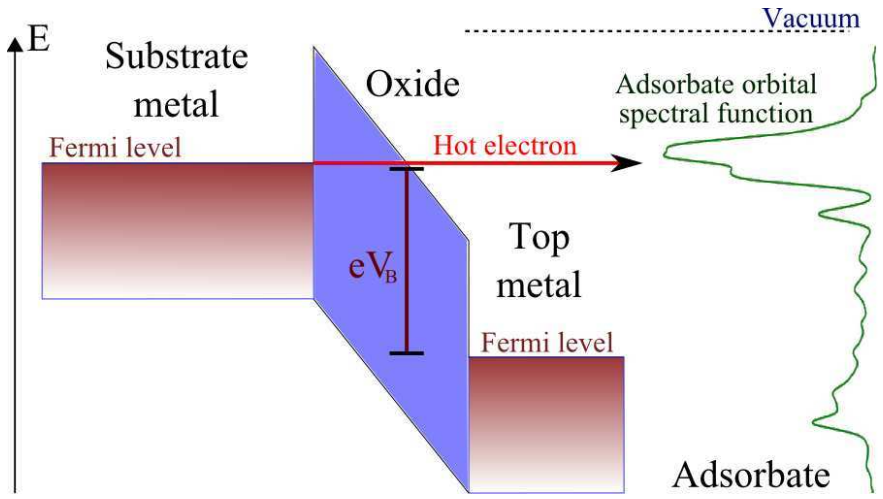

Figure 1.2: Schematic band structure of the MIM device. When a bias is applied the Fermi levels are shifted with respect to each other and electrons from the substrate metal can tunnel through the thin insulating layer and emerge as hot electrons in the top layer. If an adsorbate system is present on the top metal, a hot electron may occupy an empty adsorbate orbital and transfer energy to the adsorbate as shown in Fig. 1.1.

implies, that by changing the bias voltage, it is possible to tune the energy of hot electrons to a particular adsorbate orbital and thus maximize the possibility of a reaction. Furthermore, interaction with different unoccupied adsorbate orbitals may result in different chemical reactions and if such orbitals are well separated in energy, one has the exciting possibility of performing selective chemistry by simply tuning the MIM device to a desired reaction.

Experimentally, it has been verified that simple chemical reactions can indeed be mediated by hot electrons from an MIM device. It has also been demonstrated that large workable MIM devices can be constructed, which will emit electrons into vacuum when the bias voltage exceeds the top metal work function [101, 102, 78]. However, the flux of hot electrons produced with such devices are typically extremely low and so far only reactions with a very low reaction barrier have been observed using this method.

1.2.2 Femtosecond laser pulses

A very efficient method to produce a high flux of hot electrons at a metal surface, is by means of an intense laser pulse. In Refs. [10, 11] it was shown that NO could be desorbed from a Pt(111) surface by applying a nanosecond laser pulse (pulse duration $\sim 15\ ns$). Furthermore, the non-thermal distribution of vibrational states in the desorbed molecules and a strong dependence of the energy distribution on laser wavelength, were used to argue that hot electrons were mediating the desorption reaction. Although, the method used to produce hot electrons in such an experiment is very different from the MIM device, the basic reaction mechanism is essentially the same and changing the wavelength of the laser corresponds to tuning the bias voltage of the MIM device. However, shortly thereafter Prybyla et al. [85] used a femtosecond laser pulse (pulse duration $\sim 200\ fs$) to desorb NO from Pd(111) and measured several features, which could not be explained by a process involving single hot electrons. A mechanism involving multiple electronic excitations was identified in Ref [9] and subsequently desorption induced by femtosecond lasers has been demonstrated for several other adsorbate systems [86, 57, 96, 49]. It has also been shown that femtosecond laser pulses can induce surface hopping [95] and oxidation reactions [4, 58, 17]. The most characteristic feature of reactions involving multiple hot electrons is a power law dependence of the yield on laser fluence whereas reactions induced by single hot electrons has a linear dependence.

Reactions induced by multiple hot electrons are conceptually similar to reactions induced by single electrons and can again be understood in terms of potential energy surfaces [68]. Referring to the potentials of Fig. 1.1 one should now imaging several electrons sequentially transferring energy to the adsorbate. Thus the first electron induces a transition to the excited state but does not transfer enough energy for the adsorbate to overcome the barrier, but leaves the adsorbate with an increased vibrational energy in the ground state. The next electron excites the adsorbate again and transfers an additional amount of energy and so forth, until the adsorbate has acquired enough energy to overcome the barrier.

A somewhat orthogonal description of reactions induced by multiple electronic transitions, assumes that the excited electrons undergo rapid scattering and are well described by a hot thermal distribution function with a time dependent electronic temperature. This is illustrated in Fig. 1.3 where the resulting Fermi-Dirac distribution asserts a force on the adsorbate through a statistical occupation of the excited electronic state. The excitation of electrons happens within $\sim 100\ fs$, which is much faster than the electron-phonon coupling time

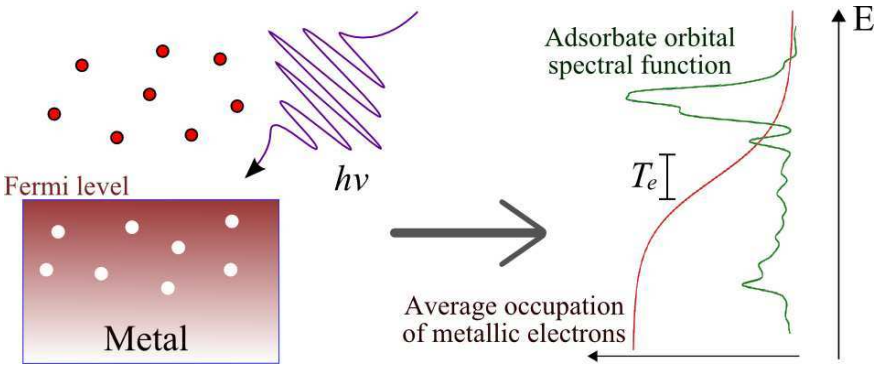

Figure 1.3: Thermal model of a reaction induced by multiple hot electrons. A femtosecond laser pulse excites a high density of electrons, which rapidly thermalize and thus allow for a statistical description. The hot electrons are then modeled by a time dependent electronic temperature $T_e(t)$, which is decoupled from the substrate temperature. The model does not involve individual transitions to the excited state potential energy surface, but assumes a small statistical occupation of the excited state, which gives rise to forces on the adsorbate.

and the electronic temperature can thus reach several thousand K. While the assumption of rapid thermalization may not always be well justified, it does lead to a beautiful and rigorous framework for describing an adsorbate under influence of a hot electron environment in terms of electronic friction and a stochastic force [69, 7, 64].

1.3 Non-Adiabatic Effects in Molecular Dynamics at Metal Surfaces

Due to a very low flux of hot electrons in the MIM device, and the difficulties in controlling electronic energies in laser experiments, reactions induced by hot electrons are so far mostly of academic interest. However, from a theoretical point of view, the basic interaction mediating the transfer of energy between adsorbates and hot electrons is identical to the interaction responsible for non-adiabatic effects in molecular dynamics at metal surfaces without hot electrons.

This can also be seen from Fig. 1.3 where the spectral function is expected to interact with metallic electrons due to a partial occupation even at low temperatures. When the adsorbate moves the spectral function will shift its position or change the broadening and this may excite electron-hole pairs in the metal and result in the adsorbate loosing energy.

The role of such non-adiabatic effects in molecular dynamics at metal surfaces is still vividly debated [63, 55, 62, 56] and often difficult to asses due to inadequacy of low dimensional models of surface dynamics. For example, unusual sticking coefficients in the measured dissociative adsorption of N_2 on Ru(0001) [23], hints at strong non-adiabatic energy loss, but has been accounted for by multi-dimensional adiabatic dynamics [20, 21]. For other reactions, such as associative desorption of N_2 from Ru(0001), non-adiabatic effects still seem to be very important [76, 22, 63] and multi-dimensional adiabatic simulations have not been able to account for large energy losses during desorption [19]. Another example is the vibrational lifetime of CO on Cu(100), which has been measured to be much shorter than the expected coupling time to substrate phonons [73], and a strong non-adiabatic coupling in this system has been confirmed by theory [84, 45, 104]. Finally, the adiabatic approximation has been shown to fail to describe the dissociation reaction of O_2 on Al(111) due to spin selection rules, which give rise to a highly non-adiabatic behavior [14, 3, 15].

1.4 Outline of the Thesis

In chapter 2, it is shown how to calculate potential energy surfaces for real systems using Density Functional Theory. Whereas the calculation of ground state potentials is a standard task, the evaluation of excited state potentials is non-trivial. A method have been developed for this particular purpose and we will discuss the methodology and constraints used to specify the nature of a desired excited state, as well as the limitations of the method. We also briefly discuss a method to simulate time propagation of hot electrons using time-dependent Density Functional Theory.

In chapter 3, a model Hamiltonian is introduced, which describes an adsorbate resonance interacting with metallic electrons and vibrational degrees of freedom. We then analyze this Hamiltonian within various approximations and derive two different approaches to non-adiabatic energy transfer at metal surfaces. In the first approach the conceptual picture is that of Fig. 1.2 and the energy transfer is treated within a framework of inelastic scattering. For the second approach, the conceptual picture is shown in Fig. 1.3, and we calculate

the reduced density matrix of the adsorbate in two different basises, leading to either a Langevin equation or a Master equation.

In chapter 4, we perform a detailed analysis of the inelastic scattering model and apply the theory to various adsorbate systems with potential energy surfaces obtained using Density Functional Theory. An equation describing the velocity distribution of hot electron mediated desorption from a Morse potential, is derived and we use parameters obtained from *ab initio* potential energy surfaces to show that the model yields good agreement with experiment. The model is then extended to include multiple scattering events and vibrational decay, which give rise to an experimentally observed power law dependence of the reaction yield on the flux of hot electrons. Finally, it is shown that with a few modifications the model can be applied to electron transport through molecules coupled to two metallic contacts, and we demonstrate that vibrational coupling can be used to control the transmission of individual electrons.

In chapter 5, we analyze the Langevin equation approach to non-adiabatic energy transfer at metal surfaces. The Langevin equation is exact for harmonic potentials when the initial state is properly included, and we compare the consequences of classical, quasiclassical, and quantized treatment of the initial state. The effect of temporal correlations in the Langevin equation is studied, and it is shown that a common approximation, which neglects temporal correlations, tends to overestimate the effect of non-adiabatic dissipation of energy.

While chapters 2 and 3 provide an introduction to the theoretical foundation of the included papers, chapters 4 and 5 focus on applications and results. Thus, one may read chapters 1-3 of the thesis and then go directly to the papers or continue with chapters 4-5, which provide a coherent and condensed summary of the most essential parts of the included papers.

Chapter 2

Density Functional Theory

In order to calculate the ground and excited state potential energy surfaces shown in Fig. 1.1, we need to solve the Scrödinger equation for the electronic Hamiltonian (1.4) while varying the nuclear coordinates. For N electrons, the many-particle wavefunction is a function of $3N$ variables, and the problem becomes prohibitly difficult to handle when more than a few electrons are involved. Density functional Theory (DFT) provides a method, which allows one to reformulate the problem in terms of a non-interacting Hamiltonian, and the many-particle wavefunction is substituted by a Slater determinant composed of single particle orbitals.

In this chapter, we will start by briefly discussing the fundamental principles of ground state DFT. We will not try give a comprehensive and self-contained introduction to the subject, but refer to the reviews [81, 24, 30] instead. In section 2.2, the results are extended to any Hamiltonian eigenstate and we will show that this generalization not only provides a way in which excited state energies can be obtained, but also gives a formal solution to the so-called non-interacting v-representability problem. Δ Self-Consistent Field (ΔSCF) is then shown to comprise a simple DFT based method, which allows one to calculate selected excited state energies for simple molecules and we generalize the concept to include excited state energies of non-stationary states. This yields a tractable method with which we can calculate potential energy surfaces, corresponding to resonant states, such as the adsorbate orbital resonance shown in Fig. 1.2. In section 2.4, we discuss time-dependent DFT as a method to simulate hot electrons tunneling into an adsorbate resonance, and show how to obtain the resonant spectral properties.

2.1 Ground State DFT

Traditionally, DFT is based on the Hohenberg-Kohn theorem [50], which states that: *Two electronic systems with external potentials that differ by more than a constant cannot have ground states with the same electron density.* This implies, that the ground state electron density uniquely determines the external potential and therefore all properties of the electronic system. In particular, for a given external potential V_{ext}^0 one can define the Hohenberg-Kohn energy functional

$$E_{HK}[\rho,\alpha] = \langle\Psi_0[\rho]|T + \alpha V_{ee}|\Psi_0[\rho]\rangle + \int d\mathbf{r} V_{ext}^0(\mathbf{r})\rho(\mathbf{r}), \tag{2.1}$$

where T is the electron kinetic energy operator, V_{ee} is the electron-electron interaction and α is a coupling constant, which may interpolate between zero and one corresponding to non-interacting and interacting electrons respectively. In this functional, the electron density ρ determines an external potential $V_{ext}[\rho]$ (through the Hohenberg-Kohn theorem), which has ρ as the ground state electron density and this potential then defines a Hamiltonian, which yields a ground state wavefunction $\Psi_0[\rho]$. For a given number of particles, the functional (2.1) has a global minimum when ρ coincides with the electron density ρ_0 corresponding to the ground state of $T + \alpha V_{ee} + V_{ext}^0$, and the ground state energy can, in principle, be found by minimizing (2.1) with respect to the density.

However, the Hohenberg-Kohn theorem guaranties uniqueness but not existence of an external potential corresponding to a given ground state density, and the functional (2.1) is only defined for densities for which such a potential exist. Furthermore, if one were to find the ground state energy by minimizing (2.1) the variation would, in principle, have to be performed on the subspace of densities for which corresponding external potentials exist. The subtle question of existence is often referred to as the v-representability problem. However, a way to circumvent the v-representability problem was proposed by Levy [61] who introduced the constrained search functional

$$E_L[\rho,\alpha] = \min_{\Psi\to\rho}\langle\Psi|T + \alpha V_{ee}|\Psi\rangle + \int d\mathbf{r} V_{ext}(\mathbf{r})\rho(\mathbf{r}). \tag{2.2}$$

In this expression one has to minimize the expectation value with respect to all wavefunctions yielding the density ρ and the ground state energy can, in principle, be found by minimizing E_L with respect to the density constrained to represent a fixed number of particles. The Levy functional is well-defined for arbitrary densities and the v-representability problem has thus been eliminated. Moreover, if ρ is the ground state density of a local external potential $V_{ext}(\mathbf{r})$,

then the minimization in (2.2) will result in the corresponding ground state $|\Psi_0\rangle$ and the Hohenberg-Kohn theorem readily follows, since if a different potential yielded the same ground state density it would also yield the same ground state $|\Psi_0\rangle$. However, this is not possible for local potentials differing by more than a constant.[1]

2.1.1 Kohn-Sham equations

Although the Levy constrained search functional defines the ground state energy rigorously, it is usually not feasible to perform the actual minimization for a given system. Instead, the density is calculated by assuming the existence of a non-interacting system with the same ground state density, but a different external potential, which is traditionally denoted $v_s[\rho(\mathbf{r})]$. To determine this potential, the functional derivatives of the interacting ($\alpha = 1$) and non-interacting ($\alpha = 0$) Levy functionals are equated giving

$$v_s[\rho_0(\mathbf{r})] = \frac{\delta E[\rho]}{\delta\rho(\mathbf{r})}\bigg|_{\rho(\mathbf{r})=\rho_0(\mathbf{r})} - \frac{\delta}{\delta\rho(\mathbf{r})}\min_{\Psi\to\rho}\langle\Psi|T|\Psi\rangle\bigg|_{\rho(\mathbf{r})=\rho_0(\mathbf{r})}. \tag{2.3}$$

The non-interacting wavefunction can be written as a Slater determinant and the Scrödinger equation reduces a set of equations for the orbitals $\varphi_i(\mathbf{r})$

$$\Big(T + v_s[\rho(\mathbf{r})]\Big)\varphi_i(\mathbf{r}) = \epsilon_i\varphi_i(\mathbf{r}), \qquad \rho(\mathbf{r}) = \sum_i |\varphi_i(\mathbf{r})|^2. \tag{2.4}$$

These are the so-called Kohn-Sham equations [59], which have to be solved self-consistently since the potential v_s is a functional of the density $\rho(\mathbf{r})$. The equations are simple in appearance, but all the complicated structure of the many-particle wavefunction $\Psi(\mathbf{r})$ has been transformed into a complicated functional dependence in the potential v_s, which needs to be approximated. The first step towards this, is to split the energy functional (2.2) with $\alpha = 1$, into terms of different physical origin and write

$$E[\rho] = T_s[\rho] + E_H[\rho] + E_{xc}[\rho] + \int d\mathbf{r} V_{ext}(\mathbf{r})\rho(\mathbf{r}), \tag{2.5}$$

where $E_H[\rho]$ is the Hartree energy given by the electrostatic interaction of the density with itself, $T_s[\rho]$ is the kinetic energy of the non-interacting Kohn-Sham

[1] If the Hamiltonians H_1 and H_2 have a common eigenstate $|\psi\rangle$ and $H_1 - H_2 = f(x)$, then $|\psi\rangle$ is also an eigenstate of $f(x)$, which is only possible if $|\psi\rangle$ is a position eigenstate. However, such a state is not an eigenstate of the kinetic energy operator.

orbitals and $E_{xc}[\rho]$ is called the exchange-correlation energy and contains the terms needed to equate (2.5) with (2.2). Similarly, the Kohn-Sham potential $v_s[\rho(\mathbf{r})]$ can be split into the terms

$$v_s[\rho(\mathbf{r})] = v_H[\rho(\mathbf{r})] + v_{xc}[\rho(\mathbf{r})] + V_{ext}(\mathbf{r}), \tag{2.6}$$

where v_H and v_{xc} are the functional derivatives of E_H and E_{xc} with respect to the density. A wide range of approximations have been constructed for E_{xc} and the choice of an approximate functional usually depends on the problem one wishes to solve. We will not delve into the involved methods of obtaining approximate exchange-correlation functionals, but simply mention that in the present thesis, we only use so-called semi-local functionals, which are based on the local exchange-correlation energy density of the homogeneous electron gas, and its first derivatives [83, 111, 44].

It should be noted that while DFT itself is rigorously defined, the existence of a non-interacting Kohn-Sham system, which reproduces the ground state density, is not guarantied and the Kohn-Sham scheme thus reintroduces a v-representability issue for the non-interacting system.

2.2 Beyond the Hohenberg-Kohn Theorem

The Hohenberg-Kohn theorem and the Levy energy functional (2.2), can be used to calculate the ground state energy of a given electronic system and as such, DFT is often referred to as a ground state theory. However, it has been shown by Görling [40] that the constrained search formalism can be generalized to excited electronic states as well. The density of an excited electronic state thus determines the external potential and therefore, all properties of an electronic system. Below we will follow Görling closely and derive this result. The construction of a Kohn-Sham like scheme for practical applications is accomplished by introducing Generalized Adiabatic Connections (GAC) between eigenstates of interacting Hamiltonians and eigenstates of non-interacting Hamiltonians.

We start by defining the Görling functional

$$E_G[\rho, \nu, \alpha] = \underset{\nu, \Psi \to \rho}{\text{stat}} \langle \Psi | T + \alpha V_{ee} | \Psi \rangle + \int d\mathbf{r} V_{ext}(\mathbf{r}) \rho(\mathbf{r}), \tag{2.7}$$

where "stat" refers to a point where the expectation value is stationary with respect to variations of the state Ψ at fixed density ρ. The functional is well defined for all well behaved densities since there is always at least one stationary

value, namely the absolute minimum. However, in general the expectation value will have several stationary points for a given density and these have to be labeled by the auxiliary quantum number ν. Thus, for a given density ρ and coupling constant α the functional (2.7) defines a set of states $|\Psi[\rho,\nu,\alpha]\rangle$ and the functional $E_G[\rho,\nu,\alpha]$ gives the expectation values of the Hamiltonian with coupling α evaluated on these states. The set of states $|\Psi[\rho,\nu,\alpha]\rangle$ will be referred to as ρ-stationary. We will now show that any Hamiltonian eigenstate is ρ-stationary and that any ρ-stationary state is an eigenstate of a Hamiltonian with an external potential being uniquely determined by ρ, ν, and α.

It is straightforward to show that any Hamiltonian eigenstate $|\Psi_i\rangle$ is also ρ-stationary. This follows from the variational principle, which states that

$$\delta\langle\Psi_i|T+\alpha V_{ee}+V_{ext}|\Psi_i\rangle=0, \tag{2.8}$$

is equivalent to the Hamiltonian eigenvalue equation $H|\Psi_i\rangle = E_i|\Psi_i\rangle$, if the variation is performed under the constraint of wavefunction normalization. The constrained variation appearing in (2.7) is exactly a subset of such variations, since the normalization requirement includes the fixed density constraint.[2]

To prove that a ρ-stationary state is an eigenstate of a Hamiltonian with external potential defined by ρ, ν, and α, we note that the general variation δ (preserving the wavefunction normalization) can be decomposed into a variation of densities δ_ρ and a variation of states corresponding to a particular density $\delta_{\Psi\to\rho}$. Formally we then write $\delta = \delta_\rho + \delta_{\Psi\to\rho}$, and since a ρ-stationary state is invariant to the latter we have

$$\begin{aligned}
&\delta\langle\Psi[\rho,\nu,\alpha]|T+\alpha V_{ee}+V_{ext}|\Psi[\rho,\nu,\alpha]\rangle\\
&=\delta_\rho\langle\Psi[\rho,\nu,\alpha]|T+\alpha V_{ee}+V_{ext}|\Psi[\rho,\nu,\alpha]\rangle\\
&=\int d\mathbf{r}\frac{\delta E_G[\rho,\nu,\alpha]}{\delta\rho(\mathbf{r})}\delta\rho(\mathbf{r}).
\end{aligned} \tag{2.9}$$

Since $\delta\rho(\mathbf{r})$ is an arbitrary variation, which conserves the particle number, it satisfies $\int d\mathbf{r}\delta\rho(\mathbf{r}) = 0$ and the last integral in (2.9) is zero if

$$\frac{\delta E_G[\rho,\nu,\alpha]}{\delta\rho(\mathbf{r})}=\mu, \tag{2.10}$$

[2]For a local external potential $V_{ext}(\mathbf{r})$ the last term in Eq. (2.7) can be included in the expectation value since $\int d\mathbf{r}V_{ext}(\mathbf{r})\rho(\mathbf{r}) = \Psi|V_{ext}|\Psi\rangle$ where $\rho(\mathbf{r}) = |\Psi(\mathbf{r})|^2$. This term only depends on ρ and is not affected by the constrained search for stationary points.

where μ is a constant. Put differently, a given ρ-stationary state $|\Psi[\rho,\nu,\alpha]\rangle$ is an eigenstate of a Hamiltonian with external potential given by

$$V_{ext}[\rho,\nu,\alpha] = -\frac{\delta}{\delta\rho(\mathbf{r})} \operatorname*{stat}_{\nu,\Psi\to\rho} \langle\Psi|T+\alpha V_{ee}|\Psi\rangle + \mu, \tag{2.11}$$

and the density thus completely determines the external potential up to an additive constant. Since we also showed that all eigenstates are ρ-stationary, this implies the following generalization of the Hohenberg-Kohn theorem: *An electron density determines the external potentials of all electronic systems that have at least one eigenstate with this electronic density.* The result is a simple generalization of DFT based on the Levy constrained search functional (2.2), which involves a special case of a ρ-stationary wavefunction, namely the ground state corresponding to the global minimum of the constrained search. However, the implications of the generalized Kohn-Sham theorem is mind boggling: the external potential and thus all properties of an electronic system, are determined by the density of any of its eigenstates!

In principle, all eigenenergies associated with a particular external potential and Hamiltonian can be found by finding all stationary densities satisfying Eq. (2.10) and evaluating the functional (2.7) at all ρ-stationary points for each of these densities. However, such a scheme is impossible to realize for practical applications and one needs a working algorithm like the Kohn-Sham scheme to actually perform a density based calculation of excited state energies.

2.2.1 Generalized Adiabatic Connections

To calculate excited state energies, one could imagine to set up a scheme similar to the Kohn-Sham equations (2.4). By the generalized Hohenberg-Kohn theorem, there exist a non-interacting model system, which has an eigenstate Φ_j with the same density as a given excited state Ψ_i. Once the density is obtained from the model system the energy can be evaluated by an equation similar to Eq. (2.5). However, since the density of the excited state is not known *a priori*, there is no general way of identifying a particular excited state of the model system as the state, which reproduces the density of the interacting excited state of interest. It should also be noted that the densities of different excited states of a particular interacting system, are reproduced by excited states of different non-interacting systems. Nevertheless, one may setup a generalized Kohn-Sham scheme like Eq. (2.4), except that the model potential v_s should depend on ν as well as on the excited state density corresponding to Ψ_i. Similarly, the energy functionals appearing in Eq. (2.5) acquires a dependence on ν, which implies

an orbital dependence in the exchange-correlation functional. Although there is no general way of constructing the relevant excited state in the model system, one may be guided by certain properties of the excited state of interest, and for simple excitations it is sometimes possible to constrain the model system in such a way that an excited state with some property is reproduced.

In spite the fact that practical applications of excited state DFT may often be hindered by technical problems related to defining and identifying corresponding states in the interacting and non-interacting systems, the generalized Hohenberg-Kohn theorem is of great fundamental interest. Besides the obvious generalization of ground state DFT, the theorem also implies a solution to the non-interacting v-representability problem. This follows from the fact that a non-interacting potential reproducing an eigenstate with a certain density, exists by construction (2.11). In ground state DFT a non-interacting potential that has a *ground state* reproducing the interacting ground state density is assumed to exist. In the generalized formalism, such a potential does not have to exist, but a non-interacting potential that has *some eigenstate* reproducing the ground state density can always (in principle) be constructed.

To formalize the connections between interacting and non-interacting systems, we follow Görling and introduce the Generalized Adiabatic Connection (GAC) as the α-path of ρ-stationary wavefunctions corresponding to a particular density ρ and auxiliary quantum number ν. Thus, one should imagine the space of all many-particle wavefunction being extended by a α-axis and a GAC is the path taken by a ρ-stationary wavefunction $\Psi[\rho, \nu, \alpha]$ for a fixed ν.[3] In Fig. 2.1 we show three possible cases of GACs involving the interacting ground state. To the left we show the usual situation where the ground state of an interacting system $\Psi_0[\rho_0]$ is connected to the ground state of a non-interacting system $\Phi_0[\rho_0]$ and the GAC coincide with the usual adiabatic connection. In the middle we show a situation where a non-interacting potential exists with a ground state $\Phi_0[\rho_0, \nu]$, which reproduces the interacting ground state density, but the non-interacting state may be connected to an interacting state $\Psi_i[\rho_0, \nu] \neq \Psi_0[\rho_0, \nu']$, since the ground state density can have several stationary points corresponding to different values of ν and the Görling functional (2.7) may satisfy $E_G[\rho_0, \nu, \alpha = 1] > E_G[\rho_0, \nu', \alpha = 1]$. In this case the non-interacting system is v-representable, but could give rise to the wrong ground

[3] The GAC may have a non-trivial structure, since the number of ρ-stationary wavefunctions belonging to a particular density may depend on α. One can therefore have situations where an adiabatic connection splits or recombines different values of ν. Here we will only consider simple adiabatic connections and refer to the discussion in Ref. [40] for the general case.

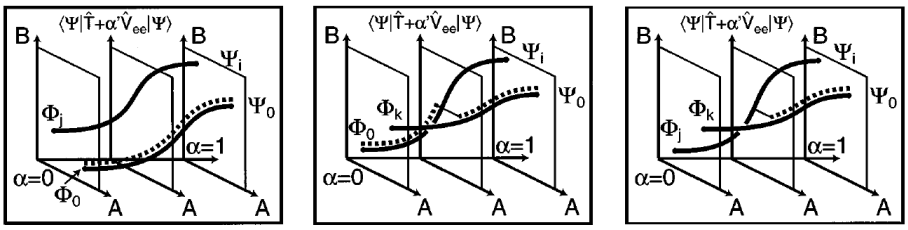

Figure 2.1: Schematic illustration of GACs in three different situations. The A-axis represent the multi-dimensional space of many-particle wavefunctions and the B-axis represents the expectation value of $T + \alpha V$. Ψ_0 and Φ_0 represent the interacting ($\alpha = 1$) and non-interacting ($\alpha = 0$) ground states respectively. Solid and dashed curves are the GAC and standard adiabatic connections respectively. Left: The usual case where the interacting ground state density can be represented by a non-interacting ground state and there is a ground state GAC coinciding with the standard adiabatic connection. Middle: In this case there is an interacting excited state Ψ_i with the same density as the ground state and the non-interacting ground state may be adiabatically connected to the this state instead of the interacting ground state. In this case the standard adiabatic connection is discontinuous at some intermediate value of α. Right: The interacting ground state is not non-interacting v-representable and the standard adiabatic connection is terminated at some intermediate value of α. The GAC is, however, well defined for the interacting ground state and a non-interacting potential may be constructed, which has an excited state with the interacting ground state density.

state energy.[4] The last case is shown to the right in Fig. 2.1, where we show a situation where a non-interacting potential with a ground state reproducing the interacting ground state density does not exist. The non-interacting system is then not v-representable, however, a non-interacting potential, which has an excited state reproducing the interacting ground state density *does* exist. The GAC thus gives a formal solution to the non-interacting v-representability problem, but for practical applications the GAC may not be particularly useful.

[4] This of course only relevant if one has a state dependent approximation for the exchange-correlation functional $E_{xc}[\rho, \nu]$.

2.3 ΔSelf-Consistent Field DFT

The method of ΔSelf-Consistent Field DFT is a simple extension of ground state DFT, where a self-consistent Kohn-Sham calculation is constrained by specifying the occupation numbers of certain Kohn-Sham orbitals. The resulting self-consistent density thus corresponds to a non-interacting excited state and is not composed of the Kohn-Sham orbitals of lowest energy. Due to the self-consistency, the potential $v_s' = v_s[\rho']$ of the non-interacting system, which gives rise to the excited state, is different than the potential $v_s = v_s[\rho_0]$ that yields the ground state density.

The method has been applied to a range of different problems [43, 54] and is often regarded as an unjustified extension of DFT, which may give reasonable results. However, the work of Görling reviewed in section 2.2, formally puts the method on a firm theoretical foundation and all that remains is to find a good approximation for the exchange-correlation functional $E_{xc}[\rho, \nu]$, which should depend on the excited state index ν as well as the density. The semi-local approximations [83, 111, 44] for the exchange-correlation functionals, which are often used for ground state DFT, are based on the ground state energy density of the homogeneous electron gas, but as a first approximation, these functionals can be used for excited state DFT calculations as well. A far more serious problem is related to the definition of the excited state of interest. ΔSCF allows one to modify the occupations numbers of the orbitals of the non-interacting system, but in general there is no systematic way of doing this and one has to be guided by physical principles and symmetries to construct a non-interacting excited state, which corresponds to a particular interacting excited state.

2.3.1 Excited states of isolated molecules

As an example we will consider the nitrogen molecule N_2. The electronic eigenstates of molecules, can be labeled according to their transformation properties under symmetry operations, which leave the electronic Hamiltonian invariant. In the case of a diatomic molecule, the Hamiltonian commutes with the component of angular momentum along the molecular axis and the eigenstates can be labeled by the quantum number M. In the context of molecular spectroscopy the many-particle eigenstates are referred to as Σ, Π, and Δ corresponding to $|M| = 0$, $|M| = 1$, and $|M| = 2$ respectively. In addition, eigenstates are labeled by the superscript $2S + 1$ where S is the total electronic spin. The ground state of N_2 is a $^1\Sigma$-state.

A common approximation, which can be used to understand the electronic

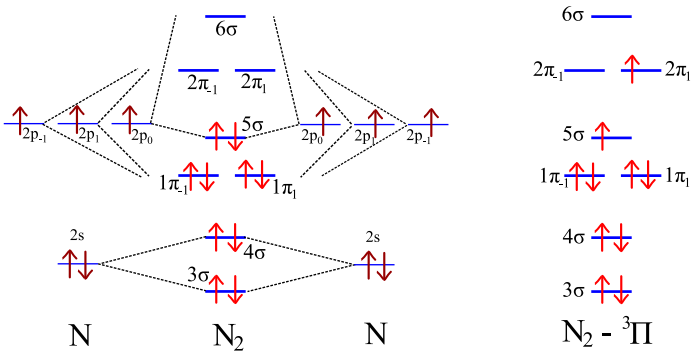

Figure 2.2: The electronic structure of N_2 in terms of molecular orbitals. To the left is shown how the orbitals of N atoms combine into the molecular orbitals used to describe N_2. To the right is a $^3\Pi$ excited state where one spin down bonding 5σ electron is moved to a spin up antibonding 2π orbital. For the $^3\Delta$ state, one would have to take the spin down electron from the bonding $1\pi_{-1}$ instead.

structure of molecules, is that of molecular orbitals, which are denoted by σ, π, and δ with angular momentum $|m| = 0$, $|m| = 1$, and $|m| = 2$ respectively. The molecular orbitals are linear combinations of the atomic orbitals s, p, and d and a schematic spectrum for N_2 in terms of these, are shown in Fig. 2.2 for the ground state and an excited $^3\Pi$ state. Depending on the whether the molecular orbitals are symmetric or antisymmetric linear combinations of atomic orbitals, they may have more or less density between the nuclei compared to the bare orbitals and are referred to as bonding or anti-bonding respectively. States composed of anti-bonding orbitals are therefore expected to have a larger adiabatic bond length than states composed of bonding orbitals.

If we focus on the unpaired orbitals, the triplet states can be approximated by

$$\begin{aligned} {}^3\Sigma_\pm(\mathbf{r}_1,\mathbf{r}_2) \approx \Big(&1\pi_{+1}(\mathbf{r}_1)2\pi_{+1}(\mathbf{r}_2) - 1\pi_{+1}(\mathbf{r}_2)2\pi_{+1}(\mathbf{r}_1) \\ &\pm 1\pi_{-1}(\mathbf{r}_1)2\pi_{-1}(\mathbf{r}_2) \mp 1\pi_{-1}(\mathbf{r}_2)2\pi_{-1}(\mathbf{r}_1)\Big)/2, \end{aligned} \tag{2.12}$$

$$ {}^3\Pi(\mathbf{r}_1,\mathbf{r}_2) \approx \Big(5\sigma(\mathbf{r}_1)2\pi_{\pm1}(\mathbf{r}_2) - 5\sigma(\mathbf{r}_2)2\pi_{\pm1}(\mathbf{r}_1)\Big)/\sqrt{2}, \tag{2.13}$$

$$ {}^3\Delta(\mathbf{r}_1,\mathbf{r}_2) \approx \Big(1\pi_{\pm1}(\mathbf{r}_1)2\pi_{\mp1}(\mathbf{r}_2) - 1\pi_{\pm1}(\mathbf{r}_2)2\pi_{\mp1}(\mathbf{r}_1)\Big)/\sqrt{2}, \tag{2.14}$$

where the ± subscripts on the Σ states denote the transformation properties when the wavefunctions are reflected through a plane containing the molecular axis. It should be noted that $\pi_{\pm 1}$ have angular momentum $m = \pm 1$ and the Π and Δ each has two-fold degeneracy corresponding to $M = \pm 1$ and $M = \pm 2$ respectively.[5] To obtain the correct total angular momentum from the constituent molecular orbitals, one should remember to include the doubly occupied 1π states in the Σ and Δ states.

The result of solving the Kohn-Sham equations (2.4) is a set of orbitals φ_i and corresponding eigenvalues ϵ_i. The physical objects of interest are the density and total energy (2.5), which are properties of the real system, whereas the eigenvalues and orbitals are auxiliary objects, which in general, do not have any physical significance. However, if the electronic many-body states are well represented by Slater determinants of single particle orbitals, the Kohn-Sham orbitals will often reproduce this orbital approximation and in the case of N_2, the Kohn-Sham orbitals are very similar to what one would obtain from the molecular orbital approximation. Because of this, we expect that the excited states of N_2 can be constructed by simply constraining the orbital occupation numbers in a Kohn-Sham calculation, and solve the equations

$$\Big(T + v_s[\tilde{\rho}(\mathbf{r})]\Big)\varphi_i(\mathbf{r}) = \epsilon_i\varphi_i(\mathbf{r}), \qquad \tilde{\rho}(\mathbf{r}) = \sum_i \tilde{f}_i|\varphi_i(\mathbf{r})|^2, \tag{2.15}$$

self-consistently. In this expression, $\tilde{\rho}$ is an excited state density defined by the occupation numbers $\tilde{f}_i$, which correspond to an excited state such as that shown in Fig. 2.2. It should be noted that in these equations, the resulting orbitals φ_i are not the same as those obtained in a ground state calculation since the potential is changed.

If a local approximation is used for $E_{xc}[\rho]$, it is assumed that the wavefunction is written as a Slater determinant, and we can only use such functionals to calculate excited states energies when this is true. In particular, to obtain the energies of the singlet states as well as the Σ states, one has to do ΔSCF calculations with non-local functionals [41]. However, the singlet energies with local functionals can be approximated by the multiplet sum method [112]. In table 2.1, we show the result of ΔSCF calculations obtained with the DFT code `GPAW` [100, 75, 25], and compare with experimental values and theoretical values obtained from time-dependent DFT. The method is seen to give reasonable, but

[5] The states with non-vanishing angular momentum $|M|$ are two-fold degenerate with eigenvalues $M = \pm|M|$ since the reflection operator R commutes with the Hamiltonian and gives $R\Psi_M = \Psi_{-M}$. The $\Sigma_\pm$ are annihilated by the angular momentum operator, but are eigenstates of R with eigenvalues ± 1 and are not degenerate.

State	Transition	$\Delta\epsilon_{KS}$	TDDFT (ALDA)	ΔSCF (LDA)	ΔSCF (RPBE)	Exp.
$^1\Pi$	$5\sigma \rightarrow 2\pi$	8.16	9.23	8.75	8.58	9.31
$^3\Pi$			7.62	7.55	7.52	8.04
$^1\Delta$	$1\pi \rightarrow 2\pi$	9.63	10.27	10.50	10.52	10.27
$^3\Delta$			8.91	8.94	8.79	8.88
$^1\Pi$	$4\sigma \rightarrow 2\pi$	11.21	13.87	11.97	12.40	13.63
$^3\Pi$			10.44	10.37	10.61	11.19

Table 2.1: Excitation energies for the N_2 molecule calculated with ΔSCF using two different approximations for the exchange-correlation functional (LDA and RPBE). The $\Delta\epsilon_{KS}$ is the Kohn-Sham eigenvalue differences, TDDFT are theoretical time-dependent DFT calculations taken from Grabo et al. [42], and Exp. is experimental values tabulated by Oddershede et al. [79] using the spectroscopic constants of Huber and Herzberg [53].

not very accurate agreement with experiment and changing the functional from LDA to RPBE does not improve the results as one would expect for a ground state calculation.

When analyzing hot electron mediated dynamics at metal surfaces, we will be interested in potential energy surfaces such as those shown in Fig 1.1. In Fig. 2.3 we show the ground state potential as a function of bond length obtained with ground state DFT and the excited $^3\Delta$ state obtained from ΔSCF. All calculations were obtained with `GPAW`. The excited potential shows the behavior expected from a molecular orbital point of view. Namely, that the minimum energy is located at a larger bond length due to the anti-bonding nature of the 2π orbital.

2.3.2 Excited states of molecules on metal surfaces

Several quantum chemical methods are able to give much more accurate results than those displayed in table 2.1 and these methods do not have problems with singlet and Σ states. Although such methods may be prohibitly time-consuming for large systems, they are certainly tractable for simple molecules like N_2 and as such, one should not regard ΔSCF as a good method for calculating excited state properties of isolated molecules.

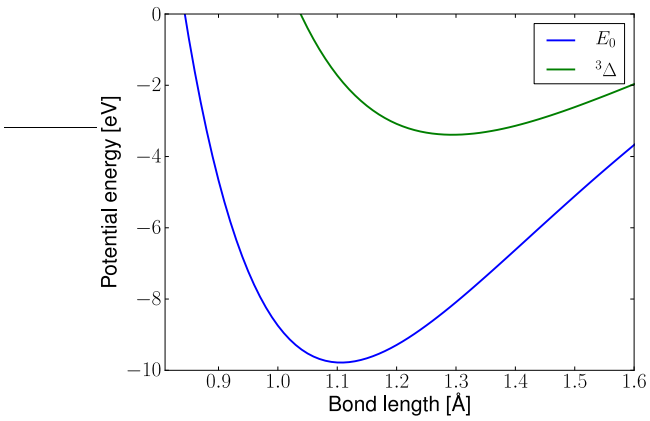

Figure 2.3: Potential energy surfaces of the ground and $^3\Delta$ excited states of the N_2 molecule as a function of bond length. In terms of molecular orbitals, the $^3\Delta$ state can be thought of as moving an electron from a bonding 1π orbital to an anti-bonding 2π orbital, which results in a minimum at larger bond length. Note that in a classical model for hot electron mediated energy transfer, such as that illustrated in Fig. 1.1, it is possible to transfer on the order of $\sim 6\ eV$ in a single excitation event between these potential energy surfaces.

A completely different matter is the problem of calculating potential energy surfaces for molecules adsorbed on metal surfaces. For such systems, DFT seems to be the only method, which allows one to handle the many degrees of freedom and ΔSCF is required in order to obtain excited state energies. However, the concept of occupation numbers constraint in Eq. (2.15), has to be generalized, since the excited state of interest is not an eigenstate of the full electronic Hamiltonian, but a state where an extra electron has been placed in an unoccupied adsorbate orbital. To perform a ΔSCF calculation on such a state we need a unique way of defining it.

Again, this is accomplished using the concept of molecular orbitals. For a total of N electrons we simply constrain the density to be

$$\rho_a(\mathbf{r}) = \sum_{i=1}^{N-1} |\varphi_i(\mathbf{r})|^2 + |\varphi_a(\mathbf{r})|^2, \tag{2.16}$$

where $\varphi_a(\mathbf{r}) = \langle \mathbf{r}|a\rangle$ is the wavefunction of the adsorbate resonance. The density is thus comprised of the $N-1$ orbitals with lowest energy and a molecular orbital, which is not an eigenstate of the Kohn-Sham equations in the presence of a metal surface. In order to perform such a calculation, a wavefunction $\varphi_a(\mathbf{r})$ is required, but here we can use the Kohn-Sham orbital of a DFT calculation for the isolated molecule, since this usually gives a good approximation for molecular orbitals. One needs to ensure that the added density only consists of unoccupied orbitals and we therefore expand the molecular orbitals in Kohn-Sham orbitals

$$\varphi_a(\mathbf{r}) = \sum_{i=1}^{\infty} c_{ai}\varphi_i(\mathbf{r}), \tag{2.17}$$

and renormalize the c_{ai} such that only empty orbitals contribute to the sum. The method is similar to that proposed by Wu et al. [108, 109, 2], where a number of electrons are constrained to be localized at a certain volume in space. However, the present approach allows for a backtransfer of charge from other orbitals, which are localized near the state φ_a and is better suited for our purpose.

The method does not provide a general way to obtain the excited state properties of a system if no prior knowledge of the excitation is given. On the other hand, if one is interested in a particular excited state and it can be constructed as in Eq. (2.16), it is possible to obtain its energy and density using DFT and ΔSCF. As an example, we consider N_2 adsorbed at a Ru(0001) surface. It is adsorbed at a top site with the molecular axis perpendicular to the surface. In the context of reactions mediated by hot electrons we will be interested in the potential energy surface associated with an excited molecular resonance as well as the ground state potential. The lowest lying unoccupied molecular orbitals of N_2, are the 2π antibonding states and the excited state potential energy surface is obtained by applying Eqs. (2.16)-(2.17). At each position of the molecule, φ_a is obtained from a calculation of the isolated molecule in its ground state. The number of electrons in the full system is conserved and the extra electron is thus taken from the Fermi level of the metal. Due to the symmetry of the 2π orbital, the most important coordinates are those perpendicular to the surface. In Fig. 2.4 we show the ground and excited state potential energy surfaces calculated as functions of the N_2 bond length and the center of mass (COM) distance to the surface, obtained with the DFT code `GPAW`. The density difference between the ground and excited states is shown and the 2π orbital is clearly seen as well as an induced image charge on the surface. As expected for an antibonding state, the bond becomes stretched when excited and the molecule

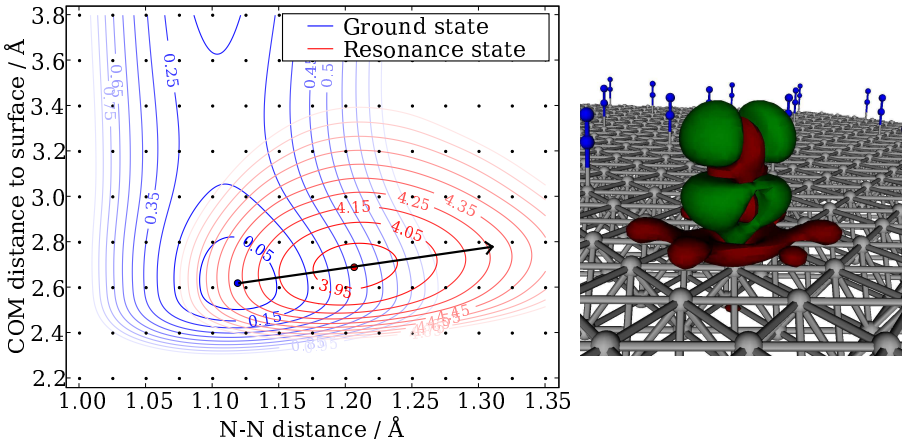

Figure 2.4: Left: Ground and excited state potential energy surfaces of N_2 adsorbed on a Ru(0001) top site. The excited state is obtained by forcing the molecular 2π orbital to be occupied according to Eq. (2.16). Right: Density difference between ground and excited state densities at the position corresponding to the minimum of the ground state potential energy surface. The green contour is excess charge in the excited state and the red contour is excess charge in the ground state. One can clearly recognize the 2π orbital and an image charge in the surface.

is seen to be stronger bound to the surface in the excited state due to interactions between the anionic molecule and the image charge.

For details on the method and comparison with inverse photoemission spectroscopy experiments, we refer to **paper I**.

2.4 Time Propagation of Hot Electrons

In this section, we will discuss a different DFT based approach, which is somewhat orthogonal to the method of ΔSCF and potential energy surfaces discussed previously. Here, we will not be concerned with non-adiabatic energy transfer, but simply consider the process of a hot electron tunneling from the metal substrate to an adsorbate orbital. The approach is based on a time-dependent extension of DFT (TDDFT) based on the Runge-Gross theorem [88], which states that there is a one-to-one mapping between time-dependent densities and the

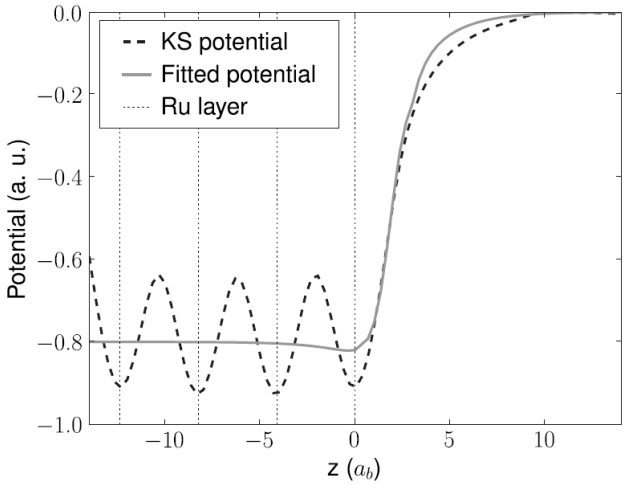

Figure 2.5: A fit of the Kohn-Sham potential at a closepacked Ruthenium surface. The dotted curve shows the self-consistent ground state Kohn-Sham potential of a four-layer Ruthenium slab averaged over the directions parallel to the surface. The solid curve shows the potential used in the time propagation simulation of a hot electron, and the vertical lines indicate the positions of the layers in the slab.

potentials under which they evolve. For details on the formalism and methodology of TDDFT we refer to Ref. [66], and here we will just note that one can construct a system of time-dependent non-interacting Kohn-Sham orbitals with a time-dependent potential that ensures that the correct time-dependent many-particle density is reproduced by the orbitals.

We will again use N_2 on Ru(0001) as a generic example. However, since the temporal propagation of electrons is a rather time consuming numeric process, we model the Ruthenium substrate by an averaged version of the Kohn-Sham potential obtained from a ground state DFT calculation of an isolated Ru(0001) slab with the `GPAW` code. This is shown in Fig. 2.5. The model system is thus composed of an N_2 molecule containing all its electrons and the slab potential, which represents the metal. To simulate an incoming hot electron, we put an electron in an energetic eigenstate of the slab potential and multiply by a phase factor $e^{ip_0 z/\hbar}$ to make the electron propagate towards the molecule with

momentum p_0.

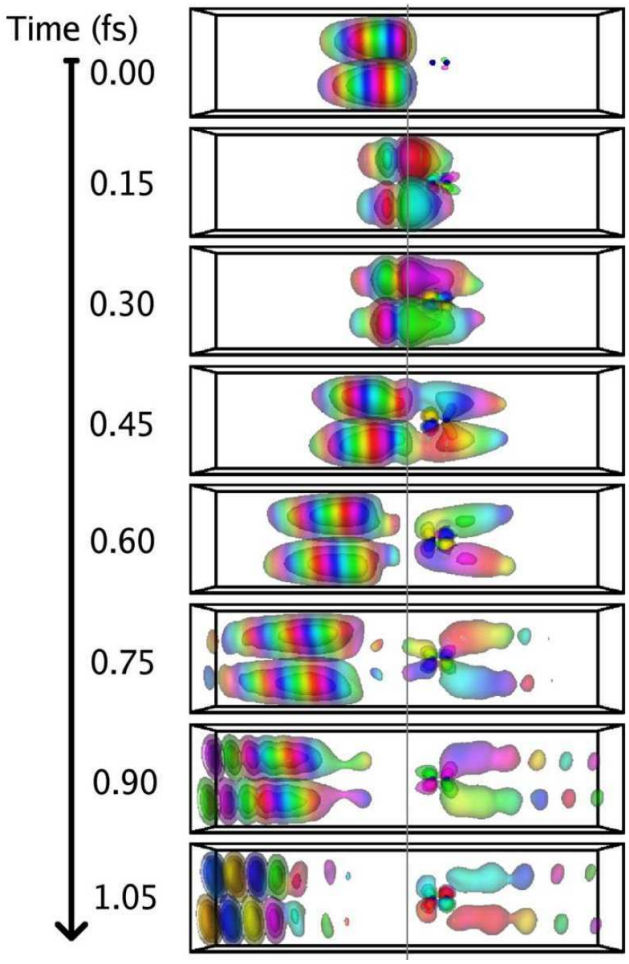

Figure 2.6: The time evolution of a hot electron with momentum $p_0 = 0.8$ a.u. directed toward the molecule. The hot electron orbital is shown at times: 0, 0.15, 0.30, 0.45, 0.60, 0.75, 0.90, and 1.05 fs. The color grading indicates the phase of the orbital. The two dots, which are visible at $t = 0$ fs, represent the positions of the nitrogen atoms and the gray line indicates the surface.

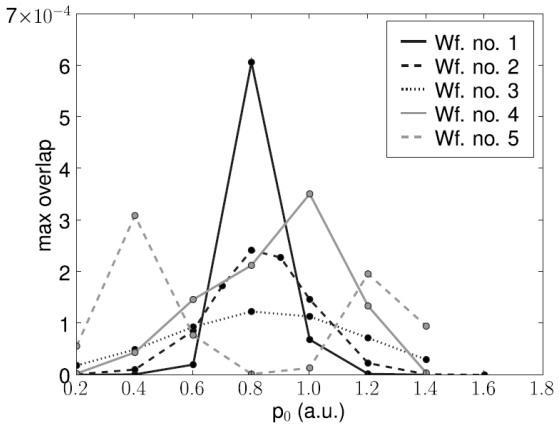

Figure 2.7: The amount of electron that gets into the 2π orbitals of the molecule within the first two femtoseconds, plotted as a function of the average momentum of the hot electron for five different initial wavefunctions.

Fig. 2.6 shows the result of a temporal propagation of the hot electron performed with the TDDFT code OCTOPUS [99]. When hitting the surface, a large fraction of the wavefunction is reflected due to the work function of the surface but a fraction of the wavefunction also ends up in the 2π states of the molecule. Part of the hot electron is apparently also transmitted into vacuum, which indicates that the hot electron has a spectral resolution extending above the vacuum level.

To quantify the probability of a hot electron making the transition to the 2π orbital of the molecule, we calculate the maximum overlap $|\langle 2\pi|\phi\rangle|^2$ of the hot electron wave function $\phi(\mathbf{r})$ with the 2π resonance during the time of propagation. The result depends on the choice of wavefunction for the initial hot electron and its momentum p_0 towards the surface, and we have repeated the calculations leading to Fig. 2.6 for five different initial orbitals (see **paper III** for a details on these wavefunctions). The result is shown in Fig. 2.7 and we see that, except for wavefunction 5, there is a maximum when the momentum is situated at ~ 0.8 a.u.

It is natural to think of the maximum overlap as a convolution of the spectral resolution of the hot electron with the 2π resonance, and we thus interpret the

excitation probability as

$$P_{transition} = \int d\varepsilon R_{2\pi}(\varepsilon) W(\varepsilon), \tag{2.18}$$

where $R_{2\pi}(\varepsilon)$ is a molecular orbital "excitation resonance" and

$$W(\varepsilon) = \sum_i |\langle \varphi_i | \phi \rangle|^2 \delta(\varepsilon_i - \varepsilon), \tag{2.19}$$

is the spectral resolution of the hot electron. For the φ_i, we can simply use the Kohn-Sham orbitals of the effective potential shown in Fig. 2.5. If we assume a Lorentzian type of excitation resonance:

$$R_{2\pi}(\varepsilon) = \frac{\alpha(\Gamma/2)^2}{(\varepsilon - \varepsilon_0)^2 + (\Gamma/2)^2}, \tag{2.20}$$

we can estimate the parameters α, Γ and ε_0 by a least squares fit of the expression (2.18) to the curves shown in Fig. 2.7. This gives the values: $\Gamma = 1.4\ eV$, $\varepsilon_0 = 9.8\ eV$, and $\alpha = 5.4 \times 10^{-3}$. The value of $\varepsilon_0 = 9.8\ eV$ may seem high, but one should keep in mind that for this system, the Fermi level lies at the highest occupied molecular orbital of the nitrogen molecule, and that the surface cannot create an image charge, which would lower the resonance energy. The $9.8\ eV$ also seems reasonable when comparing with the lowest excitation energies of the nitrogen molecule.

For an extended system with an averaged potential like the one shown in Fig. 2.5, it would be expected that the eigenstates are approximately plane waves and it would be relatively easy to construct an extended hot electron with an approximate eigenenergy, which matches the resonant energy ε_0. However, when modeling hot electrons with TDDFT, the wavefunction becomes localized in the finite super cell used in the simulation, and one cannot construct a hot electron carrying momentum towards the electron without disturbing the its spectral properties. This is shown in Fig. 2.8, where it is evident that the maximum at $p_0 = 0.8$ a.u. shown in Fig. 2.7, appears because this is the momentum, which centers the spectral resolution of the energy wavefunction on top of the resonance. It is also clear that the wavefunction with $p_0 = 0.8$ a.u. has a significant spectral width and is not a good representation of an extended plane wave. This represents a serious problem with TDDFT simulations of hot electrons, which result in an estimate of α that is too low. Nevertheless, even though we cannot represent a hot electron of definite energy in the finite

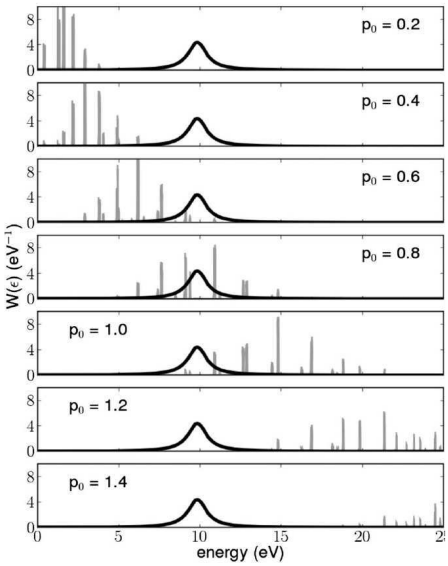

Figure 2.8: Spectral resolution of the hot electron wavefunction at different initial momenta p_0. The gray peaks show W(ε) from Eq. (2.19), where the delta functions have been replaced by Gaussians with a spread of 0.1 eV. The different subplots are for different momenta p_0 and the black curves show a Lorentzian of width $\Gamma = 1.4\ eV$ centered at $\varepsilon_0 = 9.8\ eV$. The wavefunction becomes a delta function for $p_0 = 0$ and obtains an increasing spectral width when the momentum is increased.

super cell, we can probe the molecular excitation resonance $R_{2\pi}$ by simulating scattering events using various wavefunctions with known spectral resolutions.

In **paper III**, we have repeated the TDDFT calculations with N_2 adsorbed on a Ruthenium nanoparticle and it is then possible to obtain the lifetime of the resonant 2π state. We will not go through the details here, but just mention that the result agrees with the spectral properties of the 2π state obtained from the simple model introduced above.

Chapter 3

The Non-Adiabatic Newns-Anderson Model

In general, the Hamiltonian (1.1) is to complicated to be directly applicable to models of non-adiabatic reactions at metal surfaces. Instead we will set up a model Hamiltonian inspired by the conceptual picture shown in Fig. 1.1. The foundation is the Newns-Anderson model [1, 77], which is generalized to include adsorbate degrees of freedom using potential energy surfaces. This Hamiltonian will be central to the analysis in the remainder of this thesis and within various approximations, it will be used to derive probabilities of inelastic scattering, a Master equation, and a semi-classical Langevin equation for the adsorbate coordinates.

In this chapter, we start by reviewing some properties of the Newns-Anderson model and then introduce coupling to adsorbate coordinates. As a first semi-quantitative approach, we consider the electronic excited state as a time dependent force on the adsorbate coordinate and thus obtain a forced oscillator model for the non-adiabatic energy transfer. While the model demonstrates some conceptual features of non-adiabatic dynamics, it is based on a complete disentangling of the electronic and vibrational degrees of freedom. We therefore turn to a model of inelastic scattering within the complete model Hamiltonian, which captures most of the physics involved in energy transfer mediated by hot electrons. Finally, we calculate the reduced density matrix, which gives rise to an effective equation for the adsorbate dynamics under the influence of an electronic environment.

3.1 Electronic Structure of Adsorbates

We start by neglecting the adsorbate coordinate degrees of freedom and analyze the electronic structure of a metal surface with an adsorbed atom or molecule. The adsorbate is then represented by a single localized electronic state $|a\rangle$ and the metal is represented by an infinite number of delocalized electronic states $|k\rangle$. The Hamiltonian is assumed to be diagonal in these states when the adsorbate is well separated from the metal and there is no interaction. When the adsorbate is brought into contact with the metal, $|a\rangle$ becomes hybridized with the metallic states and neither are no longer eigenstates of the Hamiltonian. This is the generic situation of our interest and, for a particular position of the adsorbate, the electronic Hamiltonian reads

$$H_{NA} = \varepsilon_0 c_a^\dagger c_a + \sum_k \varepsilon_k c_k^\dagger c_k + \sum_k \Big(V_{ak} c_a^\dagger c_k + V_{ak}^* c_k^\dagger c_a \Big), \tag{3.1}$$

where $c_a^\dagger$ creates an electron in the state $|a\rangle$ and $c_k^\dagger$ creates an electron in the state $|k\rangle$. ε_0 is the eigenenergy of the free adsorbate and ε_k are the eigenvalues of the metal without adsorbate. Since the Hamiltonian (3.1) is quadratic in electronic operators, one could in principle diagonalize it and obtain the eigenvalues ε_n of the full system. However, all the eigenstates would then be represented by delocalized orbitals and it is much more instructive to keep the basis separated in delocalized metallic states and a localized adsorbate state. The object of interest is then the spectral properties of the adsorbate state, which for a non-interacting system, can be written as a projected density of states

$$\rho_a(\varepsilon) = \sum_n |\langle n|a\rangle|^2 \delta(\varepsilon - \varepsilon_n), \tag{3.2}$$

where $|n\rangle$ are eigenstates of the Hamiltonian (3.1). The fact that $|a\rangle$ is not an eigenstate, will result in a broadening of $\rho_a(\varepsilon)$ and we will refer to such a broadened state as a resonance. Using a standard trick,[1] the projected density of states can be written

$$\rho_a(\varepsilon) = \frac{-1}{\pi} \mathrm{Im} \langle a| \frac{1}{\varepsilon - H_{NA-el} + i0^+} |a\rangle \equiv \frac{-1}{\pi} \mathrm{Im} G_R^0(\varepsilon), \tag{3.3}$$

[1] If $\eta = 0^+$ is a positive infinitesimal, then

$$\frac{1}{x + i\eta} = \mathcal{P}\frac{1}{x} - i\pi\delta(x),$$

where $\mathcal{P}$ denotes the Cauchy principal part.

where we have defined the retarded Green function of the resonance $G_R^0(\varepsilon)$. It can be evaluated from the Dyson equation with the result

$$G_R^0(\varepsilon) = \frac{1}{\varepsilon - \varepsilon_0 - \Sigma(\varepsilon) + i\Gamma(\varepsilon)/2}, \tag{3.4}$$

$$\rho_a(\varepsilon) = \frac{\Gamma(\varepsilon)/2\pi}{(\varepsilon - \varepsilon_0 - \Sigma(\varepsilon))^2 + (\Gamma(\varepsilon)/2)^2}, \tag{3.5}$$

where

$$\Gamma(\varepsilon) = 2\pi \sum_k |V_{ak}|^2 \delta(\varepsilon - \varepsilon_k), \qquad \Sigma(\varepsilon) = \frac{1}{2\pi} \mathcal{P} \int d\varepsilon' \frac{\Gamma(\varepsilon')}{\varepsilon - \varepsilon'}. \tag{3.6}$$

For an eigenstate of H_{NA} the spectral function would be a delta function centered at the eigenenergy and the result of coupling an adsorbate state to a metal surface is thus a shift in eigenenergy given by Σ and a spectral broadening given by Γ. Very often it is more useful to consider the retarded Green function in the time domain where it is defined by

$$G_R^0(t) = -i\theta(t)\langle 0|c_a(t)c_a^\dagger|0\rangle, \qquad c_a(t) = e^{iHt/\hbar} c_a e^{-iHt/\hbar}, \tag{3.7}$$

which is readily confirmed to be the Fourier transform of $G_R^0(\varepsilon)$.[2]

If the metal density of states is approximately constant in the region of the adsorbate resonance and the coupling elements V_{ak} varies slowly across the resonance, the function $\Gamma(\varepsilon)$ becomes constant and the shift $\Sigma(\varepsilon)$ vanishes. This is the very important wide band limit, which will be imposed several times in the following. The spectral function becomes a Lorentzian and the Green function in the time domain becomes an exponential $G_R^0(t) = -i\theta(t)e^{-i(\varepsilon_0 - i\Gamma/2)t/\hbar}$. An important consequence of the wide band limit is that the adsorbate acquires a well defined lifetime. If an electron is put into the state $|a\rangle$ at time $t = 0$, the probability that it is still there at time $t > 0$ is

$$P_a(t) = |\langle a|e^{-Ht/\hbar}|a\rangle|^2 = |G_R^0(t)|^2 = e^{-t/\tau}, \qquad \tau = \hbar/\Gamma, \tag{3.8}$$

and the lifetime of an electron in the adsorbate resonance is thus directly related to the width of the resonance Γ.

[2]The Fourier transform of (3.7) is defined with a factor of $e^{-0^+ t/\hbar}$ in order to secure convergence.

3.2 Non-Adiabatic Model

To include non-adiabatic effects, we now introduce coupling to adsorbate coordinates x in all terms depending on the state $|a\rangle$. We assume that the metallic states $|k\rangle$ do not couple to the adsorbate coordinates. The Hamiltonian then becomes

$$H = H_0 + \varepsilon_a(x)c_a^\dagger c_a + \sum_k \varepsilon_k c_k^\dagger c_k + \sum_k \left(V_{ak}(x)c_a^\dagger c_k + V_{ak}^*(x)c_k^\dagger c_a \right) \tag{3.9}$$

$$H_0 = T + V_0(x), \tag{3.10}$$

where we have included an adsorbate Hamiltonian H_0 with kinetic energy T and ground state potential $V_0(x)$. Referring to the potentials of Fig. 1.1, we can think of $\varepsilon_a(x)$ as the difference between ground and excited state potentials. To see this, one should simply note that we can write $\varepsilon_a(x)c_a^\dagger c_a + V_0(x) = V_1(x)c_a^\dagger c_a + V_0(x)(1 - c_a^\dagger c_a)$ with $\varepsilon_a(x) = V_1(x) - V_0(x)$ indicating that the adsorbate dynamics is governed by $V_1(x)$ when the state $|a\rangle$ is occupied and $V_0(x)$ when it is unoccupied. The off-diagonal coupling elements $V_{ak}(x)$, translate into a coordinate dependence of the spectral broadening of the resonance. The coupling and thus the broadening is expected to approach zero when the adsorbate is moved far away from the surface.

Again, the fundamental objects of interest are the Green functions which in general, have a very complicated structure when adsorbate degrees of freedom are included. It will be convenient to use a basis of the electronic single particle states $|a\rangle$ and $|k\rangle$ and eigenstates of $T + V_0(x)$, which we will denote by $|n\rangle$.

3.3 The Forced Oscillator Model

Before we delve into the involved machinery of inelastic scattering, we will consider a simple one-dimensional model of a forced oscillator, which gives a semi-quantitative picture of how non-adiabatic energy transfer is mediated [97, 33, 36]. The method assumes that we can think of the electronic and adsorbate degrees of freedom separately and thus regard the whole problem as an oscillator with a time-dependent force, which is a function of the spectral properties of the resonance.

We start by disregarding all but the diagonal coupling elements in the Hamiltonian (3.9) such that $V_{ak}(x) = V_{ak}$ are constant, and assume that the resonance is occupied at $t = 0$. The probability that the resonance is occupied for $t > 0$ is given by $P_a(t)$ (3.8) and we will think of this as the average occupation of the

resonance. In this picture we can combine the ground and excited potentials into a single time dependent potential. All relevant electronic degrees of freedom are then contained in $P_a(t)$ and the adsorbate Hamiltonian is approximated by

$$H_{FO}(t) = T + V_0(x) + V(x,t), \qquad V(x;t) = P_a(t)\varepsilon_a(x), \tag{3.11}$$

where $\varepsilon_a(x) = V_1(x) - V_0(x)$.

3.3.1 Classical energy transfer

Before we analyze the quantum dynamics resulting from Eq. (3.11) it is useful to consider a classical model of hot electron mediated energy transfer. The classical equation of motion derived from (3.11) is

$$m\ddot{x} + V_0'(x) = -P_a(t)\varepsilon_a'(x), \tag{3.12}$$

where primes denote derivatives with respect to x. It is very instructive to investigate the harmonic oscillator with a linear coupling function since it allow us to obtain exact results in a variety of models. We are thus led to consider the potential $V_0 = m\omega_0^2 x^2/2$ and the coupling function $\varepsilon_a(x) = \varepsilon_0 - fx$ corresponding to a displaced excited state potential $V_1(x) = m\omega_0^2(x-\Delta x)^2/2 - m\omega_0^2\Delta x^2/2 + \varepsilon_0$ with $\Delta x = f/m\omega_0^2$. Equation (3.12) can then be solved by a Fourier transformation giving

$$x(t) = \int_{-\infty}^{\infty} d\omega x(\omega) e^{i\omega t}, \qquad x(\omega) = \frac{fP_a(\omega)}{m(\omega_0^2 - \omega^2)}, \tag{3.13}$$

and $P_a(\omega)$ is the Fourier transform of $P_a(t)$.

In the wide band limit where $P_a(t)$ is an exponential one obtains[3]

$$x(t) = \frac{f^2}{m\omega_0(\omega_0^2 + 1/\tau^2)}\Big(\omega_0 \cos\omega_0 t - 1/\tau \sin\omega_0 t - \omega_0 e^{-t/\tau}\Big). \tag{3.14}$$

Taking the limit of $t \to \infty$ corresponding to the hot electron having left the adsorbate, gives the total energy

$$\Delta E_{Cl} = \frac{1}{2}m\omega_0^2 x^2 + \frac{1}{2}m\dot{x}^2 = \frac{f^2}{2m(\omega_0^2 + 1/\tau^2)}, \tag{3.15}$$

which is the amount of energy transferred by the hot electron.

[3] Adding a damping term $\gamma\dot{x}$ to the equation of motion shifts the real poles in the integrand in (3.13) to the upper half of the complex plane, and the integral can be calculated by the method of residues.

3.3.2 Quantum mechanical energy transfer

For a quantum mechanical treatment of the forced oscillator model (3.11), it is natural to choose a set of eigenfunctions of H_0. If the oscillator is in a state $|m\rangle$ when the time-dependent perturbation is switched on at time $t = t_0$, the probability (in the Scrödinger picture) of having made a transition to a state $|n\rangle$ at time t is [8]

$$P_{mn}(t;t_0) = |\langle m(t_0)|n(t;t_0)\rangle|^2 = |\langle m(t_0)|e^{-iH_0t/\hbar}\hat{U}(t;t_0)e^{iH_0t_0/\hbar}|n(t_0)\rangle|^2, \tag{3.16}$$

where

$$\hat{U}(t;t_0) = \mathcal{T}\Big(e^{-i\int_{t_0}^{t} dt' P_a(t')\varepsilon_a[x(t')]/\hbar}\Big), \qquad x(t) = e^{iH_0t/\hbar}xe^{-iH_0t/\hbar}, \tag{3.17}$$

and $\mathcal{T}$ denotes time ordering.

We will again consider the case of a displaced harmonic oscillator ($V_0 = m\omega_0^2x^2$ and $\varepsilon_a(x) = \varepsilon_0 - fx$). The algebraic quantization in terms of creation and annihilation operators $a^\dagger$ and a should be familiar and with these operators the forced oscillator Hamiltonian 3.11 can be written

$$H_{FO}(t) = H_0 + H_I(t) \tag{3.18}$$

$$H_0 = \hbar\omega_0(a^\dagger a + \frac{1}{2}), \qquad H_0|n\rangle = n\hbar\omega_0|n\rangle \tag{3.19}$$

$$H_I(t) = -P_a(t)fx = \lambda P_a(t)(a^\dagger + a), \qquad \lambda = -f\sqrt{\frac{\hbar}{2\omega_0 m}}. \tag{3.20}$$

It is straightforward to show that $a(t) = ae^{-i\omega_0 t}$ and the time ordering operator in Eq. (3.17) can thus readily be removed. Evaluating $\hat{U}(t;t_0)$ with the linear coupling term (3.20) then gives

$$\hat{U}(t;t_0) = e^{-iq^*a^\dagger - iqa} = e^{-|q|^2/2}e^{-iq^*a^\dagger}e^{-iqa}, \qquad q = \frac{\lambda}{\hbar}\int_{t_0}^{t} dt' P_a(t')e^{-i\omega_0 t'}, \tag{3.21}$$

where the Feynman disentangling theorem [65] was used in the second equality. The matrix element (3.16) can now be evaluated. Since we are considering transitions between Hamiltonian eigenstates, the exponentials on either side of $\hat{U}(t;t_0)$ become pure phase factors, which vanish when we take the norm. The remainder is evaluated by Taylor expanding the two exponentials containing

operators in Eq. (3.21) and keep terms where the difference in number of raising and lowering operators is equal to $m - n$. For $n \geq m$ we obtain

$$\begin{aligned} P_{mn} =& |\langle m|e^{-|q|^2/2}e^{-iq^*a^\dagger}e^{-iqa}|n\rangle|^2 \\ =& m!n!e^{-|q|^2}|q|^{2(n-m)}\left|\sum_{j=0}^{m}\frac{(-1)^j|q|^{2j}}{j!(m-j)!(n-m+j)!}\right|^2, \end{aligned} \tag{3.22}$$

which is exactly the Franck-Condon distribution of a harmonic oscillator. We could have anticipated this directly from the expression (3.21), since one can introduce a phase space rotation by defining

$$\tilde{a} = \frac{iq}{|q|}a, \qquad [\tilde{a}^\dagger, \tilde{a}] = 1, \tag{3.23}$$

and the corresponding canonical momentum and position operators $\tilde{p}$ and $\tilde{x}$. The time evolution operator can then be written as a translation operator $U = e^{-|q|(\tilde{a}-\tilde{a}^\dagger)} = e^{-i|q|\sqrt{2/\hbar\omega_0 m}\tilde{p}}$, which yields the usual definition of Franck-Condon matrix elements of a harmonic oscillator displaced by $\Delta\tilde{x} = \sqrt{2}|q|x_Q$, where $x_Q = \sqrt{\hbar/m\omega_0}$ is the quantum length of the oscillator.

To make contact to the physics involved in a hot electron scattering event, we will consider the amount of energy transferred after the hot electron has decayed and left the oscillator corresponding to $t \to \infty$. We impose the wide band limit (3.8) and get

$$|q|^2 = \frac{\lambda^2}{(\hbar\omega_0)^2 + \Gamma^2}, \tag{3.24}$$

corresponding to the Franck-Condon displacement $\Delta\tilde{x} = \Delta x/\sqrt{1 + (1/\tau\omega_0)^2}$. The transition matrix elements (3.22) are thus not determined by the overlaps between vibrational states of the ground and excited state potentials $V_0(x)$ and $V_1(x)$. Rather, it is determined by the overlaps between the ground state potential and a certain "ghost" potential, which is equal to the excited state potential with a lifetime dependent renormalization of the displacement. This is illustrated in Fig. 3.1.

If the initial state is the ground state, the distribution of transition probabilities is a Poisson distribution and the average energy transferred is

$$\Delta E = \hbar\omega_0 e^{-|q|^2}\sum_{n=0}^{\infty} n\frac{|q|^{2n}}{n!} = \hbar\omega_0|q|^2, \tag{3.25}$$

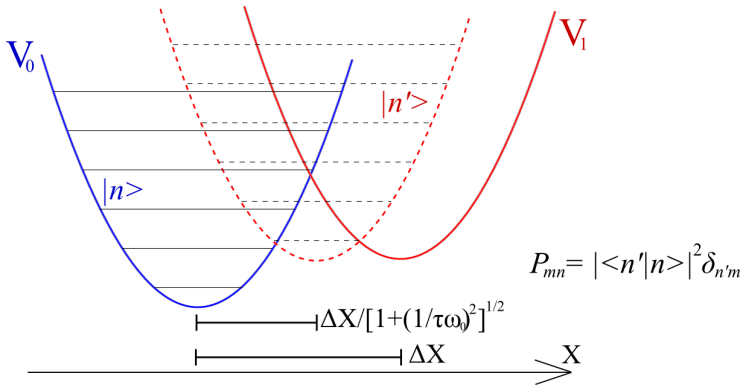

Figure 3.1: Ground and excited state potentials V_0 and V_1 of the displaced harmonic oscillator model. A hot electron is initially ($t = 0$) placed in the excited state potential and decays exponentially to the ground state. The total potential is thus $V(t) = V_1(x)e^{-t/\tau} + (1 - e^{-t/\tau})V_0(x)$. For $t \to \infty$ the probabilities of having made a vibrational transition $m \to n$ is determined by the overlaps of eigenstates of $V_0(x)$ and eigenstates of a "ghost" potential shown by the dashed line. The ghost potential is also a harmonic oscillator with a displacement depending on the spectral properties of the electronic resonance. In this figure the displacement is indicated for the wide band limit.

which is exactly the same as the classical result (3.15). This correspondence between classical and quantum mechanical results, are a special property of the harmonic oscillator and we derive a similar result when considering the density matrix below.

In the present approach, the initial assumption is that a hot metallic electron has made it to the electronic resonance, where it perturbs the adsorbate described by a harmonic oscillator, and thereby mediates energy transfer before it decays back into the metal. It is also assumed that the transition to the excited state is vertical corresponding to an infinitely fast coupling time. The initial transition to the excited electronic state, will depend on the energy of the incoming hot electron and one could include this by multiplying the transition probability (3.22) by an initial scattering factor, which one would expect to be proportional to the resonant spectral function at the energy of the incoming electron. However, we will not go into details with this, since a thorough analy-

sis of scattering using the Hamiltonian (3.9), gives rise to an intricate entangling between oscillator states and electronic states that the forced oscillator model does not capture.

3.4 Inelastic Scattering by Hot Electrons

To include the hot electron energies in the energy transfer, we need to consider the complete process as an inelastic scattering event [33]. It is then assumed that the adsorbate is unoccupied in the distant past and distant future. Furthermore, an incoming hot electron with initial energy ε_i is present in the metal in the distant past and a final state hot electron with energy ε_f is present in the metal the distant future. The differential probability that the initial hot electron with energy ε_i scatters on an adsorbate in the vibrational state n_i and transfers energy $\varepsilon_i - \varepsilon_f$ can then be written [107]

$$R_{n_i}(\varepsilon_f, \varepsilon_i) = \delta(\varepsilon_f - \varepsilon_i)[1+2\Gamma(\varepsilon_i)\mathrm{Im}G_R(n_i;\varepsilon_i)] + \Gamma(\varepsilon_f)\Gamma(\varepsilon_i)G(n_i;\varepsilon_f,\varepsilon_i), \tag{3.26}$$

where the Green functions are defined by

$$G_R(n_i;\varepsilon) = \int \frac{dt}{\hbar} e^{i\varepsilon t/\hbar}[-i\theta(t)\langle n_i|c_a(t)c_a^\dagger|n_i\rangle], \tag{3.27}$$

$$G(n_i;\varepsilon_1,\varepsilon_2) = \int \frac{d\tau ds dt}{2\pi\hbar^3} e^{i[(\varepsilon_i-\varepsilon_f)\tau+\varepsilon_f t-\varepsilon_i s]/\hbar} \times \theta(t)\theta(s)\langle n_i|c_a(\tau-s)c_a^\dagger(\tau)c_a(t)c_a^\dagger|n_i\rangle. \tag{3.28}$$

The first term of the scattering function (3.26) is thus purely elastic and the second term contains inelastic as well as elastic contributions as we shall see. The Green functions (3.27)-(3.28) are complicated objects, which are usually calculated perturbatively. However, reactions mediated by single hot electrons typically involve a large energy transfer, which cannot be handled by perturbation theory and one has to rely on model potentials where exact results for the Green functions can be obtained.

In this section, we will restrict ourselves to a one-dimensional harmonic potential, where the Green functions can be obtained exactly in the wide band limit and assume that the oscillator is initially in the ground state. The probability of a hot electron inducing the oscillator transition $0 \to n$ is then obtained by integrating $R_0(\varepsilon_f;\varepsilon_i)$ over final state energies matching the final state vibrational energy. In appendix B it is shown how to evaluate the Green functions

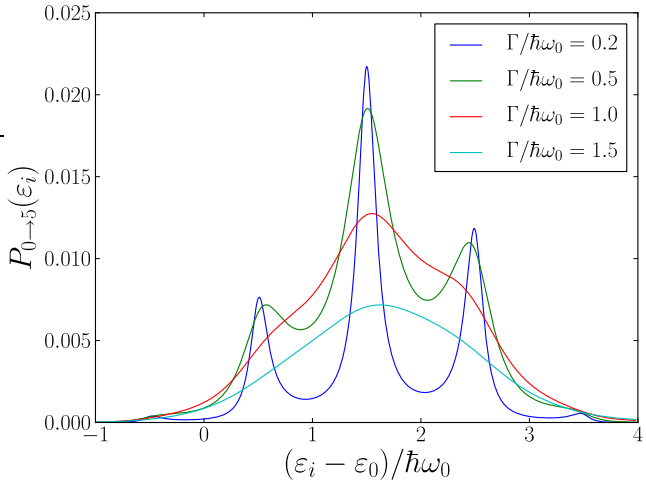

Figure 3.2: The vibrational transition probability $P_{0\to5}$ (3.29) as a function of hot electron energy ε_i calculated in the wide band limit with $g = 0.5$ at four different values of Γ. When $\Gamma < \hbar\omega_0$, one clearly sees the emergence of resonant "sidebands" separated by $\hbar\omega_0$. It is also seen that the probability distributions are centered above the resonant energy.

and the result for $n > 0$ is

$$P_{0\to n}(\varepsilon_i) = \Gamma^2 e^{-2g}\frac{g^n}{n!}\left|\sum_{j=0}^{n}(-1)^j\binom{n}{j}\sum_{k=0}^{\infty}\frac{g^k}{k!}\left(\frac{1}{\varepsilon_i - \varepsilon_0 - (j+k-g)\hbar\omega_0 + i\Gamma/2}\right)\right|^2, \tag{3.29}$$

where $g = \lambda^2/(\hbar\omega)^2$ and we used Eq. (B.19). This distribution is shown in Fig. 3.2 for the transition $n = 0 \to n = 5$ at four different values of Γ. The most significant feature is the vibrational sidebands, which are resolved when $\Gamma < \hbar\omega_0$. Each of the sidebands have width $\sim \Gamma$, are separated by $\hbar\omega_0$, and reflects that the resonant state is coupled to an oscillator of frequency ω_0. Another striking feature of the probability distributions is that they are not centered at ε_0. This can be understood as a trade off between the incoming hot electron (energy ε_i) and the inelastic scattered electron (energy $\varepsilon_i - n\hbar\omega_0$) both wanting to be close to the electronic resonance at ε_0. In general the probability distributions $P_{0\to n}(\varepsilon_i)$ are approximately centered at $\varepsilon_0 + (n/2 - g)\hbar\omega_0$. This trade off

is not present in the forced oscillator model, where the maximum probability is always centered at $\varepsilon_i = \varepsilon_0$.

There is essentially two coupling constants determining the magnitude of the transition probabilities: the coupling between the resonant state and metallic states Γ and the coupling of the resonant electron to the adsorbate vibrational states λ. In the forced oscillator model, these two constants are combined into a single coupling parameter $|q|^2$ (3.24) reflecting the average approach to the problem, whereas the coupling constants appear independently in Eq. (3.29). The transition probabilities obtained with either approach scale as $\lambda^{2n}/n!$, but the dependence on Γ is very different. This is illustrated in Fig. 3.3 where we compare the probability as a function of Γ for the transition $n = 0 \rightarrow n = 5$ using the two methods. In the forced oscillator model the initial assumption is that a hot electron has made it to the resonant state and for comparison we consider the inelastic scattering probability (3.29) with $\varepsilon_i = \varepsilon_0$. The inelastic scattering probability has a maximum at $\Gamma \sim \hbar\omega_0$ and goes to zero for $\Gamma \rightarrow 0$ and $\Gamma \rightarrow \infty$ corresponding to vanishing metal-resonance coupling and vanishing lifetime respectively. In contrast, the forced oscillator probability is a monotonously decreasing function of Γ since the model does not take into account that the coupling to metallic electrons vanish for $\Gamma \rightarrow 0$.

We will return to the inelastic scattering model in chapter 4 where we will discuss various flavors and applications of the model.

3.5 The Reduced Density Matrix

The density matrix can be used to derive equations of motion for adsorbates interacting with an environment of hot electrons. Typically, the density matrix is used to represent an ensemble of quantum mechanical states:

$$\rho_0 = \sum_i p_i |\alpha_i\rangle\langle\alpha_i|, \tag{3.30}$$

where p_i is the statistical probability of finding the state $|\alpha_i\rangle$. A well known example is the thermal ensemble where p_i can be written as Boltzmann factors e^{-E_i/k_BT} if $|\alpha_i\rangle$ are eigenstates of the Hamiltonian of the system under consideration. The density matrix then becomes a useful tool, which allows one to include temperature effects in calculations of quantum mechanical expectation values. However, for the present problem involving hot electrons interacting with an adsorbate, the power of the density matrix formalism lies in the ability

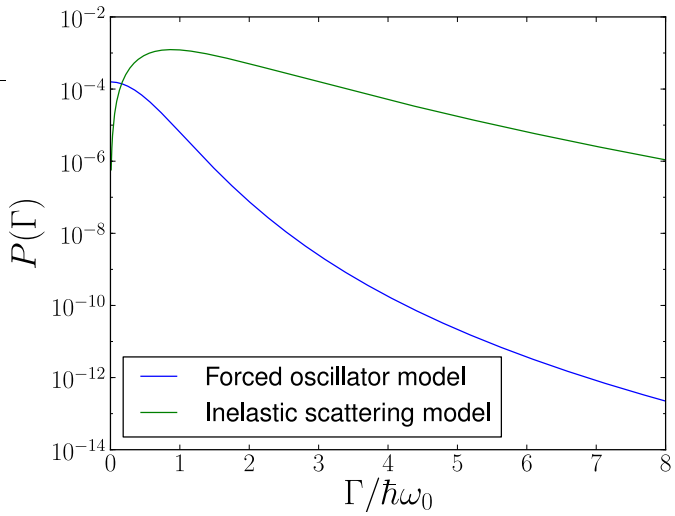

Figure 3.3: Comparison of the probability of the transition $n = 0 \rightarrow n = 5$ calculated in the wide band limit using the forced oscillator model and the inelastic scattering model with $\varepsilon_i = \varepsilon_0$ and $g = 0.5$.

to isolate the adsorbate degrees of freedom and treat the electronic degrees of freedom in terms of an effective adsorbate potential.

Consider the Hamiltonian (3.9), which is written

$$H = H_0 + H_{el} + H_I, \tag{3.31}$$

where H_0 is the adsorbate Hamiltonian (3.10), H_{el} is the pure electronic part of H given by (3.1) and H_I contains all interaction terms. If we are only interested in the state of the adsorbate regardless of the state of the electronic system, we can trace out all electronic degrees of freedom and obtain the reduced density matrix

$$\rho_{red} = \mathrm{Tr}_{el}[\rho]. \tag{3.32}$$

This operator then only acts on adsorbate states and the probability of finding the adsorbate in the state $|\alpha\rangle$ is simply given by $\langle\alpha|\rho_{red}|\alpha\rangle$. In general, however, the trace in Eq. (3.32) is a very complicated operation since the interaction term H_I entangles the adsorbate and electronic degrees of freedom.

In a time-dependent problem it is useful to analyze the time-dependent density matrix given by

$$\rho(t) = e^{-iHt/\hbar}\rho_0 e^{iHt/\hbar}, \tag{3.33}$$

and the diagonal elements give the time-dependent probabilities of being in a particular state. The equation of motion for the density matrix operator is

$$\dot{\rho} = -i[H, \rho]/\hbar, \tag{3.34}$$

where we assumed that ρ does not have any explicit time-dependence. This equation is sometimes referred to as the Liouville equation.

3.5.1 The adsorbate density matrix

As a warm up to the derivation of the Langevin equation, we consider the density matrix of an isolated adsorbate, described by the Hamiltonian H_0, in a coordinate basis. The diagonal elements of this function give the probabilities of finding the adsorbate at a particular position. We are thus led to consider the object

$$\rho(x, y; t) = \langle x|\rho(t)|y\rangle = \int dx_0 dy_0 \langle x_0|\rho_0|y_0\rangle \langle x|e^{-iH_0 t/\hbar}|x_0\rangle \langle y_0|e^{iH_0 t/\hbar}|y\rangle, \tag{3.35}$$

where two complete sets of states were inserted in the last equality. The last two matrix elements contain time evolution operators forward and backward in time and can be interpreted as propagators going from $x_0 \to x$ and $y \to y_0$ respectively. The dummy variable x_0 and y_0 can thus be regarded as initial points representing $t = 0$. It is well known that such propagators can be represented by path integrals: $\langle x|e^{-iH_0 t/\hbar}|x_0\rangle \to \int_{x_0}^{x} \mathcal{D}[x(t')] e^{iS_0[x(t')]/\hbar}$ [91], and with this substitution Eq. (3.35) becomes

$$\rho(x, y; t) = \int dx_0 dy_0 \langle x_0|\rho_0|y_0\rangle \int \mathcal{D}[x(t')]\mathcal{D}[y(t')] e^{iS_0[x(t')]/\hbar - iS_0[y(t')]/\hbar}, \tag{3.36}$$

where the action S_0 is given by

$$S_0[x(t')] = \int_0^t dt' \Big(\frac{1}{2} m\dot{x}^2(t') - V_0[x(t')]\Big), \tag{3.37}$$

and V_0 is the adsorbate potential. The action is thus a functional of the path $x(t')$ with boundary conditions $x(t'=0)=x_0$ and $x(t'=t)=x$ and the path integral $\int \mathcal{D}[x'(t)]$ in Eq. (3.36) means sum over all such paths.

We now introduce the average path $u(t')=x(t')/2+y(t')/2$ and the fluctuation $v(t')=x(t')-y(t')$. The sum of actions is expressed in terms of these variables by Taylor expanding the potentials in the fluctuation $v(t')$. Performing a partial integration on the kinetic terms then gives

$$S_0[x(t')]-S_0[y(t')]=m\dot{u}v\Big|_0^t-\int_0^t dt'\Big(m\ddot{u}v+V_0'(u)v+F(u,v)\Big), \qquad (3.38)$$

where

$$F(u,v)=2\sum_{n=1}^{\infty}\frac{(v/2)^{2n+1}}{(2n+1)!}V_0^{2n+1}(u), \qquad (3.39)$$

and $V_0^n(u)$ is the n'th derivative of the potential. Inserting this into Eq. (3.36), the density matrix becomes[4]

$$\rho(x,y;t)=\int dx_0dy_0\langle x_0|\rho_0|y_0\rangle\int\mathcal{D}[u(t')]e^{im(\dot{u}(t)v(t)-\dot{u}_0v_0)/\hbar}\int\mathcal{D}[v(t')]e^{i\widetilde{S}/\hbar},$$

with

$$\widetilde{S}[u(t'),v(t')]=-\int_0^t dt'\Big(m\ddot{u}(t')+V'(u)\Big)v(t')-\int_0^t dt'F(u(t'),v(t')),$$

and $x=u(t)+v(t)/2$, $y=u(t)-v(t)/2$.

Harmonic potential

For a harmonic potential $F(u,v)$ vanishes and $V'(u)=m\omega_0^2u$. It is then straightforward to perform the path integral in $v(t')$ and the result is a delta functional on the classical path $\ddot{u}(t')=-\omega_0^2u(t')$ for the average coordinate. If we are only interested in the probabilities of finding the particle at a given position we just need the diagonal elements of the density matrix where the end

[4]Note that v_0 and $v(t)$ represent the end points of the path and can be pulled out of the $v(t')$ path integral. However, $\dot{u}_0$ and $\dot{u}(t)$ are the derivatives at the end points and depend on a given path $u(t')$.

points satisfy $u(t) = x(t) = y(t)$ and $v(t) = 0$. In terms of these coordinates the diagonal part of the density matrix is

$$\rho_{HO}(u;t) \propto \int du_0 dv_0 \langle u_0 + v_0/2|\rho_0|u_0 - v_0/2\rangle \int \mathcal{D}[u(t')] e^{-im\dot{u}_0 v_0/\hbar} \delta(\ddot{u} + \omega_0^2 u)$$
$$\propto \int du_0 \mathcal{P}(u_0, p_0(u_0, u(t))), \tag{3.40}$$

where

$$\mathcal{P}(x,p) = \frac{1}{2\pi\hbar} \int dy \langle x + y/2|\rho_0|x - y/2\rangle e^{-ipy/\hbar}, \tag{3.41}$$

is the Wigner distribution of an initial state described by the density matrix ρ_0 and the path integral delta function has been collapsed by noting that for a given u_0 there is a unique initial momentum p_0 defined by

$$p_0 \equiv m\dot{u}_0 = \frac{m\omega_0}{\sin\omega_0 t}(u(t) - u_0 \cos\omega_0 t), \tag{3.42}$$

that connects the initial position classically with $u(t)$. The easiest way to determine the normalization is to require that $\int du \rho(u;t) = 1$ and using that $\int du_0 dp_0 \mathcal{P}(u_0, p_0) = 1$ we can finally write

$$\rho_{HO}(u;t) = \int du_0 dp_0 \mathcal{P}(u_0, p_0) \delta\Big(u(t) - [u_0 \cos\omega_0 t + p_0 \frac{\sin\omega_0 t}{m\omega_0}]\Big). \tag{3.43}$$

This result also follows directly by inserting a well known expression for the harmonic oscillator propagator [91] into Eq. (3.35), but the present derivation is much better suited for a generalization to adsorbates interacting with hot electrons.

The Wigner distribution $\mathcal{P}(x,p)$ is often referred to as a quasi-probability distribution and it is the closest one can get to defining a simultaneous differential probability distribution of finding a particle at position x with momentum p [48]. In particular it satisfies $\int dp \mathcal{P}(x,p) = \langle x|\rho_0|x\rangle$ and $\int dx \mathcal{P}(x,p) = \langle p|\rho_0|p\rangle$, which are the probability distributions for position and momentum respectively. We can thus interpret the probability of finding a particle at position $u(t)$ given by Eq. (3.43), as a sum over all initial phase space configurations, which classically connect u_0 with $u(t)$, weighted by the (quasi-)probability distribution of finding a given initial phase space point. The time evolution of the harmonic oscillator is thus purely classical and quantum effects only enter through the initial state described by ρ_0. This is a well known fact and it can be shown that

for a harmonic oscillator, the time evolution of the Wigner distribution itself is identical to the time evolution of a classical phase space distribution [48].

For anharmonic potentials, $F(u,v)$ Eq. (3.39) does not vanish and the time evolution is not classical. However, if large fluctuation paths $v(t')$ do not contribute to the path integral, we can neglect this term since it is of order v^3. The result is then again a delta function on the classical path satisfying $m\ddot{u} = -V'(u)$ and we will refer to this as the semiclassical approximation. In principle the condition for neglecting higher than first order terms in $v(t')$ has to be justified for a given set of parameters, but very often classical dynamics can be justified by other means than by analyzing the path integral.

3.5.2 Langevin equation

To obtain the time evolution of an adsorbate interacting with hot electrons, we turn to the reduced density matrix (3.32) and the Hamiltonian (3.9). An expression for the reduced density matrix in one dimension has been derived by Brandbyge et al. [7] who used a method based on influence functionals [29, 13, 93] to transform the electronic trace into an effective action. We refer to appendix B, which introduces the basic concepts of influence functionals. The effective action can then be expanded in powers of the coupling functions $\varepsilon_a(x)$ and $V_{ak}(x)$ and to second order the result for the diagonal part is

$$\rho_{red}(u;t) = \int du_0 dp_0 \mathcal{P}(u_0,p_0) \int \mathcal{D}[u(t')]\mathcal{D}[v(t')] \tag{3.44}$$
$$\times \exp\Big(-\frac{i}{\hbar}\int_0^t dt' \xi(t')v(t')/\hbar - \frac{1}{2\hbar^2}\int_0^t dt'dt'' v(t')K(t'-t'')v(t'')\Big),$$

where $u(t')$ have the additional constraint that $\dot{u}_0 = p_0/m$, $\mathcal{P}(x_0,p_0)$ is the Wigner distribution of the initial adsorbate density matrix ρ_0, and we have defined

$$\xi(t) = M\ddot{u}(t) + V'(u) + \int_0^t dt' \eta(t-t')\dot{u}(t'). \tag{3.45}$$

The dynamical friction $\eta(t)$ and the correlation function $K(t)$ are given by

$$\eta(t) = \int_{-\infty}^{\infty} \frac{d\omega}{2\pi}\Lambda(\omega)\cos(\omega t), \tag{3.46}$$

$$K(t) = \frac{\hbar}{2}\int_{-\infty}^{\infty} \frac{d\omega}{2\pi}\omega\Lambda(\omega)\coth\Big(\frac{\hbar\omega}{2k_BT_{el}}\Big)\cos(\omega t), \tag{3.47}$$

where we have defined the energy loss function

$$\Lambda(\omega) = \frac{\hbar}{\omega}\int_{-\infty}^{\infty}\frac{d\omega_1}{2\pi}\int_{-\infty}^{\infty}d\omega_2 G(\omega_1,\omega_2)\delta\Big(\omega-(\omega_2-\omega_1)\Big)\Big(n_F(\omega_1)-n_F(\omega_2)\Big), \tag{3.48}$$

and the weighted electron-hole pair density of states

$$G(u;\omega_1,\omega_2) = \sum_{q_1,q_2,q_3,q_4} A_{q_1q_2}(u;\omega_1)V'_{q_2q_3}(u)A_{q_3q_4}(u;\omega_2)V'_{q_4q_1}(u). \tag{3.49}$$

$A_{qq'}(u)$ is the spectral function of the electronic states $|q\rangle$ and $|q'\rangle$ with the electronic Hamiltonian evaluated at u and $V'_{qq'}(u)$ are the derivatives of the coupling functions $\langle q|H|q'\rangle$ evaluated at u. The expression is independent of the electronic basis and the q state could represent the Newns-Anderson basis $\{a,k\}$ or an eigenstate basis $\{n\}$. Both the friction and fluctuating force depends on the electronic temperature T_{el} through the Fermi distribution $n_F(\omega;T_{el})$.

We can interpret the expression (3.48) as an amplitude for the adsorbate to loose an amount of energy ω. The integration variables ω_1 and ω_2 then represent electron and hole energies respectively and the origin of the energy loss is an electron-hole excitation with energy conservation ensured by the delta function. The thermal occupation of holes and electrons is taken into account by the last factor, which kills the integrand unless ω_2 is above the Fermi level and ω_1 is below the Fermi level or vice versa.[5]

In addition to a second order expansion of the effective action, the reduced density matrix (3.44) is derived in the semiclassical approximation where the fluctuation path $v(t')$ is assumed small and this is the origin of derivatives and position dependence in Eq. (3.49). The semiclassical approximation was also used to arrive at the $V'(u)$ term in (3.45) and we expect the derivation of the friction and correlation function to hold, if the non-interacting molecular dynamics are well approximated by a classical equation of motion. For non-interacting dynamics we showed that the semiclassical approximation is exact for quadratic potentials (3.38)-(3.39). The analog for the interacting case is quadratic potentials and linear coupling functions: $V_{ak}(x) = V^0_{ak} + V'_{ak}x$ and $\varepsilon_a(x) = \varepsilon_0 - fx$.

Without the quadratic term $v(t')K(t'-t'')v(t')$ in the reduced density matrix (3.44), the path integral in $v(t')$ would result in a delta functional in $\xi(t)$ and the dynamics would be governed by a classical equation of motion with dynamical

[5]Note that $\Lambda(-\omega) = \Lambda(\omega)$.

friction function $\eta(t)$ (Eq. (3.45) with $\xi(t) = 0$). It is instructive to think of the last term in the exponential of (3.44), as giving rise to a Gaussian broadening of the classical path. To see this explicitly we "complete" the square in the exponential and perform the path integral in $v(t')$, which give

$$\rho_{red}(u;t) \propto \int du_0 dp_0 \mathcal{P}(u_0,p_0) \int \mathcal{D}[u(t')] e^{-\frac{1}{2}\int_0^t dt'dt''\xi(t')K^{-1}(t'-t'')\xi(t'')}, \tag{3.50}$$

where K^{-1} solves

$$\int_0^t dt'' K^{-1}(t'-t'')K(t''-t''') = \delta(t'-t'''). \tag{3.51}$$

The exponential in (3.50) can be interpreted as the probability density of taking the path $u(t')$ given the endpoints u_0 and $u(t)$ and the initial velocity $\dot{u}_0 = p_0/m$. It has a maximum at $\xi(t) = 0$ corresponding to the classical path and a broadening given by K^{-1}. However, it will be more convenient to consider the probability density of $\xi(t)$, which obviously has dimensions of a force. It is then necessary to change the path integral measure from $\mathcal{D}[u(t')]$ to $\mathcal{D}[\xi(t')]$ and it can be shown that the Jacobian of this transformation is independent of $u(t')$ [93]. The two-point correlation function of $\xi(t)$ can then be calculated by

$$\begin{aligned}
\langle \xi(t_1)\xi(t_2)\rangle &= \frac{\int \mathcal{D}[\xi(t')]\xi(t_1)\xi(t_2)e^{-\frac{1}{2}\int_0^t dt'dt''\xi(t')K^{-1}(t'-t'')\xi(t'')}}{\int \mathcal{D}[\xi(t')]e^{-\frac{1}{2}\int_0^t dt'dt''\xi(t')K^{-1}(t'-t'')\xi(t'')}} \\
&= \frac{\frac{\delta^2}{\delta J(t_1)\delta J(t_2)}\int \mathcal{D}[\xi(t')]e^{-\frac{1}{2}\int_0^t dt'dt''\xi(t')K^{-1}(t'-t'')\xi(t'')-\int_0^t dt' J(t')\xi(t')}\Big|_{J=0}}{\int \mathcal{D}[\xi(t')]e^{-\frac{1}{2}\int_0^t dt'dt''\xi(t')K^{-1}(t'-t'')\xi(t'')}} \\
&= \frac{\delta^2}{\delta J(t_1)\delta J(t_2)} e^{\frac{1}{2}\int_0^t dt'dt'' J(t')K(t'-t'')J(t'')}\Big|_{J=0} = K(t_1-t_2).
\end{aligned} \tag{3.52}$$

and it is straightforward to show that $\langle \xi(t)\rangle = 0$. This is the most compact way of specifying the statistical properties of $\xi(t)$ and Eq. (3.45) can be regarded as a classical equation motion for the adsorbate with a stochastic Gaussian distributed force $\xi(t)$.

Equation (3.45) is referred to as a Langevin equation. The interaction with a reservoir of metallic electrons is included in a frictional term $\eta\dot{x}$, which gives rise to dissipation and a random force ξ, which gives rise to fluctuations. Due

to the random force, the Langevin equation is not deterministic and one has to average a large number of trajectories to obtain physical properties. Sampling the stochastic force along an adsorbate trajectory is complicated by the fact that the correlation function contains memory and the stochastic force at a given time depends on a sampled set of stochastic forces at all previous times. However, when the electronic temperature becomes large, thermal fluctuations tend to destroy the memory and the fluctuations thus become local in time. More precisely, if Δt is a typical time scale of adsorbate motion and $k_B T_{el} \gg \hbar/\Delta t$, then we can approximate the equations (3.46)-(3.47) by

$$K(t) = 2k_B T_{el}\eta_0\delta(t), \qquad \eta(t) = 2\eta_0\delta(t), \tag{3.53}$$

with the static friction $\eta_0 = \Lambda(0)/2$. This is the so-called Markov approximation and we will investigate its consequences and range of validity in chapter 5. The Markov approximation only involves $\Lambda(0)$ and thus only includes infinitesimal electron-hole pair excitations in the (thermal) vicinity of the Fermi Level

In appendix A, we derive a model independent expression for the friction, which is expressed in terms of the electronic linear density response function. It is then straightforward to obtain an *ab initio* DFT based friction by using the non-interacting Kohn-Sham response function and one does not have to worry about the nature of the adsorbate excited state described by $\Gamma(\varepsilon)$ and ε_0. However, the derivation rests on an *a priori* assumption of classical trajectories, which is not required by the formalism based on the density matrix. Indeed, the Langevin equation (3.45) has been shown to be quantum mechanically exact in the case of a harmonic oscillator and for anharmonic potentials it gives an explicit method for performing semiclassical dynamics with proper inclusion of initial quantum states. Another advantage of the density matrix formalism is that an explicit expression is obtained for the correlation of fluctuating forces, whereas one has to add this by hand in a DFT based formalism.

Linear coupling

As a special case, we state the friction in the Markov approximation with linear coupling in the diagonal term: $\varepsilon_a(a) = \varepsilon_0 - fx$ and no coupling in the off-diagonal terms: $V_{ak}(x) = V_{ak}$. The weighted electron-hole pair density (3.49) of states then becomes independent of position: $G(\omega_1, \omega_2) = 4\pi^2\rho_a(\omega_1)\rho_a(\omega_2)$, and in the wide band limit the friction becomes

$$\eta_0 = \frac{\hbar f^2}{\pi}\int_{-\infty}^{\infty} d\varepsilon \left(\frac{\Gamma/2}{(\varepsilon-\varepsilon_0)^2 + (\Gamma/2)^2}\right)^2 \left(-\frac{dn_F(T_{el};\varepsilon)}{d\varepsilon}\right). \tag{3.54}$$

Thus, the friction is given by the convolution of the projected density of states squared with the derivative of the Fermi distribution, and its magnitude is determined by four parameters. The coupling parameter f, the electronic temperature T_{el}, the resonance position ε_0, and the resonance width Γ. At $T_{el} = 0$ the derivative of the Fermi distribution becomes a delta function and the friction is essentially given by the projected density of states squared evaluated at the Fermi level.

3.5.3 Master equation

If one is interested in the time-dependent probability for the adsorbate to be in a particular energy eigenstate rather than at a certain position, it is more convenient to consider the reduced density matrix in a basis of Hamiltonian eigenstates. For this purpose it is easier to start with the equation of motion for $\rho(t)$ (3.34), rather than using the explicit time-dependence Eq. (3.33) as we did in the path integral approach leading to the Langevin equation. Taking the electronic trace of the Liouville equation (3.34) leads to

$$\frac{d\rho_{red}}{dt} + \frac{i}{\hbar}[H_0, \rho_{red}] = \frac{-i}{\hbar}\mathrm{Tr}_{el}[H_I, \rho], \tag{3.55}$$

where $\rho_{red} = \mathrm{Tr}_{el}[\rho]$ is the reduced density matrix and we used that $\mathrm{Tr}_{el}[H_{el}\rho] = \mathrm{Tr}_{el}[\rho H_{el}]$. In a basis of eigenstates of H_0, the diagonal elements of the reduced density matrix are the time-dependent probabilities of finding the adsorbate in a particular state. The right hand side is a complicated functional, which depends on the complete history of the density matrix. However, making the self-consistent Born approximation and neglecting the off-diagonal elements of ρ_{red}, lead to the master equation [39]

$$\frac{dp_n}{dt} = \sum_{m=0}^{\infty}\Big(p_m W_{m\to n} - p_n W_{n\to m}\Big), \tag{3.56}$$

where $p_n = (\rho_{red})_{nn}(t)$ and $W_{m\to n}$ are the transition rates given by

$$W_{m\to n} = \frac{2\pi}{\hbar}\sum_{q_1,q_2} n_F(\varepsilon_{q_1})\big(1 - n_F(\varepsilon_{q_2})\big)|\langle q_1; m|H_I|q_2; n\rangle|^2\delta(\varepsilon_{q_1} - \varepsilon_{q_2} + \varepsilon_n - \varepsilon_m), \tag{3.57}$$

where $|q\rangle$ are the eigenstates of H_{el} with eigenenergies ε_q and $n_F(\varepsilon)$ is the Fermi-Dirac distribution.

The master equation Eq. 3.56 has been derived directly from Eq. (3.55) [39], but the result also follows from a straightforward hand-waving argument. The rate of change of the population in a state $|n\rangle$ is given by the rate of increase: $\sum_m p_m W_{m\to n}$ minus the rate of decrease: $p_n \sum_m W_{n\to m}$ and the expression for the transition rates (3.57) is simply Fermi's golden rule.

In the case of linear coupling on the diagonal only, we have $H_I = -fxc_a^\dagger c_a$ and using that $\langle q;m|H_I|q';n\rangle = -fx_{mn}\langle q|a\rangle\langle a|q'\rangle$, the transition rate (3.57) can be written,

$$\begin{aligned} W_{m\to n} &= \frac{2\pi}{\hbar}\sum_{q_1,q_2} n_F(\varepsilon_{q_1})\big(1-n_F(\varepsilon_{q_2})\big)|\langle q_1;m|H_I|q_2;n\rangle|^2\delta(\varepsilon_{q_1}-\varepsilon_{q_2}+\varepsilon_n-\varepsilon_m) \\ &= \frac{2\pi f^2|x_{mn}|^2}{\hbar}\sum_{q_1,q_2}\int d\varepsilon_1 d\varepsilon_2 n_F(\varepsilon_1)\big(1-n_F(\varepsilon_2)\big)|\langle q_1|a\rangle|^2|\langle q_2|a\rangle|^2 \\ &\qquad\qquad \times\delta(\varepsilon_1-\varepsilon_{q_1})\delta(\varepsilon_2-\varepsilon_{q_2})\delta(\varepsilon_1-\varepsilon_2+\varepsilon_n-\varepsilon_m) \\ &= \frac{2\pi f^2|x_{mn}|^2}{\hbar}\int d\varepsilon n_F(\varepsilon)\big(1-n_F(\varepsilon-\varepsilon_{nm})\big)\rho_a(\varepsilon)\rho_a(\varepsilon-\varepsilon_{nm}), \quad (3.58) \end{aligned}$$

where $\varepsilon_{nm} = \varepsilon_n - \varepsilon_m$ and $\rho_a(\varepsilon)$ is the projected density of states. The integrand thus gives the amplitude for having an electron at ε weighted by $\rho_a(\varepsilon)$ and a hole at $\varepsilon - \varepsilon_{nm}$ weighted by $\rho_a(\varepsilon - \varepsilon_{mn})$, which corresponds to the electronic transition associated with the adsorbate transition $m \to n$.

Harmonic potential

The Fermi golden rule expression relies on first order perturbation theory, but can be generalized to arbitrary order by introduction of the so-called T-matrix.[6] In general, it is very tedious work to obtain higher order corrections, but an exception is the harmonic oscillator with linear coupling where the T-matrix can be evaluated exactly. The result is [39]

$$W^{full}_{m\to n} = \frac{\Gamma^2}{\pi\hbar}\int d\varepsilon n_F(\varepsilon)\big(1-n_F(\varepsilon-\varepsilon_{nm})\big)\left|\sum_{k=0}^{\infty}\frac{\langle m|\tilde{k}\rangle\langle\tilde{k}|n\rangle}{\varepsilon-\varepsilon_0+(m-k+g)\hbar\omega_0+i\Gamma/2}\right|^2, \quad (3.59)$$

[6] The matrix element in Eq. (3.57) is substituted by $|\langle q_1;m|H_I|q_2;n\rangle|^2 \to |\langle q_1;m|T|q_2;n\rangle|^2$, where the T-matrix is given by the Dyson type equation [8]

$$T = H_I + H_I\frac{1}{E_{m,q_1}-H_0-H_{el}+i0^+}T,$$

and the golden rule is recovered as the lowest order expansion of the T-matrix.

where $|\tilde{k}\rangle$ are the eigenstates of a harmonic oscillator displaced by $-fx$.

It is interesting to note the appearance of the Franck-Condon overlaps $\langle m|\tilde{k}\rangle$, which we also encountered in the forced oscillator model (3.22). The expressions describe different situations though. In the forced oscillator model we considered the probability that a single electron would induce a transition $m \to n$, whereas the expression (3.59) is the rate of transitions under the influence of a reservoir of hot electrons described by T_{el}. Furthermore, the forced oscillator transition probability (3.22) was given by $|\langle m|n'\rangle|^2$ where $|n'\rangle$ was a vibrational state of the "ghost potential" shown in Fig. 3.1 The simplicity of the model thus resulted in the amplitudes for transitions being determined by the shift of the "ghost" potential only and the shift was a function of f and Γ. In contrast, the Franck-Condon overlaps appearing in (3.59) are the overlaps between the ground and "true" excited state potentials shown in Fig. 3.1. The magnitude of these overlaps are only determined by f, and the width Γ enters as an independent parameter in (3.59).

Chapter 4

Inelastic Scattering

In this chapter, we discuss various aspects of inelastic scattering as a model for hot electron assisted reactions at surfaces. We start by considering a harmonic oscillator, where exact results can be obtained in the wide band limit. First, we study a linear non-adiabatic coupling term, which typically dominates the energy transfer and corresponds to the generic model of a shifted excited state potential. However, in cases where symmetry does not permit linear coupling, a quadratic coupling term may govern the energy transfer and we will examine the consequences of quadratic coupling and discuss the relevance for certain adsorbate vibrational modes. We then apply perturbation theory to calculate inelastic scattering probabilities in a Morse potential and show how to obtain hot electron induced velocity distributions of desorbed atoms and molecules. In section 4.3, we construct a simple model for multiple inelastic scattering events in a harmonic potential, and show that the reaction yield exhibits a power law dependence on the flux of hot electrons. Finally, we turn to the seemingly very different problem of inelastic electron transport through a molecular contact and show that the fundamental aspects can be described by a process similar to hot electron mediated energy transfer.

Applications of the different models will be illustrated by examples of diatomic molecules adsorbed on specific transition metal surfaces, where the model parameters have been obtained using DFT and ΔSCF.

4.1 Quadratic Potentials

As a generic example of hot electron mediated energy transfer to adsorbates, we consider CO on various transition metals. CO typically adsorbs with the molecular axis perpendicular to the surface and the C atom closest to the surface. We will assume that the problem can be described by the Hamiltonian Eqs. (3.9)-(3.10) and to proceed systematically we would need to calculate the 6-dimensional[1] ground and excited state potentials $V_0(x)$ and $V_1(x)$. CO has an electronic structure similar to that of N_2 (Fig. 2.2) and we will assume that the coupling to hot electrons is mediated by an unoccupied 2π orbital. Thus, it is possible to use DFT and ΔSCF to map out the potential energy surfaces and we would then have complete knowledge of the problem within the Hamiltonian Eqs. (3.9)-(3.10).

However, we do not have the tools to calculate the inelastic scattering probabilities with general potentials $V_0(x)$ and $V_1(x)$. Rather, the model Eq. (3.26) involves the Green functions Eq. (3.27) and Eq. (3.28), which can be evaluated exactly for quadratic ground state potentials and linear or quadratic coupling only. It is of course possible to calculate the Green functions perturbatively within an arbitrary potential, but reactions mediated by a single hot electron typically involves very large energy transfer where perturbation theory breaks down.

4.1.1 Linear coupling

In Fig. 4.1 we show a two-dimensional cut of the potential energy surfaces for CO on Pt(111) the CO molecule is adsorbed on a top site with the molecular axis perpendicular to the surface. The desorption energy is $E_D \sim 1.4\ eV$ and this is the minimum amount of energy a hot electron should transfer to the CO molecule in order to induce a desorption event. A model with quadratic ground state and linear coupling is simply obtained by Taylor expanding the ground state potential to second order and the excited state potential to first order in

[1] One could also include the coordinates of the nearest metal atoms, which would add dimensions to the potential energy surfaces. However, due to the large difference in mass between typical transition metal atoms and CO we will neglect the metallic coordinate degrees of freedom in the following.

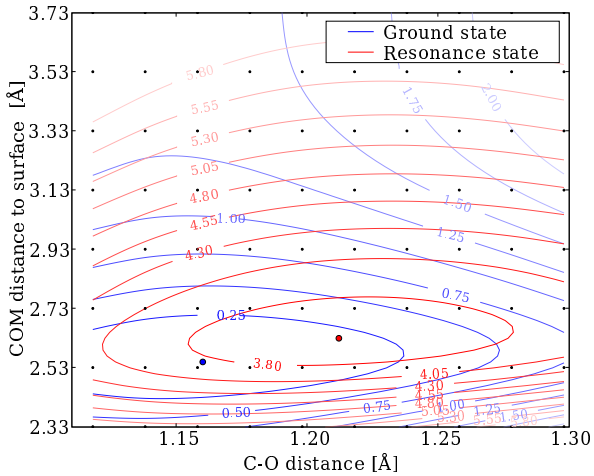

Figure 4.1: Potential energy surface for CO adsorbed on Pt(111). We have used the center of mass (COM) and internal stretch coordinates, which are the only coordinates with a linear coupling to the resonance. The blue dot is the ground state minimum and the vertical distance to the excited state potential is $\varepsilon_0 = 3.9\ eV$, which represents the distance from the Fermi level to the center of the resonance.

the vicinity of the ground state minimum x_i^0. Thus

$$H = H_0 + H_{NA} + H_I \tag{4.1}$$

$$H_0 = \sum_i \left(\frac{p_i^2}{2m_i} + \frac{1}{2} k_i x_i^2 \right), \qquad k_i = \left. \frac{\partial^2 V_0}{\partial x_i^2} \right|_{x_i = x_i^0}, \tag{4.2}$$

$$H_I = -c_a^\dagger c_a \sum_i f_i x_i, \qquad f_i = -\left. \frac{\partial V_1}{\partial x_i} \right|_{x_i = x_i^0}, \tag{4.3}$$

where H_{NA} is given in Eq. (3.1) and it was assumed that the x_i represent the normal modes.

Due to symmetry only the modes perpendicular to the surface couples linearly to the resonance. The excited state potential has vanishing first derivatives along the modes parallel to the surface since there is nearly rotational symmetry

in the surface plane. Hence, we are left with a two-dimensional model and it is straightforward to generalize the result Eq. (3.29) to two modes (see **paper II**). Denoting the internal mode by the subscript d and the COM mode by subscript z, the probability of inducing a transition from the vibrational ground state to the vibrational state $|m_d; m_z\rangle$ is[2]

$$P^{(1)}_{m_d m_z}(\varepsilon_i) = \Gamma^2 e^{-2(g_d+g_z)} \frac{g_d^{m_d} g_z^{m_z}}{m_d! m_z!} \left| \sum_{j_d=0}^{m_d} \sum_{j_z=0}^{m_z} (-1)^{j_d+j_z} \binom{m_d}{j_d} \binom{m_z}{j_z} C^{(1)}_{j_d j_z}(\varepsilon_i) \right|^2 \tag{4.4}$$

$$C^{(1)}_{j_d j_z}(\varepsilon_i) = \sum_{k=0}^{\infty} \sum_{l=0}^{\infty} \frac{g_d^k g_z^l}{k!l!} \frac{1}{\varepsilon_i - \varepsilon_0 - (j_d + k - g_d)\hbar\omega_d - (j_z + l - g_z)\hbar\omega_z + i\Gamma/2}$$

where

$$g_i = \left(\frac{\lambda_i}{\hbar\omega_i}\right)^2, \qquad \lambda_i = -f_i \sqrt{\frac{\hbar}{2m_i\omega_i}}. \tag{4.5}$$

The frequencies, coupling constants and ε_0 are readily obtained from the potential energy surface Fig. 4.1 and we get $\varepsilon_0 = 3.9\ eV$, $\hbar\omega_d = 0.196\ eV$, $\hbar\omega_z = 0.039\ eV$, $\lambda_d = -0.053\ eV$, and $\lambda_z = -0.050\ eV$.

The width of the resonance Γ, can be estimated from the projected density of states of the Kohn-Sham system shown in Fig. 4.2. Although the Kohn-Sham orbitals are in principle un-physical we expect that the projected density of state reflects the degree of hybridization of the molecular orbitals with metallic states. However, the Kohn-Sham eigenvalues typically underestimate excitation energies and the center of the projected density of state is located somewhat lower than the excitation energy of $\varepsilon_0 = 3.9\ eV$ obtained from a ΔSCF calculation.

Besides the linear coupling and quadratic ground state potential, two major approximations was imposed when deriving Eq. (4.4). First of all the model Hamiltonian Eq. (4.1) does not contain electron-electron interactions, which could easily change the scattering probabilities. However, the parameters in the model are obtained within DFT, which does take electron-electron interactions into account and one can thus regard Eq. (4.1) as an effective Hamiltonian describing scattering of renormalized particles. In a non-interacting model the projected density of states is independent of the occupation of states. In contrast, the Kohn-Sham system of an excited state is different from the ground state system since the density and thus the potential is changed. Therefore, the

[2]This expression is valid for inelastic transitions meaning that either $m_d \neq 0$ or $m_z \neq 0$.

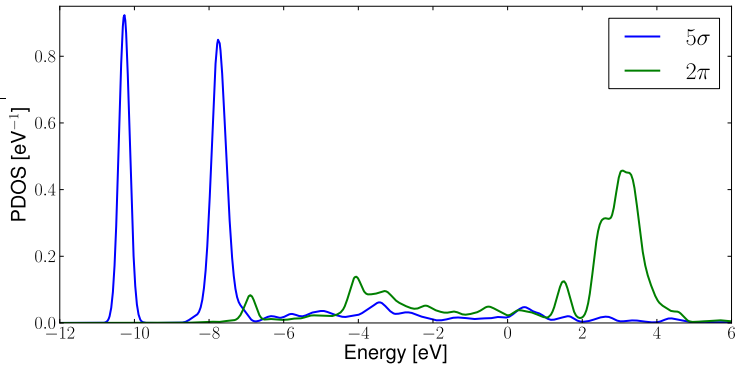

Figure 4.2: The projected density of state of the highest occupied and lowest unoccupied orbitals of N_2 adsorbed on a Pt(111) top site. The zero point is at the Fermi level. The 2π orbital is seen to acquire a significant broadening whereas the 5σ orbital splits into two distinct resonances. Both the 5σ and the 2π orbitals remain mostly occupied and mostly unoccupied respectively.

density of states projected onto a particular state will depend on whether that state is occupied or not. In Fig. 4.2 we show the projected density of states in the ground state and estimate the 2π resonance width to $\sim 1-2\ eV$. The projected density of states from a ΔSCF calculation would yield a slightly different result and we will regard this discrepancy as a uncertainty of Γ within the non-interacting model.

The second major approximation is the wide band limit in which the resonance is assumed to have a Lorentzian lineshape. Although, the 2π resonance shown in Fig. 4.2 does have a main peak with a well defined broadening, it is not exactly a Lorentzian and the projected density of states is seen to have a long tail extending below the Fermi level. In general, hybridization with the metallic *d*-band tends to split the resonance, whereas hybridization with the *sp*-band tend to produce a Lorentzian broadening. The wide band approximation is therefore expected to be good for the noble transition metals, which have a filled *d*-band located below the Fermi level and *sp*-hybridization will dominate.

Besides the fact that Γ is, at best, an ill-determined quantity, it is also instructive to keep it as a parameter and examine how its magnitude affects scattering probabilities. In Fig. 4.3 we display the rate of scattering into a vibrational state with enough energy to desorb ($\Delta E > 1.5\ eV$) as a function of

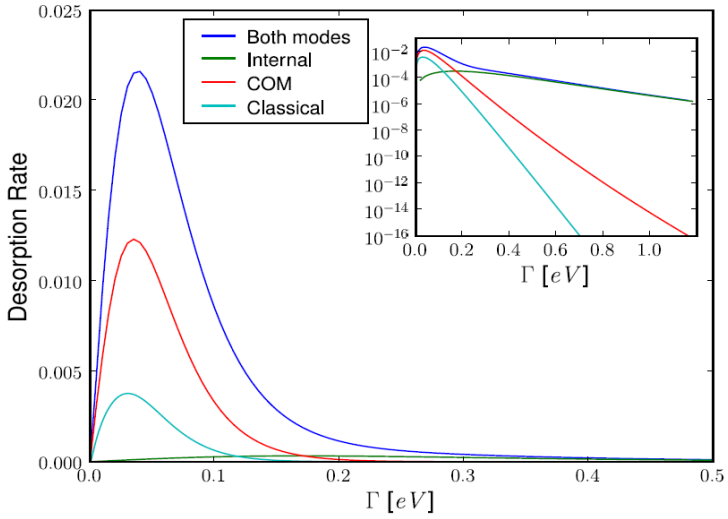

Figure 4.3: Desorption rate as a function of Γ using four different models. It should be noted that when $\Gamma > 0.4\ eV$ the internal mode completely dominates the energy transfer. Furthermore, a classical treatment of the molecule severely underestimates desorption rates when Γ becomes large.

Γ for four different models. Thus the desorption rate R_D is calculated as

$$R_D = \int \frac{d\varepsilon_i}{\hbar} P_D(\varepsilon_i), \quad P_D(\varepsilon_i) = \sum_{m_d, m_z} P_{m_d m_z}(\varepsilon_i)\theta(\hbar\omega_z m_z + \hbar\omega_d m_d - \Delta E),$$

and corresponds to the rate of desorption if the flux of incident hot electrons is uniformly distributed across the resonance. The first model is the full quantum calculation based on Eq. (4.4), in the second model we consider only the internal mode ($\lambda_z = 0$), the third model considers only the COM mode ($\lambda_d = 0$), and finally we evaluate the desorption rate using both modes but with a classical treatment of the molecule similar to Eqs. (3.12)-(3.15). First of all, it is evident that the classical model severely underestimates the desorption rate when $\Gamma > 0.2\ eV$. This also expected since for large Γ, the lifetimes of the excited electronic state becomes much short than the oscillatory period of the molecule and a quick calculation reveals that the classical action is on the order of $\hbar$ for such

processes (see **paper II** for details). Secondly, despite the fact that the coupling parameters λ_d and λ_z are of the same order of magnitude, the COM mode dominates the energy transfer at small Γ and the internal mode dominate the energy transfer at large Γ. This can be understood by comparing the lifetime of the excited electronic state with the oscillatory period of the two modes. The oscillatory period of the COM mode is five times slower than the internal mode and when Γ becomes large, the COM mode hardly has time to propagate in the excited state before it decays.

Similar behavior can be observed for CO as well as NO adsorbed on various other transition metals (see **paper II**).

4.1.2 Quadratic coupling

The linear expansion of the coupling function $\varepsilon_a(a)$ for CO on Pt(111) gave rise to two non-vanishing coupling constants perpendicular to the surface. The four remaining modes do not couple linearly to the resonance due to symmetry. However, if $\varepsilon_a(x)$ is Taylor expanded to second order the remaining modes will also couple and these modes are then described by the Hamiltonian

$$H = H_0 + H_{NA} + H_I \tag{4.6}$$

$$H_0 = \sum_i \Big(\frac{p_i^2}{2m_i} + \frac{1}{2} k_i x_i^2 \Big), \qquad k_i = \left. \frac{\partial^2 V_0}{\partial x_i^2} \right|_{x_i = x_i^0}, \tag{4.7}$$

$$H_I = c_a^\dagger c_a \sum_{ij} \frac{1}{2} (\widetilde{k}_{ij} - k_i \delta_{ij}) x_i x_j, \qquad \widetilde{k}_{ij} = \left. \frac{\partial^2 V_1}{\partial x_i \partial x_j} \right|_{x_i = x_i^0}. \tag{4.8}$$

An interesting feature of this Hamiltonian is that it cannot gives rise to classical energy transfer if the molecule is initially at the ground state minimum ($x_i = x_i^0$). The reason is of course that the minima of $V_0(x)$ and $V_1(x)$ coincide and the classical excited state force therefore vanishes at the minimum position. In the quantum model we have to take into account the vibrational ground state and the molecule is therefore not completely located at x_i^0. When a molecule described by a quantized vibrational state is excited to $V_1(x)$ the extended vibrational wave function will change according to the curvature, which is different from that of $V_0(x)$.

The probability that a hot electron induces a vibrational transition can be obtained from Eqs. (3.26)-(3.28) and the techniques developed in appendix B and the disentangling theorem [72] (see **paper IV** for details). The result is somewhat more involved than the corresponding expression for transitions

within linear coupling and here we will just state the result for a single mode with ground state frequency ω_0 and excited state curvature $\widetilde{k}$. Due to the symmetry of the coupling, it is only possible to emit or absorb $2n$ quanta of oscillation and using (B.21), we get (for $n > 0$)

$$P^{(2)}_{0\to 2n}(\varepsilon_i) = \Gamma^2(1-g_2)b_n g_2^n \left| \sum_{j=0}^{n} (-1)^j \binom{n}{j} C^{(2)}_{nj}(\varepsilon_i) \right|^2 \tag{4.9}$$

with

$$C^{(2)}_{nj}(\varepsilon_i) = \sum_{k=0}^{\infty}\sum_{l=0}^{\infty} \frac{b_l g_2^{k+l}(n+k-1)!}{k!(n-1)!} \frac{1}{\varepsilon_i - \varepsilon_0 + (\hbar\omega_0 - \hbar\omega_1)/2 - 2(j+k+l)\hbar\omega_1 + i\Gamma/2}.$$

and

$$\omega_1 = \sqrt{\widetilde{k}/m}, \qquad g_2 = \left(\frac{\omega_0-\omega_1}{\omega_0+\omega_1}\right)^2, \qquad b_n = \frac{1}{n!}\frac{\partial^n}{\partial x^n}(1-x)^{-1/2}\bigg|_{x=0}.$$

This expression should be compared to the expression for linear coupling with a single mode (3.29). With linear coupling the probability for an electron to create n bosons are proportional to the n'th order Taylor expansion of e^g and normalized by e^{-2g} whereas in the quadratic case the probability to create $2n$ bosons are proportional to the n'th order Taylor expansion of $(1-g_2)^{-1/2}$ and normalized by $(1-g_2)$.

In a model with linear coupling, the probability of exciting $2n$ vibrational quanta is proportional to g^{2n} whereas it is proportional to g_2^n in a quadratic coupled model. This implies that if $g_2 > g^2$ a quadratic coupling term will give rise to larger inelastic scattering probabilities than a linear term. Even with $g_2 < g^2$ a quadratic coupling term may have stronger effect for large n since the expansion coefficients of $(1-x)^{-1/2}$ decay slower than those of e^x. This is illustrated in figure 4.4, where the probability of transferring n vibrational quanta to the ground state is shown for linear and quadratic coupling.

Example: Frustrated rotations of CO adsorbed on Cu(100)

As an example where quadratic coupling may be of relevance, we consider CO adsorbed on Cu(100), which is well studied both theoretically [104, 45, 84] and experimentally [73, 96]. The CO molecule adsorbs at a top site with the molecular axis perpendicular to the surface and the potential energy surfaces in the perpendicular coordinates are very similar to Fig. 4.1. However, we now include

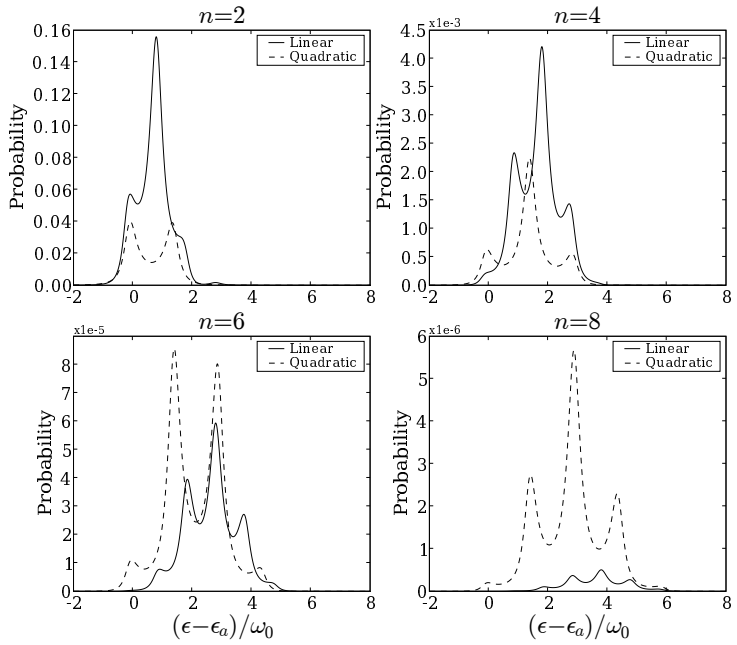

Figure 4.4: Probabilities of making the transition $0 \rightarrow n$ through resonant inelastic scattering with linear and quadratic coupling. The parameters are $\Gamma/\hbar\omega_0 = 0.5$, $g = 0.2$, and $\omega_1 = 0.75\omega_0$ ($g_2 = 0.02$). Even though $g_2 < g_1^2$ the quadratic coupling becomes dominating for large n due to the slowly decaying expansion coefficients. One should also note the spacing between peaks, which is ω_0 for linear coupling and $2\omega_1$ for quadratic coupling.

a frustrated rotational mode with quadratic coupling to the resonance. The potential energy surfaces along the frustrated rotations is shown in Fig. 4.5 along with the coupling function $\varepsilon_a(x)$. The coupling function is well approximated by a quadratic function and the parameters are displayed in Table 4.1 along with the parameters for the COM and internal stretch mode. The position of the bare resonance was calculated to $\varepsilon_0 = 2.8\ eV$ and the resonance width was estimated from the Kohn-Sham projected density of state to $\Gamma = 1\ eV$.

It should be noted that when calculating transition probabilities we should include all modes in the model, because even if the modes are not coupled di-

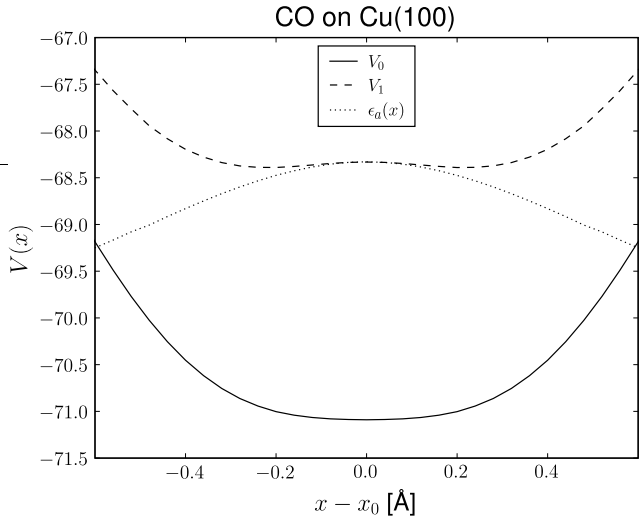

Figure 4.5: Potential energy surfaces along the frustrated rotation mode of CO adsorbed on a Cu(100) surface. The coordinate x is a generalized coordinate representing the deviation from equilibrium. $x = 0.4$ corresponds to a 24° angular deviation from the perpendicular position.

rectly they have an indirect coupling since they all interact with the resonance. It is possible to obtain expressions for the scattering matrix including more than one mode, but these are rather complicated to handle and for weakly coupled systems the physics can usually be extracted from three one-mode models. In figure 4.6 we show the calculated probabilities for a hot electron to excite the different modes of CO adsorbed on Cu(100). The internal stretch and and frustrated rotation show transition probabilities on the same order of magnitude whereas the center of mass vibrations are very unlikely to get excited. This is in accord with calculations of the electronic friction coefficients of this system [45, 104], which are very closely related to the coupling function $\varepsilon_a(x)$ [7]. The frequency of internal vibration is five times larger than both the center of mass and frustrated rotation frequencies and as shown in **paper II** the stretch mode will completely dominate the total energy transfer. Thus, in a simple model where hot electron mediated desorption [96] is reduced to calculating the probability of transferring the chemisorption energy to the adsorbate, the internal mode governs the desorption probability.

Mode	$\hbar\omega$	λ_1	λ_2
Frustrated rotation	0.037	0	-0.009
Center of mass	0.043	-0.006	~ 0
Internal stretch	0.248	-0.170	~ 0

Table 4.1: Parameters for CO adsorbed on Cu(100). All number are eV. Note that while the quadratic coupling for the two perpendicular modes are very small and thus neglectable, the linear coupling of frustrated rotation vanishes exactly due to symmetry.

4.2 Morse Potentials

While the quadratic potential is a reasonable model for the internal stretch coordinate of diatomic molecules, it does not have a reaction barrier and reaction probabilities can only be defined in terms of having transferred a sufficient amount of energy to the adsorbate. However, if the internal bond dominates the energy exchange with hot electrons, but is not involved in a given reaction, energy may be transferred from the internal bond to a reaction coordinate by anharmonic coupling and the quadratic model may give quantitatively good results. In contrast, when hot electrons transfer energy directly into the reaction coordinate it becomes necessary to consider ground state potentials, which allow for a well defined reaction path. In this section we will consider hot electron mediated desorption out of a Morse potential and calculate the velocity distribution of desorbed states.

The inelastic scattering amplitude from a bound to an unbound state Eq. (3.26) can be written

$$R_n(\varepsilon_f, \varepsilon_i) = \Gamma(\varepsilon_f)\Gamma(\varepsilon_i) \int dk \frac{dP_{nk}(\varepsilon_f, \varepsilon_i; k)}{dk d\varepsilon_f} \tag{4.10}$$

where the differential probability $\frac{dP_{nk}(\varepsilon_f,\varepsilon_i;k)}{dkd\varepsilon_f}$ of scattering into an unbound Morse state $|k\rangle$ while the hot electron goes into a metallic state ε_f is

$$\frac{dP_{nk}(\varepsilon_f, \varepsilon_i)}{dk d\varepsilon_f} = \int \frac{d\tau ds dt}{2\pi\hbar^3} e^{i[(\varepsilon_i - \varepsilon_f)\tau + \varepsilon_f t - \varepsilon_i s]/\hbar} \times G_R(t, 0; k, n) G_R^*(\tau, \tau - s; k, n), \tag{4.11}$$

To obtain this expression we have inserted a complete set of vibrational states in the two-particle Green function (3.28) and neglected the bound-bound prop-

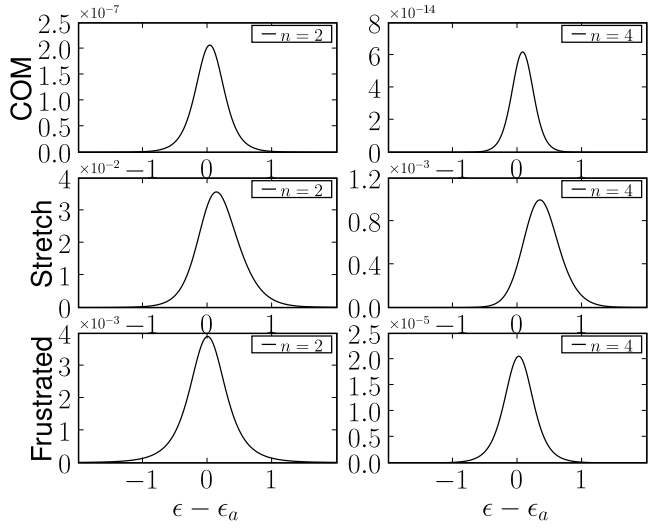

Figure 4.6: Probabilities of exciting two and four quanta of vibrations to the center of mass, internal stretch and frustrated rotational modes of CO adsorbed on Cu(100).

agators since, we are only interested in a desorption event where the adsorbate makes a transition to a free state. The retarded Green function $G_R(t_2, t_1; k, m)$ is calculated in appendix C Eq. (C.17) within the wide band limit and first order perturbation theory. Assuming a linear coupling function $\varepsilon_a(x) = -fx$, the differential scattering probability becomes

$$\frac{dP_{nk}(\varepsilon_f;\varepsilon_i)}{dk d\varepsilon_f} = \frac{f^2\Gamma^2}{(E_k - E_n)^2}\delta(\varepsilon_f - \varepsilon_i - E_k + E_n)|\langle k|x|n\rangle|^2 \times \left|\frac{1}{\varepsilon_i - \varepsilon_0 + i\Gamma/2} - \frac{1}{\varepsilon_i - \varepsilon_0 - (E_k - E_n) + i\Gamma/2}\right|^2, \tag{4.12}$$

where E_k and E_n are the Morse eigenenergies given in Eqs. (C.6) and (C.2) respectively and the matrix elements $\langle k|x|n\rangle$ are given in Eq. (C.9). The k-dependence in this expression is easily converted into a velocity dependence, since the k states become plane waves asymptotically and therefore $v = \hbar k/m$.

In Fig. 4.7 the desorption probabilities for different bound states in a Morse potential is shown (Eq. (4.12) integrated over ε_f). The main point of interest

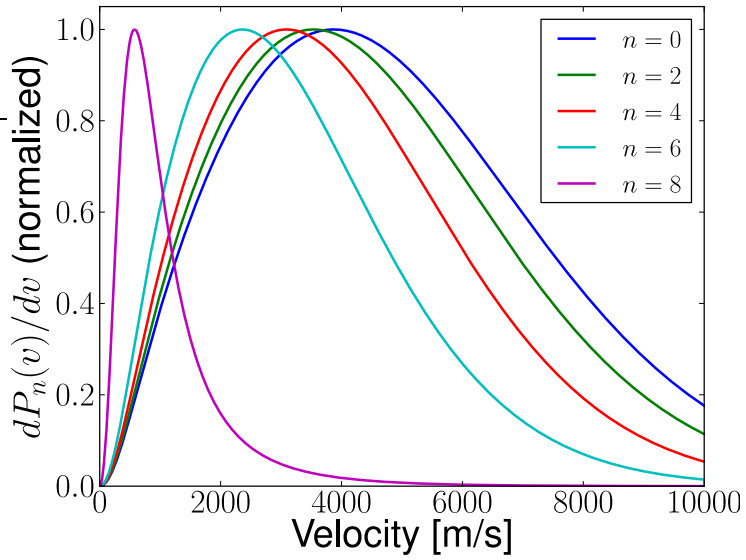

Figure 4.7: Velocity distributions of hot electron induced desorption from a Morse potential with an adsorbate in the initial vibrational state n calculated from Eq. (4.12). The parameters of the potential are $D = 2.0\ eV$, $\alpha = 3.5\text{Å}^{-}1$ and we have taken $\varepsilon_i = \varepsilon_0$, $\Gamma = 1.0\ eV$ and $m = 1\ u$. The Probabilities have been normalized to fit the figure, in fact the maximum value of $P_n(v)$ increases by an order of magnitude for each n. The $n = 8$ state thus has a much larger desorption probability than the rest.

is the maximum, which depends on the initial vibrational state n. The highly excited bound states tend to desorb into sharply peaked low velocity states whereas the low lying vibrational states tend to desorb into broadly distributed high velocity states. This feature originates from the matrix elements $\langle k|x|n\rangle$ and has the intriguing consequence that the velocity distributions of atoms or molecules desorbed by hot electrons, can probe the initial vibrational distribution of the adsorbates.

Example: Desorption of H from graphite(0001)

Experiments involving desorption of Hydrogen atoms are well suited to test the theoretical velocity distributions (Eq. (4.12) and Fig 4.7), since there is no

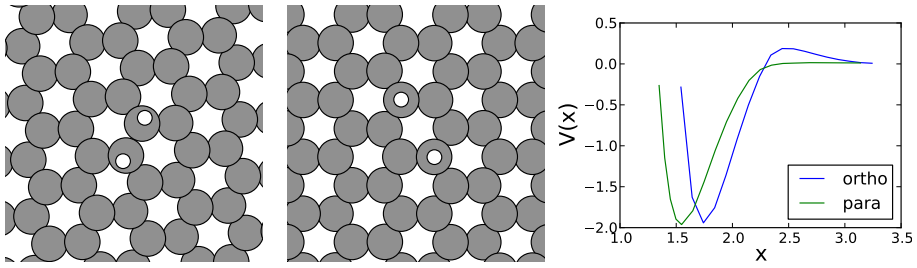

Figure 4.8: Ortho (left) and para (middle) configurations of Hydrogen adsorbed on graphene. STM studies and DFT calculations have shown that these are the preferred adsorption configurations on graphite(0001) at low Hydrogen coverage. To the right we present DFT calculations of the potential energy surfaces for desorption of a single H atom from the two configurations.

internal degrees of freedom to complicate the picture. Measurements of the velocity distributions resulting from hot electron induced desorption of Hydrogen and Deuterium from graphite(0001) have been carried out by the group of H. Zacharias in Münster and we have compared the theory with experiments. A large density of hot electrons are generated by means of a femtosecond laser pulse and it is expected that multiple scattering events are responsible for the desorption reaction.

STM studies in conjunction with DFT studies have shown that at low coverage, Hydrogen adsorbs on graphite in one of two dimer configurations [52, 51, 94] referred to as para and ortho. When considering chemical bonds on graphite(0001), a single graphene layer is an excellent approximation and the para and ortho configurations on graphene are shown in Fig. 4.8. In both configurations the desorption energy is on the order of $\sim 2\ eV$ but the desorption potential of the ortho configuration has an adsorption barrier of $\sim 0.2\ eV$ whereas the desorption potential for the para configurations shows no adsorption barrier. The desorption potential of a single Hydrogen atom in the para configuration is therefore well approximated by a Morse potential and we can compare a measured velocity distribution with the theoretical distribution Eq. (4.12).

The parameters of the model are obtained using DFT and ΔSCF. The main challenge is to identify the resonant state mediating the non-adiabatic energy transfer. To this end we have relaxed two H atoms on a graphene slab in one of the two configurations shown in Fig. 4.8 and then removed all atoms except one

	α	D	f	ε_0
para	3.5	1.97	0.27	3.85
ortho	3.5	2.1	0.57	3.81

Table 4.2: Ground and excited state parameters for the ortho and para potentials shown in Fig. 4.8. The para potential is well approximated by a Morse potential with parameters D and α, but for the ortho potential we have simply approximated D by the distance from the bottom of the potential to the top of the adsorption barrier, and α by the best fit of the ortho potential cut at the barrier to a Morse potential with fixed D. The parameters are in eV and Å^{-1}.

Hydrogen and the Carbon atom nearest to it. A DFT calculation has then been carried out on this "CH" atom and the lowest unoccupied Kohn-Sham orbital turns out to have an anti-bonding nature. This orbital has then been projected onto the density of states of the full graphene slab with two hydrogen atoms and it is observed that the orbital is still mostly unoccupied a semi-localized in energy with a width of $\sim 1.5\ eV$. The lowest unoccupied orbital of the "CH" atom thus serves as a good orbital for doing ΔSCF calculations and we can map out an excited potential energy surface $V_1(x)$ of this state. However, since the model (4.12) only handles linear coupling we use the approximation

$$\varepsilon_a(x) = V_1(x) - V_0(x) \approx \varepsilon_0 - fx, \qquad f = -\frac{d}{dx}V_1(x)\Big|_{x=x_0}, \tag{4.13}$$

and obtain the parameters displayed in table 4.2

In order to apply the model (4.12) we also need the probability of being in the n'th vibrational state at the time a hot electron desorbs the atom. Since multiple electrons are expected to participate in the reaction it is natural to assume that a number of hot electrons produce a distribution of vibrational states P_n before a final hot electron desorbs the molecule. To get this distribution we note that an expression for bound-bound transitions can be obtained exactly as we got Eq. (4.12) and it is then possible to calculate the distribution of vibrational states induced by each hot electron. We have chosen to use a distribution P_n resulting from five initial hot electrons scattering events with the parameters displayed in table 4.2 and $\varepsilon_i = \varepsilon_0$. This choice may seem a bit arbitrary, but while the actual desorption probability depends sensitively on the number of hot electrons contributing to the reaction, the qualitative conclusions regarding

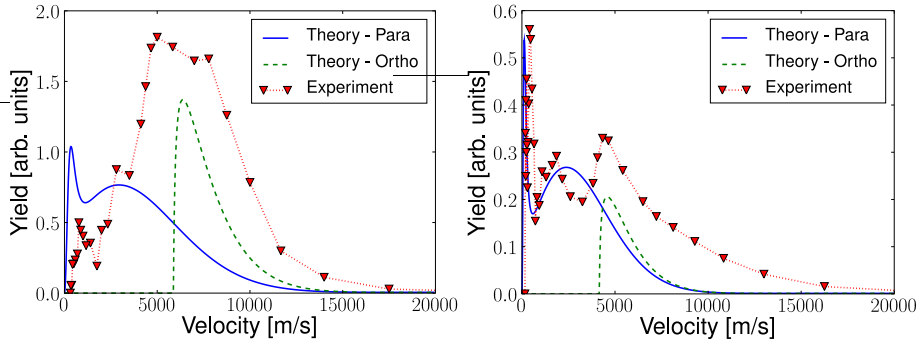

Figure 4.9: Measured and calculated velocity distributions for Hydrogen (left) and Deuterium (right) desorbed from graphite(0001) by means of a femtosecond laser pulse. The sharp low velocity peak results from desorption out of the highest vibrationally excited state in the para configuration.

the velocity distribution will not depend on the initial hot electrons.[3] We will return to an analysis of multiple scattering events in section 4.3.

We can then calculate $P(k) = \sum_n P_n P_{nk}$, which is shown in Fig 4.9 and compare the result to experimentally measured yields. For details on the experimental setup we refer to **paper VII**. The theoretical velocity distribution from the ortho configuration was obtained by assuming a Morse potential ending at the top of the adsorption barrier and then accelerating the desorbed atoms after the barrier. This is the reason why the velocity distribution of the ortho configuration has an onset at $\sim 4 - 5.5\ km/s$ and the calculated peak has a good correspondence with the measured high velocity peak. In contrast, the para configuration has no adsorption barrier and allow desorption of arbitrarily slow atoms. In fact, the calculated velocity distribution shows a bimodal structure with a sharp very low velocity peak and a broadened peak centered at $\sim 3\ km/s$. Referring to Fig. 4.7, we see that there is a straightforward interpretation of this structure: the low velocity peak originates from atoms, which were in the highest vibrational state, whereas the broad high velocity peak originates from lower vibrational states.

It would be very interesting to measure velocity distributions at different

[3] Alternatively one can assume that the hot electrons induce a (hot!) thermal distribution of vibrational states. This assumption gives distributions very similar to those shown in Fig 4.9.

Laser intensities to see how the relative intensity of the low velocity peak. If the above conjecture is true, one would expect an increased laser fluence would increase the population of atoms in the highest vibrational states and thus increase the relative intensity of the low velocity peak. In **paper VIII**, we discuss a different set of measurements where an extreme UV laser is used. Again, we find good agreement between theory and experiments, although we have to extend the model with a certain uniform para adsorption configuration, which is expected to be present at high coverage (see appendix D).

4.3 Power Laws

Most of the experimental observations of surface reactions induced by hot electrons, have involved electrons excited by a femtosecond laser pulse (see Fig 1.3). A characteristic feature of such experiments is the emergence of a power law dependence of the reaction yield on the laser fluence $Y \sim F^n$, indicating that multiple hot electrons are involved in the reaction [85, 9, 86, 58, 57, 69, 17, 49, 96, 12, 18, 95, 106]. While it is easy to predict a non-linear dependence of the laser fluence when multiple hot electrons are involved in a reaction, the power law dependence is not obvious *a priori* and the exponent n have mostly been reported as an empirical parameter characterizing a given experiment. A model for Desorption Induced by Multiple Electronic Transitions (DIMET) was first proposed by Misewich et al. [68], who regarded a desorption event as the result of multiple transitions between vibrational state in the desorption potential. The conceptual picture is a sequential climbing of bound states in the potential as shown in Fig. 4.10.

A different way of handling the multiple electronic excitations was proposed by Brandbyge et al. [7] and is illustrated in Fig. 1.3. In that picture, the hot electrons are assumed to thermalize rapidly and are described by a time-dependent electronic temperature $T_e(t)$. The concept of a thermal distribution of hot electrons is extremely practical because the complicated distribution of hot electron energies is described by a single time-dependent parameter, which can be fitted to experiments or calculated from the parameters of the metal. On the other hand, it has been shown that the thermalization time of a distribution of excited electrons in metals, can be as large as ~ 1 *ps* [27, 28], which is close to the reaction time in such experiments, and the non-thermal properties of the hot electrons may then be important.

In this section, we will construct a simple model for incoherent multiple inelastic scattering and show that it gives rise to a power law dependence when

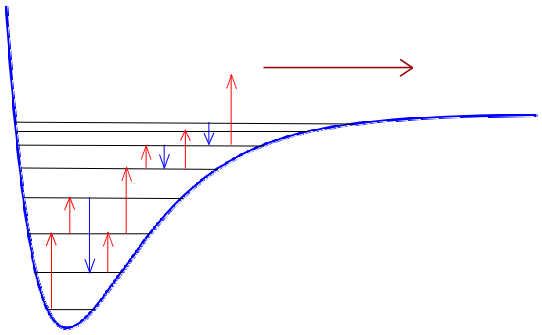

Figure 4.10: Principle of DIMET. The adsorbate desorbs by sequential excitations of hot electrons (red arrows), which may be disturbed by spontaneous decay of vibrational states (blue arrows).

scattering probabilities are obtained from the model (4.1). With a simplifying assumption the power law can be derived analytically within the model and we obtain a simple physical interpretation of the exponent n, which represents the number of adsorbate vibrational states participating in the reaction.

4.3.1 Incoherent model of multiple inelastic scattering

Suppose we know the transition probabilities $P_{nm}(\varepsilon_i)$ of a hot electron induced transition from a vibrational state m to a different vibrational state n in some adsorbate potential $V_0(x)$. Assuming that the adsorbate is initially in the state $n = 0$, we can then write the distribution of vibrational states after a single electron with energy ε_1 has scattered on the adsorbate:

$$Q_1(n;\varepsilon_1) = P_{0n}(\varepsilon_1). \tag{4.14}$$

After a time interval Δt_1, a second electron of energy ε_2 scatters on the adsorbate and induces a new distribution of vibrational states:

$$Q_2(n;\varepsilon_1,\varepsilon_2) = \sum_m p_m(Q_1;\Delta t_1) P_{mn}(\varepsilon_2), \tag{4.15}$$

where $p_m(Q_1;\Delta t_1)$ is the probability of being in the vibrational state m given the time interval Δt_1 and the initial distribution Q_1. This scheme can be continued

to included l sequential scattering events separated by $(l-1)$ time intervals and the distribution induced by the l'th hot electron is

$$Q_l(n;\{\varepsilon_i\}) = \sum_m p_m(Q_{l-1};\Delta t_{l-1}) P_{mn}(\varepsilon_l), \tag{4.16}$$

where $\{\varepsilon_i\}$ is the set of l hot electron energies and Q_{l-1} has been determined by the previous scattering event and so forth.

Here, it has been assumed that the individual scattering events are incoherent, meaning that we describe the system by the probabilities of being in a particular state only and not the complete quantum state of the adsorbate. This corresponds to neglecting the off-diagonal elements of the reduced density matrix introduced in section 3.5, which is the approximation leading to the master equation (3.56).

The total reaction probability of the l'th electron can now be obtained by calculating

$$P_l^R = \sum_n p_n(Q_{l-1};\Delta t_{l-1}) Q_{l-1}(n) P_R(n;\varepsilon_l), \tag{4.17}$$

where $P_R(n;\varepsilon_l)$ is the reaction probability of the adsorbate given that it is in the n'th vibrational state and the hot electron has energy ε_l. The reaction probability will depend on the model one is considering. For example, in the case of desorption of Hydrogen from graphite it would be given by

$$P_R^{Morse}(n;\varepsilon_i) = \int dk d\varepsilon_f \frac{dP_{nk}(\varepsilon_f,\varepsilon_i)}{dk d\varepsilon_f}, \tag{4.18}$$

whereas in the quadratic models considered in section 4.1, the reaction probability would be obtained by truncating the potential such that

$$P_R^{Harmonic}(n;\varepsilon_i) = \theta(E_R - \hbar\omega_0 n). \tag{4.19}$$

In the quadratic case it is thus assumed that a reaction will happen once the adsorbate reaches a vibrational state equivalent of the reaction energy E_R. In Eq. (4.17) one would then put $P_R(n) = 1$ and truncate the sum such that it starts at $n = n_R \sim E_R/\hbar\omega_0$.

4.3.2 Independent bosons

A major challenge in applying the multiple scattering model (4.14)-(4.17) is the inclusion of vibrational decay incorporated in the function $p_m(Q_k, \Delta t_k)$. An

exception is the case of a harmonic potential in which the vibrational state $|n\rangle$ can be regarded as n independent bosons. If a single boson is assumed to decay exponentially with a life time T_{vib}, the probability that m out of n bosons survive the time interval Δt, is given by the binomial distribution:

$$p(m|n) = \frac{n!}{m!(n-m)!}(e^{-\Delta t/T_{vib}})^m(1-e^{-\Delta t/T_{vib}})^{n-m}, \tag{4.20}$$

where the prefactor takes into account the combinatorics of picking m out of n identical objects.[4] To obtain the probability of being in the m'th vibrational state after the time interval Δt, we have to sum over all vibrational states n weighted by their probability $Q(n)$ and we get

$$p_m(Q_k(n), \Delta t_k) = \sum_{n=m}^{\infty} Q_k(n)\frac{n!}{m!(n-m)!}(e^{-\Delta t/T_{vib}})^m(1-e^{-\Delta t/T_{vib}})^{n-m}. \tag{4.21}$$

The model Eqs. (4.14)-(4.17) and Eq. (4.21) can now applied if we can obtain an expression for $P_{mn}(\varepsilon)$. As a simple starting point, we can consider the forced oscillator model from section 3.3, which gave rise to a Franck-Condon distribution of transition probabilities Eq. (3.22). The probability of making the transition $m \to n$ scales as $\alpha^{n-m}/(n-m)!$ and in the following we will examine the consequences of assuming transition probabilities of the form

$$P_{mn} = e^{-\alpha}\frac{\alpha^{n-m}}{(n-m)!}, \qquad \alpha = \frac{\lambda^2}{(\hbar\omega_0)^2 + (\Gamma/2)^2}, \tag{4.22}$$

for $n \geq m$ and $P_{mn} = 0$ for $n < m$. Repeated use of the algorithm (4.14)-(4.17) with these probabilities and equal time interval $\Delta t_i = \Delta t$ then reveals that to leading order in α one has

$$Q_k(n) = \frac{\alpha^n}{n!}\left(\sum_{j=0}^{k-1} e^{-j\Delta t/T_{vib}}\right)^n. \tag{4.23}$$

We then consider a large flux $e^{-\Delta t/T_{vib}} \sim 1 - \Delta t/T_{vib}$, sum up the geometric series, take the limit $k \to \infty$ corresponding to steady state, and get

$$Q(n) = \frac{\alpha^n}{n!}(T_{vib}J_0)^n, \tag{4.24}$$

[4] The transition rate $W_{nm} \sim 1/T_{vib}$ for going from the n'th to the m'th vibrational state is in fact given exactly by Eq. (3.59), but the present assumption serves as a simple and intuitive expression, which reproduces the first order golden rule expression (3.58) and satisfies $\sum_{m=0}^{n} p(m|n)$=1.

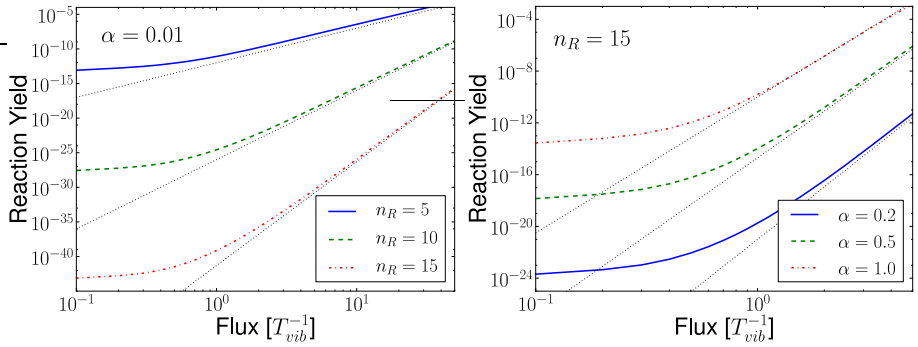

Figure 4.11: The yield as a function of electron flux obtained using the transition probabilities in equation (4.22) for different values of α and n_R. Left: A small α the yield becomes an exact power law in the flux of hot electrons with exponent $n = n_R$. Right: For larger values of α the power law exponent decreases slightly.

where $\Delta t = 1/J_0$. Thus, for small α the reaction probability (4.17) will be dominated by such a term with $n = n_R$. Here, J_0 is the flux of hot electrons incident on the adsorbate and since we expect that J_0 is proportional to the laser fluence F and $Q(n)$ is proportional to the reaction yield Y, the expression (4.24) becomes $Y \propto F^{n_R}$.

The power law emerges from summing up the detailed combinatorics of all possible ways of rising through the vibrational states in the potential well. The leading order in α means that decay and reexcitation are not contributing since such processes would involve additional factors of α, but the decay factor (4.20) is still most important, since it introduces the flux J_0. It should be noted that although the power law becomes exact when in the limit of small α where decay does not contribute, the exponent cannot be interpreted as the number of electrons necessary to induce a reaction. Rather, both direct excitations $0 \to n_R$ by a single electron and sequential excitations $0 \to 1 \to 2 \to \ldots \to n_R$ by n_R electrons contribute to the sum resulting in Eq. (4.24). In figure 4.11 we show the reaction yields for three values of n_R and they are seen to approach power laws of the form $Y \propto J_0^{n_R}$ for large fluxes. Even if α is not small, equations (4.14)-(4.17) tend to conserve the power law although the exponent becomes reduced from the value of n_R when terms beyond leading order are not vanishing. In figure 4.11 we show the yield when $n_R = 15$ for $\alpha = 0.2$, $\alpha = 0.5$, and $\alpha = 1.0$. At large fluxes the yields are well approximated by power laws

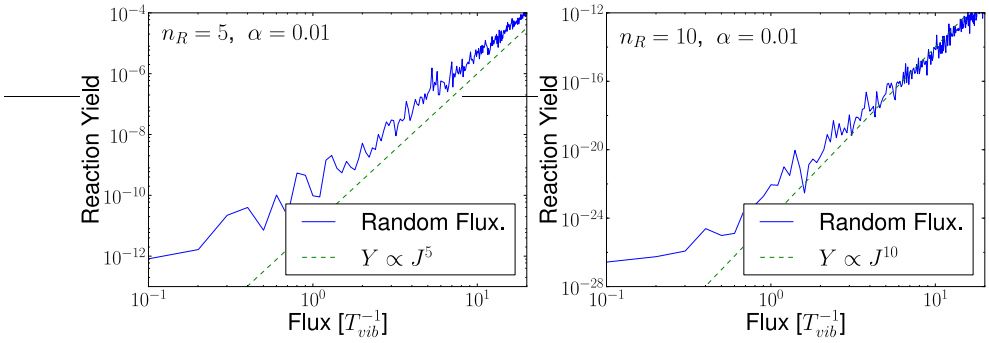

Figure 4.12: The reaction yield as a function of flux calculated from the algorithm (4.14)-(4.17) and with the time intervals randomly drawn form the exponential distribution $p(t) \sim e^{-t/\Delta t}$. Δt is the average temporal separation between scattering events and inversely proportional to the average flux. The power law is clearly seen as an average trend in the yields.

with exponents 14, 12, and 10 respectively. We should also note, that while the absolute magnitude of the yield depends on the number of scattering events k included in the algorithm, the power law exponent becomes independent of k after a few scattering events.

One might worry that the fixed time interval Δt between scattering events is too crude an approximation for the random nature of hot electrons interacting with the adsorbate. However, a sequence of time intervals $\{t_k\}$ with an average of Δt would lead to the replacement $j\Delta t \to \sum_{i=1}^{j} t_{k-i}$ in (4.23), which is well approximated by $j\Delta t$ for large j. In Fig. 4.12 we show the reaction yield calculated from equations (4.14)-(4.17) but with the time intervals randomly drawn from an exponential distribution $p(t) \sim e^{-t/\Delta t}$. It is evident that the power law is indeed conserved on average.

The interpretation of the power law exponent as the number of contributing vibrational states can be used to identify the reaction channel of a given adsorbate system. For example, in the study of hot electron mediated desorption of NO from Pd(111) [85] a power law with exponent $n \simeq 3.3$ was found. The internal stretch vibration corresponds to an energy of $\hbar\omega \simeq 210\ meV$ whereas the other modes have vibrational energies $\hbar\omega \leq 70\ meV$. Since the adsorption energy is $E_a \simeq 1.0\ eV$ we conclude that the power law exponent $n_R \sim E_a/\hbar\omega$ has to arise from sequential excitation of the internal stretch vibration and sub-

sequent anharmonic energy transfer to the desorption coordinate. In contrast, the study of hot electron induced surface diffusion of atomic oxygen on Pt(111) [95], gave rise to a power law with exponent $n \simeq 15$, which fits very well with an experimental diffusion barrier of $E_d \simeq 0.8\ eV$ and vibrational modes on the order $\hbar\omega \sim 50\ meV$.

Example: Desorption of CO from Cu(111)

The Poissonian transition probabilities (4.22) were chosen because they allow for an analytical derivation of the power laws shown in Fig. 4.11. However, the power laws also emerge if one uses the Franck-Condon overlaps (3.22), which were the true transition probabilities derived from the forced oscillator model in section 3.3. Furthermore, it is possible to derive an approximate expression for the inelastic scattering probabilities $P_{mn}(\varepsilon_i)$[5] within the linear model Eqs. (4.1)-(4.5), which makes it possible to include the effect of the hot electron energies $\{\varepsilon_i\}$.

As an example we calculate the fluence dependent transfer of energy from hot electrons to a CO molecule adsorbed on Cu(111), mediated by excitation of an unoccupied 2π orbital. CO adsorbs with the molecular axis perpendicular to the surface and the symmetry of the adsorbed molecule thus only allows a linear coupling to the center of mass (COM) and internal stretch vibrations of CO. The system can thus be modelled by the linear model with two quadratic modes (4.1)-(4.5), and the parameters for CO chemisorbed at a Cu(111) bridge site have been calculated with the `GPAW` code. We have modelled the surface by a three layer (4×4) supercell with the top layer relaxed, a grid-spacing of 0.2Å, and a 4×4 surface K-point sampling. With the RPBE [44] functional, we find $\varepsilon_0 = 2.4\ eV$, $\hbar\omega = 231\ meV$ and $\lambda = -118\ meV$ for the internal stretch vibration, and $\hbar\omega = 42\ meV$ and $\lambda = -4\ meV$ for the COM vibration. The internal mode completely dominates the transfer of energy from hot electrons to the molecule since it has a much larger coupling λ, and the quantum of energy is five times larger than for the COM mode.

In figure 4.13, we have used Eqs. (4.14)-(4.17) with hot electrons at $\varepsilon = 2.0\ eV$ corresponding to the laser frequency used in [86], to calculate reaction rates, which require energies corresponding to 3, 4, 5 and 6 internal vibrational excitations. In the non-linear regime corresponding to reactions induced by multiple scattering events, the rates are very well approximated by power laws with $n = 2.8$, $n = 3.6$, $n = 4.3$, and $n = 5.1$. Varying the parameters in the

[5] It is in fact possible to derive the transition probabilities exactly, but the procedure is extremely cumbersome (see **paper II** for details)

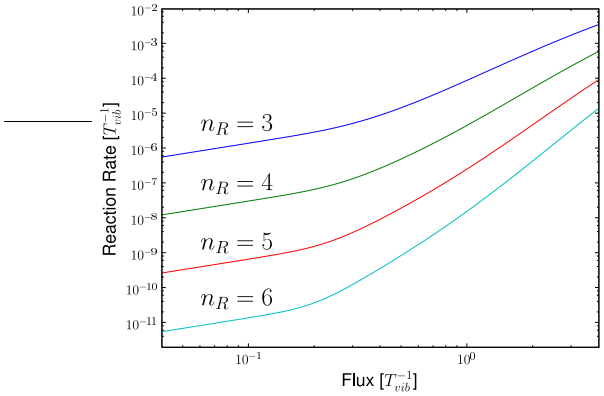

Figure 4.13: The reaction yield of CO on Cu(111) as a function of hot electron flux for four reaction energies. For large flux the reaction rates are seen to be well represented by power laws with exponents that increase with increasing reaction quantum number n_R.

model reveals that in general, one always obtains very good power law fits with exponents $n \sim n_R$. Increasing the energy of the hot electrons above the resonant energy ε_0 tend to decrease n.

4.4 Vibrationally Mediated Transmission of Electrons

In the final section of this chapter, we turn to a seemingly very different class of problems. Namely, the transmission of electrons through a molecule coupled to two metal contacts. Understanding such processes is a major step toward the realization of molecular electronics devices and both theoretical and experimental investigations of the subject have shown substantial progress during the past two decades [98]. In the context of non-adiabatic models, a particularly interesting aspect of electron transport is the coupling to molecular vibrations and several experiments have established that such coupling can have a significant effect on the I-V characteristics of single-molecule junctions [80, 110, 82, 92, 60]. Here, we will not delve into the involved theoretical models designed to incorporate the effect of electron-electron interaction in electronic transport [37, 38, 31, 26], but simply focus on a primitive model, which includes the effect of molecular

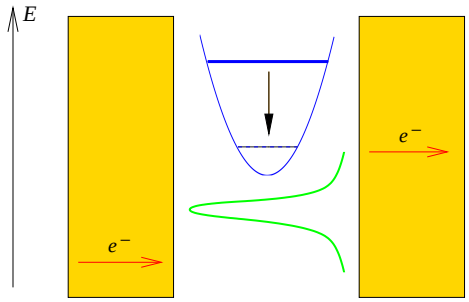

Figure 4.14: A molecule between two metal contacts is represented by a resonant state (for example the lowest unoccupied molecular orbital) and a vibrational potential. If the molecule is initially vibrationally excited, an off-resonant electron below the resonance may tunnel through the molecule by absorbing a quantum of vibration. When the molecule is initially in its vibrational ground state, transmission is not possible.

vibrations exactly. It will be shown that control of the vibrational states of a molecule sandwiched between two metallic contacts, allows one to control the transmission of single electrons through the molecule.

We start by noting the similarity between transmission through a molecular junction with coupling to vibrational states and hot electron induced energy transfer to adsorbates. A molecular junction can be regarded as an adsorbate/substrate system with coupling to an additional substrate, and a hot electron scattering on the adsorbate from one substrate then has the additional possibility of tunneling through the molecule and ending up in the second substrate. Such an event will be referred to as a transmission of an electron, and may or may not be accompanied by energy loss to the vibrational modes of the molecule.

Referring to Fig. 3.2, we see that the incoming electron is more likely to loose energy to vibrations if it is detuned above the resonance. However, we could also imagine the opposite scenario where the molecule is initially vibrationally excited and it would then be expected that the incoming electron is most likely to gain energy from the vibrations if it is detuned below the resonance. In fact, there could be situations where the incoming electrons are detuned in such a way that a transmission event is *only* possible if it is accompanied by a vibrational downward transition of the molecule and transmission is therefore impossible

unless the molecule is vibrationally excited. The conceptual picture of such an event is sown in Fig. 4.14: Since transmission is only allowed combined with a downward vibrational transition, only one or a few electrons may tunnel through the junction and the transmission channel will be closed once the vibrational mode reaches the ground state.

Inspired by these considerations, we perform a quantitative analysis based on the model transport Hamiltonian [107]

$$\begin{aligned} H_{trans} =& \varepsilon_0 c_a^\dagger c_a + \sum_i \hbar\omega_i b_i^\dagger b_i + \sum_i \lambda_i c_a^\dagger c_a (b_i^\dagger + b_i) \\ &+ \sum_k \epsilon_{Lk} c_{Lk}^\dagger c_{Lk} + \sum_k \left(V_{Lk} c_a^\dagger c_{Lk} + V_{Lk}^* c_{Lk}^\dagger c_a \right) \\ &+ \sum_k \epsilon_{Rk} c_{Rk}^\dagger c_{Rk} \sum_k \left(V_{Rk} c_a^\dagger c_{Rk} + V_{Rk}^* c_{Rk}^\dagger c_a \right), \end{aligned} \tag{4.25}$$

where $c_a^\dagger$ is the creation operator for the resonant state, $c_{Lk}^\dagger$ and $c_{Rk}^\dagger$ are creation operators for metallic states in the left and right metal contact respectively and $b_i^\dagger$ are creation operators for the vibrational normal modes of the molecule with frequencies ω_i. Thus, the electronic states of the left and right contacts are coupled through the molecular resonance, which is coupled to molecular vibrations with coupling strengths λ_i. Note that this is exactly the quadratic model with linear coupling Eq. (4.1) except that the resonance has been coupled to an additional metal substrate. We impose the wide band limit in which the contact density of states is constant in the region of the resonance and the resonance hybridization with metallic states is determined by the parameters

$$\Gamma_L = 2\pi \sum_k |V_{Lk}|^2 \delta(\varepsilon_0 - \epsilon_{Lk}), \tag{4.26}$$

and a similar expression for the coupling to the right lead Γ_R. Without the vibrational coupling, the resonance spectral function would then be a Lorentzian with full width at half maximum given by $\Gamma = \Gamma_L + \Gamma_R$. We will be interested in the regime $\Gamma,\ k_B T \ll \hbar\omega_i$, but we will not restrict ourselves to the classical limit $\Gamma \ll k_B T$ where the current through the molecule can be expressed in terms of rate equations [6, 70, 71]. Instead, we consider the transmission probability $T_{mn}(\varepsilon_i, \varepsilon_f)$ for an electron with initial state energy ε_i to be transmitted while the adsorbate makes the transition $m \to n$. It can derived in complete analogy with Eqs. (3.26) and (4.11) and the result is

$$T_{mn}(\varepsilon_i) = \Gamma_L \Gamma_R \int \frac{dsdt}{\hbar^2} e^{i\varepsilon_i (t-s)/\hbar} G_R(t, 0; n, m) G_R^*(t, t-s; n, m),$$

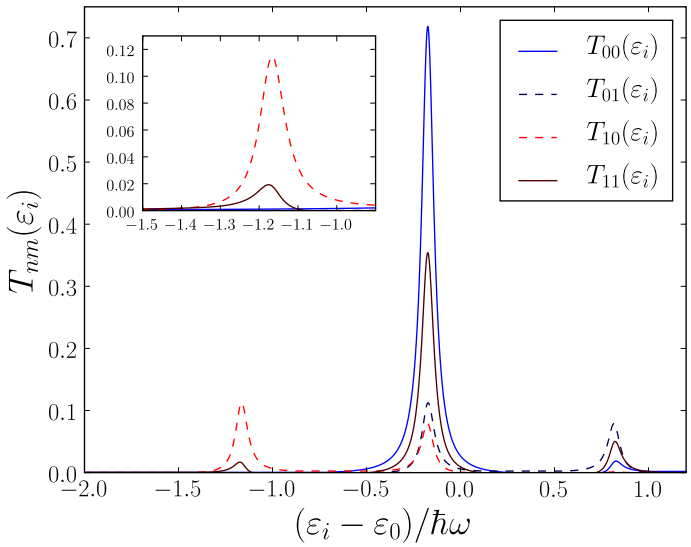

Figure 4.15: Transmission probabilities calculated from (4.25) as a function of incoming electron energy with $\Gamma_L = \Gamma_R = 0.04\hbar\omega$ and $\lambda = 0.4\hbar\omega$. Below the resonance energy ε_0 the ground state transmission functions $T_{00}(\varepsilon_i)$ and $T_{01}(\varepsilon_i)$ essentially vanish. The insert shows the lower sideband, where stimulated emission of a vibrational quantum $T_{10}(\varepsilon_i)$ is the dominating transmission channel.

with

$$G_R(t_2, t_1; n, m) = -i\theta(t_2 - t_1)\langle n, 0|c_a(t_2)c_a^\dagger(t_1)|m, 0\rangle. \tag{4.27}$$

In **paper VI**, we have used a model with a single mode to calculate the four transmission probabilities, where the initial and final states take the values of zero and one and the results are shown in Fig. 4.15. It is seen that incoming electrons with energies below $\varepsilon_0 - \hbar\omega$ have a vanishing probability of transmission ($\sum_n T_{0n}$) when the molecule is in its vibrational ground state. This means that if a bias voltage is applied such that the Fermi level of the upstream contact is at $\varepsilon_F = \varepsilon_0 - \hbar\omega$ no current will be observed when the molecule is in its vibrational ground state. If the molecule is vibrationally excited, e.g. by means of a IR laser, transmission becomes possible through the low lying vibrational transmission sideband (T_{11} and T_{10}). However, the first electron, which is transmitted through the T_{10} channel induces a transition to the vibrational ground

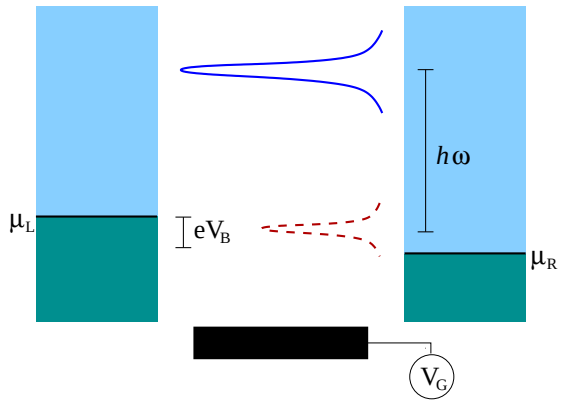

Figure 4.16: The principle of single electron transmission. A small bias is applied such that the bias window just covers the resonance: $eV_B \sim \Gamma$ and a gate voltage is tuned such that the resonance is located at: $\varepsilon_0 \sim \mu_L - eV_B/2 + \hbar\omega$. In the vibrational ground state the transmission function T_{00} (solid line) is zero in the bias window. Exciting the first vibrational state changes the transmission function, which is dominated by the inelastic part T_{10} (dashed line) in the bias window. A vibrational excitation of the molecule will thus result in a single electron (or a few if T_{11} does not vanish) being transmitted.

state and thus closes the transmission channel completely. Hence, if electrons are present at the lower sideband energy it is possible to induce transmission of one or a few electrons by exciting the vibrational mode of the molecule.

Typically, in experiments with electron transport through molecular junctions, the electrons being transmitted originate from the Fermi level of one of the metal substrates and the contact can be "tuned" by adjusting a bias and a gate voltage. The setup is illustrated in Fig. 4.16 where a small bias voltage $V_B \sim \Gamma/e$ has been applied and a gate voltage V_G has been tuned such that the position of the resonance is located $\hbar\omega$ above the bias window. It is crucial that the electronic resonance has a width much smaller than the quantum of vibration ($\Gamma \ll \hbar\omega$), since otherwise there will be a small but constant transmission probability when the molecule is in the vibrational ground state.

Chapter 5

The Langevin Equation

In this chapter, we study various aspects of a Langevin dynamical approach to non-adiabatic dynamics at surfaces. The method is well suited for situations where multiple hot electrons are involved and these are assumed to be described by a thermal distribution. This also includes the zero temperature limit where the Langevin equation becomes a useful tool to investigate non-adiabatic effects in reactions at metal surfaces, which are not assisted by hot electrons. On the other hand, reactions induced by single hot electrons, as relevant to experiments with MIM devices (see Fig. 1.2), are not well suited for this kind of modelling.

As shown in section 3.5, the Langevin equation can be derived from the reduced density matrix. The derivation assumes a certain semiclassical expansion of paths, which becomes exact for quadratic potentials with linear non-adiabatic coupling. The Langevin equation has a classical appearance, but involves an integral over all initial phase space points weighted by the Wigner distribution of the initial vibrational quantum state. In section 5.1, we demonstrate the importance of proper inclusion of the initial quantum state and compare with a classical and a quasiclassical approach. In section 5.2, we investigate the consequences of temporal correlations in the fluctuating forces, and show that at low temperatures, such correlations are needed in order to conserve the energy of the vibrational ground state.

As in section 3.4, we will illustrate applications of the theory by examples of diatomic molecules adsorbed on transition metal surfaces with model parameters obtained from DFT and ΔSCF.

5.1 Quantum Corrections

Since the master equation (3.56) and Langevin equation (3.45) are representations of the reduced density matrix in different basises, one should be able to obtain the same result using either approach. If one is interested in the probability of an adsorbate being in a simple vibrational state, it is natural to apply the master equation, since it gives the temporal evolution of such probabilities directly. For complicated reactions, however, the Langevin equation is preferable, since it gives the probability for the adsorbate to make it to a particular position along a certain reaction coordinate.

To show how quantized states are incorporated into the Langevin equation, we consider a single harmonic oscillator with linear non-adiabatic coupling. The Hamiltonian describing the system is thus given by Eq. (4.1) with a single mode. It is straightforward to take the initial state into account, since it follows from Eq. (3.44) that one should propagate the adsorbate starting from all phase space points and then weigh the result by the Wigner distribution of the initial state. Such a procedure would result in a probability distribution for the adsorbate of being at a particular phase space point (x, p) at time t. For a harmonic potential the time evolution of the classical phase space distribution is identical to that of the Wigner distribution [48] and it is then possible to obtain the probability of being in the vibrational state n at time t. To see this we note that

$$\begin{aligned} p_n(t) &= \langle n|\rho_{red}(t)|n\rangle = \int dxdy\rho_{red}(t;x,y)\varphi_n^*(x)\varphi_n(y) \qquad (5.1)\\ &= \int dudv\rho_{red}(t;u+v/2,u-v/2)\int d\tilde{v}\varphi_n^*(u+\tilde{v}/2)\varphi_n(u-\tilde{v}/2)\delta(v-\tilde{v})\\ &= \frac{1}{2\pi\hbar}\int dudv\rho_{red}(t;u+v/2,u-v/2)\int d\tilde{v}dp\varphi_n^*(u+\tilde{v}/2)\varphi_n(u-\tilde{v}/2)e^{ip(v-\tilde{v})/\hbar}\\ &= 2\pi\hbar\int dudp\mathcal{P}_n(u,p)\mathcal{P}(t;u,p), \end{aligned}$$

where $\mathcal{P}_n(u,p)$ is the Wigner distribution of the pure state density matrix $\rho_n = |n\rangle\langle n|$ and we identify $\mathcal{P}(t;u,p)$ with the classical phase space distribution at time t.

The pure state Wigner distributions in a quadratic potential is given by [48]

$$\mathcal{P}_n(x,p) = \frac{(-1)^n}{\pi\hbar}e^{-\mathcal{H}(x,p)/E_0}L_n(2\mathcal{H}(x,p)/E_0), \qquad (5.2)$$

where $\mathcal{H}(x,p) = p^2/2m + m\omega^2x^2/2$ is the classical Hamiltonian, $E_0 = \hbar\omega_0/2$, and L_n is the n'th Laguerre polynomial. Since $\mathcal{P}_n$ is only a function of the

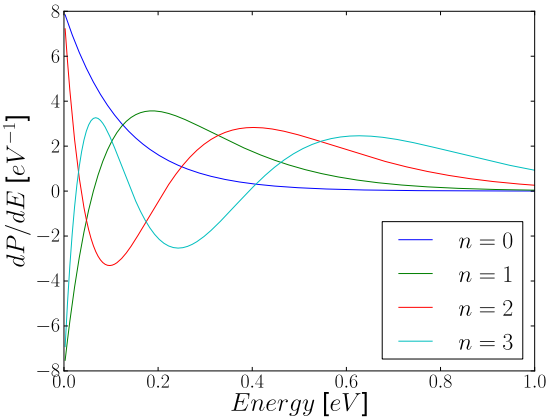

Figure 5.1: The energy distributions given by Eq. (5.5) for the lowest four vibrational states of a harmonic oscillator with zero point energy $E_0 = 0.125\ eV$. The corresponding quasiclassical distributions are deltafunctions centered at $E_0(2n+1)$.

Hamiltonian energy we can write

$$\begin{aligned} p_n &= 2\pi\hbar \int_0^\infty dE \mathcal{P}_n(E) \frac{dP}{dE} \\ &= 2(-1)^n \int_0^\infty dE e^{-E/E_0} L_n(2E/E_0) \frac{dP}{dE}, \end{aligned} \tag{5.3}$$

with

$$\frac{dP}{dE} = \int dx dp \mathcal{P}(x,p) \delta(E - \mathcal{H}(x,p)). \tag{5.4}$$

Note that the distribution dP/dE is not a true probability distribution since it is not strictly positive, but it can be rigorously translated into the quantum mechanical probabilities p_n. On the other hand, we can obtain the distribution dP_n/dE associated with a particular vibrational state $|n\rangle$ by replacing $\mathcal{P}(x,p)$ in Eq. (5.4) with $\mathcal{P}_n(x,p)$. Using that $dxdp = \hbar d\varphi d\mathcal{H}/2E_0$ with φ being a phase space angle, the integral can then be evaluated to

$$\frac{dP_n}{dE} = \frac{(-1)^n}{E_0} e^{-E/E_0} L_n(2E/E_0). \tag{5.5}$$

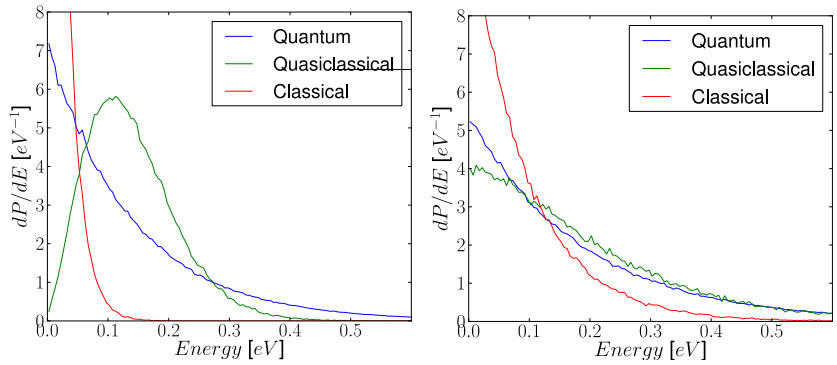

Figure 5.2: The continuous energy distributions dP/dE obtained from Langevin dynamics with a constant $T_{el} = 4000$ using quantum, quasiclassical, and classical boundary conditions. The initial quantum state is the vibrational ground state. Left: $t = 0.1\ ps$. Right: $t = 0.5\ ps$. After a while both the quasiclassical and classical distributions approach the quantum distribution.

The distributions Eq. (5.5) are shown in Fig. 5.1 for the first four vibrational states with $E_0 = 0.125\ eV$. The structure of the distributions is in sharp contrast to that obtained in the quasiclassical (QC) approach, where the energy is fixed at E_n and the energy distribution of the n'th state is $dP_n^{(QC)}/dE = \delta(E - E_n)$ with $E_n = \hbar\omega(n + 1/2)$. This gives rise to completely different and and even negative probabilities. For example, using $dP_0^{(QC)}/dE = \delta(E - E_0)$ immediately yields $p_0 = p_1 = -p_2 = 0.74$ from Eq. (5.3).

We have performed Langevin dynamics using Eqs. (3.45) and (3.54) within the Markov approximation (3.53) using the parameters $m = 6.86\ amu$, $\hbar\omega_0 = 0.25\ eV$, $\varepsilon_0 = 2.6\ eV$, $\Gamma = 2.0\ eV$, and $f = 8.7\ eV/\AA$. These parameters were chosen to mimic the internal vibrational mode of CO adsorbed on Cu(100) considered below, but presently we will just think of them as a realistic set of parameters, which we use to compare different model calculations. The adsorbate is initially in its ground state described by the Wigner distribution

$$\mathcal{P}_0(x_0, p_0) = \frac{1}{\pi\hbar} e^{-x_0^2/x_Q^2 - p_0^2/p_Q^2}, \tag{5.6}$$

with the quantum length and momentum given by

$$x_Q = \sqrt{\hbar/m\omega}, \qquad p_Q = \sqrt{\hbar m\omega}. \tag{5.7}$$

The distribution is even in both momentum and position and since the frictional decay is much slower than the vibrational time of oscillation, the final state phase space distribution can be assumed to be even in the initial phase space point. For simplicity we assume a constant electronic temperature at $T_{el} = 4000\ K$ and integrate the Langevin equation for $t = 1\ ps$. For each point on an initial (6x6) positive phase space grid with a spacing $0.5x_Q \times 0.5p_Q$, we run a large number of Langevin trajectories (~ 30000) and record the final state energy. The final state energy distribution is then obtained by summing the distributions resulting from each initial phase space point $dP/dE(E; x_0, p_0)$ weighted by the initial state Wigner distribution $\mathcal{P}(x_0, p_0)$:

$$\frac{dP(E)}{dE} = \int dx_0 dp_0 \mathcal{P}(x_0, p_0) \frac{dP(E; x_0, p_0)}{dE}. \tag{5.8}$$

In Fig. 5.2 we show this distribution at $t = 0.1\ ps$ and $t = 0.5\ ps$ along with the distributions resulting from quasiclassical (initial phase space points with $\mathcal{H}(x_0, p_0) = E_0$) and classical initial condition (initial phase space point $x_0 = p_0 = 0$). On long time scales the distributions will forget the initial conditions and approach a Boltzmann distribution at the appropriate temperature. However, on timescales less than a picosecond there is still plenty of memory of the initial state and the classical and quasiclassical distributions, which start as delta functions at $E = 0$ and $E = E_0$ respectively, are completely wrong at timescales on the order of 0.1 ps. The quasiclassical initial conditions approach the correct distribution faster than the classical one since the initial state contains the right amount of energy, which just needs to be redistributed.

With the interaction Hamiltonian $H_I = -fc_a^\dagger c_a x$ it is easy to calculate the transition rates Eq. (3.58) with the result:

$$\begin{aligned} W_{m\to n} =& m\delta_{m,n+1} \frac{\pi f^2}{M\omega} \int d\varepsilon \rho_a(\varepsilon)\rho_a(\varepsilon + \hbar\omega) n_F(\varepsilon)\big(1 - n_F(\varepsilon + \hbar\omega)\big) \\ &+ (m+1)\delta_{m,n-1} \frac{\pi f^2}{M\omega} \int d\varepsilon \rho_a(\varepsilon)\rho_a(\varepsilon - \hbar\omega) n_F(\varepsilon)\big(1 - n_F(\varepsilon - \hbar\omega)\big). \end{aligned} \tag{5.9}$$

Using the parameters above we can then integrate the master equation Eq. (3.56) and compare the probabilities p_n with those obtained from the Langevin equation Eqs. (5.3) and (5.8). This is shown in Fig. 5.3 for the four lowest vibrational states. As expected we see a close correspondence between the master equation approach and Langevin dynamics with correct phase space sampling. In contrast, the classical initial conditions result in completely wrong probabilities

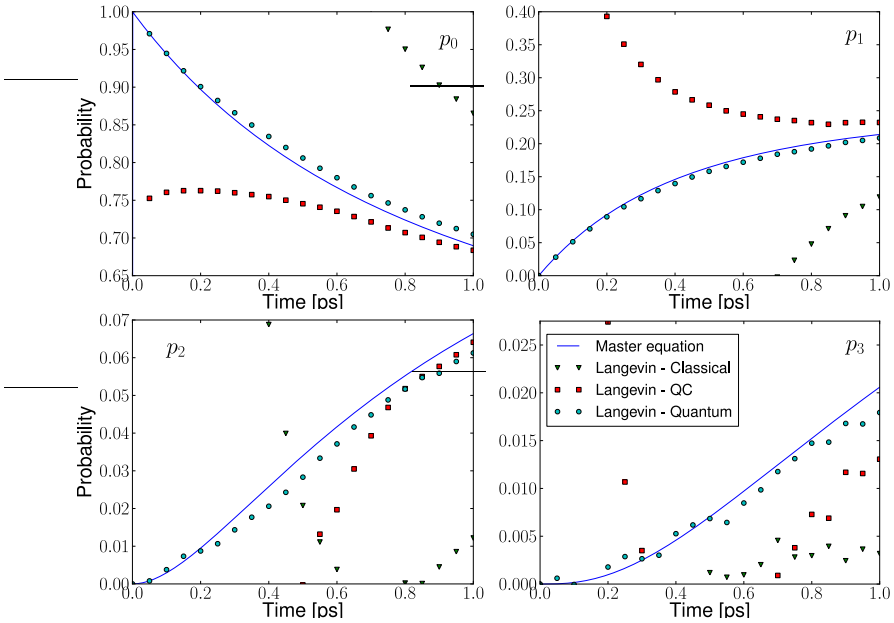

Figure 5.3: The time dependent probabilities p_n for being in the vibrational state $|n\rangle$ obtained with the master equation and Langevin dynamics with three kinds of initial conditions. The correct quantum initial conditions are seen to give results nearly identical to the master equation, whereas the classical and quasiclassical initial conditions give wrong results.

and the quasiclassical initial conditions only result in sensible probabilities after $\sim 0.5\ ps$.

It should be noted, that the quasiclassical initial conditions gives a good description of average quantities and the average energy $\langle E \rangle = \sum_n p_n E_n$ is very well approximated by the quasiclassical approach, even at short timescales. However, if one were to model a surface reaction with a barrier by a truncated harmonic potential the quasiclassical approach is likely to fail. For example, the adsorption energy of CO on Cu(100) is $\sim 0.6\ eV$ and as a simple model for hot electron induced desorption one could use the present oscillator truncated above the desorption energy. This means that $p_2 + p_3$ would be a measure of the desorption probability and from Fig. 5.3 it is clear that for times $< 0.5\ ps$

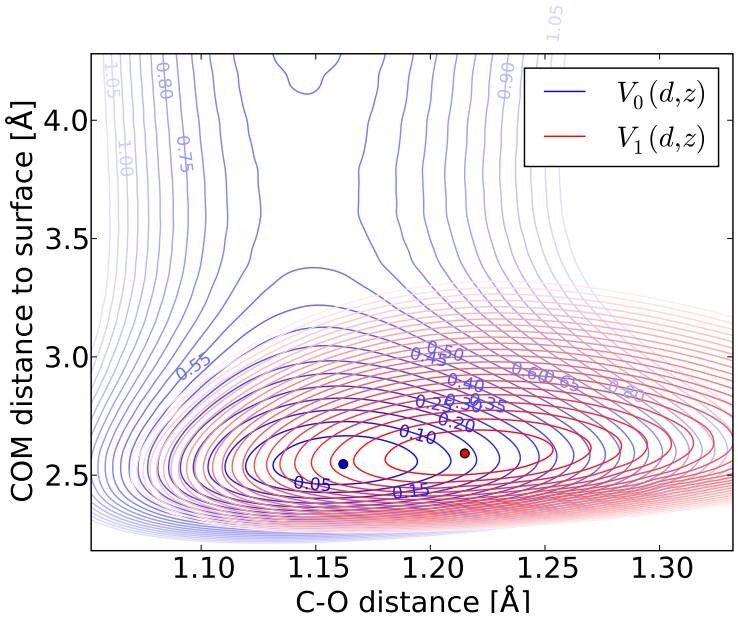

Figure 5.4: Potential energy surfaces for the ground and excited state of CO adsorbed at a Cu(100) top site. The contours are at 0.05 eV intervals and the desorption barrier is at 0.57 eV. The extra electron in the anti-bonding 2π orbital is seen to stretch th C-O bond. The center of mass is moved slightly out from the surface in spite of the attraction to the image charge.

one would severely miscalculate the desorption probability.

Example: Desorption of CO from Cu(100)

As an example illustrating the effect of including the initial quantum state, we consider the case of desorption of CO from Cu(100) mediated by transient excitation of the CO 2π resonance. The ground and excited state potential energy surfaces has been calculated with the code `GPAW` and is shown in Fig. 5.4 in terms of the COM and internal stretch coordinates. Within the Markov approximation the Langevin equation for multiple modes is

$$\xi_i(t) = M\ddot{x}_i(t) + \frac{\partial V_0(u)}{\partial x_i} + \sum_j \eta_{ij}(x)\dot{x}_j(t'), \tag{5.10}$$

	$\hbar\omega_i$	$f_i(\varepsilon_F)$	$M_i/\eta_{ii}(0;0)$
Internal	0.248 eV	4.3 eV/Å	2.7 ps
COM	0.043 eV	-3.6 eV/Å	16 ps

Table 5.1: Parameters for the internal vibration and center of mass mode for CO adsorbed on a Cu(100) top site.

where the static friction tensor is given by

$$\eta_{ij}(x) = \frac{-\hbar}{\pi}\int_{-\infty}^{\infty} d\varepsilon \left(\frac{\Gamma(x)/2}{(\varepsilon-\varepsilon_a(x))^2+(\Gamma(x)/2)^2}\right)^2 f_i(\varepsilon;x) f_j(\varepsilon;x)\frac{dn_F(T;\varepsilon)}{d\varepsilon}, \tag{5.11}$$

with

$$f_i(\varepsilon;x) = \frac{\varepsilon_a(x)-\varepsilon}{\Gamma(x)}\cdot\frac{\partial\Gamma(x)}{\partial x_i} - \frac{\partial\varepsilon_a(x)}{\partial x_i}, \tag{5.12}$$

and the correlation function of the Gaussian distributed stochastic forces is

$$\langle \xi_i(t)\xi_j(t')\rangle = 2k_B T_{el}\eta_{ij}\delta(t-t'). \tag{5.13}$$

In addition to the potential energy surfaces, which determine $\varepsilon_a(x)$, we also need the position dependent resonance width $\Gamma(x)$. We assume that the width does not depend on the internal stretch coordinate and has an exponential decay in the COM coordinate such that $\Gamma \sim \Gamma_0 e^{-(z-z_0)/z_\Gamma}$, where z_0 is the COM minimum position and z_Γ and Γ_0 are estimated from the projected density of state at various COM positions. We find $z_\Gamma = 0.7$ *Å* and $\Gamma_0 = 2$ eV and the desorption energy is determined to be $E_D = 0.57$ eV in excellent agreement with the experimental value [96].

The ground state potential energy surface is well approximated by a quadratic potential in the internal mode and a Morse potential in the center of mass mode. The two modes are nearly decoupled and in Tab. 5.1 we display the parameters associated with the two modes at the ground state minimum. Since the friction tensor is additive in contributing orbitals, we can simply multiply the expression (5.11) by a factor of four to account for the degeneracy of the 2π orbital and spin, or equivalently, multiply the frictional force by a factor of two, which for the internal mode, reproduces the parameters used to produce Figs. 5.2 and 5.3. The excitation energy at the ground state minimum is $\varepsilon_0 = 2.6$ eV and the

diagonal elements of the friction tensor Eq. (5.11) at the equilibrium position and zero temperature can be roughly related to the vibrational lifetimes of the modes: $\tau_i = M_i/\eta_{ii}$. We note that the calculated vibrational lifetimes in Tab. 5.1 are in good agreement with previous calculations using a different method [84, 45, 104].

To model a particular surface experiment where a femtosecond laser pulse induces a surface reaction, one would need a detailed model for the time dependent distribution of hot electrons resulting from the laser pulse. Here we just wish to examine the qualitative impact of including quantum initial states in the dynamics and therefore, we will take a very simple model for the hot electrons and assume a thermal pulse with a Gaussian temporal shape $T_{el}(t) = T_{max}e^{-t^2/2\Delta t^2}$ with $T_{max} = 4000\ K$ and $\Delta t = 0.5\ ps$. Under the influence of this pulse we have performed Langevin dynamics with Eq (5.10) with classical quasiclassical and quantized initial conditions in both the internal and center of mass mode using the potentials shown in Fig. 5.4. The Langevin equation is integrated from 2 ps prior to the center of the pulse to 4 ps after the center of the pulse. Due to the very weak coupling between the two modes, the initial conditions of the internal mode have almost no influence on desorption probabilities. With fully quantized initial conditions (vibrational ground state) of the COM mode we find a desorption probability of $P_{Quan} = 3.7 \times 10^{-6}$, whereas we find $P_{QC} < \times 10^{-6}$ and $P_{Clas} < 10^{-6}$ when using quasiclassical and classical initial conditions respectively (10^6 trajectories did not result in a single desorption event). We note, that when calculating the fluctuating forces Eq. (5.13), it is most important to take into account the correlation between the two modes determined by the off-diagonal elements of the friction tensor.

Although a quantization of the internal mode does not influence the desorption probability it may have a large impact on the distribution of vibrational states of the desorbed molecules. Due to the low desorption probabilities we have started the molecule with a COM momentum of $p = 3p_Q$ corresponding to $0.19\ eV$, since otherwise we were not able to get good statistics for the energy distribution of desorbed molecules. However, because of the very weak coupling between the two modes, we do not expect this to have a large influence on the internal energy distribution. The resulting vibrational distributions of desorbed molecules can be translated into a distribution of vibrational states p_n using Eq. (5.3). The classical initial conditions lead to $p_0 > 1$ and $p_1 < 0$ whereas quasiclassical initial conditions give $p_1/p_0 = 0.22$ and quantized initial conditions give $p_1/p_0 = 0.092$, which is in agreement with Ref. [96]. In general, quasiclassical initial conditions tend to overestimate p_1 and underestimate p_0 and p_2 as is seen in Fig. 5.3. In the present case, the error on p_1/p_0 is more than

a factor of two. For long interaction times and high temperatures the quasiclassical approximation becomes better and we have repeated the above analysis with $T_{max} = 6000\ K$, which yields close agreement between the vibrational probabilities resulting from quasiclassical and quantized initial conditions.

For additional details on this system we refer to **paper IX**.

5.2 Memory Effects

The Langevin equation was derived by tracing out the electronic degrees of freedom from the density matrix of the full system. The result is a simple classical equation for the adsorbate coordinate, but the price to be paid for this severe reduction of degrees of freedom, is the emergence of a stochastic force with memory as is evident from Eqs. (3.47) and (3.52). The physical origin of the stochastic force is a combination of thermal and quantum fluctuations in the electron gas interacting with the adsorbate and the memory simply reflects that if a stochastic force has the value F_0 at a given time, then it is most likely to have a similar value immediately after. In reality, the memory does not extend beyond the duration of a typical quantum fluctuation and when integrating the Langevin equation one only needs to take into account the previous stochastic forces in a time interval on the order of a fluctuation.

When a reaction is driven by hot electrons the stochastic force is typically dominated by thermal fluctuations and the duration of a fluctuation is on the order $\tau_T \sim \hbar/k_B T_{el}$ where T_{el} is a temperature used to describe the distribution of hot electrons. When the time step Δt needed to integrate the Langevin equation becomes much larger than the timescale of fluctuations $\Delta t \gg \tau_T$, one obtains the well known Markov expression (5.13), where the stochastic forces are uncorrelated in time. For molecules like N_2 and, CO the oscillatory period for the internal vibrational mode is on the order of $\sim 15\ ps$ and with a standard Verlet integration method, one typically needs a timestep of $\Delta t = 1\ ps$ to describe the ground state. A first estimate of the validity of the Markov approximation can thus be obtained as: $T_{el} \gg \hbar/(\Delta t k_B) \sim 2900\ K$, but to get a better quantitative estimate of the validity of the Markov approximation, we can consider the correlation time t_c given by

$$t_c^2 = \frac{\int dt t^2 K(t)}{\int dt K(t)}. \tag{5.14}$$

It should be noted that the correlation time is only a function of the electronic system and does not depend on the non-adiabatic coupling f. We have calcu-

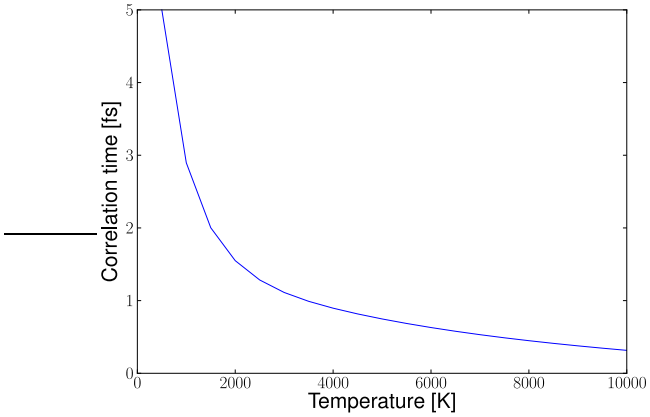

Figure 5.5: The correlation time Eq. (5.14) as a function of temperature. Below 3500 K the correlation time becomes larger than a femtosecond, which is the largest time step we can use in the molecular dynamics, and non-Markovian processes therefore begins to influence the dynamics below this temperature.

lated t_c as a function of temperature and the result is shown in Fig. 5.5. For molecular dynamics requiring a time step no larger than $\sim 1\ fs$, we see that the correlation time becomes larger than this when the electronic temperature comes below 3500 K. Thus, below this temperature non-Markovian processes play an important role in the dynamics.

5.2.1 Quadratic Potential

The fluctuating force $\xi(t)$ in the Langevin equation, vanishes within the Markov approximation Eq. (3.53) when $T_{el} \to 0$. With a quadratic potential it is then possible to solve the Langevin equation analytically, which gives the time-dependent energy

$$E_{Markov}(t) = E_0 e^{-t/\tau}, \qquad \tau = 2M/\Lambda(0), \tag{5.15}$$

where E_0 is the initial energy. However, as discussed in section 5.1 the Langevin equation is quantum mechanically exact for a harmonic potential if the initial conditions are accounted for correctly and the total energy should thus not be allowed to decay below $\hbar\omega_0/2$. The problem is that the Markov approximation

neglects all non-thermal excitations of the electronic system and leads to pure dissipation at $T_{el} \to 0$. In reality, an oscillating adsorbate will induce (non-thermal) excitations of the electron gas, which may then influence the propagation of the adsorbate. In general, it is therefore expected that the Markov approximation tends to underestimate the influence of the electronic system on the adsorbate. This non-Markovian effect should vanish at high temperatures, where thermal excitations of the electronic system dominate.

In Fig. 5.6 we show the time evolution of the average energy of a harmonic oscillator interacting with a thermal reservoir of electrons at six different temperatures. The average energy is calculated using the full non-Markovian correlation function (3.47) and within the Markov approximation (3.53). The initial state was chosen as the vibrational ground state and included exactly by phase space sampling the Wigner distribution as described in section 5.1. The parameters used are chosen as $\Gamma = 2.0\ eV$, $\varepsilon_0 = 2.6\ eV$, $\hbar\omega = 0.25\ eV$, and $f = -8.7\ eV/\AA$, which are the same values used in Figs. 5.2 and 5.3. The failure of the Markov approximation and resulting decay of the average energy is clearly seen at low temperatures. In particular, at $T_{el} = 500\ K$ the Markov approximation gives rise to exponentially decaying energy whereas the energy remains nearly fixed at $E \approx E_0$ when memory effects are included. For high temperatures ($T_{el} > 3000\ K$), thermal excitations dominate and the Markov approximation becomes reliable. In all calculations we have converged the results by decreasing the time steps.

In Fig. 5.7 we show the average energy of the harmonic oscillator after 5 ps of interaction with a thermal reservoir of electrons. The energy is calculated with non-Markovian Langevin dynamics, Markovian Langevin dynamics, the master equation with rates obtained from Eq. (3.58), and the master equation with exact rates (3.59). The non-Markovian Langevin approach matches the exact non-perturbative Master equation approach, whereas the perturbative Master equation fails at high temperatures and the Markovian Langevin approach fails at low temperatures. It may be surprising that the non-Markovian Langevin equation reproduces the exact and not the perturbative master equation. However, as described in section 3.5, the perturbative derivation of the master equation is based on a direct evaluation of the reduced density matrix to second order in the non-adiabatic coupling, while the Langevin equation is derived by constructing an effective action to second order in the non-adiabatic coupling. Thus, while the reduced density matrix calculated from the effective action only becomes exact in the small friction limit, it does contain terms to all orders in the non-adiabatic coupling and is a much better approximation for large frictional coupling and high temperatures than the direct perturbative

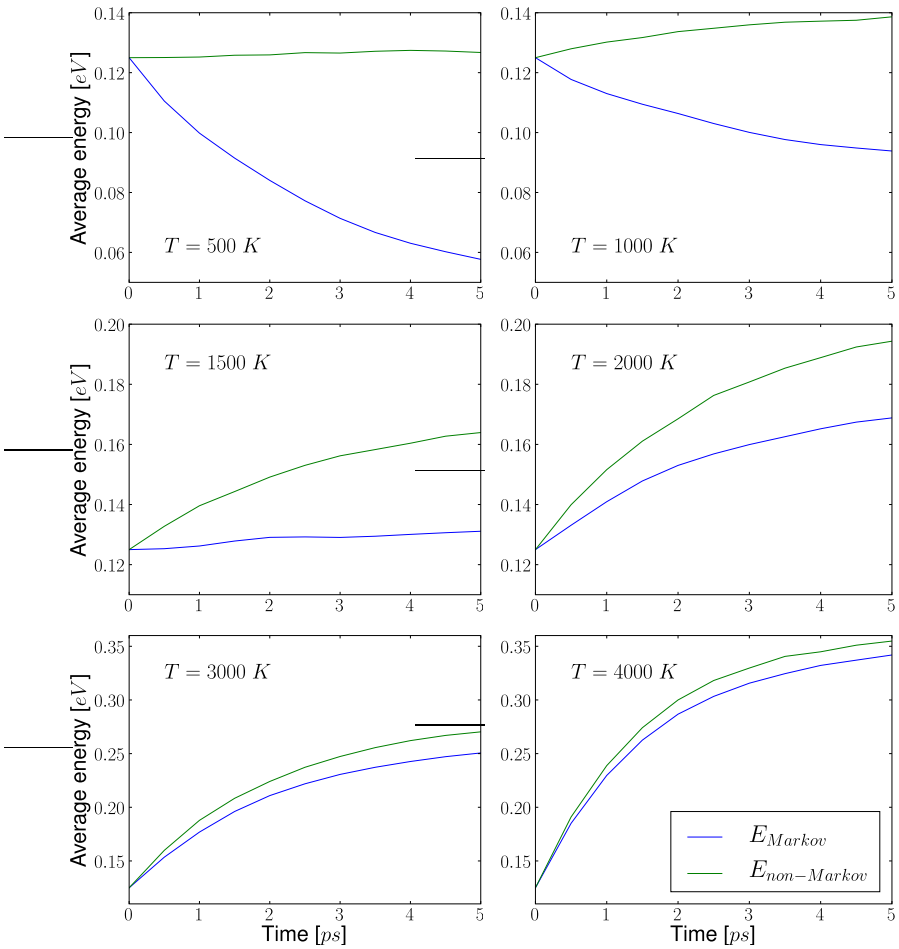

Figure 5.6: Average energy of a harmonic oscillator interacting with a thermal reservoir of electrons at six different temperatures evaluated using Langevin dynamics with memory and using the Markov approximation. The Markov approximation fails below $T_{el} = 3000\ K$ where quantum fluctuations are important.

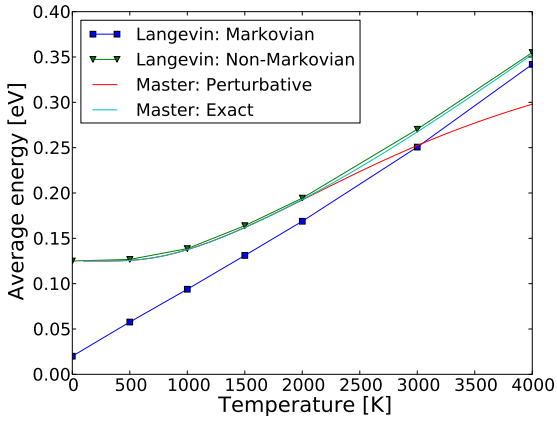

Figure 5.7: Average energy of a harmonic oscillator after 5 *ps* of interaction with a thermal reservoir of hot electrons. The non-Markovian Langevin equation and the non-perturbative master equation both give the correct dependence, whereas the Markovian Langevin equation fails at low temperatures and the perturbative master equation fails at high temperatures.

derivation leading to the master equation Eq. (3.56).

It may seem like a complete overkill to apply a non-adiabatic Langevin dynamics to a harmonic potential when the results are readily obtainable from the master equation approach. However, for anharmonic potentials it is not possible to derive transition rates for the master equation exactly and the best approximation is then the non-Markovian Langevin equation.

Example: Associative Desorption of N_2 from Ru(0001)

As an example of a potential where the master equation approach is not readily applicable, we consider the well-known reaction of associative desorption of N_2 from Ru(0001). This system has been subject to extensive experimental [23, 22, 76] and theoretical [76, 20, 21, 19, 63] studies and much evidence points to a non-adiabatic dissipation of energy during associative desorption. In contrast to other examples in the present thesis, this example does not involve hot electrons, but for comparison with experiment we consider a substrate and thus electronic temperature of $T = 900\ K$

We are not aiming at a detailed quantitative study, but we wish to investigate

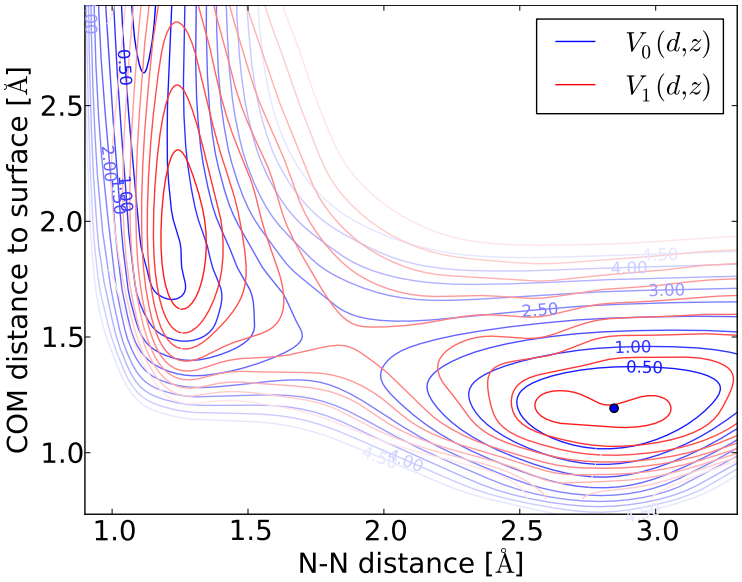

Figure 5.8: Ground and excited state potential energy surfaces of N_2 adsorbed on Ru(0001). The excited state was obtained by occupying the 2π orbital of N_2.

the qualitative effects of including memory in a Langevin dynamical approach to the problem. We thus restrict ourselves to the COM and internal stretch degrees of freedom with the molecular axis being parallel to the surface. For details on this desorption path we refer to Murphy et al. [76]. The ground and excited state potential energy surfaces has been calculated with the DFT code `GPAW` in terms of these coordinates and are shown in Fig. 5.8. We wish to integrate the Langevin equation (5.10) using a two-dimensional version of the correlation function (3.47), as well as within the Markov approximation (5.13). The position dependent resonance width is approximated by $\Gamma(x) = \Gamma_0 e^{-(z-z_t)/z_\Gamma}$ with $\Gamma_0 \approx 3.0\ eV$ and $z_\Gamma \approx 0.5\ \AA$. Here, z is the COM coordinate and z_t is its value at the transition state.

To examine the impact of non-adiabatic dissipation of energy and, in particular, the validity of the Markov approximation, we have considered four representative initial conditions leading to desorption. All four are initially at the transition state with a kinetic energy of 0.1 eV. The kinetic energy is then

Mode	z-	z+	d-	d+
Markovian	0.31	0.49	0.079	0.10
non-Markovian	0.13	0.42	0.053	0.10

Table 5.2: Average energy loss (all numbers in eV) of trajectories leading to desorption for four different initial conditions with and without the Markov approximation at $T = 900\ K$. The initial conditions were all at the transition state with a kinetic energy of 0.1 eV. d and z denotes initial momentum in the internal vibrational mode and the center of mass mode respectively and - and + denotes the sign of the initial momentum. In general, the Markov approximation tends to underestimate the effect of fluctuating forces, which results in too much dissipation.

concentrated in positive or negative center of mass momentum or positive or negative internal momentum. Table 5.2 displays the average energy loss in a desorption event of the four initial conditions with and without the Markov approximation. The reason for the large difference is due to the average time spend in the exit channel, which for initial negative internal momentum is $\sim 125\ fs$ and for initial positive center of mass momentum is $\sim 250\ fs$. The shift to lower dissipation in non-Markovian dynamics is what we would expect from Fig 5.6 and in general, memory effects seems to increase the importance of fluctuating forces and thus decrease the overall dissipation of energy.

Chapter 6

Summary and Outlook

Since it is nearly impossible to handle the full Hamiltonian (1.1), the solution to a particular non-adiabatic problem starts with an approximation, which captures the essential physics of the problem. In the present thesis, we have analyzed various models of non-adiabatic dynamics at surfaces based on potential energy surfaces and the model Hamiltonian (3.9). The main tools for obtaining the potential energy surfaces, have been DFT and its ΔSCF extension, which were generalized to include non-stationary states in section 2.2.

A model of inelastic scattering has been used to obtain probabilities for reactions mediated by single hot electrons for a range of systems. A major problem with this model is that perturbation theory does not apply when one is interested in large energy transfer, and we are restricted to quadratic potentials and the wide band limit, where the excitation probabilities can be obtained exactly. The price to pay for this simplification is that a product state cannot be properly defined, and one has to identify the reaction probability with the probability of reaching the reaction energy in the harmonic potential. For diatomic molecules on transition metals, the dominating channel of energy transfer is the internal vibrational mode, which is well described by a harmonic oscillator, and we expect the quadratic model to give a realistic estimate of the probability for transferring a given amount of energy into this mode. In section 4.1 we have assumed that a molecule will simply desorb if it has enough energy in any of the vibrational modes combined (Fig. 4.3). However, one could estimate the actual desorption probability given an internal vibrational state of the molecule and

the *ab initio* potential energy surfaces Fig. 4.1, using Langevin dynamics with frictional decay of the vibrational state Eq. (5.11) and phase space sampling of the internal vibrational state. Although we have not pursued this aspect of the desorption dynamics, the calculations should be straightforward and it would certainly be interesting to get an estimate of the effect of anharmonic coupling, as well as a comparison of different transition metals. For example, the normal modes of CO on Cu(100) are much closer to those of the free molecule than for CO on Pt(111), which indicates a weaker anharmonic coupling in the former case.

Another drawback of the inelastic scattering model is the wide band approximation, in which the resonant projected density of states becomes a Lorentzian. For alkali metals, which have only s valence electrons, the approximation is expected to work well, since the s-band is rather broad and flat. In contrast, the transition metals, which we are particularly interested in, have a d-band, which tends to introduce a splitting of resonances into bonding and anti-bonding states. For the noble metals, the d-band is well situated below the Fermi level and the wide band approximation is expected to be well justified for unoccupied states, but when one moves to the left in the periodic table, the d-band approaches the unoccupied states and the wide band approximation becomes progressively worse. This picture is confirmed by the Kohn-Sham projected density of states, which starts to deviate from a Lorentzian when one moves to the left in the periodic table starting from the noble metals. The derivation of the expression for inelastic scattering amplitudes (3.26)-(3.28), assumes that the resonance is initially unoccupied, but if the d-band splits the resonance and the lower part moves below the Fermi level, this assumption breaks down and one needs to derive a scattering amplitude, which incorporates the Fermi level. This is already evident in the 2π resonance of CO on Pt(111) shown in Fig. 4.2, where it is seen that the projected density of states has a tail extending below the Fermi level.

In the case of reactions induced by multiple hot electrons, we have derived a power law for the dependence of reaction yield on electron flux. The derivation is only valid for quadratic potentials and the power law will most likely break down for anharmonic potentials. However, the internal mode of diatomic molecules is typically well approximated by a quadratic potential and if this mode constitutes the dominating channel for hot electron mediated energy transfer, then the quadratic model is well justified and the interpretation of the power law exponent is maintained. Nevertheless, there is still an implicit assumption of rapid anharmonic energy transfer to the reaction mode, which needs to be verified as discussed above. It should also be possible to use perturbation theory

to derive decay rates between vibrational states in anharmonic potentials and extend the model to arbitrary potential energy surfaces.

When multiple hot electrons are involved, a reaction can be induced by sequential climbing of the vibrational states of the potential. This allows for perturbative calculations of transition probabilities and the inelastic scattering model can be extended to, for example, a Morse potential, where it is possible to obtain adsorbate velocity distributions induced by hot electrons. In Fig. 4.7 we showed the velocity distribution resulting from direct desorption induced by hot electrons, given an initial vibrational state n. All vibrational transitions of the Morse potential are possible within first order perturbation theory, but we expect the fidelity of perturbation theory to decrease when the energy difference involved in the transitions increases. Thus, for the velocity distributions in Fig. 4.7, the large n calculations are trustworthy whereas the small n calculations are more dubious. The most interesting part of the experimental observations shown in Fig. 4.9, is the low velocity peak, which we believe originate from the highest vibrational state, and that transition is well represented within perturbation theory. However, we cannot exclude that higher order perturbation theory could yield low velocity distributions for the lower vibrational states as well, and it would therefore be very interesting to investigate how second order perturbation theory modifies the results.

In addition to inelastic scattering we have studied the Langevin dynamics approach to hot electron mediated dynamics at surfaces. The method is only applicable to adsorbates interacting with a thermal reservoir of electrons and therefore rests on the assumption of rapid thermalization of hot electrons following, for example, excitation by a laser pulse. This raises the question of the role of nascent non-thermal electrons and it would be very interesting to compare with inelastic scattering models, which can handle any distribution of hot electrons. However, such a study would again require inelastic scattering using many-particle states and a Fermi level as discussed above.

We have analyzed the effect of proper initial state phase space sampling in Langevin dynamics, and compared with quasiclassical and classical initial conditions. For a one-dimensional truncated harmonic oscillator, the initial state is the only quantum mechanical effect and the Langevin equation becomes exact for small frictional coupling. This allows for a comparison with a master equation approach and, as expected, the agreement is excellent. Applied to an *ab initio* potential energy surface, such as the desorption potential of CO from Cu(100), we only observe a small effect on the desorption probability, but a

significant effect on the distribution of vibrational states of desorbed molecules.

The static friction calculated from the Kohn-Sham states described in appendix A, gives a true *ab initio* expression, where one does not have to consider, which physical process gives rise to the non-adiabatic coupling. In the present thesis, we have chosen to perform Langevin dynamics with the electronic friction and fluctuating forces derived from the model Hamiltonian (3.9) and potential energy surfaces. With that method, one has to know the nature of the resonance, which gives rise to the friction as well as the resonant spectral properties as a function of position, and it may seem like a completely inferior method compared to the Kohn-Sham approach. However, the derivation of the Langevin equation from the model Hamiltonian has the great advantage that it yields the exact correlation function of fluctuating forces and it becomes possible to study the effect of temporal correlations. We have shown that, for a harmonic oscillator, temporal correlations is needed in order to conserve energy of the vibrational ground state and, in general, neglecting temporal correlations tends to overestimate the role of non-adiabatic dissipation of energy. Our calculations were based on a very simple assumption for the frictional force, but it would be interesting to do non-Markovian Langevin dynamics with the Kohn-Sham based semi-empirical correlation function given in Eq. (A.15).

As a final remark we wish to point to the existence of several studies of non-adiabatic dynamics using different theoretical approaches than those presented in this thesis [113, 32, 89, 90, 105]. Like inelastic scattering and Langevin dynamics, these approaches have their advantages as well as shortcomings and the best choice of model depends on the nature of a particular problem.

Appendix A

Non-Adiabatic Energy Transfer from Classical Trajectories

If the nuclear degrees of freedom are assumed to be well approximated by a classical trajectory $x(t)$, it is possible to derive a model-independent expression for non-adiabatic energy transfer. The analysis is well-known and we will follow the derivation of Trail et al. closely [103]. For a classical trajectory the nuclear coordinates enter as parameters in the full Hamiltonian (1.1) and we can construct the trajectory-dependent electronic Hamiltonian

$$H[x(t)] = T_{el} + V_{el} + V_{ext}[x(t)], \tag{A.1}$$

where T_{el} is the electronic kinetic energy, V_{el} is the electron-electron interaction and V_{ext} is the electron-nuclei interaction, which depends on the trajectory $x(t)$. The instantaneous expectation value of the energy is then $E(t) = \langle\psi(t)|H[x(t)]|\psi(t)\rangle$, where $|\psi(t)\rangle$ is the time-dependent many-electron state, which is governed by the Scrödinger equation $i\hbar|\dot{\psi}(t)\rangle = H[x(t)]|\psi(t)\rangle$. The change in energy is

$$\begin{aligned}\dot{E}(t) &= \langle\dot{\psi}(t)|H[x(t)]|\psi(t)\rangle + \langle\psi(t)|H[x(t)]|\dot{\psi}(t)\rangle + \langle\psi(t)|\frac{d}{dt}H[x(t)]|\psi(t)\rangle \\ &= \langle\psi(t)|\frac{d}{dt}V_{ext}[x(t)]|\psi(t)\rangle,\end{aligned} \tag{A.2}$$

where the Scrödinger equation was used to cancel the first two terms. $E(t)$ represents the total change in electronic energy along the trajectory $x(t)$, but we are only interested in the-non-adiabatic energy transfer. To obtain this we can subtract the adiabatic part $E_0(t)$, defined as the eigenvalue of the instantaneous ground state $|\psi_0(t)\rangle$, which satisfies $H[x(t)]|\psi_0(t)\rangle = E_0(t)|\psi_0(t)\rangle$. The change in adiabatic energy can be written

$$\begin{aligned}\dot{E}_0(t) &= \langle\dot{\psi}_0(t)|E_0(t)|\psi_0(t)\rangle + \langle\psi_0(t)|E_0(t)|\dot{\psi}_0(t)\rangle + \langle\psi_0(t)|\frac{d}{dt}H[x(t)]|\psi_0(t)\rangle \\ &= \langle\psi_0(t)|\frac{d}{dt}V_{ext}[x(t)]|\psi_0(t)\rangle, \end{aligned} \tag{A.3}$$

where we used $\frac{d}{dt}\langle\psi_0(t)|\psi_0(t)\rangle = 0$ to cancel the two first terms.[1] The non-adiabatic rate of change in energy can now be written

$$\dot{E}_{non-ad}(t) = \dot{E}(t) - \dot{E}_0(t) = \dot{x}(t)\int d\mathbf{r}\frac{d}{dx}V_{ext}[\mathbf{r};x(t)]\delta n(\mathbf{r},t), \tag{A.4}$$

where $\delta n(\mathbf{r},t) = n(\mathbf{r},t) - n_0(\mathbf{r},t)$ and n and n_0 are the densities of $|\psi\rangle$ and $|\psi_0\rangle$ respectively.

If one assumes weak non-adiabatic coupling the change in density can be evaluated within linear response and δn can be written

$$\delta n(\mathbf{r},t) = \int_{-\infty}^{t} dt' \int d\mathbf{r}'\chi(\mathbf{r},\mathbf{r}',t-t';x(t))\delta V(\mathbf{r}',t'), \tag{A.5}$$

where $\chi(\mathbf{r},\mathbf{r}',t-t';x(t))$ is the electronic linear density response function and δV is the change in external potential resulting from a change in nuclear coordinates. If it is assumed that the electronic response time is much faster than the timescale of nuclear motion, we can write

$$\delta V(\mathbf{r},t') = \frac{dV_{ext}(\mathbf{r};x(t))}{dx}(x(t') - x(t)), \tag{A.6}$$

and equation (A.4) becomes

$$\dot{E}_{non-ad}(t) = \dot{x}(t)\int_{-\infty}^{t} dt'\widetilde{\Lambda}[t-t';x(t)]x(t'), \tag{A.7}$$

[1] The derivation is nothing but a variant of the well-known Hellman-Feynman theorem, which states that the derivative of an adiabatic potential energy surface can be evaluated as $\langle\psi(t)|\nabla V_{ext}(x)|\psi_0\rangle$.

with the memory function

$$\widetilde{\Lambda}[t-t';x(t)] = \int d\mathbf{r}d\mathbf{r}' \frac{dV_{ext}(\mathbf{r};x(t))}{dx}\Big[\chi(\mathbf{r},\mathbf{r}',t-t';x(t)) - \delta(t-t')\int_{-\infty}^{t} dt''\chi(\mathbf{r},\mathbf{r}',t-t'';x(t))\Big]\frac{dV_{ext}(\mathbf{r}';x(t))}{dx}. \tag{A.8}$$

The adsorbate equation of motion can now be obtained by imposing energy conservation on the combined adsorbate-electron system. The adsorbate energy is $E_0 = M\dot{x}^2/2 + V_0(x)$ and equating its temporal derivative with $-\dot{E}_{non-ad}(t)$ finally gives

$$M\ddot{x}(t) + \frac{dV_0}{dx} = -\int_{-\infty}^{t} dt'\widetilde{\Lambda}[t-t';x(t)]x(t'), \tag{A.9}$$

and the usual velocity dependent frictional force can be obtained by performing a partial integration on the right hand side.

It is instructive to consider the Fourier transform of (A.8), which becomes

$$\widetilde{\Lambda}(\omega;x) = \int d\mathbf{r}d\mathbf{r}' \int_0^{\infty} dt' \frac{dV_{ext}(\mathbf{r};x)}{dx}\chi(\mathbf{r},\mathbf{r}',t';x)\Big[e^{-i\omega t'}-1\Big]\frac{dV_{ext}(\mathbf{r}';x)}{dx}, \tag{A.10}$$

where we have put $x \equiv x(t)$. The Markov approximation is obtained by taking the low frequency limit of this expression and Taylor expanding to first order in ω. We thus write $\Lambda(\omega,x) = -i\omega\eta(x)$ with $\eta(x)$ being the first derivative of the memory function with respect to ω. Inserting this into equations (A.7) then gives

$$\dot{E}_{non-ad}(t) = \eta(x(t))\dot{x}(t)^2, \tag{A.11}$$

which finally yields the equation of motion in the Markov approximation

$$M\ddot{x} + \frac{dV_0}{dx} = -\eta(x)\dot{x}, \tag{A.12}$$

where

$$\eta(x(t)) = \int d\mathbf{r}d\mathbf{r}' \int_0^{\infty} dt' \frac{dV_{ext}(\mathbf{r};x)}{dx} t'\chi(\mathbf{r},\mathbf{r}',t';x)\frac{dV_{ext}(\mathbf{r}';x)}{dx}. \tag{A.13}$$

It has been assumed that the nuclei could be described by a single degree of freedom x, but in the case of N degrees of freedom the derivatives in (A.13) are simply replaced by gradients and the friction becomes a $N \times N$ dimensional tensor.

Non-interacting friction

When no electron interactions are present the response function can be expressed in terms of single particle orbitals $\phi_j(\mathbf{r})$ and the friction can be written

$$\eta^0(x) = \pi\hbar \sum_{i,j} \left|\langle\phi_i|\frac{dV_{ext}}{dx}|\phi_j\rangle\right|^2 \int d\varepsilon \delta(\varepsilon - \varepsilon_i)\delta(\varepsilon - \varepsilon_j)\Big(-\frac{dn_F}{d\varepsilon}\Big), \qquad \text{(A.14)}$$

where n_F is the Fermi distribution, which depends on the electronic temperature T_{el}. Within DFT, it is natural to replace the external potential with the Kohn-Sham potential (2.3) and use the Kohn-Sham orbitals for ϕ_i and Eq. (A.14) then allows one to perform DFT based molecular dynamics with electronic friction [103, 63, 64]. Compared to the formalism introduced in section 3.5, a friction tensor based on DFT has the advantage that it does not rely on potential energy surfaces or a knowledge of the spectral properties of a particular adsorbate orbital mediating the non-adiabatic energy transfer. The method naturally incorporates all adsorbate orbitals contributing to the friction and one does not have to make any assumptions on the nature of the frictional coupling.

Fluctuating forces

The present derivation does not yield the statistical properties of the fluctuating force. In the Markov approximation one can incorporate fluctuations by assuming a Gaussian distributed uncorrelated force as in Eq. (3.53), but a general expression for the temporal correlation does not emerge from the present analysis. One of the advantages of the density matrix formalism applied in section 3.5 is that it leads to an explicit expression for the statistical properties of the fluctuating force. To this end, it should be noted that there is a striking similarity between the energy loss function $\Lambda(\omega)$ in Eq. (3.48) and the memory function $\widetilde{\Lambda}(\omega)$ in Eq. (A.8). In both cases, the Markov approximation was obtained in the small frequency limit and it is tempting to associate $\omega\Lambda(\omega)$ with $2\mathrm{Im}\widetilde{\Lambda}(\omega)$. Referring to Eq. (3.47) it is then natural to introduce an empirical Gaussian distributed stochastic force with the correlation function

$$K_{emp}(t) = \hbar \int_{-\infty}^{\infty} \frac{d\omega}{2\pi} \mathrm{Im}\widetilde{\Lambda}(\omega) \coth\Big(\frac{\hbar\omega}{2k_B T_{el}}\Big)\cos(\omega t). \qquad \text{(A.15)}$$

and include it in Eq. (A.9).

Appendix B

Path Integral Representations

In this appendix, we derive various path integral representations of propagators, which will become extremely useful for obtaining an expression for the reduced density matrix and exact evaluation of certain Green functions. The path integral representation of propagators often gives a renewed insight into the underlying physics, although the mathematical complexity can be somewhat larger. In its simplest form the path integral formulation of quantum mechanics states that quantum mechanical propagators can be represented as a sum over all possible paths weighted by e^{iS},[1] where S is the action for that path. The amplitude for finding the particle in a state $|x(t)\rangle$ given that it was at $|x_0\rangle$ at t_0 can thus be written

$$\langle x|e^{-iH(t-t_0)}|x_0\rangle = \int \mathcal{D}[x(t')]e^{iS[x(t')]}, \qquad S = \int_{t_0}^{t} dtL[\dot{x}(t'), x(t')], \quad \text{(B.1)}$$

where $L[\dot{x}(t'), x(t')]$ is the Lagrangian of the path $x(t')$, typically given by the kinetic energy minus the potential energy. In this expression $\int \mathcal{D}[x(t')]$ means a (properly normalized) sum over all paths from $x_0(t_0)$ to $x(t)$.

[1] In this appendix we will take $\hbar = 1$ and all actions will therefore be dimensionless.

B.1 The Newns-Anderson Retarded Green Function

The Newns-Anderson Hamiltonian is given in Eq. (3.1) and repeated here for reference

$$H_0 = \varepsilon_0 c_a^\dagger c_a + \sum_k \epsilon_k c_k^\dagger c_k + \sum_k \Big(V_{ak} c_a^\dagger c_k + V_{ak}^* c_k^\dagger c_a \Big). \tag{B.2}$$

The retarded Green function

$$G_R^0(t) = -i\theta(t)\langle a|e^{-iHt}|a\rangle, \tag{B.3}$$

can be evaluated easily using a Dyson equation approach, but by expressing it as a sum over paths, we will see that each path can be understood as sequence of jumps between the resonance and the metallic band. In the wide band limit the time spend in the metal band goes to zero and the electron thus spends all the time of propagation in the resonant state. This fact becomes extremely useful when evaluating Green functions where interactions with an adsorbate coordinate are included.

The path integral representation is derived by dividing the time interval t, into N intervals of length $\Delta t = t/N$. When N becomes sufficiently large, we can take $e^{-iHt} = (e^{-iH\Delta t})^N \approx (1 - iH\Delta t)^N$. We then insert $N-1$ complete sets of states $|n\rangle$ such that the Green function becomes a sum over N-fold products of matrix elements

$$G_R^0(t) \approx -i\theta(t) \sum_{\{n_i\}} \langle a|1 - iH_0\Delta t|n_1\rangle\langle n_1|1 - iH_0\Delta t|n_2\rangle \ldots \langle n_{N-1}|1 - iH_0\Delta t|a\rangle, \tag{B.4}$$

where the sum runs over all states in each of the $N-1$ complete sets $\{n_i\}$. Assuming that $\langle a|k\rangle = 0$ the states $|n\rangle$ can either be $|a\rangle$ or $|k\rangle$ and the matrix elements $\langle a|1 - iH_0\Delta t|a\rangle = e^{-i\varepsilon_0\Delta t}$, $\langle k_1|1 - iH_0\Delta t|k_2\rangle = \delta_{k_1k_2}e^{-i\epsilon_k\Delta t}$, and $\langle a|1 - iH_0\Delta t|k\rangle = -iV_{ak}\Delta t$ represent propagation in the resonance, propagation in the band, and a jump from the band to the resonance respectively. When we take the limit $N \to \infty$, Eq. (B.4) becomes formally exact and the jumps between band and resonance become instantaneous. It is then most convenient to order the terms in Eq. (B.4) according to the number of jumps. Since the endpoints of the time interval is at the resonance, a jump into the band has to be accompanied by a jump back into the resonance and each such "band excursion"

comes with a factor of $-\sum_k |V_{ak}|^2 e^{-i\epsilon_k \tau_i}$ where τ_i is the time spend in the i'th excursion into band. It is also clear that p excursions into the resonance has to be accompanied by $p+1$ resonant propagation factors $e^{-i\varepsilon_0 \sigma_i}$ where σ_i is the i'th time interval in the resonant state. Finally, for a given number of band excursions we have to integrate over all possible band and resonance time intervals and the retarded Green function becomes

$$G_R^0(t) = -i \int_0^\infty d\sigma_0 e^{-i\varepsilon_0 \sigma_0} \sum_{p=0}^{\infty} \Big(- \int_0^\infty \int_0^\infty d\sigma d\tau \sum_k |V_{ak}|^2 e^{-i\epsilon_k \tau} e^{-i\varepsilon_0 \sigma} \Big)^p \times \delta\Big(\sigma_0 + \sum_{j=1}^{p} (\sigma_j + \tau_j) - t\Big), \tag{B.5}$$

where the delta function has been introduced to ensure that the time intervals sum to t and the theta function has become redundant.[2] We can use the delta function to eliminate the σ_i integration variables in the exponentials and get

$$G_R^0(t) = -ie^{-i\varepsilon_0 t} \int_0^\infty d\sigma_0 \sum_{p=0}^{\infty} \Big(- \int_0^\infty \int_0^\infty d\sigma d\tau \Gamma(\tau) \Big)^p \times \delta\Big(\sigma_0 + \sum_{j=1}^{p} (\sigma_j + \tau_j) - t\Big), \tag{B.6}$$

with the environment time evolution operator given by.

$$\Gamma(t) \equiv \sum_k |V_{ak}|^2 e^{-i(\epsilon_k - \epsilon_0)t} = \int_{-\infty}^{\infty} \frac{d\omega}{2\pi} \Gamma(\omega) e^{-i(\omega - \varepsilon_0)t}. \tag{B.7}$$

By using that $\delta(t) = (1/2\pi) \int d\omega e^{i\omega t}$ it is now possible to evaluate (B.6) and recover the result (3.4) as the Fourier transform of Eq (B.6). In the wide band limit, $\Gamma(t) = \Gamma\delta(t)$, which implies that the electron does not spend any time in the band and the retarded Green function becomes a sum over paths, which are composed of *instantaneous* excursions into the band. We use the notation χ to represent a position in state space and $\int \mathcal{D}[\chi(t')] e^{iS_0[\chi(t')]}$ as a formal expression representing the sum over all paths weighted by the Newns-Anderson action S_0.

[2] The $p = 0$ term just involves the delta function $\delta(\sigma_0 - t)$.

B.2 Influence Functionals

We will now derive an influence functional formalism, which can be used to incorporate the interactions with an environment into an effective potential governing the dynamics. The formalism was pioneered by Feynman and Vernon [29] and has subsequently been used to develop the reduced density matrix formalism [13, 93]. We will follow the analysis of Hedegård [46, 47], which is most useful for the present purpose of modeling adsorbates interacting with hot electrons.

We consider Hamiltonians of the type

$$H = H_0 + H_e + H_I, \tag{B.8}$$

where H_0 is the Hamiltonian of an isolated particle, H_e is the Hamiltonian of a certain environment and H_I couples the environment to the particle. The object of our interest is the propagator of the particle described by H_0 under the influence of the environment. The propagator is written

$$G(x,t;x_0,t_0;y) = \langle y;0|\Psi(x,t)\Psi^\dagger(x_0,t_0)|y;0\rangle, \tag{B.9}$$

where x denotes the state of the particle described by H_0 and y denotes the state of the environment described by H_e. $\Psi^\dagger(x,t) = e^{iHt}\Psi^\dagger(x)e^{-iHt}$ is a quantum field operator, which creates a particle in the state $|x(t)\rangle$[3] and $|y,0\rangle$ denotes a state with the environment in the state y and no particle. It should be noted that (B.9) propagates the particle described by x from t_0 to t at fixed y and the expression is therefore not the same as $\langle x,y|e^{-iH(t-t_0)}|x_0,y\rangle$. Rather, we will formally write it as

$$G(x,t;x_0,t_0;y) = \langle y|e^{iH_et}\langle x|e^{-iH(t-t_0)}|x_0\rangle e^{-iH_et_0}|y\rangle, \tag{B.10}$$

where $\langle x|e^{-iH(t-t_0)}|x_0\rangle$ is now an operator acting in the environment space and we used that $e^{-iHt}|y;0\rangle \propto e^{-iH_et}|y;0\rangle$. A path integral representation of this operator can now be derived by the usual discretization of the time interval $t-t_0$ into N small pieces of size $\Delta t = (t-t_0)/N$ and insertion of a complete set of particle states x_i between each time interval. This leads to a product of

[3] We use the quantum field operators, which are typically used to create a particle at the *position* x, but the analysis might as well be done for a fermionic creation operator $c_a^\dagger$ and we will thus think of both x and y as abstract states and the field operators represent general creation and annihilation operators of any such state.

operators (in y space) of the type

$$\begin{aligned}\langle x_{i+1}|e^{-iH\Delta t}|x_i\rangle &\approx \langle x_{i+1}|1 - iH_0\Delta t - iH_e\Delta t - iH_I(x_i)\Delta t|x_i\rangle \\ &\approx \langle x_{i+1}|e^{-iH_0\Delta t}|x_i\rangle e^{-i\widetilde{H}_I(x_i)\Delta t},\end{aligned} \tag{B.11}$$

with

$$\widetilde{H}_I(x_i) = H_e + H_I(x_i), \tag{B.12}$$

where $H_I(x_i)$ is the interaction operator with all particle operators being replaced by the c-number appearing in the matrix element in Eq. (B.11). We can then write

$$\begin{aligned}\langle x|e^{-iH(t-t_0)}|x_0\rangle \approx \int dx_1 dx_2 \ldots dx_{N-1} &\langle x_N|e^{-iH_0\Delta t}|x_{N-1}\rangle\langle x_{N-1}|e^{-iH_0\Delta t}|x_{N-2}\rangle \\ &\times \ldots \langle x_1|e^{-iH_0\Delta t}|x_0\rangle e^{-i\widetilde{H}_I(x_N)\Delta t}e^{-i\widetilde{H}_I(x_{N-1})\Delta t}\ldots e^{-i\widetilde{H}_I(x_0)\Delta t},\end{aligned}$$

with $x_N = x(t)$. The expression becomes formally exact in the limit of $N \to \infty$ and we will represent the resulting infinite number of integrals with the usual $\int \mathcal{D}[x(t')]$. However, since the operators $\widetilde{H}_I$ do not commute at different times, we have to time order the exponential operators and get

$$\langle x|e^{-iH(t-t_0)}|x_0\rangle = \int \mathcal{D}[x(t')]e^{iS_0[x(t')]}\mathcal{T}\Big(e^{-i\int_{t_0}^{t} dt'\widetilde{H}_I[x(t')]}\Big), \tag{B.13}$$

where $\mathcal{T}$ denotes time ordering. We can then finally write

$$G(x,t;x_0,t_0;y) = \int \mathcal{D}[x(t')]e^{iS_0[x(t')]}\langle y|\widetilde{U}[x(t')]|y\rangle, \tag{B.14}$$

where

$$\widetilde{U}[x(t')] = e^{iH_e t}\mathcal{T}\Big(e^{-i\int_{t_0}^{t} dt'\widetilde{H}_I[x(t')]}\Big)e^{-iH_e t_0} \tag{B.15}$$

is the environment time evolution operator.

The dynamics of the environment has thus been separated from the time evolution of the particle. However, the price we pay is an explicit path dependence in the environment part of the propagator. In general it is not possible to evaluate $\widetilde{H}_I[x(t')]$ on all possible paths, but below we will consider two examples where the formalism can be used to derive exact results for particles interacting with an environment.

B.2.1 Resonant fermion in bosonic environment

We start by considering a resonant electron in a bosonic environment. In this case H_0 is the Newns-Anderson Hamiltonian (B.2) and the environment is a bosonic field:

$$H_e = \sum_i \Big(\frac{p_i^2}{2m_i} + \frac{1}{2} m_i \omega_i^2 y_i^2 \Big) = \sum_i \hbar\omega_i \Big(a_i^\dagger a_i + \frac{1}{2} \Big). \tag{B.16}$$

The interaction is mediated by the resonant state and is written

$$H_I = c_a^\dagger c_a \varepsilon_a(y), \tag{B.17}$$

where the coupling function $\varepsilon_a(y)$ depends on all bosonic coordinates y_i.

Referring to (B.14), the particle state x represents the state of the electron and the particle path $x(t')$, represents a sequence of jumps between the resonant state $|a\rangle$ and metallic states $|k\rangle$. We will denote the particle path by $\chi(t')$ and write

$$G_R(t,t_0;y) = -i\theta(t-t_0)\langle y|c_a(t)c_a(t_0)^\dagger|y\rangle = \int \mathcal{D}[\chi(t')] e^{iS_0[\chi(t')]} \langle y|\widetilde{U}[\chi(t')]|y\rangle.$$

Evaluating this expression requires a calculation of the last matrix element on all possible paths, which is not possible in general. However, one exception is the wide band limit, where $\widetilde{H}_I$ becomes particularly simple. In section B.1 it was shown that the Newns-Anderson retarded Green function could be written as a sum of paths, where each path consisted of a sequence of jumps between the metallic band and the resonant state. In the wide band limit, the electron spends all the time in the resonant state and the Hamiltonian becomes $\widetilde{H}_I = H_e + \varepsilon_a(y)$, which is path- and therefore also time-independent. One can then remove the time ordering operator and write the retarded Green function

$$G_R(t,t_0;y) = G_R^0(t,t_0)\langle y|e^{iH_e t} e^{-i[H_e+\varepsilon_a(y)](t-t_0)} e^{-iH_e t_0}|y\rangle, \tag{B.18}$$

where $G_R^0(t,t_0)$ is given by Eq. (3.7). The single-particle Green function (3.27) appearing in the inelastic scattering probability (3.26) is exactly given by this expression if we let y represent an eigenstate $|n\rangle$ of the environment Hamiltonian. The environment matrix element can then be evaluated exactly using a generalization of the Baker-Hausdorff formula [72] when $\varepsilon_a(y)$ is linear or quadratic in the bosonic coordinates. For details we refer to **Paper IV** and here we simply state the results for a single mode with frequency ω_0.

With linear coupling to the resonant state ($H_I = \lambda c_a^\dagger c_a y$) we obtain[4]

$$G_R^{(1)}(n;t) = -i\theta(t)e^{-(i\varepsilon_0+\Gamma/2)t}e^{-g(1-i\omega_0 t-e^{-i\omega_0 t})}L_n[g|1-e^{i\omega_0 t}|^2], \quad g = \Big(\frac{\lambda}{\omega_0}\Big)^2,$$

where $L_n(x)$ is the n'th Laguerre polynomial. Similarly, the four-point Green function $G(n;\tau,s,t) = \langle n|c_a(\tau-s)c_a^\dagger(\tau)c_a(t)c_a^\dagger(0)|n\rangle$ appearing in Eq. (3.28) becomes

$$\begin{aligned} G^{(1)}(n;\tau,s,t) &= G_R^0(t)\bar{G}_R^0(s)e^{ig\omega_0(t-s)}e^{-gf(\tau,s,t)}L_n[gf(\tau,t,s)+gf^*(\tau,t,s)], \\ f(\tau,s,t) &= 2-e^{-i\omega_0 t}-e^{i\omega_0 s}+e^{-i\omega_0\tau}(1-e^{-i\omega_0 t})(1-e^{i\omega_0 s}). \end{aligned} \tag{B.19}$$

With quadratic coupling ($H_I = \kappa c_a^\dagger c_a y^2$), the retarded Green function becomes

$$\begin{aligned} G_R^{(2)}(n;t) = G_R^0(t)e^{i(n+1/2)\omega_0 t}\Big(\cosh(i\omega_1 t)+\frac{\omega_0+2\kappa}{\omega_1}\sinh(i\omega_1 t)\Big)^{-n-\frac{1}{2}} \\ \times\sum_{l=0}^{[n/2]}\frac{\kappa^{2l}n!}{\omega_1^{2l}(l!)^2(n-2l)!}\sinh^{2l}(i\omega_1 t), \end{aligned} \tag{B.20}$$

where $\omega_1 = \omega_0(1+4\kappa/\omega_0)^{1/2}$ and $[n/2]$ is the integer part of $n/2$. It is also straightforward to obtain the two-particle Green function with quadratic coupling (see **Paper IV**), but here we will just state the result for the vibrational ground state:

$$\begin{aligned} G^{(2)}(n=0;\tau,s,t) = G_R^0(t)\bar{G}_R^0(s)e^{i\omega_0(t-s)/2}e^{B(t)/2+B(-s)/2} \\ \times\sum_{m=0}^{\infty}e^{2im\omega_0(t-\tau)}\frac{A^m(t)A^m(-s)(2m)!}{(m!)^2}, \end{aligned} \tag{B.21}$$

where

$$A(t) = \frac{-\kappa\tanh(i\omega_1 t)}{\omega_1+(\omega_0+2\kappa)\tanh(i\omega_1 t)}, \tag{B.22}$$

$$B(t) = -\ln\Big(\cosh(i\omega_1 t)+\frac{\omega_0+2\kappa}{\omega_1}\sinh(i\omega_1 t\Big). \tag{B.23}$$

[4]Note that without loss of generality we can restrict ourselves to the case of $t_0 = 0$.

B.2.2 Bosons in fermionic environment

As another example where the influence functional formalism is useful, we consider the time-dependent density matrix of a boson interacting with a thermal reservoir of electrons. The boson will now play the role of the particle and is described by the coordinates x_i. Thus

$$H_0 = \sum_i \Big(\frac{p_i^2}{2m_i} + \frac{1}{2} m_i \omega_i^2 x_i^2 \Big) = \sum_i \hbar\omega_i \Big(a_i^\dagger a_i + \frac{1}{2} \Big), \tag{B.24}$$

and H_e is the Newns-Anderson Hamiltonian given in (B.2). The density matrix in a coordinate representation can be written

$$\begin{aligned} \rho(x, x'; t) &= \langle x | e^{-iHt} \rho(0) e^{iHt} | x' \rangle \\ &= \int dx_0 dx_0' \langle x | e^{-iHt} | x_0 \rangle \langle x_0 | \rho(0) | x_0' \rangle \langle x_0' | e^{iHt} | x' \rangle. \end{aligned} \tag{B.25}$$

Since the state $|x\rangle$ only contains the particle degrees of freedom, the expression (B.25) is a product of three operators acting in the environment space. Two of these are exactly of the form (B.13) with $t_0 = 0$ and we can write

$$\begin{aligned} \rho(x, x'; t) = \int dx_0 dx_0' \int \mathcal{D}[x(t')] \mathcal{D}[x'(t')] e^{iS_0[x(t')] - iS_0[x'(t')]} \\ \times e^{-iH_e t} \widetilde{U}[x(t')] \langle x_0 | \rho(0) | x_0' \rangle \widetilde{U}^\dagger[x'(t')] e^{iH_e t}, \end{aligned} \tag{B.26}$$

where $x(t')$ is a path from x_0 to $x(t)$ and $x'(t')$ is a path from $x'(t)$ to x_0'. By tracing out the environment degrees of freedom we obtain the reduced density matrix:

$$\begin{aligned} \rho_{red}(x, x'; t) = \int dx_0 dx_0' \rho_0(x_0, x_0') \int \mathcal{D}[x(t')] \mathcal{D}[x'(t')] e^{iS_0[x(t')] - iS_0[x'(t')]} \\ \times F[x(t'), x'(t')], \end{aligned} \tag{B.27}$$

where

$$F[x(t'), x'(t')] = \mathrm{Tr}_e \Big(\widetilde{U}^\dagger[x'(t')] \widetilde{U}[x(t')] \rho_e \Big), \tag{B.28}$$

and we assumed that the particle and environment initially decouples: $\rho(0) = \rho_0 \otimes \rho_e$.

The functional $F[x(t'), x'(t')]$ depends on the two paths $x(t')$ and $x'(t')$ and we can regard it as a thermal average of the time evolution operator

$$U_\gamma(0,0') = \mathcal{T}_\gamma\Big(e^{-i\int_\gamma d\tau \widetilde{H}_I[x_\gamma(\tau)]}\Big), \tag{B.29}$$

where $x_\gamma(\tau)$ is a path, which runs from $t = 0$ to t and then back to $t = 0$ and $\mathcal{T}_\gamma$ is the time ordering operator on that path. We will use the linked cluster theorem to obtain a useful expression for the influence functional. This is accomplished by replacing $H_I[x_\gamma(t')]$ with $\lambda H_I[x_\gamma(t')]$ in U_γ and differentiate:

$$\frac{d}{d\lambda}U_\gamma^{(\lambda)}(0,0') = -i\int_\gamma d\tau U_\gamma^{(\lambda)}(0,\tau)e^{iH_e\tau}H_I[x_\gamma(\tau)]e^{-iH_e\tau}U_\gamma^{(\lambda)}(\tau,0'). \tag{B.30}$$

Multiplying by ρ_e and taking the environment trace give a differential equation for $F_\lambda[x(t'), x'(t')]$ subject to the boundary condition $F_0[x(t'), x'(t')] = 1$. The solution can be verified to be

$$F_\lambda[x(t'), x'(t')] = e^{-i\int_0^\lambda d\lambda' \int_\gamma d\tau \mathcal{F}_{\lambda'}(\tau)}, \tag{B.31}$$

with

$$\mathcal{F}_\lambda(\tau) = \frac{\mathrm{Tr}_e\Big(U_\gamma^{(\lambda)}(0,\tau)e^{iH_e\tau}H_I[x_\gamma(\tau)]e^{-iH_e\tau}U_\gamma^{(\lambda)}(\tau,0')\rho_e\Big)}{\mathrm{Tr}_e\Big(U_\gamma^{(\lambda)}(0,0')\rho_e\Big)}. \tag{B.32}$$

The reduced density matrix can then finally be written

$$\rho_{red}(x,x';t) = \int dx_0 dx_0' \rho_0(x_0,x_0') \int \mathcal{D}[x(t')]\mathcal{D}[x'(t')]e^{iS_{eff}[x(t'),x'(t')]}, \tag{B.33}$$

with the effective action

$$S_{eff}[x(t'), x'(t')] = S_0[x(t')] - S_0[x(t')] - \int_0^1 d\lambda \int_\gamma d\tau \mathcal{F}_\lambda(\tau). \tag{B.34}$$

The last part of the effective action couples the two paths $x(t')$ and $x'(t')$ and can be expressed in terms of Green functions time ordered on the γ-contour. A perturbative expansion of these Green functions to second order in H_I with $x(t) = x'(t) \equiv u$, yields the expression (3.44) [7].

Appendix C

The Morse Potential

The Morse potential is a useful model for a barrierless desorption potential. The quantization of the potential is well known and in this appendix we will state expressions for the bound state energies and certain useful matrix elements. We then derive a perturbative expression for the Retarded Green function of the Newns-Anderson Hamiltonian coupled to a Morse oscillator, and use the result to calculate the scattering amplitude for reactions induced by hot electrons.

C.1 Quantization

The Morse Hamiltonian is

$$H_0 = \frac{p^2}{2m} + D\Big(e^{-2\alpha(x-x_0)} - 2e^{-\alpha(x-x_0)}\Big), \tag{C.1}$$

where D is the depth of the potential, x_0 is the minimum position, and $1/\alpha$ is the width of the potential. The potential has a number of bound energy eigenstates and a continuum of unbound states, which are shown schematically in Fig. C.1. The quantization was first performed by Morse in 1929 [74].

Bound states

For $E < 0$, the eigenenergies comprise a finite discrete set. It is useful to introduce the dimensionless variable $N = \sqrt{2mD/\hbar^2\alpha^2} + 1/2$ in terms of which

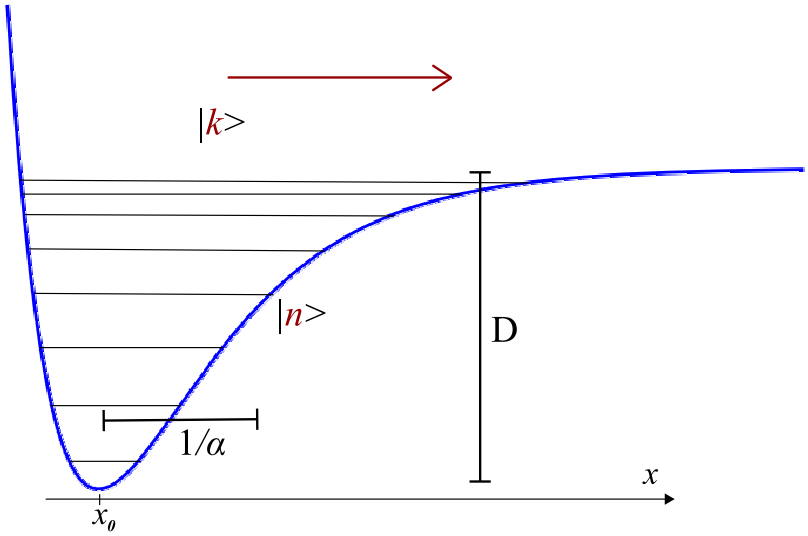

Figure C.1: The Morse potential with parameters x_0, α, and D. There is a finite number of bound states $|n\rangle$ and a continuum of unbound state $|k\rangle$, which become plane waves in the asymptotic region $x \to \infty$.

the eigenvalues can be written

$$E_n = -\frac{\hbar^2 a^2}{2m}(N-n)^2, \qquad 0 \le n \le [N], \tag{C.2}$$

where $[N]$ denotes the integer part of N.

The eigenfunctions are

$$\varphi_n(x) = A_n z^{N-n} e^{-z/2} L_n^{2N-2n}(z), \qquad z = (2N+1)e^{-\alpha(x-x_0)}, \tag{C.3}$$

where

$$A_n = \sqrt{\frac{\alpha n!(2N-2n)}{\Gamma(2N-n+1)}}, \tag{C.4}$$

and $L_n^{2N-2n}(z)$ is the generalized Laguerre polynomial

$$L_n^a(z) = \frac{z^{-a}e^z}{n!}\frac{d^n}{dx^n}\left(z^{n+a}e^{-z}\right). \tag{C.5}$$

Here $\Gamma(x) = \int t^{x-1}e^{-t}dt$ is the Gamma function, which should not be confused with the imaginary part of the resonant self-energy Eq. (3.6). While this notation is a bit unfortunate, it is traditional and the meaning of Γ should be clear from the context.

Continuum states

The continuum of bound states become plane waves asymptotically and have the plane wave eigenvalues

$$E_k = \frac{\hbar^2 k^2}{2m}. \tag{C.6}$$

The analytical structure of the eigenfunctions is rather complicated and we refer to Lima et al. [16] for details.

Matrix elements

The matrix elements of the position operator were calculated in Ref. [16] and are stated here for convenience. For $m > n$ the bound-bound matrix elements are

$$\langle n|x|m\rangle = \frac{2(-1)^{m-n+1}}{\alpha(m-n)(2N-n-m)}\sqrt{\frac{(N-n)(N-m)\Gamma(2N-m+1)m!}{\Gamma(2N-n+1)n!}}, \tag{C.7}$$

and the diagonal matrix elements can be expressed in terms of the digamma-function $\psi(x) = \frac{d}{dx}\ln\Gamma(x)$:

$$\langle n|x|n\rangle = \frac{1}{\alpha}[\ln(2N+1) + \psi(2N-n+1) - \psi(2N-2n+1) - \psi(2N-2n)]. \tag{C.8}$$

The bound-unbound matrix elements are

$$\langle k|x|n\rangle = \frac{(-1)^{n+1}|\Gamma(ik/\alpha - N)|}{\pi\alpha^{3/2}[(N-n)^2 + (k/\alpha)^2]}\sqrt{\frac{k/\alpha\sinh(2\pi k/\alpha)(2N-2n)}{n!\Gamma(2N-n+1)}}|\Gamma(1+N+ik/\alpha)|^2, \tag{C.9}$$

and for the unbound-unbound elements $\langle k|x|k'\rangle$ we will again refer to Lima et al. [16], since these have a non-trivial analytical structure.

C.2 Coupling to the Newns-Anderson Model

We will now obtain an expression for the retarded Green function of the Newns-Anderson type resonance coupled to a Morse potential. With the coupling function $\varepsilon_a(x)$ we are then led to consider the Hamiltonian

$$H = H_0 + H_{NA} + H_I, \tag{C.10}$$

$$H_I = c_a^\dagger c_a \varepsilon_a(x), \tag{C.11}$$

where H_{NA} is given in Eq. (3.1) and H_0 is given in Eq. (C.1). One of the main objects of interest is the retarded Green function

$$G_R(t_1, t_0; m, n) = -i\theta(t_1 - t_0)\langle m, 0|c_a(t_1)c_a^\dagger(t_0)|n, 0\rangle, \tag{C.12}$$

where m and n represent (bound or unbound) eigenstates of H_0, $|n, 0\rangle$ is a state with no electron, and $c_a(t) = e^{iHt/\hbar}c_a e^{-iHt/\hbar}$. Unlike the case of a harmonic oscillator, it is not possible to evaluate the Green function exactly for simple coupling functions. However, it is possible to make some progress within perturbation theory to which we now turn.

It is most convenient to express the operators in the interaction picture and we write the propagator

$$\langle m, 0|c_a(t_1)c_a^\dagger(t_0)|n, 0\rangle = \langle m, 0|\hat{c}_a(t_1)\hat{U}(t_1 - t_0)\hat{c}_a^\dagger(t_0)|n, 0\rangle, \tag{C.13}$$

with

$$\hat{U}(t_1, t_0) = \mathcal{T}\Big(e^{-i\int_{t_0}^{t_1} dt' \hat{H}_I(t')/\hbar}\Big), \quad \hat{c}_a(t) = e^{i(H-H_I)t/\hbar}c_a e^{-i(H-H_I)t/\hbar}. \tag{C.14}$$

To first order in the interaction one obtains

$$\langle m, 0|c_a(t_1)c_a^\dagger(t_0)|n, 0\rangle = -i\int_{t_0}^{t_1} dt' \langle m, 0|\hat{c}_a(t_1)\hat{c}_a^\dagger(t')\hat{c}_a(t')\varepsilon_a(\hat{x}(t'))\hat{c}_a^\dagger(t_0)|n, 0\rangle. \tag{C.15}$$

Since H_0 and H_{NA} commute, we can write $e^{-i(H-H_I)t/\hbar} = e^{-iH_0 t/\hbar}e^{-iH_{NA}t/\hbar}$ and the matrix element can be split into a fermionic and bosonic part. Thus

$$\begin{aligned} G_R(t_1, t_0; m, n) &= -\theta(t_1 - t_0)\int_{t_0}^{t_1} \frac{dt'}{\hbar}\langle m|\varepsilon_a(\hat{x}(t'))|n\rangle\langle 0|\hat{c}_a(t_1)\hat{c}_a^\dagger(t')\hat{c}_a(t')\hat{c}_a^\dagger(t_0)|0\rangle, \\ &= \theta(t_1 - t_0)\langle m|\varepsilon_a(x)|n\rangle\int_{t_0}^{t_1} \frac{dt'}{\hbar}e^{i(E_m - E_n)t'/\hbar}G_R^0(t_1, t')G_R^0(t', t_0). \end{aligned} \tag{C.16}$$

In the second step we have inserted a complete set of states in the fermionic propagator and used that only the vacuum state survives, since $\hat{c}_a(t')\hat{c}_a^\dagger(t_0)$ conserves the number of particles. In the wide band limit, the bare Green function $G_R^0(t_1,t')$ is an exponential (Eq. (3.7)) and $G_R^0(t_1,t')G_R^0(t',t_0) = G_R^0(t_1,t_0)$. Within first order perturbation theory the Green function (with $m \neq n$) then becomes

$$G_R(t_1,t_0;m,n) = G_R^0(t_1,t_0)\langle m|\varepsilon_a(x)|n\rangle \frac{e^{i(E_m-E_n)t_1/\hbar} - e^{i(E_m-E_n)t_0/\hbar}}{i(E_m-E_n)}. \tag{C.17}$$

Appendix D

Hydrogen Adsorption on Graphene

In Ref [52] it was shown that at low coverage, Hydrogen adsorbs on graphite(0001) in one of two dimer configurations referred to as para and ortho. The two configurations are shown in Fig. 4.8. The preference of ortho and para configurations has subsequently been traced to the local density of states induced by a single adsorbed Hydrogen atom [94].

At higher coverages (> 0.02 monolayer) the Hydrogen atoms tend to adsorb in larger clusters of unknown structure. In this appendix, we present some calculations for the adsorption energy of various periodic configurations at a coverage of 0.25 monolayer. There is an infinity of such configurations, but we have focused on nine rather symmetric structures, which are shown and given reference names in Fig. D.1. From the results of Ref. [94] it is expected that the preferred configurations are those, which optimize the number of mutual para and ortho interactions between any two pairs of Hydrogen atoms.

The average binding energy per H atom is displayed in table Tab. D.1 for each of the configurations, and the expected preference to mutual ortho and para configurations is indeed observed. The strongest bound configuration is the uniform para configuration where every Hydrogen atom is in a para configuration to its three nearest neighbor Hydrogen atoms. The Hydrogen atoms in this structure are in a super honey comb lattice with a lattice parameter twice that of the graphene lattice. Another strongly bound structure is the orthochain, where each hydrogen atom is in a ortho configuration with two other

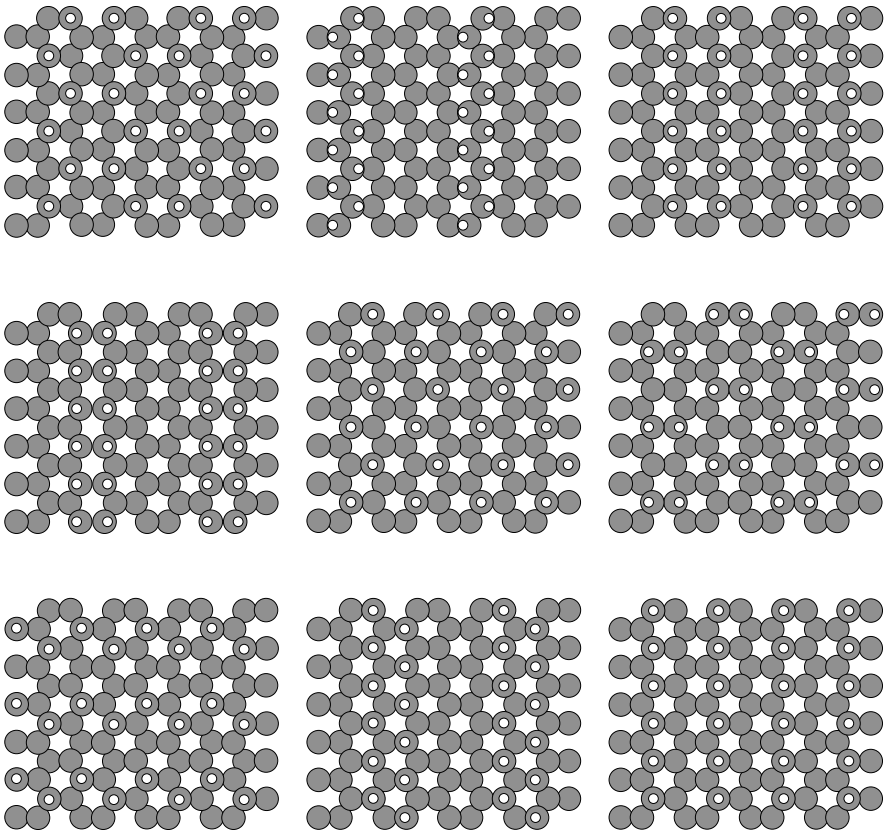

Figure D.1: Various periodic configurations of H adsorbed on graphene at 0.25 monolayer coverage. Top row: uniform para, orthochain, paraband. Middle row: orthoband, parachain, orthotwin. Bottom row: metachain, metaband, metaline.

Configuration	Average binding energy	Desorption energy
Uniform para	1.70	2.69
Orthochain	1.57	2.39
Paraband	1.33	1.94
Orthoband	1.28	1.43
Parachain	1.23	1.69
Orthotwin	1.21	1.50
Metachain	0.50	0.34
Metaband	0.49	0.21
Metaline	0.48	0.14

Table D.1: Average binding energies and desorption energies for the configurations shown in Fig. D.1. The average binding energy is per adsorbed H atom relative to a free H atoms and a pure graphene slab. The desorption energy is the energy required to desorb the first H atom. All numbers are in eV.

Hydrogen atoms. The atoms in the parachain configuration also have two nearest para neighbors, but the distance between each chain is unfavorable and the binding energy is lowered. The three structures: paraband, orthoband, and orthotwin have a single favorable nearest neighbor and have intermediate binding energies. Finally, in the three meta configurations, no Hydrogen atom has a favorable nearest neighbor and the atoms are weakly bound.

Furthermore, the three para configurations show no barrier to adsorption of "the last" atom, whereas the ortho configurations all show barriers of $\sim 0.08 - 0.20\ eV$. Thus at high coverages, clusters of the uniform para configuration are expected to dominate although many different adsorbate structures will probably be present. It should be noted that for this structure, both the average binding energy and desorption energy are larger than those for the ortho and para dimers at low coverage, which are $\sim 1.25\ eV$ and $\sim 2.0\ eV$ respectively.

Bibliography

[1] P. W. Anderson. Localized magnetic states in metals. *Phys. Rev.*, 124:41, 1961.

[2] J. Behler, B. Delley, K. Reuter, and M. Scheffler. Nonadiabatic potential-energy surfaces by constrained density-functional theory. *Phys. Rev. B*, 75:115409, 2007.

[3] J. Behler, K. Reuter, and M. Scheffler. Nonadiabatic effects in the dissociation of oxygen molecules at the al(111) surface. *Phys. Rev. B*, 77:115421, 2008.

[4] M. Bonn, S. Funk, Ch. Hess, D. N. Denzler, C. Stampfl, M. Scheffler, M. Wolf, and G. Ertl. Phonon- versus electron-mediated desorption and oxidation of co on ru(0001). *Science*, 285:1042, 1999.

[5] M. Born and R. Oppenheimer. Zur quantentheorie der moleküle. *Annalen der Physik*, 84:457, 1927.

[6] S. Braig and K. Flensberg. Vibrational sidebands and dissipative tunneling in molecular transistors. *Phys. Rev. B*, 68:205324, 2003.

[7] M. Brandbyge, P. Hedegård, T. F. Heinz, J. A. Misewich, and D. M. Newns. Electronically driven adsorbate excitation mechanism in femtosecond-pulse laser desorption. *Phys. Rev. B*, 52:6042, 1995.

[8] H. Bruus and K. Flensberg. *Many-Body Quantum Theory in Condensed Matter Physics*. Oxford University Press, 2004.

[9] F. Budde, T. F. Heinz, M. M. T. Loy, J. A. Misewich, F. de Rougemont, and H. Zacharias. Femtosecond time-resolved measurement of desorption. *Phys. Rev. Lett.*, 66:3024, 1991.

[10] S. A. Buntin, L. J. Richter, R. R. Cavanagh, and D. S. King. Optically driven surface reactions: Evidence for the role of hot electrons. *Phys. Rev. Lett.*, 61:1321, 1988.

[11] S. A. Buntin, L. J. Richter, D. S. King, and R. R. Cavanagh. State-resolved evidence for hot carrier driven surface reaction: Laser-induced desorption of no from pt(111). *J. Chem. Phys*, 91:6429, 1989.

[12] L. Cai, X. Xiao, and M. M. T. Loy. Femtosecond laser desorption of co from the pt(111) surface. *Surf. Sci. Lett.*, 464:727, 2000.

[13] A. O. Caldeira and A. J. Leggett. Path integral approach to quantum brownian motion. *Physica A.*, 121:587, 1983.

[14] C. Carbogno, J. Behler, A. Gross, and K. Reuter. Fingerprints for spin-selection rules in the interaction dynamics of o_2 at al(111). *Phys. Rev. Lett.*, 101:096104, 2008.

[15] C. Carbogno, J. Behler, K. Reuter, and A. Gross. Signatures of nonadiabatic o_2 dissociation at al(111): First-principles fewest-switches study. *Phys. Rev. B*, 81:035410, 2010.

[16] E. F de Lima and J. E. M. Hornos. Matrix elements for the morse potential under an external field. *J. Phys. B*, 38:815, 2005.

[17] S. Deliwala, R. J. Finlay, J. R. Goldman, T. H. Her, W. D. Mieher, and E. Mazur. Surface femtochemistry of o_2 and co on pt(111). *Chem. Phys. Lett.*, 242:617, 1995.

[18] D. N. Denzler, C. Frischkorn, M. Wolf, and G. Ertl. Surface femtochemistry: Associative desorption of hydrogen from ru(001) induced by electronic excitations. *J. Chem. Phys. B*, 108:14503, 2004.

[19] C. Díaz, A. Perrier, and G. J. Kroes. Associative desorption of n_2 from ru(0001): A computational study. *Chem. Phys. Lett.*, 434(4-6):231 – 236, 2007.

[20] C. Díaz, J. K. Vincent, G. P. Krishnamohan, R. A. Olsen, G. J. Kroes, K. Honkala, and J. K. Nørskov. Multidimensional effects on dissociation of n_2 on ru(0001). *Phys. Rev. Lett.*, 96(9):096102, 2006.

[21] C. Díaz, J. K. Vincent, G. P. Krishnamohan, R. A. Olsen, G. J. Kroes, K. Honkala, and J. K. Nørskov. Reactive and nonreactive scattering of n_2 from ru(0001): A six-dimensional adiabatic study. *J. Chem. Phys.*, 125:114706, 2006.

[22] L. Diekhöner, L. Hornekær, H. Mortensen, E. Jensen, A. Baurichter, V. V. Petrunin, and A. C. Luntz. Indirect evidence for strong nonadiabatic coupling in n_2 associative desorption from and dissociative adsorption on ru(0001). *J. Chem. Phys.*, 117:5018, 2002.

[23] L. Diekhöner, H. Mortensen, A. Baurichter, and A. C. Luntz. *J. Chem. Phys.*, 115:3356, 2001.

[24] R. M. Dreizler and E. K. U. Gross. *Density Functional Theory.* Springer, 1990.

[25] J. Enkovaara et al. Electronic structure calculations with gpaw: a real-space implementation of the projector augmented-wave method. *J. Phys.: Condens. Matter*, 22:253202, 2010.

[26] J. S. Evans and T. V. Voorhis. Dynamic current suppression and gate voltage response in metal-molecule-metal junctions. *Nano Lett.*, 9:2671, 2009.

[27] W. S. Fann, R. Storz, H. W. K. Tom, and J. Bokor. Direct measurement of nonequilibrium electron-energy distributions in subpicosecond laser-heated gold films. *Phys. Rev. Lett*, 68:2834, 1992.

[28] W. S. Fann, R. Storz, H. W. K. Tom, and J. Bokor. Electron thermalization in gold. *Phys. Rev. B*, 46:13592, 1992.

[29] R. P. Feynman and F. L. Vernon. The theory of a general quantum mechanical system interacting with a linear dissipative system. *Ann. Phys. (N.Y.)*, 24:118, 1963.

[30] C. Fiolhais, F. Nogueira, and M. A. L. Marques (Eds.). *A Primer in Density Functional Theory.* Springer, 2003.

[31] T. Frederiksen, M. Paulsson, M. Brandbyge, and A.-P. Jauho. Inelastic transport theory from first principles: Methodology and application to nanoscale devices. *Phys. Rev. B*, 75:205413, 2007.

[32] C. Frischkorn and M. Wolf. Femtochemistry at metal surfaces: Nonadiabatic reaction dynamics. *Chem. Rev.*, 106:4207, 2006.

[33] J. W. Gadzuk. Inelastic resonance scattering, tunneling, and desorption. *Phys. Rev. B*, 44:13466, 1991.

[34] J. W. Gadzuk. Resonance-assisted hot electron femtochemistry at surfaces. *Phys. Rev. Lett.*, 76:4234, 1996.

[35] J. W. Gadzuk. Role of secondary electrons in hot-electron femtochemistry at surfaces using tunnel junctions. *J. Vac. Sci. Technol. A*, 15:1520, 1997.

[36] J. W. Gadzuk. Intramolecular dynamics due to electron transitions: from photoelectron spectroscopy to femtochemistry. *J. Elec. Spec.*, 98-99:321, 1999.

[37] M. Galperin and M. A. Ratner. On the line widths of vibrational features in inelastic electron tunneling spectroscopy. *Nano. Lett.*, 4:1605, 2004.

[38] M. Galperin, M. A. Ratner, and A. Nitzan. Molecular transport junctions: vibrational effects. *J. Phys. Condens. Matter.*, 19:103201, 2007.

[39] S. Gao. Quantum kinetic theory of vibrational heating and bond breaking by hot electrons. *Phys. Rev. B*, 55:1876, 1997.

[40] A. Görling. Density-functional theory beyond the hohenberg-kohn theorem. *Phys. Rev. A*, 59:3359, 1999.

[41] A. Görling. Proper treatment of symmetries and excited states in a computationally tractable kohn-sham method. *Phys. Rev. Lett.*, 85:4229, 2000.

[42] T. Grabo, M. Petersilka, and E.K.U. Gross. Molecular excitation energies from time-dependent density functional theory. *J. Mol. Structure (Theochem)*, 501:353, 2000.

[43] O. Gunnarsson and B. I. Lundqvist. Exchange and correlation in atoms, molecules, and solids by the spin-density-functional formalism. *Phys. Rev. B*, 13:4274, 1976.

[44] B. Hammer, L. B. Hansen, and J. K. Nørskov. Improved adsorption energetics within density-functional theory using revised perdew-burke-ernzerhof functionals. *Phys. Rev. B*, 59:7413, 1999.

[45] M. Head-Gordon and J. C. Tully. Molecular-orbital calculations of the lifetime of the vibrational modes of co on cu(100). *Phys. Rev. B*, 46:1853, 1992.

[46] P. Hedegård. Light quantum particles in a metallic environment. *Phys. Rev. B*, 35:533, 1987.

[47] P. Hedegård. Quantum diffusion in a metallic environment. *Phys. Rev. B*, 35:6127, 1987.

[48] M. Hillery, R. F. O'Connell, M. O. Scully, and E. P. Wigner. Distribution functions in physics. *Phys. Rep.*, 106:121, 1984.

[49] W. Ho. Femtosecond lase-induced dynamical quantum processes on solid surfaces (dqpss). *Surf. Sci.*, 363:166, 1996.

[50] P. Hohenberg and W. Kohn. Inhomogeneous electron gas. *Physical Review*, 136:864, 1964.

[51] L. Hornekær, E. Rauls, W. Xu, Ž. Šljivančanin, R. Otero, I. Stensgaard, E. Lægsgaard, B. Hammer, and F. Besenbacher. Clustering of chemisorbed h(d) atoms on the graphite (0001) surface due to preferential sticking. *Phys. Rev. Lett.*, 97:186102, 2006.

[52] L. Hornekær, Ž. Šljivančanin, W. Xu, R. Otero, E. Rauls, I. Stensgaard, E. Lægsgaard, B. Hammer, and F. Besenbacher. Metastable structures and recombination pathways for atomic hydrogen on the graphite (0001) surface. *Phys. Rev. Lett.*, 96:156104, 2006.

[53] K. P. Huber and G. Herzberg. *Molecular Spectra and Molecular Structure IV: Constants of Diatomic Molecules*. Van Nostrand Reinhold, New York, 1979.

[54] R. O. Jones and O. Gunnarsson. The density functional formalism, its applications and prospects. *Rev. Mod. Phys.*, 61:689, 1989.

[55] J. I. Juaristi, M. Alducin, R. Díez Muiño, H. F. Busnengo, and A. Salin. Role of electron-hole pair excitations in the dissociative adsorption of diatomic molecules on metal surfaces. *Phys. Rev. Lett.*, 100:116102, 2008.

[56] J. I. Juaristi, M. Alducin, R. Díez Muiño, H. F. Busnengo, and A. Salin. Juaristi et al. reply:. *Phys. Rev. Lett.*, 102:109602, 2009.

[57] F.-J. Kao, D. G. Busch, D. Cohen, D. Gomes da Costa, and W. Ho. Femtosecond laser desorption of molecularly adsorbed oxygen from pt(111). *Phys. Rev. Lett.*, 71:2094, 1993.

[58] F.-J. Kao, D. G. Busch, D. Gomes da Costa, and W. Ho. Femtosecond versus nanosecond surface photochemistry: O_2+co on pt(111) at 80 k. *Phys. Rev. Lett.*, 70:4098, 1993.

[59] W. Kohn and L. J. Sham. Self-consistent equations including exchange and correlation effects. *Physical Review*, 140:1133, 1965.

[60] R. Leturcq, C. Stamper, K. Inderbitzin, L. Durrer, C. Hierold, E. Mariani, M. G. Schultz, F. von Oppen, and K. Ensslin. Franck-condon blockade in suspended carbon nanotube quantum dots. *Nature Physics*, 5:327–331, 2009.

[61] M. Levy. Universal variational functionals of electron densities, first-order density matrices, and natural spin-orbitals and solution of the v-representability problem. *Proc. Natl. Acad. Sci. USA*, 76:6062, 1979.

[62] A. C. Luntz, I. Makkonen, M. Persson, S. Holloway, D. M. Bird, and M. S. Mizielinski. Comment on "role of electron-hole pair excitations in the dissociative adsorption of diatomic molecules on metal surfaces". *Phys. Rev. Lett.*, 102:109601, 2009.

[63] A. C. Luntz and M. Persson. How adiabatic is activated adsorption/associative desorption? *J. Chem. Phys.*, 123:074704, 2005.

[64] A. C. Luntz, M. Persson, S. Wagner, C. Frischkorn, and M. Wolf. Femtosecond laser induced associative desorption of h2 from ru(0001). comparison of first principles theory with experiment. *J. Chem. Phys.*, 124:244702, 2006.

[65] G. D. Mahan. *Many-Particle Physics*. Plenum Press, New York and London, 1981.

[66] M. A. L. Marques, C. A. Ullrich, F. Nogueira, A. Rubio, K. Burke, and E. K. U. Gross (Eds.). *Time-Dependent Density Functional Theory*. Springer, 2006.

[67] D. Menzel and R. Gomer. Desorption from metal surfaces by low-energy electrons. *J. Chem. Phys.*, 41:3311, 1964.

[68] J. A. Misewich, T. F. Heinz, and D. M. Newns. Desorption induced by multiple electronic transitions. *Phys. Rev. Lett.*, 68:3737, 1992.

[69] J. A. Misewich, A. Kalamarides, T. F. Heinz, U. Höfer, and D. M. Newns. Vibrationally assisted electronic desorption: Femtosecond surface chemistry of o_2/pd(111). *J. Chem. Phys.*, 100:736, 1994.

[70] A. Mitra, I. Aleiner, and A. J. Millis. Phonon effect in molecular transistors: Quantal and classical treatment. *Phys. Rev. B*, 69:245302, 2004.

[71] A. Mitra, I. Aleiner, and A. J. Millis. Semiclassical analysis of the nonequilibrium local polaron. *Phys. Rev. Lett.*, 94:076404, 2005.

[72] H. Mitter and K. Yamazaki. A factorization theorem for an exponential operator. *Lett. Math. Phys*, 8:321, 1984.

[73] M. Morin, N. J. Levinos, and A. L. Harris. Vibrational energy transfer of co/cu(100): Nonadiabatic vibration/electron coupling. *J. Chem. Phys.*, 96:3950, 1992.

[74] P. M. Morse. Diatomic molecules according to the wave mechanics. ii. vibrational levels. *Phys. Rev.*, 34:57, 1929.

[75] J. J. Mortensen, L. B. Hansen, and K. W. Jacobsen. Real-space grid implementation of the projector augmented wave method. *Phys. Rev. B*, 71:035109, 2005.

[76] M. J. Murphy, J. F. Skelly, A. Hodgson, and B. Hammer. Inverted vibrational distributions from n_2 recombination at ru(001): Evidence for a metastable molecular chemisorption well. *J. Chem. Phys.*, 110:6954, 1999.

[77] D. M. Newns. Self-consistent model of hydrogen chemisorption. *Phys. Rev.*, 178:1123, 1969.

[78] G. Nielsen, L. B. Thomsen, M. Johansson, O. Hansen, and I. Chorkendorff. Electron emission from mos electron emitters with clean and cesium covered gold surfaces. *App. Surf. Sci*, 225:7657, 2009.

[79] J. Oddershede, N. E. Grüner, and G. H. F. Diercksen. Comparison between equation of motion and polarization calculations. *Chem. Phys.*, 97:303, 1985.

[80] H. Park, J. Park, A. K. L. Lim, E. H. Anderson, A. P. Alivisatos, and P. L. McEuen. Nanomechanical oscillations in a single-c_60 transistor. *Nature*, 407:57–60, 2000.

[81] R. G. Parr and W. Yang. *A Primer in Density Functional Theory of Atoms and Molecules*. Oxford University Press, 1989.

[82] A. N. Pasupathy et al. Vibration-assisted electron tunneling in c_140 transistors. *Nano Lett.*, 5:203–207, 2005.

[83] J. P. Perdew, K. Burke, and M. Ernzerhof. Generalized gradient approximation made simple. *Phys. Rev. Lett.*, 77:3865, 1996.

[84] B. N. J. Persson and M. Persson. Vibrational lifetime for co adsorbed on cu(100). *Solid State Commun.*, 36:175, 1980.

[85] J. A. Prybyla, T. F. Heinz, J. A. Misewich, M. M. T. Loy, and J. H. Glownia. Desorption induced by femtosecond laser pulses. *Phys. Rev. Lett.*, 64:1537, 1990.

[86] J. A. Prybyla, H. W. K. Tom, and G. D. Aumiller. Femtosecond time-resolved surface reaction: Desorption of co from cu(111) in ¡ 325 fsec. *Phys. Rev. Lett.*, 68:503, 1992.

[87] P. A. Redhead. Interaction of slow electrons with chemisorbed oxygen. *Can. J. Phys.*, 42:886, 1964.

[88] E. Runge and E. K. U. Gross. Density-functional theory for time-dependent systems. *Phys. Rev. Lett.*, 52:997, 1984.

[89] P. Saalfrank. Quantum dynamical approach to ultrafast molecular desorption from surfaces. *Chem. Rev.*, 106:4116, 2006.

[90] P. Saalfrank, M. Nest, I. Andrianov, T. Klamroth, D. Kröner, and S. Beyvers. Quantum dynamics of laser-induced desorption from metal and semiconductor surfaces and related phenomena. *J. Phys.: Condens. Matter*, 18:1425, 2006.

[91] J. J. Sakurai. *Modern Quantum Mechanics*. Addison-Wesley, 1994.

[92] S. Sapmaz, P. J.-Herrero, Y. M. Blanter, C. Dekker, and H. S. J van der Zant. Tunneling in suspended carbon nanotubes assisted by longitudinal phonons. *Phys. Rev. Lett.*, 96:026801, 2006.

[93] A. Schmid. On a quasiclassical langevin equation. *J. Low Temp. Phys.*, 49:609, 1982.

[94] Ž. Šljivančanin, E. Rauls, L. Hornekaer, W. Xu, F. Besenbacher, and B. Hammer. Extended atomic hydrogen dimer configurations on the graphite(0001) surface. *The Journal of Chemical Physics*, 131:084706, 2009.

[95] K. Stépán, J. Gűdde, and U. Hőfer. Time-resolved measurement of surface diffusion induced by femtosecond laser pulses. *Phys. Rev. Lett.*, 94:236103, 2005.

[96] L. M. Struck, L. J. Richter, S. A. Buntin, R. R. Cavanagh, and J. C. Stephenson. Femtosecond laser-induced desorption of co from cu(100): Comparison of theory and experiment. *Phys. Rev. Lett.*, 77:4576, 1996.

[97] M. Šunjić and A. Lucas. Phonon contribution to the x-ray photoemission linewidths in polar crystal films. *Chem. Phys. Lett.*, 42:462, 1976.

[98] N. J. Tao. Electron transport in molecular junctions. *Nature Nanotechnology*, 1:173, 2006.

[99] OCTOPUS is a freely available real space time-dependent density functional theory code (see `www.tddft.org/programs/octopus/`).

[100] `GPAW` is freely available as a part of the CAMPOS software: `www.camd.dtu.dk/Software`.

[101] L. B. Thomsen, G. Nielsen, S. B. Vendelbo, M. Johansson, O. Hansen, and I. Chorkendorff. Ultralarge area mos tunnel device for electron emission. *Phys. Rev. B*, 76:155315, 2007.

[102] L. B. Thomsen, G. Nielsen, S. B. Vendelbo, M. Johansson, O. Hansen, and I. Chorkendorff. Electron emission from ultralarge area metal-oxide-semiconductor electron emitters. *Vac. Sci. Technol. B*, 27:562, 2009.

[103] J. R. Trail, D. M. Bird, M. Persson, and S. Holloway. Electron-hole pair creation by atoms incident on a metal surface. *J. Chem. Phys.*, 119:4539, 2003.

[104] J. C. Tully, M. Gomez, and M. Head-Gordon. Electronic and phonon mechanisms of vibrational relaxation: Co on cu(100). *J. Vac. Sci. Technol. A*, 11:1914, 1993.

[105] T. V. Voorhis, T. Kowalczyk, B. Kaduk, L.-P. Wang, C.-L. Cheng, and Q. Wu. The diabatic picture of electron transfer, reaction barriers, and molecular dynamics. *Annu. Rev. Phys. Chem.*, 61:149, 2010.

[106] S Wagner, H Ostrom, A. Kaebe, M. Krenz, M. Wolf, A. C. Luntz, and C. Frischkorn. Activated associative desorption of c + o → co from ru(001) induced by femtosecond laser pulses. *New J. Phys.*, 10:125031, 2008.

[107] N. S. Wingreen, K. W. Jacobsen, and J. W. Wilkins. Inelastic scattering in resonant tunneling. *Phys. Rev. B*, 40:11834, 1989.

[108] Q. Wu and T. V. Voorhis. Direct optimization method to study constrained systems within density-functional theory. *Phys. Rev. A*, 72:24502, 2005.

[109] Q. Wu and T. V. Voorhis. Constrained density functional theory and its application in long-range electron transfer. *J. Chem. Theor. Comp.*, 2:765, 2006.

[110] L. H. Yu, Z. K. Keane, J. W. Ciszek L. Cheng, M. P. Stewart, J. M. Tour, and D. Natelson. Inelastic electron tunneling via molecular vibrations in single-molecule transistors. *Phys. Rev. Lett.*, 93:266802, 2004.

[111] Yingkai Zhang and Weitao Yang. Comment on generalized gradient approximation made simple. *Phys. Rev. Lett.*, 80:890, 1998.

[112] T. Ziegler, A. Rauk, and E. J. Baerends. On the calculation of multiplet energies by the hartree-fock-slater method. *Theor. Chim. Acta*, 43:261, 1977.

[113] F. M. Zimmerman and W. Ho. State resolved studies of photochemical dynamics at surfaces. *Surf. Sci. Rep.*, 22:127, 1995.

Included Papers

Paper I

J. Gavnholt, T. Olsen, M. Engelund, and J. Schiøtz
Delta self-consistent field as a method to obtain potential energy surfaces of excited molecules on surfaces
Phys. Rev. B **78**, 075441 (2008).

Δ self-consistent field method to obtain potential energy surfaces of excited molecules on surfaces

Jeppe Gavnholt, Thomas Olsen, Mads Engelund,* and Jakob Schiøtz†
Danish National Research Foundation's Center for Individual Nanoparticle Functionality (CINF), Department of Physics, Technical University of Denmark, DK-2800 Kongens Lyngby, Denmark
(Received 9 June 2008; revised manuscript received 15 July 2008; published 27 August 2008)

We present a modification of the Δ self-consistent field (ΔSCF) method of calculating energies of excited states in order to make it applicable to resonance calculations of molecules adsorbed on metal surfaces, where the molecular orbitals are highly hybridized. The ΔSCF approximation is a density-functional method closely resembling standard density-functional theory (DFT), the only difference being that in ΔSCF one or more electrons are placed in higher lying Kohn-Sham orbitals instead of placing all electrons in the lowest possible orbitals as one does when calculating the ground-state energy within standard DFT. We extend the ΔSCF method by allowing excited electrons to occupy orbitals which are linear combinations of Kohn-Sham orbitals. With this extra freedom it is possible to place charge locally on adsorbed molecules in the calculations, such that resonance energies can be estimated, which is not possible in traditional ΔSCF because of very delocalized Kohn-Sham orbitals. The method is applied to N_2, CO, and NO adsorbed on different metallic surfaces and compared to ordinary ΔSCF without our modification, spatially constrained DFT, and inverse-photoemission spectroscopy measurements. This comparison shows that the modified ΔSCF method gives results in close agreement with experiment, significantly closer than the comparable methods. For N_2 adsorbed on ruthenium (0001) we map out a two-dimensional part of the potential energy surfaces in the ground state and the 2π resonance. From this we conclude that an electron hitting the resonance can induce molecular motion, optimally with 1.5 eV transferred to atomic movement. Finally we present some performance test of the ΔSCF approach on gas-phase N_2 and CO in order to compare the results to higher accuracy methods. Here we find that excitation energies are approximated with accuracy close to that of time-dependent density-functional theory. Especially we see very good agreement in the minimum shift of the potential energy surfaces in the excited state compared to the ground state.

DOI: 10.1103/PhysRevB.78.075441 PACS number(s): 31.15.xr, 31.50.Df, 82.20.Gk

I. INTRODUCTION

Density-functional theory[1,2] (DFT) has proved to be a vital tool in gaining information on many gas-surface processes. This may be surprising, since DFT is only valid for relaxed systems in their ground state and therefore not directly applicable to dynamical situations. However, often the electrons relax much faster than the time scale of the atomic movement, such that the electron gas can be considered relaxed in its ground state at all times. Then potential energy surfaces (PES) of the ground state obtained by DFT, or any other method, can be used to describe the motion of atomic cores. This is the Born-Oppenheimer approximation.

In some situations, however, the Born-Oppenheimer approximation is not valid. This is for example the case when the electronic system is excited by a femtosecond laser[3,4] or hot electrons are produced with a metal-insulator-metal junction.[5] The Born-Oppenheimer approximation also breaks down if the time scales for the electronic and nuclear motions are comparable or if the separations between the electronic states are very small, such that transitions between the electronic states will occur. In these situations it is necessary to go beyond the Born-Oppenheimer approximation either by considering the coupling between electronic states[6,7] where it becomes necessary to obtain PESs of excited states, or by an electronic friction model.[8,9]

The problem of calculating excitation energies is being approached in many different ways, even within DFT. Time dependent density-functional theory[10] (TDDFT) gives, compared to the computational cost, good agreement with experiments for excitations in atoms and molecules.[11] However, TDDFT suffers some problems in excitations involving charge transfer.[12] The GW approximation[13,14] can be used to gain accurate excitation energies for molecules and clusters. The embedding method,[15,16] which combines high-accuracy quantum chemistry methods with DFT, makes it possible to handle larger periodic systems with great accuracy. The embedding theory has been applied to estimate PESs of excited molecules on surfaces.[17] However, the computational cost and involved complexity are still very high. Our aim has been to find a method, which at a computational cost close the level of ground-state DFT, can estimate excited-state energies of molecules on surfaces with reasonable accuracy. Such a method would make it more feasible to consider a large range of systems in search of systems with interesting or desired properties.

Constrained DFT (Refs. 7, 18, and 19) and Δ self-consistent field (ΔSCF) (Refs. 20 and 21) are two different approaches, which both can be considered as small extensions of ground-state DFT, such that the computational cost lies close to that of ground-state DFT. In constrained DFT an additional potential is introduced and varied until a certain constraint on the electrons is fulfilled. The simplest approach is to lower (or increase) the potential in a certain part of space until you have the desired number electrons in this area.[18] A different approach is to introduce potentials on the orbitals in a localized basis set, which depends on the orbitals' positions in space.[7] In Sec. III we will argue that when

considering molecular resonance states on surfaces it may be problematic with such a strict constraint on the electrons, since a part of the charge may return to the surface on a much shorter time scale than the lifetime of the resonance.

In the ΔSCF scheme the positions of the electrons are controlled by controlling the occupation of the Kohn-Sham (KS) states as the system reaches self-consistency. The ΔSCF scheme has for a long time been justified in cases, where the excited state corresponds to the lowest state of a given symmetry.[22] The scheme has, however, often been applied to more general cases. More recently, Görling[23] extended the KS formalism to include excited states, such that ΔSCF gets a formal justification in the general case, although a special unknown orbital-dependent exchange-correlation potential should be used for the excited states. In practical implementations standard exchange-correlation potentials from ground-state DFT are typically used.

This traditional way of just controlling the occupation of the KS orbitals has some limitations. For example when a molecule is placed on a metallic surface the molecular orbitals will hybridize with the orbitals in the surface, such that the molecular orbitals will be spread over several KS states. For such systems there is no good way of representing a resonance on the molecule as a change in the occupations of the KS orbitals. The optimal thing one can do within this scheme is to occupy the KS orbital with the largest overlap with the molecular orbital in question, but this overlap can be quite small and highly system size dependent. This problem was also pointed out by Hellman *et al.*[21] and Behler *et al.*[7]

In this paper we modify the ΔSCF approach, such that electrons are allowed to occupy arbitrary linear combinations of KS orbitals. In this way one achieves much better control on the position of the excited electron. As is the case for traditional ΔSCF some knowledge of the resonance is needed in order to apply the method. The method is especially relevant in Newns-Anderson-type[24,25] systems, where a resonance can be attributed to a known single level, which has been hybridized through interactions with other states. This includes systems with molecules adsorbed on metal surfaces and molecules trapped between to metal contacts.

The modification we propose only has minor implications on the way practical calculations are performed, which is very similar to performing an ordinary ground-state DFT calculation. In the following we will go through the details of the method and apply it to a few diatomic molecules on metallic surfaces. The obtained results will be compared to the ordinary ΔSCF method, spatially constrained DFT, and inverse-photoemission spectroscopy (IPES) measurements. Finally we present some tests on the performance of the ΔSCF approach on N_2 and CO in the gas phase.

II. METHOD

In the following we go through the differences between the linear-expansion ΔSCF method we propose, ordinary ΔSCF, and standard DFT. We start by stating the modification of the KS equations when considering an electron excited from the Fermi level to a higher lying state. Then we show how this affects the energy calculation. Finally we generalize the approach to other types of excitations.

A. Kohn-Sham equations

The fundamental KS equations[2] represent a practical way of finding the ground-state electron density for a given external potential and a given number of electrons through an iterative process

$$\left[-\frac{\nabla^2}{2}+v_{\mathrm{KS}}[n](\mathbf{r})\right]\psi_i(\mathbf{r})=\epsilon_i\psi_i(\mathbf{r}), \tag{1}$$

$$n(\mathbf{r})=\sum_{i=1}^{N}\psi_i^*(\mathbf{r})\psi_i(\mathbf{r}), \tag{2}$$

$$v_{\mathrm{KS}}[n](\mathbf{r})=v_{\mathrm{ext}}(\mathbf{r})+\int d\mathbf{r}'\frac{n(\mathbf{r}')}{|\mathbf{r}-\mathbf{r}'|}+\frac{\delta E_{xc}}{\delta n(\mathbf{r})}, \tag{3}$$

where v_{KS} is the KS potential, E_{xc} is the exchange-correlation energy, and N is the number of electrons. As seen from Eq. (2) only the N orbitals with lowest energy contribute to the density, i.e., the electrons are placed in these orbitals.[26] In ordinary ΔSCF one estimates properties of excited states by placing the electrons differently. For example the HOMO-LUMO gap in a molecule could be estimated by replacing Eq. (2) with

$$n(\mathbf{r})=\sum_{i=1}^{N-1}\psi_i^*(\mathbf{r})\psi_i(\mathbf{r})+\psi_a^*(\mathbf{r})\psi_a(\mathbf{r}), \tag{4}$$

where $\psi_a(\mathbf{r})$ is the KS orbital resembling the LUMO from the ground-state calculation. Naturally, the KS orbitals found when solving these modified KS equations will differ from the ones found in an ordinary DFT calculation due to the change in the Hamilton through the change in the density when different orbitals are occupied.

In the linear-expansion ΔSCF method we propose, the excited electron is not forced to occupy a KS orbital, but can occupy any orbital that is a linear combination of empty KS orbitals

$$\psi^{\mathrm{res}}(\mathbf{r})=\sum_{i=N}^{M}a_i\psi_i(\mathbf{r}), \tag{5}$$

where M is the number of KS orbitals in the calculation. In practice this means that the KS many-particle wave function is no longer just a Slater determinant of N KS orbitals, but a Slater determinant of $N-1$ KS orbitals and $\psi^{\mathrm{res}}(\mathbf{r})$. Only empty KS orbitals are included in the linear expansion, since otherwise $\psi^{\mathrm{res}}(\mathbf{r})$ will not be orthogonal to the filled KS orbitals. Equation (2) is then replaced with

$$n(\mathbf{r})=\sum_{i=1}^{N-1}\psi_i^*(\mathbf{r})\psi_i(\mathbf{r})+\sum_{i,j=N}^{M}a_i^*a_j\psi_i^*(\mathbf{r})\psi_j(\mathbf{r}). \tag{6}$$

Since the expansion coefficients a_i in principle could have any value some *a priori* knowledge are needed in order to choose good values. In the case of molecular resonances on surfaces the expansion coefficients are chosen such that

$\psi^{\mathrm{res}}(\mathbf{r})$ resembles the relevant molecular orbital as much as possible, i.e.,

$$a_i = \frac{\langle \psi_i | \phi \rangle}{\left(\sum_i |\langle \psi_i | \phi \rangle|^2 \right)^{1/2}}, \tag{7}$$

where ϕ is the molecular orbital. This is consistent with a Newns[24] and Anderson[25] picture, where the resonance corresponds to an electron getting in the molecular orbital, but the resonance broadening and energy shift are due to hybridization with the metallic bands and an image charge effect.

In calculations with k-point sampling the linear expansion is performed independently in all k points. In the linear-expansion ΔSCF one then avoids the difficulties one can encounter in choosing which KS state to occupy in each k point in the traditional way of performing ΔSCF calculations. For example, one may risk occupying different bands in each k point, when just choosing the KS orbital with the largest overlap with the molecular orbital in each k point.

B. Energy

The energy calculation, which is performed after the KS equations have reached self-consistency, is not significantly different in the linear-expansion ΔSCF scheme compared to ordinary DFT. The Hartree energy is evaluated directly from the density, which is also the case for the exchange-correlation energy if an orbital independent functional is used. So in linear-expansion ΔSCF these terms are evaluated exactly as in ordinary DFT. In ordinary DFT the kinetic energy is evaluated as

$$T[n(\mathbf{r})] = \sum_{i=1}^{N} \langle \psi_i | -\frac{\nabla^2}{2} | \psi_i \rangle = \sum_{i=1}^{N} \epsilon_i - \int v_{\mathrm{KS}}[n](\mathbf{r}) n(\mathbf{r}) d\mathbf{r}, \tag{8}$$

where the last equality is seen directly from Eq. (1). Similarly the expression for the kinetic energy in the linear-expansion ΔSCF is found to be

$$T[n(\mathbf{r})] = \sum_{i=1}^{N-1} \epsilon_i + \sum_{i=N}^{M} |a_i|^2 \epsilon_i - \int v_{\mathrm{KS}}[n](\mathbf{r}) n(\mathbf{r}) d\mathbf{r}. \tag{9}$$

For orbital-dependent exchange-correlation functionals some effort must be put into ensuring that the exchange-correlation energy is evaluated correctly. This should however be quite straightforward since all the occupied orbitals are known.

C. Gradients

Gradients of PESs are easily evaluated in ordinary DFT due to the Hellman-Feynman theorem. The Hellman-Feynman theorem, however, only applies to eigenstates and not linear expansions of eigenstates. Due to this there is no easy way of gaining the gradients in a linear-expansion ΔSCF calculation. In Sec. IV C we will show that the Hellman-Feynman gradients do in fact not match the true gradients.

D. Other excitations

Above we only considered excitations where an electron is removed from the Fermi energy and placed in some specified orbital. The method is, however, easily extended to other types of excitations by representing each removed and each added electrons as linear expansions of KS orbitals. Equation (6) then gains an extra sum for each extra linear expansion. In cases of removed electrons the sign should of course be negative and the sum be over KS states below the Fermi energy. Similarly Eq. (9) gains extra sums.

E. Implementation

We have implemented the method in GPAW,[27,28] which is a real-space DFT code that uses the projector-augmented waves[29,30] (PAW) formalism to represent the core electrons. The self-consistent electron density is determined by an iterative diagonalization of the KS Hamiltonian and Pulay mixing of the resulting density.[31] For calculations on single molecules we use the local-density approximation[32] (LDA) as well as revised Perdew-Burke-Ernzerhof (RPBE) (Ref. 33) to describe exchange and correlation effects. The LDA is used because we compare to TDDFT results obtained using the adiabatic local-density approximation (ALDA),[34] and RPBE is used to see whether or not the generalized gradient description improves results. For calculations on molecules at surfaces we only use RPBE because this is designed to perform well for molecules adsorbed on transition-metal surfaces.

The projection step described in Sec. II A can easily be approximated within the PAW formalism if the atomic orbitals are chosen as partial waves; see Appendix for details.

For reasons of comparison we have also made a few linear-response TDDFT (lrTDDFT) calculations. These have been made using the OCTOPUS code,[35,36] which is a real-space TDDFT code using norm-conserving pseudopotentials to represent core electrons.

III. MOLECULES ON SURFACES

The linear-expansion ΔSCF method is especially relevant for molecules on metallic surfaces because the molecular state, due to hybridization, is spread over many KS states, i.e., it is necessary to write the resonant state as a linear combination of KS states. In this section we will make a detailed investigation of the 2π resonance of N_2 on a ruthenium (0001) surface. Furthermore we apply the proposed method to several diatomic molecules on different metallic surfaces and compare the results to other methods and experiments. Finally we map out a part of the PESs for N_2 on ruthenium (0001) and use it to estimate how much energy could possibly be put into molecular motion from an electron hitting the resonance.

A. 2π resonance energy for N_2 on ruthenium

The two top panels in Fig. 1 show the 2π resonance energy for N_2 on a ruthenium (0001) surface as a function of the system size, i.e., the surface unit cell and the number of ruthenium layers.

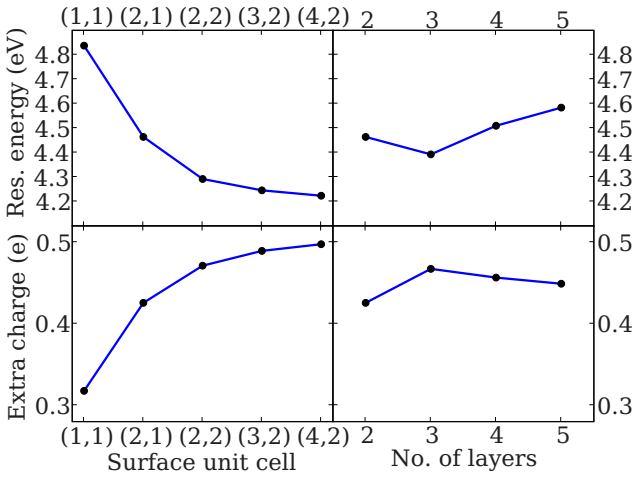

FIG. 1. (Color online) Upper row: The 2π resonance energy of N_2 molecule on a ruthenium surface. Lower row: The extra charge on the N_2 molecule in the resonance compared to a ground-state calculation. Left panels are for two layers and different surface cells, i.e., different N_2 coverages. Right panels are for a (2,1) surface cell and different number of layers. The extra amount of charge is estimated using Bader decomposition (Refs. 37 and 38).

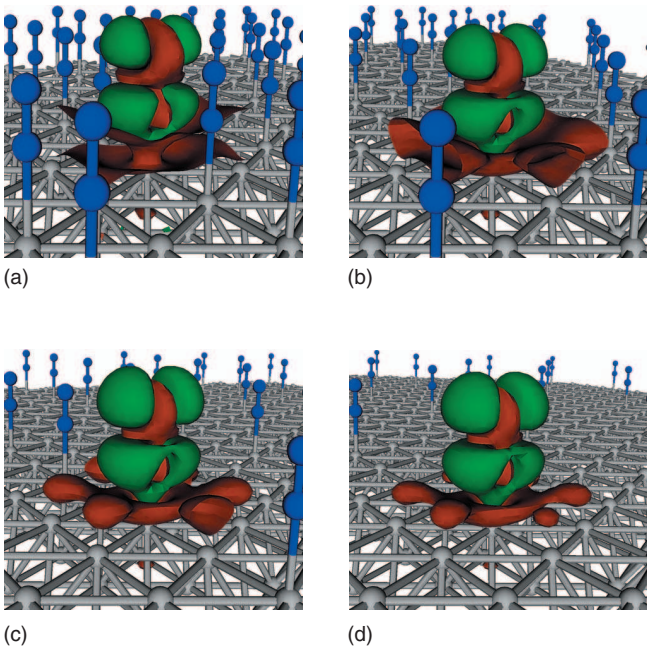

FIG. 2. (Color) The change in charge distribution due to the excitation. Green: more charge (0.01 a.u. contour), red: less charge (−0.01 a.u. contour). The four figures are for four different surface unit cells: (1,1), (2,1), (2,2), and (4,2). Gray atoms are ruthenium and blue atoms are nitrogen. The periodic images of the atoms are also shown, whereas the density changes are only shown in one unit cell.

The resonance energy is the total-energy difference between a resonant calculation and a ground-state calculation, both performed with atomic positions corresponding to the minimum of the ground-state PES (vertical resonance energies). We minimize the energy in the ground-state calculations by keeping all surface atoms frozen and found that the nitrogen molecule is placed on top with the two nitrogen atoms placed 2.084 and 3.201 Å above the surface. In the resonance calculation the $2\pi_y$ orbital of the N_2 molecule has been expanded on all KS states above the Fermi energy. This expansion has been used as ψ^{res} in Eq. (5). Although an extra electron is placed on the molecule we keep the total number of electrons unchanged, such that the unit cell is neutral. This is reasonable because a charged molecule will form an image charge in the surface, keeping the entire system neutral.

The resonance energy is converged to within 0.1 eV at a surface unit cell of (2,2). The rather large variation in energy for smaller unit cells is probably due to dipole interactions between periodic images. This is confirmed by a simple estimation of the dipol-dipol interaction energies. The resonance energy is not influenced significantly by the number of layers in the ruthenium, indicating that the charge redistribution only occurs very near to the surface. That the charge redistribution is local is confirmed by Fig. 2, which shows the change in charge between the resonance calculation and the ground-state calculation for four different surface unit cells.

For the larger unit cells, where the resonance energy has converged, a clearly localized image charge is seen below the nitrogen molecule and above the first layer of ruthenium atoms. The area with extra charge clearly resembles the 2π orbital of nitrogen, indicating that the 2π orbital is well represented by the linear expansion of KS orbitals. Figure 2 also reveals that some charges are redistributed within the molecule.

In order to get an estimate of the size of the charge redistribution we also performed Bader decomposition[37,38] on the density found in the ground-state calculation and the resonance calculation. The two bottom panels in Fig. 1 show the extra charge assigned to the nitrogen molecule in the resonance calculation compared to the ground-state calculation as a function of system size. The converged value is close to 0.5 electron charge, i.e., only half of the electron is placed on the nitrogen molecule according to the Bader decomposition. This discrepancy could either be due to the ambiguity in the way one chooses to assign charge to the atoms or a more physical effect of charge going back into the surface when extra charge is placed on the molecule. The former reason is very likely, since the image charge is located very close to the molecule.

In order to investigate the effect of charge going back into the surface we start by considering the 2π orbital itself. Figure 3 shows the density of KS states and the projected density of states (PDOS) for the 2π orbital for the ground-state calculation and the resonance calculation. In the ground-state calculation a part of the long tail of the PDOS goes below the Fermi energy, i.e., a small part of the 2π orbital is occupied here. In the resonance calculation the PDOS has moved upward in energy such that the tail no longer goes below the Fermi energy, i.e., some charges go back into the surface as charge is placed on the molecule. Similar effects are seen for the other molecular orbitals as visualized in Fig. 4, which shows the PDOS for the 3σ, 4σ, 1π, and 5σ orbitals. Again it is seen that all the PDOSs are shifted up in energy as more

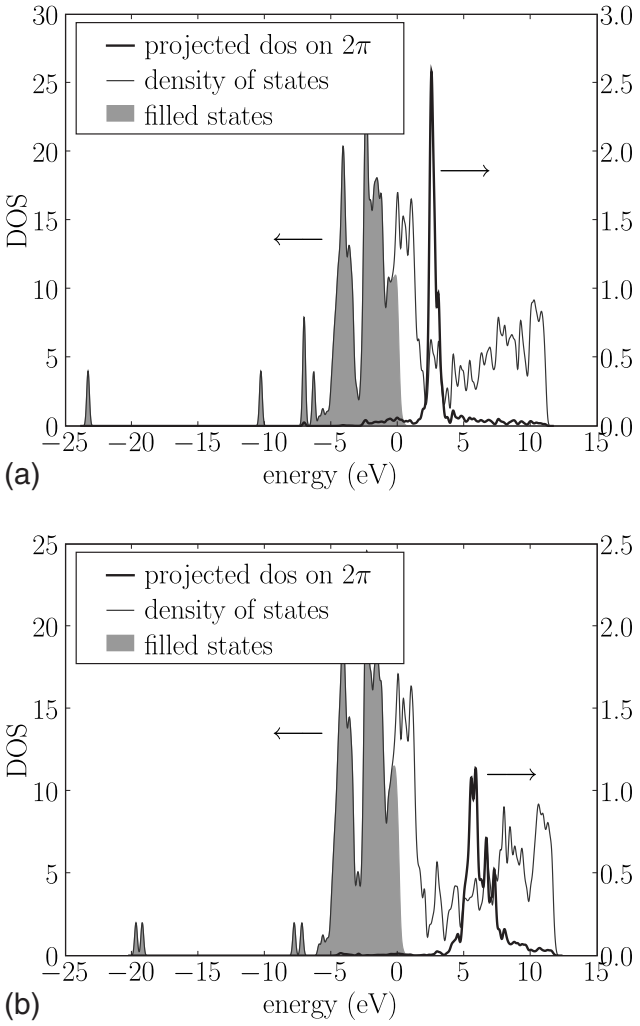

FIG. 3. The density of states for a N_2 molecule on a ruthenium slab and the projected density of states on the 2π orbital of the N_2 molecule. Top: Ground-state calculation. Bottom: Resonance calculation.

charge is placed on the molecule. Almost the entire PDOSs are still under the Fermi level, but small ripples can be seen above the Fermi level, also contributing to the amount of charge going back into the surface.

This backtransfer of charge is not an unwanted effect, since we try to model the long-lived resonance state, i.e., the reasonably localized peak in the PDOS in Fig. 3. The backtransfer of charge is due to some on the energy scale very delocalized bands, indicating a much shorter lifetime, i.e., the backtransfer is expected to happen on a much shorter time scale than the decay of the resonance. It is however clear from Figs. 3 and 4 that the charge backtransfer in this case is far from the 0.5 electron indicated by the Bader decomposition. We then conclude that the main part of the discrepancy in this situation can be assigned to the ambiguity in the way charge is assigned to the different atoms. We also find that one gets significant different results by assigning charge in a different manner, for example, by dividing the charge by a flat plane midway between the surface and the molecule.

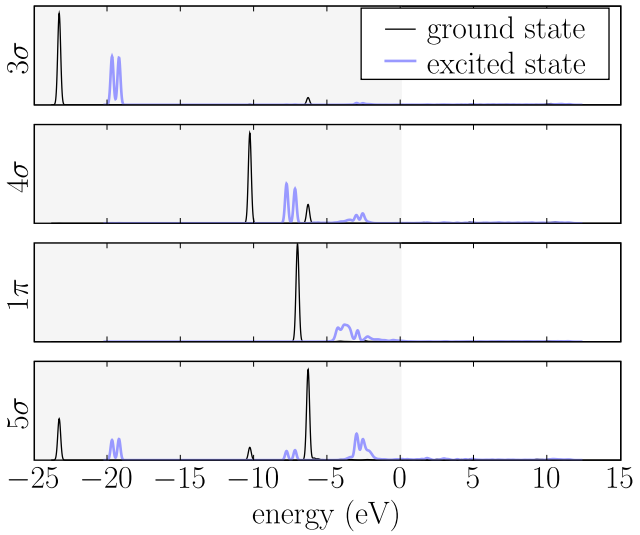

FIG. 4. (Color online) Projected density of states (PDOS) on the 3σ, 4σ, 1π, and 5σ orbitals of a N_2 molecule sitting on a ruthenium slab. The PDOSs are plotted for both the ground-state calculation and the resonance calculation. The gray area indicates energies below the Fermi level.

B. Comparison with inverse-photoemission spectroscopy experiments

In Table I we have tested the linear-expansion ΔSCF method against inverse-photoemission spectroscopy measurements and compared the results to spatially constrained DFT and ordinary ΔSCF calculations. The modified ΔSCF values are all calculated in exactly the same manner as for N_2 on ruthenium in Sec. III A. In all cases the molecules sit on top, and all surface atoms were kept fixed during the minimization of the molecular degrees of freedom. For the

TABLE I. Comparison of the 2π resonance energies for different diatomic molecules on different surfaces found by spatially constrained DFT, ordinary ΔSCF, our modified ΔSCF, and experiments. The experimental results have been obtained from inverse-photoemission spectroscopy measurements. All energies are in eV. We have not included lrTDDFT calculations, since it is not applicable to periodic systems.

System	Constrained DFT	ΔSCF (orig.)	ΔSCF (this work)	Experiment
N_2 on Ni(001)	2.2	3.5	4.0	4.4[a]
CO on Ni(001)	2.2	3.2	4.2	4.0[a]/4.5[b]
NO on Ni(001)	2.2	0.6	1.4	1.6[a]/1.5[c]
CO on Ni(111)	2.8	4.3	4.4	4.4[c]
NO on Ni(111)	2.7	0.5	1.4	1.5[b]
CO on Pd(111)	4.6	4.1	4.9	4.7[d]
CO on Pd step	2.8	3.2	4.5	4.0[d]

[a]Johnson and Hulbert (Ref. 39).
[b]Reimer *et al.* (Ref. 40).
[c]Reimer *et al.* (Ref. 41).
[d]Rogozik and Dose (Ref. 42).

TABLE II. The positions of the molecules in the systems from Table I. All positions are relative to the closest surface atom. The z direction is normal to the surface. At the Pd step the CO molecule is tilted over the step, which is the reason for the composant in the y direction. All numbers are in Angstroms.

Surface	Molecule	Pos. of 1. atom	Pos. of 2. atom
Ni(001)	N_2	N: (0,0,1.638)	N: (0,0,2.798)
	CO	C: (0,0,1.456)	O: (0,0,2.621)
	NO	N: (0,0,1.404)	O: (0,0,2.580)
Ni(111)	CO	C: (0,0,1.774)	O: (0,0,2.941)
	NO	N: (0,0,1.758)	O: (0,0,2.935)
Pd(111)	CO	C: (0,0,1.904)	O: (0,0,3.064)
Pd step	CO	C: (0,0.586,1.801)	O: (0,0.844,2.934)

Ni (001) surface we used three atomic layers, for the Ni (111) and Pd surfaces we used two atomic layers. The positions of the molecules in their minimized position are given in Table II. All resonance energies are vertical from the minimum of the ground-state PES. The relevant resonance for all the considered systems is the 2π resonance.

The spatially constrained DFT method was suggested by Wu and Van Voorhis.[18,19] In the calculations we perform here we divide the space into two areas divided by the flat plane mid between the surface and the lowest atom in the molecule. We the apply a potential $V=V_0[1+\exp(\frac{z_0-z}{\Delta z})]^{-1}$, with $\Delta z=0.2$ Å and z_0 being the z value of the dividing plane. V_0 is varied until an extra electron is placed on the molecules side of the dividing plane compared to the unconstrained calculation. The energy is then calculated as described by Wu and Van Voorhis.[18,19] The results using the original ΔSCF method have all been obtained by forcing an electron in the KS orbital with the largest overlap with the 2π orbital.

The results obtained with our proposed modification of the ΔSCF method are seen to agree quite well with the experimental results, better than the spatially constrained DFT and the original ΔSCF methods. All the results obtained by the original ΔSCF approach lie too low, which is due to the fact that the large hybridization of the molecular orbitals makes it impossible to place sufficient charge on the molecule. However, a significant problem with this method is that PESs often become discontinuous if one chooses to occupy the KS orbital with the largest overlap with the molecular orbital, since this can be different orbitals at different configurations.

The major problem with the spatially constrained DFT method seems to be that it in some cases is a too strict criterion to force an extra electron on the molecule, which reflects itself in similar resonance energies for CO and NO. We find that the backtransfer of charge discussed in Sec. III A is significant for adsorbed NO and essential to obtain the resonance energies we find with the modified ΔSCF method. This indicates that the spatially constrained DFT approach is more suited for systems with a smaller coupling than one has on the metallic surfaces considered here. The good agreement between our modified ΔSCF method and experiments indicates that this method is preferable for these kinds of systems and that the backtransfer effect is indeed physically reasonable.

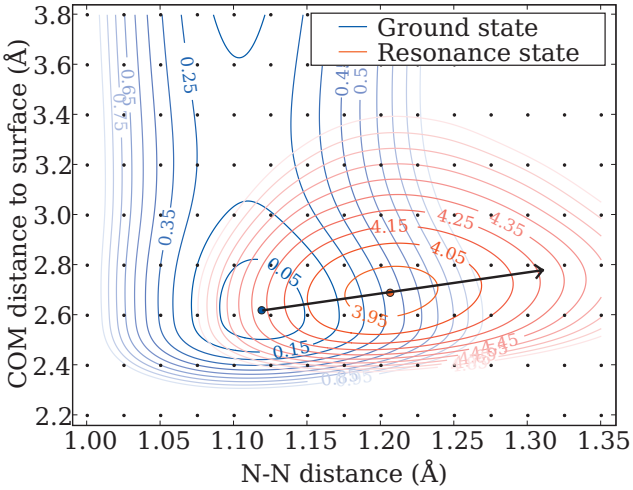

FIG. 5. (Color) Potential energy surfaces (PES) for a nitrogen molecule on a close-packed ruthenium surface in the ground state and the $2\pi_y$ resonance as a function of the distance between the two nitrogen atoms and the distance from the surface to the center of mass of the nitrogen molecule. The energies are in eV. The small dots represent the points where the energy has been calculated in order to generate the surfaces. The black arrow represents a possible trajectory of the system in the resonance state (see text).

C. Potential energy surfaces for N_2 on ruthenium

In Fig. 5 we have mapped out a part of the potential energy surfaces for a nitrogen molecule on a ruthenium (0001) surface in the ground state and the $2\pi_y$ resonances. We limit ourselves to two dimensions, which at least is reasonable in the ground state, since here it is well known that the molecule sits vertically on an on-top site. In the resonance state we have tried to rotate the molecule a small angle around the surface atom in the x and y directions at several points on the PES. In all cases this leads to an increase in energy, i.e., it also seems reasonable to stay within the two dimensions in the resonance state. Here we will only apply the PES to a simple estimate of the possible energy transfer into molecular motion from an electron hitting the resonance. For a more detailed analysis it is necessary to include other dimensions.

The ground-state PES looks as expected, with a small barrier for desorption and a local minimum corresponding to the adsorption configuration. The resonance PES has a shifted minimum, which indicates that an electron hitting this resonance could induce molecular motion, since a sudden shift between the PESs would leave the system far away from the minimum, such that the atoms would start to move. The maximum possible energy gain assuming classical ion dynamics from a single electron hitting the resonance can be roughly estimated by following the black arrow in Fig. 5. The system is most likely situated at the local minimum of the ground-state PES when the electron hits the resonance. The black arrow shows a possible trajectory of the system in

TABLE III. Vertical excitation energies for the N_2 molecule taken from the minimum-energy configuration of the ground state. All theoretical results are obtained using LDA as the *xc* potential (and ALDA for the *xc* kernel in the lrTDDFT calculations).

State	Transition	$\Delta\epsilon_{KS}$[a]	TDDFT[b] (ALDA)	ΔSCF (LDA)	ΔSCF (RPBE)	Exp.[c]
$a^1\Pi$			9.23	8.75	8.58	9.31
	$5\sigma\rightarrow 2\pi$	8.16				
$B^3\Pi$			7.62	7.55	7.52	8.04
Singlet-triplet splitting:			1.61	1.20	1.06	1.27
$w^1\Delta$			10.27	10.50	10.52	10.27
	$1\pi\rightarrow 2\pi$	9.63				
$W^3\Delta$			8.91	8.94	8.79	8.88
Singlet-triplet splitting:			1.36	1.56	1.73	1.39
$o^1\Pi$			13.87	11.97	12.40	13.63
	$4\sigma\rightarrow 2\pi$	11.21				
$C^3\Pi$			10.44	10.37	10.61	11.19
Singlet-triplet splitting:			3.43	1.60	1.79	2.44

[a]KS eigenvalue differences.
[b]Linear-response calculations taken from Grabo *et al.* (Ref. 44).
[c]Computed by Oddershede *et al.* (Ref. 45) using the spectroscopic constants of Huber and Herzberg (Ref. 46).

the resonance state until the resonance decays and the system returns to the ground-state PES. The potential energy after the electron event in this optimal situation is approximately 1.5 eV higher than before the event. This is seen to be more than enough to desorb the molecule. A more detailed analysis involving calculations of the possible vibrational excitations and the probabilities of exciting them will be the topic of a future publication. Such an analysis will have to take all six degrees of freedom of the molecule into account.

The PESs show that the center of mass is shifted away from the surface when the resonance is occupied. This may seem counterintuitive since the charged molecule is attracted to the generated image charge in the surface. However, the resonance weakens the bond between the nitrogen atoms, such that the distance between them increases, which shifts the center of mass outwards as the lower atom is not free to move closer to the surface. This effect is more significant than the decrease in the ruthenium-nitrogen distance due to the mentioned image charge effect.

IV. SMALL MOLECULES

In the following we present some small tests performed on N_2 and CO. These small systems have the advantage that they make it possible to compare to more accurate linear-response time-dependent density-functional theory calculations. When possible we also compare to experiments. The only advantage of our modified ΔSCF compared to ordinary ΔSCF for these molecules is the possibility of handling degenerate states without getting convergence problems, i.e., the following should be viewed as a test of the ΔSCF approach rather than a test of our modification. We are especially interested in confirming the ability to predict the shift of the minimum when going from the ground-state PES to the excited-state PES, which we in Sec. III C argued is very important when considering molecular motion induced by an electron hitting a molecular resonance.

A. Excitation energies

We have used the linear-expansion ΔSCF in combination with the multiplet sum method[43] to calculate excitation energies for different excitations in the N_2 and CO molecules. The results are presented in Tables III and IV, respectively. The 4σ and 5σ states are both represented by a single KS orbital. The 1π and 2π states are both double degenerate, so they are both represented as a linear combination of two KS orbitals: $|\pi\rangle=\frac{1}{\sqrt{2}}|\pi_{\mathrm{KS},a}\rangle+i\frac{1}{\sqrt{2}}|\pi_{\mathrm{KS},b}\rangle$, where $|\pi_{\mathrm{KS},a}\rangle$ and $|\pi_{\mathrm{KS},b}\rangle$ are the two degenerate KS orbitals. The imaginary unit i has been included in order to get the correct angular momentum of the excited states (Π and Δ). This would not be possible using traditional ΔSCF, where one only has the freedom to change occupation numbers of the KS states. Due to the rotational symmetry of the density found from these states the calculations do not suffer from any convergence difficulties. That is not the case if one just occupies one of the degenerate KS orbitals. Only the Δ states are included in the $1\pi\rightarrow 2\pi$ transitions in Tables III and IV, since the Σ states cannot be estimated by the multiplet sum method.[43] This is, however, not a problem for the kinds of systems for which

TABLE IV. Vertical excitation energies for the CO molecule taken from the minimum-energy configuration of the ground state. All theoretical results are obtained using LDA as the *xc* potential (and ALDA for the *xc* kernel in the lrTDDFT calculations).

State	Transition	$\Delta\epsilon_{KS}$[a]	TDDFT[b] (ALDA)	ΔSCF (LDA)	ΔSCF (RPBE)	Exp.[c]
$A^1\Pi$			8.44	7.84	7.81	8.51
	$5\sigma\rightarrow 2\pi$	6.87				
$a^3\Pi$			6.02	6.09	6.02	6.32
Singlet-triplet splitting:			2.42	1.75	1.79	2.19
$D^1\Delta$			10.36	10.82	10.73	10.23
	$1\pi\rightarrow 2\pi$	9.87				
$d^3\Delta$			9.24	9.72	9.55	9.36
Singlet-triplet splitting:			1.12	1.10	1.18	0.87
$C^1\Pi$				13.15	13.09	
	$4\sigma\rightarrow 2\pi$	11.94				
$c^3\Pi$			11.43	12.26	12.09	11.55
Singlet-triplet splitting:				0.89	1.00	

[a]KS eigenvalue differences.
[b]Linear-response calculations taken from Gonis *et al.* (Ref. 47).
[c]Computed by Nielsen *et al.* (Ref. 48).

this method is intended, such as molecules on surfaces where high-accuracy alternatives are still lacking.

In general the excitation energies found by the linear-expansion ΔSCF method look quite good for the low-lying excitations. The accuracy is only slightly worse than that of lrTDDFT and significantly better than just taking KS eigenvalue differences. The singlet triplet splittings are also rather close to the experimental values. The method however seems to struggle a bit more in the higher lying $4\sigma\rightarrow 2\pi$ transitions. This could indicate that the method should only be applied to low-lying excitations. Changing the exchange-correlation functional from LDA to RPBE does not affect the accuracy significantly although a small tendency toward better performance is seen for the higher lying excitations. We note, however, that the intended application of ΔSCF do not include simple diatomic molecules, where more accurate quantum chemical methods are available.

B. Excited potential energy surfaces

The shapes of the potential energy surfaces can in some cases be more important than the exact height of them, i.e., a constant error is not so critical. This is for example the case when considering chemistry induced by hot electrons.[5,49] In order to get an idea of the accuracy with which the linear-expansion ΔSCF method reproduces correct shapes of potential energy surfaces we have calculated the potential energy surfaces for the ground state and two excited states in the N_2 molecule. These are plotted in Fig. 6 together with results from lrTDDFT calculations.

The small differences between the two ground-state curves are due to the fact that they have been calculated with two different codes. Both codes are real-space codes, but gpaw uses the PAW formalism to represent the core electrons whereas OCTOPUS uses norm-conserving pseudopotentials. The calculations have been made with the same grid spacing

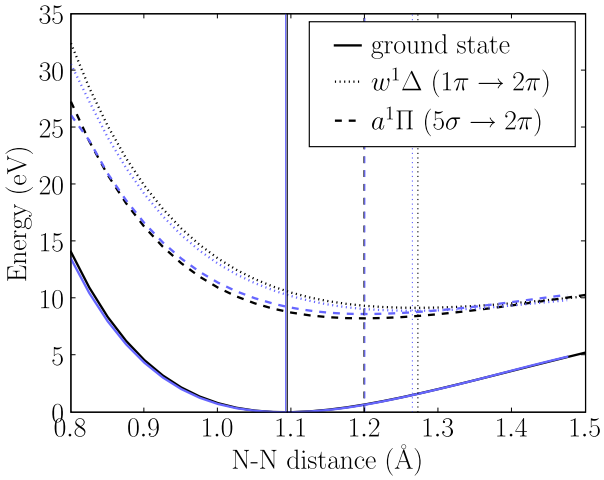

FIG. 6. (Color online) The energy as a function of bond length for the N_2 molecule in the ground state and two excited states. The black lines correspond to ΔSCF calculations, the gray (online: light blue) lines correspond to linear-response calculations. The linear-response calculations have been made using OCTOPUS (Refs. 35 and 36). The vertical lines indicate the positions of the minima.

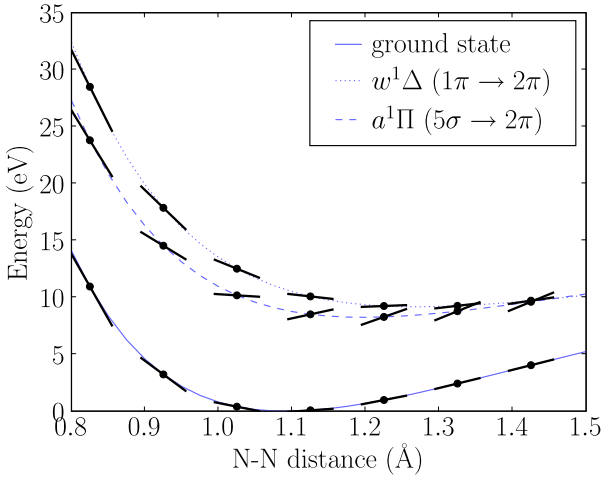

FIG. 7. (Color online) The energy as a function of bond length for the N_2 molecule in the ground state and two excited states. The short thick lines indicate the size of the gradients.

and unit-cell size and with the same exchange-correlation potential (LDA/ALDA).

The shapes of the potential energy surfaces found from the two different methods are seen to be very similar. Especially the predicted positions of the minima are seen to agree very well. The shifting of the minima toward larger bond lengths is also the expected behavior, since an electron is moved from a bonding orbital to an antibonding orbital. When going to bond lengths beyond 2 Å we start having problems with convergence problems in the ΔSCF calculations, since the 2π orbital ceases to exist. This is not a problem we have encountered in the systems with a molecule on a surface.

The good agreement between ΔSCF and lrTDDFT probably reflects that ΔSCF and ignoring the history dependence of the exchange-correlation potential in TDDFT are related approximations. For example, the density obtained in ΔSCF would be stationary if evolved in time with TDDFT.

C. Gradients

As mentioned in Sec. II C the Hellman-Feynman theorem does not apply in the linear-expansion ΔSCF method. This is verified by the calculations shown in Fig. 7. Here the energies of the ground state and two excited states in the N_2 molecule are plotted as a function of the bond length. The short thick lines indicate the gradient given by calculated Hellman-Feynman forces. For the ground state the agreement is as expected perfect, but for the excited states there is a clear mismatch. Unfortunately this implies that it is computationally heavy to do dynamics or minimizations in the excited states.

V. SUMMARY

We have extended the ΔSCF method of calculating excitation energies by allowing excited electrons to occupy linear combinations of KS states instead of just single KS states. This solves the problems encountered for molecules near surfaces, where the molecular orbitals hybridize, such that none of the KS orbitals can be used to represent an extra electron placed on the molecule. The method has been implemented in gpaw[27,28] and applied to several systems.

From calculated potential energy surfaces of N_2 on a ruthenium surface we concluded that an electron hitting the 2π resonance in this system can induce molecular dynamics due to the different positions of the minima of the ground-state PES and the resonance PES. Through a simple analysis we found that one electron can optimally place 1.5 eV in the atomic motion, more than enough to desorb the molecule.

We find good agreement between the model and inverse photoemission experiments for several diatomic molecules on different metallic surfaces. For the considered systems we find significantly better agreement with experiments using the modified ΔSCF method compared to spatially constrained DFT and traditional ΔSCF.

Finally we applied the method to N_2 and CO in their gas phases we found that excitation energies are estimated with quite good accuracy for the lower lying excitations, comparable to that of TDDFT. Especially the shape of the potential energy surfaces and the positions of the minima agree well with TDDFT results.

ACKNOWLEDGMENTS

The authors wish to thank Jens Jørgen Mortensen and Anders Hellman for fruitful discussions. The Center for Individual Nanoparticle Functionality (CINF) is sponsored by the Danish National Research Foundation. This work was supported by the Danish Center for Scientific Computing.

APPENDIX: OVERLAPS USING PAW PSEUDOWAVE FUNCTION PROJECTIONS

The projector augmented wave[29] method utilizes that one can transform single-particle wave functions $|\psi_n\rangle$ oscillating wildly near the atom core (all-electron wave functions) into smooth well-behaved wave functions $|\tilde{\psi}_n\rangle$ (pseudowave functions) which are identical to the all-electron wave functions outside some augmentation sphere. The idea is to expand the pseudowave function inside the augmentation sphere on a basis of smooth continuations $|\tilde{\phi}_i^a\rangle$ of partial waves $|\phi_i^a\rangle$ centered on atom a. The transformation is

$$|\psi_n\rangle = |\tilde{\psi}_n\rangle + \sum_{i,a} (|\phi_i^a\rangle - |\tilde{\phi}_i^a\rangle)\langle \tilde{p}_i^a|\tilde{\psi}_n\rangle, \tag{A1}$$

where the projector functions $|\tilde{p}_i^a\rangle$ inside the augmentation sphere a fulfills

$$\sum_i |\tilde{p}_i^a\rangle\langle\tilde{\phi}_i^a| = 1, \quad \langle \tilde{p}_i^a|\tilde{\phi}_j^a\rangle = \delta_{ij}, \quad |\mathbf{r} - \mathbf{R}^a| < r_c^a. \tag{A2}$$

Suppose we have an atom adsorbed on a metal surface and we wish to perform a ΔSCF calculation where a certain atomic orbital $|a\rangle$ is kept occupied during the calculation. If the orbital is hybridized with the metal states we need to find the linear combination which constitutes the orbital. This can

always be done if a sufficient number of unoccupied KS orbitals is included in the calculation

$$|i\rangle = \sum_n c_{ni}|\psi_n\rangle, \quad c_{ni} = \langle\psi_n|i\rangle. \tag{A3}$$

Since the partial waves are typically chosen as atomic orbitals we just need to consider the quantity

$$\langle\psi_n|\phi_i^a\rangle = \langle\tilde{\psi}_n|\phi_i^a\rangle + \sum_{j,a'}\langle\tilde{\psi}_n|\tilde{p}_j^{a'}\rangle(\langle\phi_j^{a'}|\phi_i^a\rangle - \langle\tilde{\phi}_j^{a'}|\phi_i^a\rangle) \approx \langle\tilde{\psi}_n|\tilde{p}_i^a\rangle. \tag{A4}$$

If we were just considering a single atom, the last equality would be exact inside the augmentation sphere since the partial waves would then be orthogonal and the pseudopartial waves are dual to the projectors in Eq. (A2). When more than one atom is present there are corrections due to overlap of partial waves from neighboring atoms and noncompleteness of projectors/pseudopartial waves between the augmentation spheres. However using $\langle\tilde{\psi}_n|\tilde{p}_i^a\rangle$ is a quick and efficient way of obtaining the linear combination, since these quantities are calculated in each step of the self-consistence cycle anyway. The method can then be extended to molecular orbitals by taking the relevant linear combinations of $\langle\tilde{\psi}_n|\tilde{p}_i^a\rangle$.

*Present address: Department of Micro- and Nanotechnology, Technical University of Denmark, DK–2800 Kongens Lyngby, Denmark.
†schiotz@fysik.dtu.dk

[1] P. Hohenberg and W. Kohn, Phys. Rev. **136**, B864 (1964).
[2] W. Kohn and L. J. Sham, Phys. Rev. **140**, A1133 (1965).
[3] A. C. Luntz, M. Persson, S. Wagner, C. Frischkorn, and M. Wolf, J. Chem. Phys. **124**, 244702 (2006).
[4] M. Bonn, S. Funk, C. Hess, D. N. Denzler, C. Stampfl, M. Scheffler, M. Wolf, and G. Ertl, Science **285**, 1042 (1999).
[5] J. W. Gadzuk, Phys. Rev. Lett. **76**, 4234 (1996).
[6] W. Lichten, Phys. Rev. **131**, 229 (1963).
[7] J. Behler, B. Delley, K. Reuter, and M. Scheffler, Phys. Rev. B **75**, 115409 (2007).
[8] K. Bohnen, M. Kiwi, and H. Suhl, Phys. Rev. Lett. **34**, 1512 (1975).
[9] M. Brandbyge, P. Hedegård, T. F. Heinz, J. A. Misewich, and D. M. Newns, Phys. Rev. B **52**, 6042 (1995).
[10] E. Runge and E. K. U. Gross, Phys. Rev. Lett. **52**, 997 (1984).
[11] M. Petersilka, E. K. U. Gross, and K. Burke, Int. J. Quantum Chem. **80**, 534 (2000).
[12] M. E. Casida, F. Gutierrez, J. Guan, F. Gadea, D. Salahub, and J. Daudey, J. Chem. Phys. **113**, 7062 (2000).
[13] L. Hedin, Phys. Rev. **139**, A796 (1965).
[14] G. Onida, L. Reining, and A. Rubio, Rev. Mod. Phys. **74**, 601 (2002).
[15] T. Klüner, N. Govind, Y. A. Wang, and E. A. Carter, J. Chem. Phys. **116**, 42 (2002).
[16] D. Lahav and T. Klüner, J. Phys.: Condens. Matter **19**, 226001 (2007).
[17] D. Kröner, I. Mehdaoui, H. Freund, and T. Klüner, Chem. Phys. Lett. **415**, 150 (2005).
[18] Q. Wu and T. Van Voorhis, Phys. Rev. A **72**, 024502 (2005).
[19] Q. Wu and T. Van Voorhis, J. Phys. Chem. A **110**, 9212 (2006).
[20] R. O. Jones and O. Gunnarsson, Rev. Mod. Phys. **61**, 689 (1989).
[21] A. Hellman, B. Razaznejad, and B. I. Lundqvist, J. Chem. Phys. **120**, 4593 (2004).
[22] O. Gunnarsson and B. I. Lundqvist, Phys. Rev. B **13**, 4274 (1976).
[23] A. Görling, Phys. Rev. A **59**, 3359 (1999).
[24] D. M. Newns, Phys. Rev. **178**, 1123 (1969).
[25] P. W. Anderson, Phys. Rev. **124**, 41 (1961).
[26] Often an electronic temperature is introduced to improve convergence, such that the electrons are distributed by a Fermi-Dirac distribution. This can also be done in the proposed method.
[27] J. J. Mortensen, L. B. Hansen, and K. W. Jacobsen, Phys. Rev. B **71**, 035109 (2005).
[28] The GPAW code including the implementation of ΔSCF is available as a part of the CAMPOS software, www.camp.dtu.dk/Software
[29] P. E. Blöchl, Phys. Rev. B **50**, 17953 (1994).
[30] P. E. Blöchl, C. J. Först, and J. Schimpl, Bull. Mater. Sci. **26**, 33 (2003).
[31] G. Kresse and J. Furthmuller, Comput. Mater. Sci. **6**, 15 (1996).
[32] D. M. Ceperley and B. J. Alder, Phys. Rev. Lett. **45**, 566 (1980).
[33] B. Hammer, L. B. Hansen, and J. K. Nørskov, Phys. Rev. B **59**, 7413 (1999).
[34] A. Zangwill and P. Soven, Phys. Rev. A **21**, 1561 (1980).
[35] OCTOPUS is a freely available real-space time-dependent density-functional theory code (see www.tddft.org/programs/octopus/).
[36] A. Castro, H. Appel, M. Oliveira, C. Rozzi, X. Andrade, F. Lorenzen, M. Marques, E. Gross, and A. Rubio, Phys. Status Solidi B **243**, 2465 (2006).
[37] G. Henkelman, A. Arnaldsson, and H. Jónsson, Comput. Mater. Sci. **36**, 354 (2006).
[38] R. F. W. Bader, *Atoms in Molecules: A Quantum Theory* (Oxford University Press, New York, 1990).
[39] P. D. Johnson and S. L. Hulbert, Phys. Rev. B **35**, 9427 (1987).
[40] W. Reimer, T. Fink, and J. Küppers, Surf. Sci. **186**, 55 (1987).
[41] W. Reimer, T. Fink, and J. Küppers, Surf. Sci. **193**, 259 (1988).
[42] J. Rogozik and V. Dose, Surf. Sci. **176**, L847 (1986).
[43] T. Ziegler, A. Rauk, and E. J. Baerends, Theor. Chim. Acta **43**, 261 (1977).
[44] T. Grabo, M. Petersilka, and E. Gross, J. Mol. Struct.: THEOCHEM **501-502**, 353 (2000).
[45] J. Oddershede, N. E. Grüner, and G. H. F. Diercksen, Chem. Phys. **97**, 303 (1985).
[46] K. P. Huber and G. Herzberg, *Molecular Spectra and Molecular Structure IV: Constants of Diatomic Molecules* (Van Nostrand Reinhold, New York, 1979).
[47] *Electron Correlations and Materials Properties*, edited by A. Gonis, N. Kioussis, and M. Ciftan (Plenum, New York, 1999).
[48] E. S. Nielsen, P. Jørgensen, and J. Oddershede, J. Chem. Phys. **73**, 6238 (1980).
[49] P. Saalfrank, Surf. Sci. **390**, 1 (1997).

Paper II

T. Olsen, J. Gavnholt, and J. Schiøtz
Hot-electron-mediated desorption rates calculated from excited state potential energy surfaces
Phys. Rev. B **79**, 035403 (2009).

Hot-electron-mediated desorption rates calculated from excited-state potential energy surfaces

Thomas Olsen, Jeppe Gavnholt, and Jakob Schiøtz*
Department of Physics, Danish National Research Foundation's Center of Individual Nanoparticle Functionality (CINF), Technical University of Denmark, DK-2800 Kongens Lyngby, Denmark
(Received 13 October 2008; revised manuscript received 24 November 2008; published 6 January 2009)

We present a model for desorption induced by (multiple) electronic transitions [DIET (DIMET)] based on potential energy surfaces calculated with the delta self-consistent field extension of density-functional theory. We calculate potential energy surfaces of CO and NO molecules adsorbed on various transition-metal surfaces and show that classical nuclear dynamics does not suffice for propagation in the excited state. We present a simple Hamiltonian describing the system with parameters obtained from the excited-state potential energy surface and show that this model can describe desorption dynamics in both the DIET and DIMET regimes and reproduce the power-law behavior observed experimentally. We observe that the internal stretch degree of freedom in the molecules is crucial for the energy transfer between the hot electrons and the molecule when the coupling to the surface is strong.

DOI: 10.1103/PhysRevB.79.035403 PACS number(s): 31.15.xr, 71.15.Qe, 71.38.−k, 82.20.Gk

I. INTRODUCTION

The advent of femtosecond lasers has initiated major progress in the study of nonadiabatic surface dynamics on a wide range of systems. Photoinduced desorption had already been observed for a few adsorbate systems[1,2] using low-intensity nanosecond laser pulses, but high-intensity femtosecond laser pulses have been shown to induce desorption in a large class of adsorbate systems[3–10] and induce chemical reactions which cannot proceed by thermal heating.[11]

The mechanism attributed to these reactions is excitation of substrate electrons by the laser pulse. A single hot electron can then interact with an initially unoccupied adsorbate resonance, thus asserting a force on the adsorbate nuclei which may then lead to desorption induced by electronic transitions (DIET). Using femtosecond lasers, it is possible to reach high densities of excited electrons resulting in a different dominating mechanism—desorption induced by multiple electronic transitions (DIMET) (Ref. 12) where several hot electrons interact with the adsorbate.

A different method to produce hot electron based on a metal-insulator-metal (MIM) heterostructure was suggested by Gadzuk.[13] With an ideal MIM device, it is possible to tune hot electrons to any desired resonance of an adsorbate system and the approach thereby suggests the highly attractive possibility of performing selective chemistry at surfaces. Such devices have been constructed and characterized[14] and comprise a promising candidate for future hot-electron femtochemistry experiments.

The theoretical framework to describe the nonadiabatic dynamics resulting from a hot electron interacting with an adsorbate is usually based on the concept of potential energy surfaces (PESs). In the Born-Oppenheimer approximation the electrons are assumed to remain in their ground state and are thus decoupled from the nuclei. This allows one to map out a ground-state PES for the nuclei by calculating the electronic energy for each position of the nuclei. Similarly, when an initially unoccupied resonance becomes occupied, a new excited-state PES arises which has its minimum at a different location from the ground-state PES and a force is exerted on the adsorbate. Several models have emerged to deal with nonadiabatic dynamics at surfaces, but they are usually limited by the difficulty to obtain reliable excited-state PESs and most theoretical results are based on model potentials.[15–20]

An often used method to treat the extreme DIMET regime with many contributing electrons is using an electronic friction model.[21–23] The hot electrons are then assumed to thermalize rapidly and the influence of the electrons on the adsorbate is treated statistically using an electronic temperature which can be several thousands of Kelvins. The conceptual picture is that of a hot Fermi distribution with a tail partially overlapping an adsorbate resonance and thereby exerting a force on the adsorbate. However, correct calculation of the temperature-dependent friction still requires knowledge of the excited-state PES.

The subject of this paper will be the application of two-dimensional excited-state PESs to calculate desorption probabilities. We will be particularly interested in the DIET regime where the hot electron has a known energy as relevant for the MIM device and the few-electron DIMET regime. Although the friction models have enjoyed some success,[24,25] there is still a need of a microscopic nonstatistical model of DIMET to test the assumption of thermally equilibrated electrons and to bridge the gap to the DIET regime. Furthermore, the hot-electron femtochemistry relevant to the MIM device can certainly not be described using an electronic temperature since all electrons are tuned to a specific energy.

We start by summarizing the method of linear-expansion delta self-consistent field extension of density-functional theory (ΔSCF-DFT) (Ref. 26) used to calculate the excited-state PESs and note some qualitative features using CO on Pt(111) as an example. We then discuss the models used to obtain desorption probabilities based on the calculated potential energy surfaces. First an adiabatic model in which the adsorbate jumps between the ground- and excited-state potentials is presented. A general nonadiabatic Newns-Anderson-type[27,28] model is then introduced and the connection to potential energy surfaces is explained. This model with linear coupling has previously been solved[29] and applied to the one-dimensional desorption problem with model parameters.[16] We extend these results to a two-

dimensional adsorbate and obtain the nonadiabatic coupling parameters from calculated excited-state potential energy surfaces. In the DIET regime, the model will be used to show that for small excited-state lifetimes the main channel of energy transfer is the internal degree of freedom and we emphasize its importance in desorption dynamics. We compare the calculated desorption probabilities for CO and NO on four transition-metal surfaces and note some general features of the desorption dynamics. The scattering probabilities obtained in the model are then generalized to include adsorbates in any vibrationally excited state which allow us to extend the calculations to include a substrate temperature and to treat the DIMET regime within the model. In Appendix A it is shown how to expand excited states within the projector augmented wave (PAW) formalism, and in Appendix B the results and generalizations of scattering amplitude calculations are summarized.

II. POTENTIAL ENERGY SURFACES

The potential energy surfaces were obtained using the code GPAW (Refs. 30 and 31) which is a real-space density-functional theory (DFT) code that uses the projector augmented wave method.[32,33] In all our calculations we used the revised Perdew-Burke-Ernzerhof (RPBE) exchange-correlation functional[34] since this has been designed to perform well for molecules adsorbed on surfaces and has been shown to perform better than the original PBE functional[35] both for isolated molecules[36] and for adsorbed molecules. For each metal we set up a closed-packed surface consisting of three atomic layers with the top layer being relaxed. 10 Å of vacuum was then introduced above the slab and 0.25 monolayer of adsorbate molecules relaxed at either top or at hcp hollow site. We then mapped out two-dimensional ground-state potential energy surfaces in terms of the internal stretch and the center of mass (COM) to surface distance coordinate using 12 irreducible k points and a grid spacing of 0.2 Å.

To find the excited-state potential energy surfaces, we use the method of linear-expansion delta self-consistent field (ΔSCF) which we have published in a previous work[26] and implemented in GPAW. In the previous publication we have tested the method against inverse photoemission spectroscopy and found that it performed well for molecules chemisorbed on surfaces.[26] In each step of the self-consistency cycle an electron is removed from the Fermi level, the density of an excited state is added to the total density, and the band energy of this state is added to the total energy. To get the band energy right, we need to expand the excited state on the Kohn-Sham (KS) orbitals found in each iteration. The method is thus a generalization of the usual ΔSCF where occupations numbers are changed. Instead of changing occupation numbers we occupy an orbital which is not an eigenstate of the KS Hamiltonian but a superposition of eigenstates, in such a way that the state is as close as possible to the original molecular state. We refer to Appendix A for details on how to do this within the projector augmented wave formalism. The excited states used in this paper are the antibonding 2π orbitals of NO and CO.

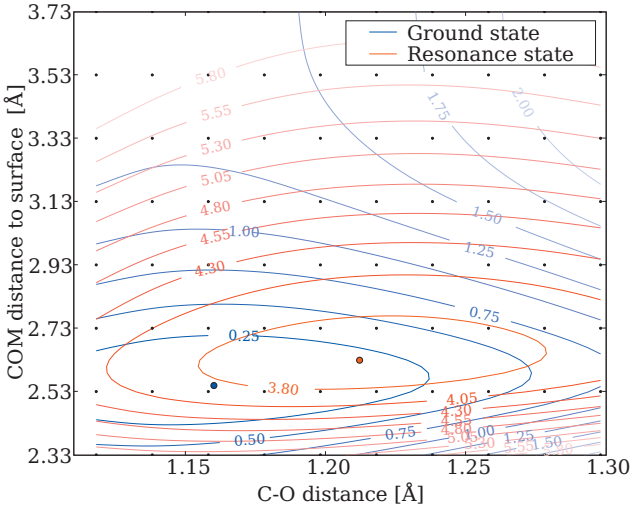

FIG. 1. (Color) Ground- and excited-state (2π) potential energy surfaces for CO adsorbed on Pt(111) top site. The coverage is 0.25 monolayer.

In the previous publication,[26] we investigated the influence of the interactions between neighboring supercells for different supercell sizes and found that the size dependency of the excitation energy is consistent with an electrostatic dipole-dipole interaction. Already for a (2×2) surface cell, the interaction energy has become small, and furthermore this interaction energy will have little influence on the slope of the excited-state PES and thus little influence on the calculated desorption rates. For this reason and to keep the calculations manageable, we use a (2×2) surface cell.

As an example we show the two-dimensional excited-state PES superimposed on a ground-state PES in the case of CO on Pt(111) top site in Fig. 1. The molecules adsorb with the molecular axis perpendicular to the surface with carbon closest to the top site. Due to the symmetry of the 2π orbital and the geometry at the ground-state minimum, we cannot induce forces parallel to the surface if the molecule is at the ground-state minimum when excited. The excited state could have unstable extremal points with respect to the degrees of freedom parallel to the surface; but the model we apply in this work only depends on the degrees of freedom with nonvanishing derivatives on the excited-state PES and we thus assume that the COM and internal stretch degrees of freedom should capture the essential desorption dynamics of the considered systems.

Since the excited molecule has an extra electron in an antibonding orbital the excited molecule is expected to have a larger equilibrium bond length and this is also what we observe. A popular and conceptually simple way of explaining desorption in one-dimensional models of DIET is the Antoniewicz mechanism,[37] where the excited molecule induces an image charge on the surface which results in an attractive force on the surface. The excited molecule is then accelerated toward the surface and eventually decays to the steep wall of the ground-state Morse potential. From Fig. 1 we observe a qualitatively different behavior: the COM of the excited molecules experience a repulsive force accelerating the COM of the molecule away from the surface. This is

due to the effect of the bond-length expansion and the fact that the 2π orbital has a large density in the vicinity of the carbon atom which gives a repulsion that dominates the image charge attraction. It will be shown below that for the considered systems, it is primarily excitation of the internal degree of freedom which is responsible for the large energy transfers leading to desorption. The potential energy surfaces for CO adsorbed on Pd, Rh, and Ru show very similar qualitative features.

III. MODELS

The time scale at which adsorbates dissipate energy to the substrate is typically on the order of picoseconds[38] and since the oscillation times for the two modes is ~15–50 fs (see Sec. IV A) we will assume that the molecule has plenty of time to desorb if it has absorbed the required energy from a hot electron. This is the major assumption we will impose and thus when we refer to desorption rates in the following, it is the rate of transferring at least of the energy needed for a molecule to desorb.

Assuming a Lorentzian resonance with full width at half maximum (FWHM) $\Gamma=\hbar/\tau$ centered at ϵ_a, the probability that a hot electron of energy ε desorbs the molecule becomes

$$P_{\mathrm{des}}^{\mathrm{ad}}(\varepsilon)=\frac{(\Gamma/2)^2}{(\varepsilon-\epsilon_a)^2+(\Gamma/2)^2}\frac{1}{\tau}\int_0^\infty P(t_d)e^{-t_d/\tau}dt_d, \tag{1}$$

where $P(t_d)$ is the probability of a desorption event when the molecule is excited at $t=0$ and decays at time $t=t_d$. Using classical dynamics, the probability $P(t_d)$ can be obtained by propagating the molecule on the excited-state PES according to the forces, evaluate the energy gain ΔE after time t_d, and set $P(t_d)=1$ if $\Delta E>E_{\mathrm{des}}$ and $P(t_d)=0$ if $\Delta E<E_{\mathrm{des}}$. However, the short lifetime of the excited electron implies that classical molecular propagation on the excited-state PES may not be a good approximation.

In fact, the classical limit is obtained when the action $S=\int dtL[\dot{x}(t),x(t)]$ on a representative path satisfies

$$|S|\gg\hbar. \tag{2}$$

Assuming a quadratic excited-state potential of frequency ω and initial potential energy E_0, we can evaluate the action on a classical path between initial time t_i and final time t_f. For generic time scales one just obtains the usual condition of high excitation numbers $E_0\gg\hbar\omega$, whereas for $\omega\Delta t\ll 1$, the additional condition of $E_0\Delta t\gg\hbar$ needs to be satisfied in order to apply classical dynamics. In the case of CO on Pt(111) we have $E_0\sim 0.3$ eV (Fig. 1) and $\tau\sim 1$ fs (Fig. 8) which gives $E_0\Delta t\sim\hbar$. Thus molecular propagation on the excited-state PES is not expected to follow the classical equations of motion. Below we will show an example where a classical analysis underestimates desorption probabilities by several orders of magnitude.

This scheme could be extended to a quantum dynamical treatment of the molecule by propagating the molecular wave function using a two-PES Hamiltonian. However, the method still rests on the Born-Oppenheimer approximation and the adiabatic concept of potential energy surfaces and thus cannot be expected to fully capture the nonadiabatic entangled dynamics of the resonant electron and adsorbate coordinates.

Instead we consider a Newns-Anderson-type[27,28] Hamiltonian with substrate states $|k\rangle$, a resonant state $|a\rangle$, adsorbate coordinates x_i, an adiabatic adsorbate ground-state potential $V_0(x_i)$, and a nonadiabatic coupling of the resonant electron to adsorbate coordinates $\varepsilon_a(x_i)$,

$$H=T(\dot{x}_i)+V_0(x_i)+\varepsilon_a(x_i)c_a^\dagger c_a+\sum_k\epsilon_k c_k^\dagger c_k+\sum_k(V_{ak}c_a^\dagger c_k+V_{ak}^*c_k^\dagger c_a). \tag{3}$$

The strength of the electronic coupling is expressed through the function

$$\Gamma(\varepsilon)=2\pi\sum_k|V_{ak}|^2\delta(\varepsilon-\epsilon_k). \tag{4}$$

The model as such neglects the electron-electron interaction, but we assume that the important part of the electron-electron interactions is the restructuring of the metallic electrons when the resonance is occupied and that we can capture this effect in an effective nonadiabatic coupling. To do this we note that we can obtain $\varepsilon_a(x_i)$ as the expectation value differences of Eq. (3) with the adsorbate at x_i with and without an electron in the state $|a\rangle$. Applying this to an interacting problem leads us to identify $\varepsilon_a(x_i)=V_1(x_i)-V_0(x_i)$, where $V_1(x_i)$ and $V_0(x_i)$ are the potential energy surfaces of excited and ground states which we have obtained with linear-expansion ΔSCF-DFT.

In the following we will apply the wideband limit which means that the individual coupling coefficients V_{ak} are assumed to vary slowly in energy and the density of states $\rho(\varepsilon)$ is taken as constant in the vicinity of the resonance. This gives an energy-independent coupling $\Gamma=2\pi\rho(\epsilon_a)\Sigma_k|V_{ak}|^2$ and the resonance spectral function corresponding to the electronic part of Eq. (3) becomes a Lorentzian with FWHM Γ.

Even in the wideband limit it is quite difficult to handle model (3) analytically with arbitrary coupling function $\varepsilon_a(x_i)$. In particular, we would like to calculate the probability that an incoming substrate electron of energy ε_i scatters inelastically on the resonance and is reflected back into the substrate with final energy ε_f. Fortunately, the potential energy surfaces we are considering are close to being quadratic in the region of interest (see Fig. 1) and the ground- and excited-state potentials have approximately the same curvature. Taylor expanding $V_0(x_i)$ to second order and $\varepsilon_a(x_i)$ to first order in the vicinity of the ground-state equilibrium positions x_i^0 then gives

$$H=\epsilon_a c_a^\dagger c_a+\sum_k\epsilon_k c_k^\dagger c_k+\sum_k(V_{ak}c_a^\dagger c_k+V_{ak}^*c_k^\dagger c_a)+\sum_i\hbar\omega_i\left(a_i^\dagger a_i+\frac{1}{2}\right)+\sum_i\lambda_i c_a^\dagger c_a(a_i^\dagger+a_i), \tag{5}$$

with $\epsilon_a=V_1(x_i^0)-V_0(x_i^0)$ and

$$\lambda_i = \frac{l_i}{\sqrt{2}} \frac{\partial}{\partial x_i} V_1 \Big|_{x_i = x_i^0}, \quad l_i = \sqrt{\frac{\hbar}{m_i \omega_i}}, \tag{6}$$

where we have assumed that an appropriate transformation to normal coordinates has been performed. Note that if the ground- and excited-state potentials are exactly quadratic with equal second derivatives, we can relate the coupling constants to the positions x_i^1 of the excited-state potential minimum as $\lambda_i^2 = \hbar \omega_i \Delta V_i$ with $\Delta V_i = \frac{1}{2} m_i \omega_i^2 |x_i^1 - x_i^0|$. The quantity $g_i = (\lambda_i / \hbar \omega_i)^2$ then corresponds to an "initial quantum number" on the excited-state surface and this becomes the effective dimensionless coupling constant in the model (see Appendix B). Hamiltonian (5) has previously been subjected to detailed analysis in the context of inelastic scattering[29] and applied to desorption dynamics[16] for the case of a one-dimensional adsorbate with model parameters.

Below we extend the results of Refs. 16 and 29 to a two-dimensional adsorbate and calculated the coupling parameters λ_i from excited-state potential energy surfaces. We also calculate scattering amplitudes for an adsorbate initially in a vibrationally excited state which enable us to apply the model to the DIMET regime.

A. DIET

In Eq. (B8) we show how to calculate the scattering probability $P_{n_i,n_j}(\varepsilon_i)$ that an incoming electron of energy ε_i excites the (n_i, n_j) mode of a two-dimensional harmonic oscillator. The probability of transferring E_R or more energy to the adsorbate can then be found by calculating

$$P_R(\varepsilon_i) = \sum_{n_i,n_j} P_{n_i n_j}(\varepsilon_i)\, \theta(\hbar \omega_i n_i + \hbar \omega_j n_j - E_R), \tag{7}$$

where $\theta(x)$ is the Heaviside step function. The desorption rate can then be calculated by integrating this expression with the current density of incoming hot electrons. One should note that the probability $P_{n_i n_j}$ of exciting the (n_i, n_j) modes in a two-mode model is not just given by the product of single mode probabilities P_n in a one-mode model. This is due to an indirect coupling of the two modes through the resonance. The result can be generalized to include the substrate temperature and we will examine the consequences of this below.

B. DIMET

If we assume that the time between individual inelastic-scattering events is much longer than the scattering time itself, it is possible to regard multiple-electron desorption events as sequence of single-electron-scattering events. Since we have extended the inelastic-scattering probabilities to include situations where the molecule is initially in a vibrationally excited state, it is also possible to treat DIMET events within model (5). As an example, let us assume a single vibrational mode which is initially unoccupied ($n=0$). When a hot electron with energy ε_1 scatters inelastically on the resonance the result will be a probability distribution $P_{n_1}(\varepsilon_1)$ for all vibrationally excited states n of the molecule. If a second electron with energy ε_2 now scatters on the resonance, the probability distribution will change to $P_{n_2}(\varepsilon_1, \varepsilon_2)$ and so forth. The probability $P_{n_2-n_1}(\varepsilon_2, n_1)$ of exciting the state n_2 given that the initial state was n_1 is calculated in Eq. (B6) and we can write

$$P_{n_2}(\varepsilon_1, \varepsilon_2) = \sum_{n_1=0}^{\infty} P_{n_2-n_1}(\varepsilon_2, n_1) P_{n_1}(\varepsilon_1), \tag{8}$$

for a two-electron event and similar expressions for multiple-electron events. Given an initial distribution of hot electrons, we may then calculate the probability of a desorption event with any number of contributing electrons.

TABLE I. Parameters for CO adsorbed at top site on four transition metals. All numbers are in eV.

Metal	ϵ_a	ω_z	ω_d	λ_z	λ_d
Pt(111)	3.89	0.054	0.255	−0.142	−0.145
Pd(111)	3.64	0.061	0.256	−0.082	−0.164
Rh(111)	3.80	0.048	0.247	−0.129	−0.132
Ru(0001)	3.74	0.054	0.255	−0.134	−0.120

IV. RESULTS

A. Parameters

The parameters in desorption model (5) are the width of the resonance Γ, the frequencies of the normal modes ω_i, the excitation energy ϵ_a, and the nonadiabatic coupling coefficients λ_i. We cannot calculate Γ from first principles but we estimate its value from the Kohn-Sham projected density of states. It is typically on the order of 1 eV, but it will be instructive to treat it as a free parameter and examine how it affects desorption probabilities.

The frequencies are obtained from a standard normal-mode analysis and ϵ_a is obtained as the excitation energy at the ground-state potential minimum. The coupling coefficients are determined by mapping out a small area of the excited-state potential energy surface in the immediate vicinity of the ground-state potential. In each of the considered systems, we optimize the area such that it is small enough to be linear but large enough to suppress numerical fluctuations in the excited-state energies. We then fit a linear function to this area and transform the derivatives to the normal modes.

In all the considered systems the calculated normal modes are similar but not identical to the standard COM and internal stretch modes. For example, with CO on Pt(111) the internal stretch and COM modes are, respectively, $\mathbf{d}=(-1, 0.75)$ and $\mathbf{z}=(1,1)$, whereas the calculated modes are in the directions $\mathbf{d}=(-1, 0.68)$ and $\mathbf{z}=(1, 1.11)$ with respect to the (x_C, x_O) coordinates normal to the surface. Since the desorption probabilities are quite sensitive to the value of the nonadiabatic coupling constants, it is important that we take the derivatives on the excited-state PES with respect to the correct normal modes.

Tables I and II below display the calculated parameters. We have only examined CO at on-top sites and NO at hcp hollow sites. NO is seen to have much lower nonadiabatic

TABLE II. Parameters for NO adsorbed at hcp hollow site on four transition metals. All numbers are in eV.

Metal	ϵ_a	ω_z	ω_d	λ_z	λ_d
Pt(111)	1.71	0.039	0.196	−0.050	−0.053
Pd(111)	1.48	0.055	0.201	−0.046	−0.053
Rh(111)	1.82	0.073	0.277	−0.042	−0.020
Ru(0001)	2.14	0.042	0.192	−0.052	−0.006

coupling coefficients and excitation energies than CO. The low excitation energies are due to the fact that NO already has one electron in the antibonding orbital and the resonance thus has to lie close to the Fermi level of the metal. The small coupling coefficients can also be traced to the ground-state occupation of the 2π orbital on NO. In the Kohn-Sham picture we can imagine the resonance corresponding to 2π lying right at the Fermi level being partially occupied. When an extra electron is put into the orbital, the resonance energy is increased due to the Hartree repulsion and the initial partial occupation is lost. In the true system things are more complicated, but the qualitative features are the same: exciting NO results in less charge being transferred to the molecule than exciting CO and thus a weaker nonadiabatic coupling. Thus it is much harder to transfer energy to adsorbed NO compared to CO in a one-electron event; but since the resonance is located much closer to the Fermi level a thermal distribution of hot electrons is likely to result in more frequent scattering events than for CO.

B. DIET desorption rates

The probability that a single electron with energy ε_i scatters inelastically and transfers the energy E_R to an adsorbate can be calculated in model (5) with Eq. (7). Our basic assumption is that rate of energy dissipation to the substrate is much longer than the time of a desorption event, and when we refer to desorption rates in the following it will mean the rates of transferring the energy needed for a molecule to desorb in a truncated quadratic potential.

In Fig. 2 we display the probability that an incoming electron will scatter with an energy loss in excess of the desorption energy ($\Delta E > 1.5$ eV) for three values of the resonance width. When only a single mode is considered we see the appearance of oscillator sidebands with an energy spacing of $\hbar\omega$. At larger resonance width the sidebands are washed out and the probability takes the form of a Lorentzian which is detuned by $\delta\epsilon_a \sim \Delta E/2$. A simple way to understand this detuning is as a compromise where both the incoming and outgoing electrons are closest to the resonance. Thus we see the emergence of an *effective* inelastic resonance with a center that is detuned dependent on the desorption energy and a shape which is highly dependent on the lifetime. Such a probability distribution could not have been obtained in a model where the transfer of energy to the adsorbate is decoupled from the probability of capturing the electron, and the desorption probability would always be a Lorentzian (in the wideband limit) centered at ϵ_a and multiplied by a factor

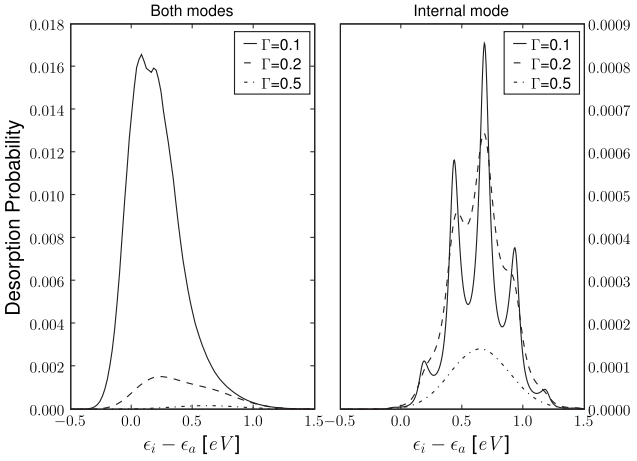

FIG. 2. Desorption probability for CO adsorbed on Pt(111) for three different values of the resonance width. For $\Gamma > 0.5$ the one- and two-mode probability distributions become identical Lorentzians with an integrated probability that decays exponentially with resonance width (see Fig. 3).

dependent on the details of the potential energy surfaces. For $\Gamma > 0.5$ eV the COM degree of freedom becomes unimportant and the desorption probabilities obtained using both modes and only the internal degree of freedom become identical.

Assuming an energy-independent current of hot electrons we can integrate the desorption probabilities in Fig. 2 to obtain a desorption rate normalized to the incident flux of electrons. In Fig. 3 we show how each of the two modes contributes to the desorption rate and compare with a calculation within the classical adiabatic model (1). The two single mode rates are obtained by setting g_d and g_z to zero in

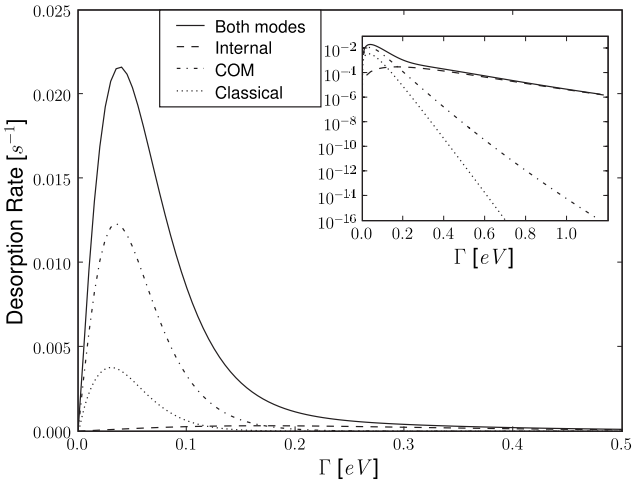

FIG. 3. Desorption rate for CO adsorbed on Pt(111) as a function of resonance width Γ. In the wide resonance (short lifetime) regime the rate is seen to be completely governed by the internal stretch excitation, whereas the COM excitation is governing the desorption rate in the narrow resonance (long lifetime) regime. The classical rate becomes several orders of magnitude smaller than the quantum rate at large resonance width. The inset shows the same data on a logarithmic scale.

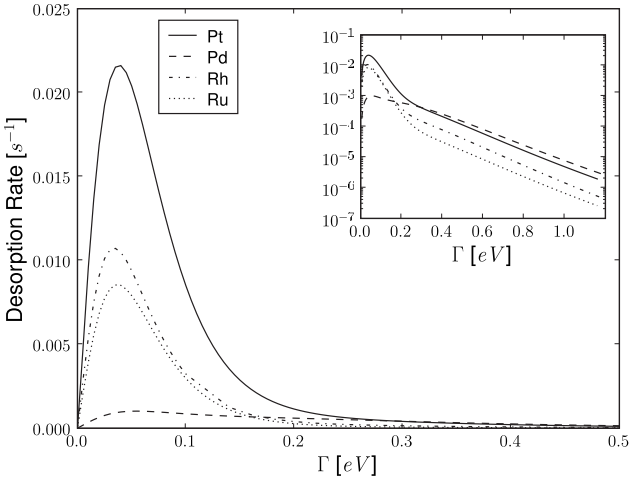

FIG. 4. Rates of transferring 1.5 eV to CO on four transition metals.

Eq. (B8). It is seen that it is the internal stretch mode that governs the energy transfer completely in the large width regime and the COM mode governs the energy transfer at low width. The reason for this partitioning is the time scale associated with the two different modes. As seen from Tables I and II the nonadiabatic coupling constants have approximately the same magnitude for the two modes. However, the period of oscillation is five times larger for the COM mode and for small lifetimes there is not enough time to transfer energy to the COM mode. From Fig. 3 we see that the maximum rate of energy transfer in each mode occurs when $\Gamma \sim \hbar\omega_i$. The desorption rate decreases at small resonance width, since the hot electron then becomes weakly coupled to the resonant state

In Figs. 4 and 5 we show a comparison of CO and NO adsorbed on the different transition metals. Again comparing with Tables I and II it is seen that it is the coupling to the internal mode alone which controls the magnitude of the desorption rate at large resonance width. Since the internal

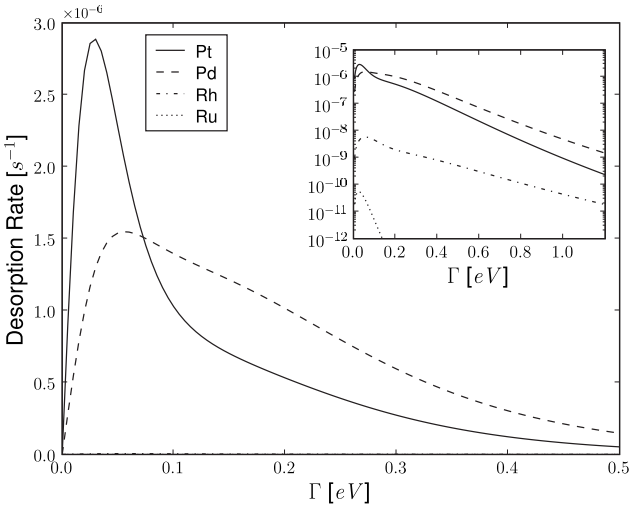

FIG. 5. Rates of transferring 1.0 eV to NO on four transition metals.

TABLE III. Desorption energies and calculated maximum desorption probability for CO adsorbed at top site on four transition metals. All numbers except $P_D^{\max}$ are in eV.

Metal	E_D	Γ	$\delta\varepsilon$	$P_D^{\max}$
Pt(111)	1.37[a]	1.0	0.6	2×10^{-5}
Pd(111)	1.48[a]	1.5	0.7	7×10^{-7}
Rh(111)	1.45[a]	1.2	0.7	1×10^{-6}
Ru(0001)	1.49[a]	0.9	0.7	2×10^{-6}

[a]Experimental values taken from Abild-Pedersen and Andersson (Ref. 39).

degree of freedom seems to control the rate of energy transfer in the physical range of the resonance width (typically $0.5<\Gamma<1.5$) we will ignore the COM degree of freedom in the following.

Comparison of CO and NO

So far we have analyzed some general features of desorption probabilities and their dependence on the nonadiabatic coupling parameters and the lifetime $\tau=\hbar/\Gamma$. Now we will compare the desorption probabilities of CO and NO on four transition-metal surfaces using experimentally determined desorption energies. Although substantial experimental data exist for various systems including CO and NO, a direct comparison to experimental data is difficult since experimental desorption yields are highly dependent on the distribution of hot electrons in the substrate which depends on the detailed physical properties of the metal and the applied laser pulse. The distribution of hot electrons resulting from a given laser pulse could in principle be calculated from first principles; however, we will make no attempt of such a calculation here but simply compare desorption probabilities of single-electron events as relevant for the MIM device.[13,14] In Tables III and IV we summarize the desorption energy E_d, the estimated resonance width Γ, the detuning of the energy at which the incoming electron has the maximum probability of transferring the desorption energy $\delta\varepsilon=\varepsilon_i^{\max}-\epsilon_a$, and the maximum desorption probability $P_D^{\max}=P_D(\varepsilon_i^{\max})$ for the four transition metals (the maximum probability is detuned from ϵ_a, as shown in Fig. 2). The detuning very nicely follows the rule of thumb that $\delta\varepsilon\sim E_D/2$ in accordance with the picture of a compromise between the incoming and outgoing elec-

TABLE IV. Desorption energies and calculated maximum desorption probability for NO adsorbed at hcp hollow site on four transition metals. All numbers except $P_D^{\max}$ are in eV.

Metal	E_D	Γ	$\delta\varepsilon$	$P_D^{\max}$
Pt(111)	1.29[a]	0.8	0.6	3×10^{-11}
Pd(111)	1.17[b]	0.6	0.6	5×10^{-9}
Rh(111)	1.68[b]	0.4	0.8	2×10^{-15}
Ru(0001)	1.49[c]	0.3	0.7	3×10^{-22}

[a]Croci *et al.* (Ref. 40).
[b]Vang *et al.* (Ref. 41).
[c]Butler *et al.* (Ref. 42).

trons both being as close as possible to the center of the resonance ϵ_a.

In general it is easier for a single electron at the right energy to mediate a desorption event involving CO than with NO from all the considered systems. However, in a femtosecond laser-pulse experiment the resulting hot-electron distribution would have much lower occupation numbers at the CO resonances than at a typical NO resonance. For example, taking platinum as an example with a thermal electron distribution at 5000 K and referring to Tables I and II, we see that the electronic occupation numbers at the resonance energy of CO and NO relates as $f(\epsilon_{NO})/f(\epsilon_{\mathrm{NO}}) \sim 150$. We should also note that the excited-state potential energy surfaces for adsorbed NO are only quadratic in a small region near the minimum and Hamiltonian (5) is thus not expected to describe NO as accurately as CO.

The desorption probabilities are highly dependent on the resonance width Γ which we can only estimate roughly from the Kohn-Sham projected density of states. In addition, the electronic lifetime of CO on Pt(111) has been shown to be highly dependent on coverage[3] since the 2π electrons become delocalized and quasistationary at certain coverages. Furthermore, both CO and NO are known to form adsorbate structures which is more involved[41,43] than the simple periodic coverage of 0.25 monolayer considered here and the dependence of nonadiabatic coupling coefficients on coverage certainly deserves a study of its own.

However, from Figs. 4 and 5 we do observe the general trends that NO has a much weaker nonadiabatic coupling to the surfaces than CO and that for both CO and NO the coupling to Pt and Pd is similar, whereas the coupling is weaker for Rh and very low for Ru. This decrease in nonadiabatic coupling could hint at a simple dependence on the number of *d*-band electrons. Investigating this will be the subject of future work.

C. DIMET desorption rates

To get an idea of desorption probabilities in the DIMET regime, we will start by examining how an initial excitation influences the probability of transferring a given number of vibrational quanta. When the oscillator is in an excited vibrational state there is also the possibility of stimulated emission of vibrational quanta where the incoming hot electron gains energy by the scattering event.

In Fig. 6 the maximum probability of transferring Δn quanta is shown for a range of initial quantum numbers n. We treat n as a continuous variable since in the case of a thermal ensemble of states the initial quantum number is simply replaced by a Bose distribution. There is a striking increase in the probabilities of transferring energy to the oscillator if the oscillator is already excited. For example, the probabilities of exciting $0 \rightarrow 3$ and $3 \rightarrow 6$ are 3×10^{-3} and 2×10^{-2}, respectively, although both transitions involve the same energy transfer. Thus if we compare the one-electron event $P_{0\rightarrow 6} = 6 \times 10^{-6}$ with the product of the two probabilities $P_{0\rightarrow 3\rightarrow 6} = 6 \times 10^{-5}$, we get an order-of-magnitude difference and we still need to include the other channels for transferring six quanta in a two-electron event.

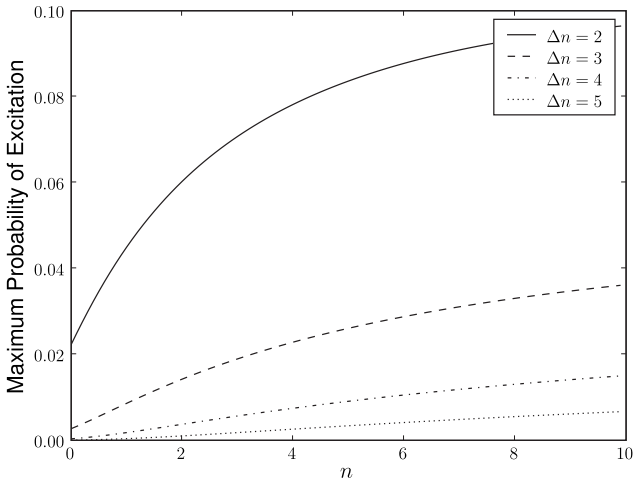

FIG. 6. Maximum probability of transferring Δn vibrational quanta given that the initial state is n with $\Gamma = 1.0$ eV.

This also implies that the effect of a finite substrate temperature is twofold. The occupation numbers of excited vibrational states will be nonzero, meaning that less energy transfer is needed to desorb the molecule and the likelihood of a given energy transfer is increased if the molecule is thermally excited. However at room temperature the probability that the internal mode is in its first-excited state is on the order of 10^{-5} and we can safely neglect the effect of temperature.

A hallmark of the DIMET regime is the power-law dependence of the desorption rate on the laser fluence $R \sim F^n$ where n depends on the particular adsorbate/substrate system considered.[4] It is by no means trivial that the desorption rate should follow a power law and calculating the exponent of a particular system is a major challenge of any DIMET model.

It is reasonable to assume that the laser fluence is proportional to the flux of hot electrons hitting the molecule, since the desorption rate typically becomes linear[44] for small fluences corresponding to the DIET regime. As a simple model for the desorption rate we then consider a given flux J of hot electrons at a fixed energy ε_i hitting the resonance in equally spaced time intervals $\Delta t = 1/J$. We assume that each vibrational quantum has a fixed lifetime T_{vib} and that desorption occurs immediately if the vibrational energy reaches the desorption energy E_D. The probability that one vibrational quantum survives the time interval Δt is $e^{-\Delta t/T_{\mathrm{vib}}}$ and the probability of decay is $(1-e^{-\Delta t/T_{\mathrm{vib}}})$. The probability that the first electron excites the nth vibrational state is then simply the DIET probability,

$$Q_1(n) = P_n(\varepsilon_i, 0), \tag{9}$$

where $P_n(\varepsilon_i, 0)$ is given by Eq. (B6). The probability of the adsorbate being in the nth vibrational state after the second electron has scattered is

$$Q_2(n) = \sum_{m=0}^{\infty} p(m) P_{n-m}(\varepsilon_i, m), \tag{10}$$

where $P_{n-m}(\varepsilon_i, m)$ is the probability of the transition $m \rightarrow n$ [Eq. (B6)] and $p(m)$ is the probability that the adsorbate was initially in the state m given by

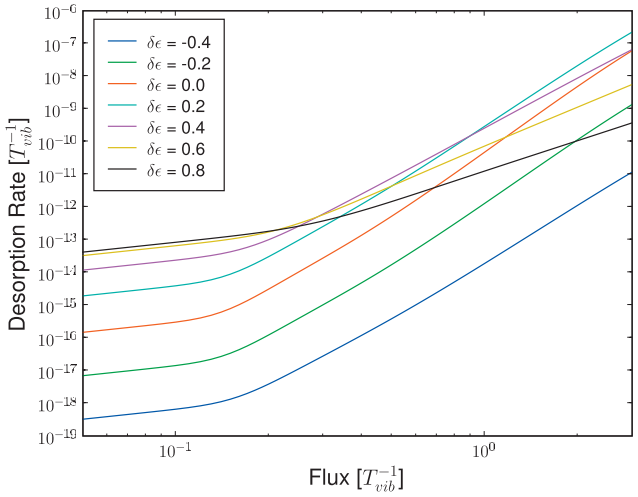

FIG. 7. (Color) Desorption rate as a function of electron flux per adsorption site. For small electron flux the rate is linear in the flux corresponding to the DIET regime, whereas for larger electron flux the rate obeys a power law ($R \sim J^n$ with $n > 1$) corresponding to the DIMET regime. In this figure we show the desorption rate of NO on Pt(111) using the parameters given in Table IV and in seven different values of detuning.

$$p(m) = \sum_{k=m}^{\infty} Q_1(k) \binom{k}{m} (e^{-\Delta t/T_{\mathrm{vib}}})^m (1 - e^{-\Delta t/T_{\mathrm{vib}}})^{k-m} \times \theta(E_d - \hbar\omega k). \quad (11)$$

Thus we only sum over values of k below the desorption energy since states above E_D would previously have been desorbed by assumption. Similarly the probability $Q_3(n)$ of being in the nth excited state after the third scattering event can be expressed in terms of $Q_2(n)$ and so forth. The desorption probability of the Nth electron is then

$$P_N^{\mathrm{des}} = \sum_n Q_N(n)\theta(\hbar\omega n - E_D). \quad (12)$$

When enough time intervals are included the probabilities converge such that $P_N^{\mathrm{des}} = P_{N-1}^{\mathrm{des}}$ and the desorption rate is $R(J) = JP_N^{\mathrm{des}}$ with $J = 1/\Delta t$.

In Fig. 7 we show the rate for NO on Pt(111) with $\Gamma = 0.8$ eV. The desorption energy corresponds to 8 vibrational quanta. Note that changing the lifetime T_{vib} in this model just corresponds to rescaling the flux. The similarity to similar experimental figures[44] is striking. At small flux the rate is linear whereas it obeys a power law ($R \sim J^n$ with $n > 1$) at higher fluences. The fit to a power law is very good for fluxes above 0.2 T_{vib}^{-1}. For small values of the detuning ($-0.4 < \delta\varepsilon < 0.2$ eV) we find that $5.5 < n < 6$, in good agreement with Ho.[44] For large positive values of the detuning the exponent decreases dramatically which is probably due the fact that fewer transitions dominate the dynamics in this region. This means that even though the results were obtained using the simple electron flux $J(\varepsilon_i) = J_0\delta(\varepsilon_i - \epsilon_a - \delta\varepsilon)$ we would most likely obtain the same exponent if we generalized the model to any flux localized within ± 0.2 eV of the resonance.

Although the correspondence with the experimentally found exponent may be fortuitous in such a simple model, the power law itself is very robust to changes in the parameters and we obtain similar power laws for CO on Pt(111). For example, changing the value of Γ results in an overall shift of the rates but the exponents are essentially unchanged. Indeed the exponents appear to be determined mainly by the number of vibrational quanta needed for desorption.

V. SUMMARY AND DISCUSSION

We have previously presented a method to obtain excited-state potential energy surfaces for molecules chemisorbed at metal surfaces.[26] In this paper the method has been applied and combined with a nonadiabatic quantum model to obtain desorption probabilities for CO and NO on four transition-metal surfaces.

The model we have applied allows us to predict the probability that a hot electron will transfer a given amount of energy to the different vibrational modes of an adsorbate. Our main conclusion is the significant role of the internal degree of freedom and the failure of classical mechanics to describe the excited-state adsorbate propagation. Combining the model with a simple picture of the decay and re-excitation of vibrational states reproduces the characteristic power laws of DIMET experiments and yields the exponent associated with a given adsorbate/substrate system.

The model we have used for calculating the energy-transfer rates obviously represents a very simplified view of the dynamics. First of all it is a model of noninteracting electrons. We assume that we can include the important part of the electron-electron interactions by using nonadiabatic coupling coefficients λ_i obtained from the interacting density with linear-expansion ΔSCF-DFT. The approximation amounts to assuming ballistic hot electrons and instantaneous restructuring of the electronic environment when occupying the resonance. Although this may be the case in some metallic systems, electron-electron interactions could have effects which go beyond a simple renormalization of the nonadiabatic coupling. The linear nonadiabatic coupling regime leading to Eq. (5) corresponds to an assumption of equal curvature on the ground- and excited-state PESs. This is a good approximation for CO but NO has a very shallow excited-state PES on some of the transition metals and there the approximation may not be as good.

Furthermore the model assumes that the ground-state potential is quadratic and that the excited-state potential is simply a shifted ground-state potential. At least in the COM direction it is clear from Fig. 1 that the ground-state potential deviates significantly from a quadratic potential and since we are concerned with high-lying vibrational excitations, this deviation could perhaps have an important effect. It may be possible to include anharmonic terms in the Hamiltonian and calculate different scattering amplitudes perturbatively but this will be left for future work.

We have focused on the molecules CO and NO, since they have a conceptually simple structure and a vast amount of experiments have been performed on these systems. However, it is well known that generalized gradient approxima-

tion (GGA)–DFT calculations of CO adsorbed an Pt(111) predict CO to bind at a hollow site in contradiction to the experimentally observed top site.[45] While the difference in adsorbtion energy appears to be less with GPAW than in the calculations presented in Ref. 45, possibly due to the use of the PAW method instead of ultrasoft pseudopotentials, the difference is still 80 meV and the inability to predict the correct binding site is worrying. On the other hand, the existence in the calculation of another adsorption site with a slightly lower energy is unlikely to change the local shape in the potential energy surface enough to *qualitatively* change the results obtained here. In addition, we see a very similar behavior for CO on Ru(0001), where DFT does predict the right adsorption site (the top site). We have thus chosen to put CO at the experimentally observed top site as the hollow site would lead to a smaller surface molecule distance and thus very different screening and desorption rate.

As previously mentioned the value of Γ is estimated from the Kohn-Sham projected density of states, but we do not know how well this estimate matches the true value and as such we have mostly treated Γ as a free parameter. In fact the object of interest in the problem is the spectral function of the resonant state; but even if we had a reliable way of determining this function we would have to make the wideband approximation (where the spectral function is a Lorentzian of width Γ) in order to calculate scattering rates. Nevertheless it would be very interesting to calculate this function to get an idea of the validity of the wideband approximation and to obtain a trustworthy value of Γ.

We have not made any attempt to predict how the distribution of energy evolves after a molecule returns to its electronic ground state, but assume that the dissipation of energy is slow enough that the adsorbate will desorb if the desorption energy has been transferred. This is of course a rather crude assumption and the rate of energy transfer should be accompanied by a detailed molecular propagation on the full-dimensional ground-state PES to improve the results. Ground-state molecular dynamics would also be necessary to obtain branching ratios when there is a possibility of different chemical reactions induced by hot electrons.

However the model we have presented captures some of the essential features of nonadiabatic dynamics. For example, the appearance of an effective inelastic resonance which is detuned from the electronic resonance by an amount depending on the energy transfer is a pure nonadiabatic result and would never have emerged from an adiabatic model. Furthermore the exponents in the DIMET power laws appear to be determined by the number of vibrational quanta needed for desorption and thus communicate the quantum nature of the dynamics.

ACKNOWLEDGMENTS

We would like to acknowledge the help and advice of Jens Jørgen Mortensen on implementing and using linear-expansion ΔSCF in GPAW. The Center for Individual Nanoparticle Functionality (CINF) is sponsored by the Danish National Research Foundation. This work was supported by the Danish Center for Scientific Computing.

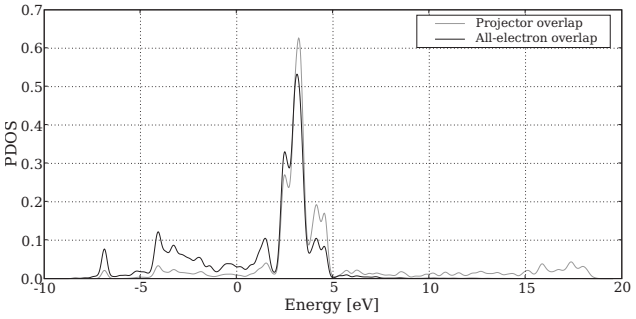

FIG. 8. Ground-state calculation of CO adsorbed on Pt(111) top site. The projected density of states of the 2π orbitals using the methods of projector or pseudowave-function overlap and all-electron wave-function overlap are compared. In the projector overlap method the orbital is defined by $|\tilde{p}_{2\pi}\rangle = \frac{1}{\sqrt{13}}(3|\tilde{p}_x\rangle_C - 2|\tilde{p}_x\rangle_O)$ which is the orbital most similar to the gas-phase calculation. The long high-energy tail of the projector overlap signals an inaccuracy of the method and makes excited-state calculations dependent on the number of unoccupied bands. Thus we use the all-electron overlaps to determine expansion coefficients in this work.

APPENDIX A: PROJECTING KS STATES ON A MOLECULAR ORBITAL IN PAW

The PAW method[32] utilizes that one can transform single-particle wave functions $|\psi_n\rangle$ oscillating wildly near the atom core (all-electron wave functions) into smooth well-behaved wave functions $|\tilde{\psi}_n\rangle$ (pseudowave functions) which are identical to the all-electron wave functions outside some augmentation sphere. The idea is to expand the pseudowave function inside the augmentation sphere on a basis of smooth continuations $|\tilde{\phi}_i^a\rangle$ of partial waves $|\phi_i^a\rangle$ centered on atom a. The transformation is

$$|\psi_n\rangle = |\tilde{\psi}_n\rangle + \sum_{i,a} (|\phi_i^a\rangle - |\tilde{\phi}_i^a\rangle)\langle\tilde{p}_i^a|\tilde{\psi}_n\rangle, \tag{A1}$$

where the projector functions $|\tilde{p}_i^a\rangle$ inside the augmentation sphere a fulfills

$$\sum_i \langle\tilde{p}_i^a|\tilde{\phi}_i^a\rangle = 1, \quad \langle\tilde{p}_i^a|\tilde{\phi}_j^a\rangle = \delta_{ij}, \quad |\mathbf{r} - \mathbf{R}^a| < r_c^a.$$

The method of linear-expansion ΔSCF involves expanding a molecular orbital $|\varphi_i\rangle$ in Kohn-Sham states $|\psi_n\rangle$ and does a self-consistent calculation with an additional density corresponding to the orbital.[26] The simplest way of getting the expansion coefficients is using the projector overlaps $\langle\psi_n|\varphi_i\rangle \sim \langle\tilde{\psi}_n|\tilde{p}_i^a\rangle$ which is calculated in each iteration anyway. However, this method turns out to be too inaccurate in the case of CO on Pt(111) due to nonvanishing projector overlaps for highly energetic Kohn-Sham states as shown in Fig. 8. This implies that the expansion coefficients depend on the number of unoccupied bands included in the calculation

To calculate the overlaps $\langle\psi_n|\varphi_i\rangle$ exactly, one should start by performing a gas-phase calculation of the molecule or atom which is to be used in the ΔSCF calculation. The pseudowave function $\tilde{\psi}_i(x)$ corresponding to the orbital to be occupied is then saved along with the projector overlaps

$\langle \tilde{p}_k^a | \tilde{\psi}_i \rangle$ and the ΔSCF calculation is initialized. In each step of the calculation we can then do a numerical integration to obtain the expansion coefficients by

$$c_{ni} = \langle \psi_n | \psi_i \rangle = \langle \tilde{\psi}_n | \tilde{\psi}_i \rangle + \sum_{a,j,k} \langle \tilde{\psi}_n | \tilde{p}_j^a \rangle (\langle \phi_j^a | \phi_k^a \rangle - \langle \tilde{\phi}_j^a | \tilde{\phi}_k^a \rangle) \times \langle \tilde{p}_k^a | \tilde{\psi}_i \rangle, \tag{A2}$$

where Eq. (A1) was used. Note that there is only a single sum over atoms (and only the ones in the molecule) and that the cross terms of pseudowave or all-electron wave function does not contribute. This can be seen using the arguments following Eq. 20 of Ref. 33.

APPENDIX B: CALCULATING THE INELASTIC-SCATTERING PROBABILITY

Here we briefly summarize the calculation leading to the inelastic-scattering probabilities in model (5).[29] An explicit expression for the probability has previously been obtained[29] for a single mode at initially in the ground state. Here we will extend the result to an explicit expression for any number of modes initially in a thermal ensemble of vibrationally excited states.

From Hamiltonian (3) the differential reflection matrix $R(\varepsilon_i, \varepsilon_f)$ which is defined as the probability per unit final-state energy that an incoming hot electron with energy ε_i scatters on the resonance into a final state of ε_f can be expressed in terms of the four-point Green's function. The inelastic part is contained in the expression,

$$R_{\mathrm{in}}(\varepsilon_i, \varepsilon_f) = \Gamma(\varepsilon_f)\Gamma(\varepsilon_i) \int\int\int \frac{d\tau ds dt}{2\pi\hbar^3} e^{i[(\varepsilon_i - \varepsilon_f)\tau + \varepsilon_f t - \varepsilon_i s]/\hbar} \times G(\tau, s, t), \tag{B1}$$

where the Green's functions is

$$G(\tau, s, t) = \theta(s)\theta(t)\langle c_a(\tau - s) c_a^\dagger(\tau) c_a(t) c_a^\dagger(0) \rangle,$$

$$c(t) = e^{iHt/\hbar} c(0) e^{-iHt/\hbar}, \tag{B2}$$

and $\langle\ \rangle$ denotes a thermal ensemble of oscillator states. The expression is valid for any nonadiabatic coupling function $\varepsilon_a(x)$, but in general it can be very hard to obtain an expression for the Green's function. An exception is the wideband limit with linear coupling corresponding to Hamiltonian (5).[29] The Green's function then becomes

$$G(\tau, s, t) = \theta(t)\theta(s) e^{-i\epsilon_a (t-s)/\hbar - \Gamma(t+s)/2\hbar} \times \exp\left(\sum_i g_i [i(t-s)\omega_i - (1+n_i) f_i - n_i f_i^*] \right), \tag{B3}$$

where ϵ_a is center of the resonance, n_i is the Bose distribution, $g_i = (\lambda_i / \hbar\omega_i)^2$ is the effective coupling constant of the mode i, and

$$f_i(\tau, s, t) = 2 - e^{-i\omega_i t} - e^{i\omega_i s} + e^{-i\omega_i \tau}(1 - e^{i\omega_i t})(1 - e^{i\omega_i s}). \tag{B4}$$

The integrals in scattering matrix (B1) can be evaluated by writing the exponentials in Eq. (B3) as Taylor expansions and performing the τ integral. This leaves the remaining two integrals as complex conjugates which are evaluated by writing factors such as $(1 - e^{i\omega_i t})^m$ by their binomial expansions. For a single oscillator with thermal occupation n we obtain the inelastic reflection matrix,

$$R_{\mathrm{in}}(\varepsilon_i, \varepsilon_f, n) = \Gamma^2 e^{-2g(1+2n)} \sum_{m_1=0}^{\infty} \sum_{m_2=0}^{\infty} \frac{g^{m_1+m_2}(1+n)^{m_1} n^{m_2}}{m_1!\, m_2!} \times \delta(\varepsilon_i - \varepsilon_f - (m_1 - m_2)\hbar\omega) \times F(m_1, m_2), \tag{B5}$$

with

$$F(m_1, m_2) = \left| \sum_{i=0}^{m_1} \sum_{j=0}^{m_2} (-1)^{i+j} \binom{m_1}{i} \binom{m_2}{j} \times \sum_{k=0}^{\infty} \sum_{l=0}^{\infty} \frac{g^{k+l}(1+n)^k n^l}{k!\, l!} \times \frac{1}{\varepsilon_i - \epsilon_a - (i - j + k - l - g)\hbar\omega + i\Gamma/2} \right|^2.$$

Although the expression looks rather complicated it has a simple interpretation. Integrating over final-state energies in the vicinity of $\Delta n = m_1 - m_2$ gives the probability of transferring $\Delta E = \Delta n \hbar\omega$ to the oscillator if the energy of the incoming electron is ε_i,

$$P_{\Delta n}(\varepsilon_i, n) = \Gamma^2 e^{-2g(1+2n)} \left[\frac{g^{\Delta n}(1+n)^{\Delta n}}{\Delta n!} F(\Delta n, 0) + \frac{g^{\Delta n+1}(1+n)^{\Delta n+1} g n}{(\Delta n + 1)!} F(\Delta n + 1, 1) + \frac{g^{\Delta n+2}(1+n)^{\Delta n+2}(gn)^2}{(\Delta n + 2)!\, 2!} F(\Delta n + 2, 2) + \cdots \right], \tag{B6}$$

where the first term is the probability of adding Δn bosons, the second term is the probability for removing (coupling ng) one, and adding [coupling $(n+1)g$] $\Delta n + 1$ bosons and so forth.

We can also evaluate the differential reflection matrix for N oscillators initially in the ground state with frequencies and coupling constants ω_i and g_i, respectively. The result is

$$R_{\mathrm{in}}(\varepsilon_i,\varepsilon_f)=\Gamma^2 e^{-2\Sigma_{i=1}^N g_i}\sum_{m_1=0}^{\infty}\cdots\sum_{m_N=0}^{\infty}\frac{g_1^{m_1}\cdots g_N^{m_N}}{m_1!\cdots m_N!}\delta\left(\varepsilon_i-\varepsilon_f-\sum_{i=1}^{N}m_i\hbar\omega_i\right)\left|\sum_{j_1=1}^{m_1}\cdots\sum_{j_N=1}^{m_N}(-1)^{\Sigma_{i=1}^N j_i}\binom{m_1}{j_1}\cdots\binom{m_N}{j_N}\right.$$

$$\left.\times\sum_{L_1=0}^{\infty}\cdots\sum_{l_N=0}^{\infty}\frac{g_1^{l_1}\cdots g_N^{l_N}}{l_1!\cdots l_N!}\frac{1}{\varepsilon_i-\epsilon_a+i\Gamma/2-\sum_{i=1}^{N}(j_i+l_i-g_i)\hbar\omega_i}\right|^2. \tag{B7}$$

It is amusing that result (B5) for a one-mode system with initial excitation number n follows from result (B7) if we regard Eq. (B5) as a two-mode system at $T=0$ with energies $\hbar\omega$ and $-\hbar\omega$ and coupling constants $g(n+1)$ and gn, respectively. For convenience we state the probability of exciting the (m_d,m_z) state from the ground state in the two-dimensional model with modes d and z,

$$P_{m_d m_z}(\varepsilon_i)=\Gamma^2 e^{-2(g_d+g_z)}\frac{g_d^{m_d}g_z^{m_z}}{m_d!\,n_z!}\left|\sum_{j_d=1}^{m_d}\sum_{j_z=1}^{m_z}(-1)^{j_d+j_z}\binom{m_d}{j_d}\binom{m_z}{j_z}\sum_{k=0}^{\infty}\sum_{l=0}^{\infty}\frac{g_d^k g_z^l}{k!\,l!}\frac{1}{\varepsilon_i-\epsilon_a-(j_d+k-g_d)\hbar\omega_d-(j_z+l-g_z)\hbar\omega_z+i\Gamma/2}\right|^2. \tag{B8}$$

Elastic scattering

The elastic part of the scattering matrix for a single oscillator with thermal occupation number n is

$$R_{\mathrm{el}}(\varepsilon_i,\varepsilon_f,n)=\delta(\varepsilon_i-\varepsilon_f)[1+2\ \mathrm{Im}\ G_R(\varepsilon_i)],$$

$$G_R(\varepsilon)=\int\frac{dt}{\hbar}e^{i\varepsilon t/\hbar}G_R(t),$$

$$G_R(t)=-i\theta(t)\langle n|c_a(t)c_a^{\dagger}(0)|n\rangle. \tag{B9}$$

We can use the linked cluster theorem to derive the retarded Green's function and get the result

$$G_R(t)=-i\theta(t)e^{-g(1+2n)}e^{(-i\epsilon_a-ig\hbar\omega-\Gamma/2)t/\hbar}\sum_{m_1=0}^{\infty}\sum_{m_2=0}^{\infty}\frac{g^{m_1}n^{m_1}g^{m_2}(1+n)^{m_2}}{m_1!\,m_2!}e^{-i(m_2-m_1)\omega t}. \tag{B10}$$

We can then calculate the elastic part of the scattering probability and get

$$P_{\mathrm{el}}(\varepsilon_i,n)=1-\Gamma^2 e^{-g(1+2n)}\sum_{m_1=0}^{\infty}\sum_{m_2=0}^{\infty}\frac{g^{m_1}n^{m_1}g^{m_2}(1+n)^{m_2}}{m_1!\,m_2!}\frac{1}{(\varepsilon_i-\epsilon_a-[m_2-m_1-g]\hbar\omega)^2+(\Gamma/2)^2}. \tag{B11}$$

When calculating the elastic-scattering probability one should also remember to include the $m_1=m_2$ terms in Eq. (B5).

The n in the expressions above denote the Bose distribution and not a specific state $|n\rangle$, but in the context of DIMET our main point of interest is the probability that a oscillator initially in the state $|n_i\rangle$ scatters inelastically to the state $|n_f\rangle$. However, the expression in the case of a pure state is very similar to the thermal ensemble, the only difference being that we should make the substitution

$$e^{-g_i n_i(f_i+f_i^*)}\rightarrow L_{n_i}[g(f_i+f_i^*)] \tag{B12}$$

in Eq. (B3), where $L_n(x)$ is the nth Laguerre polynomial. The expression involving Laguerre polynomials is somewhat more complicated to handle numerically and therefore we have chosen to work with the thermal ensemble expressions instead. In the range of parameters in the present work, the thermal ensemble expressions are very good approximations since $L_n(x)$ have the same first-order Taylor expansion as e^{-nx} and for $t<\hbar/\Gamma$ we get $g_i f_i<0.001$.

*schiotz@fysik.dtu.dk

[1] S. A. Buntin, L. J. Richter, R. R. Cavanagh, and D. S. King, Phys. Rev. Lett. **61**, 1321 (1988).
[2] S. A. Buntin, L. J. Richter, D. S. King, and R. R. Cavanagh, J. Chem. Phys. **91**, 6429 (1989).
[3] F. Fournier, W. Zheng, S. Carrez, H. Dubost, and B. Bourguignon, Phys. Rev. Lett. **92**, 216102 (2004).
[4] J. A. Prybyla, T. F. Heinz, J. A. Misewich, M. M. T. Loy, and J. H. Glownia, Phys. Rev. Lett. **64**, 1537 (1990).
[5] J. A. Prybyla, H. W. K. Tom, and G. D. Aumiller, Phys. Rev. Lett. **68**, 503 (1992).
[6] F. Budde, T. F. Heinz, M. M. T. Loy, J. A. Misewich, F. de Rougemont, and H. Zacharias, Phys. Rev. Lett. **66**, 3024 (1991).
[7] J. A. Misewich, A. Kalamarides, T. F. Heinz, U. Höfer, and D. M. Newns, J. Chem. Phys. **100**, 736 (1994).
[8] L. M. Struck, L. J. Richter, S. A. Buntin, R. R. Cavanagh, and J. C. Stephenson, Phys. Rev. Lett. **77**, 4576 (1996).
[9] P. T. Howe and H. L. Dai, Surf. Sci. **451**, 12 (2000).
[10] L. Cai, X. Xiao, and M. M. T. Loy, Surf. Sci. Lett. **464**, L727 (2000).
[11] M. Bonn, C. Hess, S. Funk, J. H. Miners, B. N. J. Persson, M. Wolf, and G. Ertl, Phys. Rev. Lett. **84**, 4653 (2000).
[12] J. A. Misewich, T. F. Heinz, and D. M. Newns, Phys. Rev. Lett. **68**, 3737 (1992).
[13] J. W. Gadzuk, Phys. Rev. Lett. **76**, 4234 (1996).
[14] L. B. Thomsen, G. Nielsen, S. B. Vendelbo, M. Johansson, O. Hansen, and I. Chorkendorff, Phys. Rev. B **76**, 155315 (2007).
[15] J. W. Gadzuk, L. J. Richter, S. A. Buntin, D. S. King, and R. R. Cavanagh, Surf. Sci. **235**, 317 (1990).
[16] J. W. Gadzuk, Phys. Rev. B **44**, 13466 (1991).
[17] J. W. Gadzuk, Surf. Sci. **342**, 345 (1995).
[18] S. M. Harris, S. Holloway, and G. R. Darling, J. Chem. Phys. **102**, 8235 (1995).
[19] J. W. Gadzuk, J. Vac. Sci. Technol. A **15**, 1520 (1997).
[20] P. Saalfrank, G. Boendgen, K. Finger, and L. Pesce, J. Chem. Phys. **251**, 51 (2000).
[21] A. Nourtier, J. Phys. (Paris) **38**, 479 (1977).
[22] D. M. Newns, T. F. Heinz, and J. A. Misewich, Prog. Theor. Phys. Suppl. **106**, 411 (1991).
[23] M. Brandbyge, P. Hedegård, T. F. Heinz, J. A. Misewich, and D. M. Newns, Phys. Rev. B **52**, 6042 (1995).
[24] A. C. Luntz and M. Persson, J. Chem. Phys. **123**, 074704 (2005).
[25] A. C. Luntz, M. Persson, S. Wagner, C. Frischkorn, and M. Wolf, J. Chem. Phys. **124**, 244702 (2006).
[26] J. Gavnholt, T. Olsen, M. Engelund, and J. Schiøtz, Phys. Rev. B **78**, 075441 (2008).
[27] P. W. Anderson, Phys. Rev. **124**, 41 (1961).
[28] D. M. Newns, Phys. Rev. **178**, 1123 (1969).
[29] N. S. Wingreen, K. W. Jacobsen, and J. W. Wilkins, Phys. Rev. B **40**, 11834 (1989).
[30] The GPAW code is available as a part of the CAMPOS software: www.camd.dtu.dk/Software
[31] J. J. Mortensen, L. B. Hansen, and K. W. Jacobsen, Phys. Rev. B **71**, 035109 (2005).
[32] P. E. Blöchl, Phys. Rev. B **50**, 17953 (1994).
[33] P. E. Blöchl, C. J. Först, and J. Schimpl, Bull. Mater. Sci. **26**, 33 (2003).
[34] B. Hammer, L. B. Hansen, and J. K. Nørskov, Phys. Rev. B **59**, 7413 (1999).
[35] J. P. Perdew, K. Burke, and M. Ernzerhof, Phys. Rev. Lett. **77**, 3865 (1996).
[36] S. Kurth, J. P. Perdew, and P. Blaha, Int. J. Quantum Chem. **75**, 889 (1999).
[37] P. R. Antoniewicz, Phys. Rev. B **21**, 3811 (1980).
[38] J. D. Beckerle, M. P. Casassa, R. R. Cavanagh, E. J. Heilweil, and J. C. Stephenson, Phys. Rev. Lett. **64**, 2090 (1990).
[39] F. Abild-Pedersen and M. P. Andersson, Surf. Sci. **601**, 1747 (2007).
[40] M. Croci, C. Felix, G. Vandoni, W. Harbich, and R. Monot, Surf. Sci. **307–309**, 460 (1994).
[41] R. T. Vang, J. G. Wang, J. Knudsen, J. Schnadt, E. Lægsgaard, I. Steensgaard, and F. Besenbacher, J. Phys. Chem. B **109**, 14262 (2005).
[42] D. A. Butler, B. Berenbak, S. Stolte, and A. W. Kleyn, Phys. Rev. Lett. **78**, 4653 (1997).
[43] M. Ø. Pedersen, M. L. Bocquet, P. Sautet, E. Lægsgaard, I. Stensgaard, and F. Besenbacher, Chem. Phys. Lett. **299**, 403 (1999).
[44] W. Ho, Surf. Sci. **363**, 166 (1996).
[45] P. J. Feibelman, B. Hammer, J. K. Nørskov, F. Wagner, M. Scheffler, R. Stumpf, R. Watwe, and J. Dumesic, J. Phys. Chem. B **105**, 4018 (2001).

Paper III

J. Gavnholt, A. Rubio, T. Olsen, K. S. Thygesen, and J. Schiøtz
Hot-electron-assisted femtochemistry at surfaces: A time-dependent density functional theory approach
Phys. Rev. B **79**, 195405 (2009).

PHYSICAL REVIEW B **79**, 195405 (2009)

Hot-electron-assisted femtochemistry at surfaces: A time-dependent density functional theory approach

Jeppe Gavnholt,[1] Angel Rubio,[2] Thomas Olsen,[1] Kristian S. Thygesen,[3] and Jakob Schiøtz[1,*]

[1]*Department of Physics, Danish National Research Foundation's Center for Individual Nanoparticle Functionality (CINF), Technical University of Denmark, DK-2800 Kongens Lyngby, Denmark*

[2]*Dpto. Fisica de Materiales, European Theoretical Spectroscopy Facility (ETSF), Universidad del Pais Vasco, E-20018 Donostia-San Sebastian, Spain*

[3]*Department of Physics, Center for Atomic-scale Materials Design (CAMD), Technical University of Denmark, DK-2800 Kongens Lyngby, Denmark*

(Received 15 January 2009; revised manuscript received 6 April 2009; published 6 May 2009)

Using time-evolution time-dependent density functional theory (TDDFT) within the adiabatic local-density approximation, we study the interactions between single electrons and molecular resonances at surfaces. Our system is a nitrogen molecule adsorbed on a ruthenium surface. The surface is modeled at two levels of approximation, first as a simple external potential and later as a 20-atom cluster. We perform a number of calculations on an electron hitting the adsorbed molecule from inside the surface and establish a picture, where the resonance is being probed by the hot electron. This enables us to extract the position of the resonance energy through a fitting procedure. It is demonstrated that with the model we can extract several properties of the system, such as the presence of resonance peaks, the time electrons stay on the molecule before returning to the surface when hitting a molecular resonance and the lowering of the resonance energy due to an image charge effect. Finally we apply the TDDFT procedure to only consider the decay of molecular excitations and find that it agrees quite well with the width of the projected density of Kohn-Sham states.

DOI: 10.1103/PhysRevB.79.195405 PACS number(s): 31.15.ee, 73.20.Hb, 82.20.Gk

I. INTRODUCTION

In most chemical processes the intrinsic barriers are overcome due to the randomly directed thermal energy of the atomic cores. This sets some limitations on the possibility of controlling chemical reactions since the thermal energy will distribute itself among all degrees of freedom in the system; i.e., the energy cannot be directed toward, for example, splitting of a certain molecule or desorption of another. Furthermore, in order to get a satisfactory turnover frequency, in some catalyzed reactions, the temperature may need to be so high that the catalyst becomes unstable and degrades over time.

In hot-electron-assisted femtochemistry at surfaces[1–8] the hot electrons (electrons with an energy significantly above the Fermi level) interact with molecular resonances, which gives rise to an electron-phonon coupling. This will initiate motion mainly in those vibrational modes where the coupling is high; i.e., it is possible to direct energy toward certain vibrational modes. This has been demonstrated in an experiment by Bonn *et al.*,[8] who were able to form carbon dioxide from carbon monoxide and oxygen on a ruthenium (0001) surface with the help of hot electrons. This is normally impossible because the carbon monoxide desorbs before the carbon dioxide formation when the temperature is raised. The effect is explained by the hot-electrons injecting energy into the vibrational modes of the adsorbed atomic oxygen so that the barrier forming carbon monoxide can be overcome at a lower temperature.

In most femtochemistry experiments the hot electrons are generated using a femtosecond laser pulse. Each pulse excites a lot of electrons in the metal surface. Due to the high electron density the electron-electron scattering thermalize the hot electrons very rapidly, on a femtosecond time scale, giving rise to an electronic temperature, which is much higher than the phonon temperature. The phonons and electrons will equilibriate much slower, on a picosecond time scale, i.e., for several picoseconds there are electrons present, which have sufficient energy to interact with otherwise unreachable molecular resonances. The high concentration of high-energy electrons even makes it possible to observe multielectron processes, such as desorption induced by multiple electronic transitions, which has been observed for a variety of systems.[9] However, the thermal distribution of electrons does not make it possible to target a specific molecular resonance, in particular one cannot inject electrons into a high-energy resonance without also injecting them into lower-energy resonances, if present.

Another approach to generate hot electrons, by the use of a metal-insulator-metal (MIM) junction, has been suggested by Gadzuk.[7] If the insulating layer in the junction is sufficiently thin and a finite bias is applied, electrons will tunnel from near the Fermi level of the first metal into the other metal, where they can have an energy significantly above the Fermi level; i.e., they will be hot electrons. If the second metal layer is also very thin, these electrons will be able to reach the surface of the other metal and perhaps induce chemistry. The advantage of such a device is that it should, at least theoretically, be possible to target certain molecular resonances by tuning the energy of the hot electrons. The disadvantage being that it will probably not be possible to generate a high electron flux, i.e., only single-electron processes can be observed. Such a MIM device, where the first metal has been substituted by a highly doped silicon layer, has recently been created,[10] and its ability to induce chemical reactions is currently being investigated.

We have previously investigated the hot-electron interaction with different diatomic molecules on different transition-metal surfaces, by applying an electron-phonon interaction model to potential-energy surfaces, which are obtained from the delta self-consistent field method.[11,12] The purpose of this paper is to investigate a different approach, based on time-evolution time-dependent density functional theory (TDDFT), for modeling hot electrons interacting with molecular resonances. TDDFT provides, in principle, an exact framework to describe nonequilibrium processes as the ones relevant in femtochemistry and transport. The price one has to pay in TDDFT is that all correlation effects are embedded in an exchange and correlation kernel that should be nonlocal in space and time. However, most functional in use nowadays are not designed to cope with nonequilibrium situations but still it is common practice to apply local and semilocal functionals to those situations. Further work is needed in the development of nonlocal and frequency-dependent exchange-correlation functionals, which would have impact beyond the present studies. The hope is, however, that such an approach with a simple exchange-correlation functional can still give supplementary information about the occurring processes. Of specific interest are the cross section for exciting the resonance and the lifetime the molecular excitations, which are very important when considering the possibility of hot-electrons inducing chemistry.[12] Another nice feature of the time-evolution approach is that it offers the possibility of simulating the entire event of one hot electron hitting a molecule, i.e., it offers a more physically intuitive picture. Finally it is also worth mentioning that TDDFT provides a multicomponent approach,[13] where the electron and nuclei motion can be directly coupled. This provides the hope that the TDDFT approach presented here in the future can involve a direct calculation of the induced molecular motion. A related approach is TDDFT-based Ehrenfest dynamics, which has, e.g., recently been used to study the interaction of a hydrogen atom with a jellium cluster.[14]

In the following we will start by giving a description of how the time-evolution TDDFT calculations have been performed. After this we present the simulations of the entire event of a hot electron hitting a molecule at a surface. We start by considering a simple model system and then move on to a more realistic system. Finally we will investigate the lifetime of molecular excitations by starting time-evolution TDDFT calculations from the excited state. All the way through we will focus on nitrogen adsorbed on ruthenium, although the methods presented of course are general.

II. METHOD

The main type of calculation performed in this paper is a time-evolution TDDFT calculation, which we have done with the freely available OCTOPUS code.[15,16] We use an adiabatic local-density approximation (ALDA) (Ref. 17) description of the exchange-correlation functional. Nonadiabatic effects and initial state dependence of the exchange-correlation functional are not accounted for by the simple local-density approximation (LDA)-type functional. However, this is not a serious drawback for the present work where we are more interested in getting a qualitative rather than a quantitative picture of the process of hot-electron-induced femtochemistry at metal surfaces. To describe core electrons we use norm-conserving pseudopotentials from the Fritz-Haber Institute[18] generated using the Troullier-Martins scheme.[19] OCTOPUS uses a real-space grid to represent wave functions and densities. After some convergence tests we found that a grid spacing of 0.18 Å gives sufficient accuracy. The Kohn-Sham equations are propagated using a combination of the exponential midpoint rule[20] and a Krylov subspace approximation to the exponential matrix operator.[21] The optimal time step for the type of systems considered here was found to be 0.001 fs, so this time step has been used in all calculations presented in this paper.

The time-evolution TDDFT calculations have not been started from the ground state but still ground-state calculations have been used in the generation of the initial states as it will be clear from Secs. III and IV. Unless otherwise specified the ground-state calculations have been made using the OCTOPUS code with a LDA (Ref. 22) description of the exchange-correlation interactions to maintain consistency with the TDDFT calculations. In each cycle toward self-consistency in the Kohn-Sham equations a Broyden mixing[23] of the seven preceding densities is performed and the Hamiltonian is diagonalized iteratively using the conjugate-gradient method. The occupations of the Kohn-Sham states follow a Fermi-Dirac distribution with an electronic temperature of 0.1 eV, which is necessary in order to get convergence.

III. EXCITING AN ADSORBED MOLECULE

In this section we consider the entire event of a single electron hitting a molecule adsorbed at a surface. We will start from a situation where an electron is placed inside the surface and has a momentum toward the molecule sitting on the surface. This means that we do not consider the creation of the hot electron but the simulated situation is very similar to that found in the MIM device, where hot electrons come from inside the surface with a sufficiently low rate, such that the hot electrons do not affect each other. Naturally, we expect the interaction between the hot electron and the molecular resonance to depend on the starting state of the hot electron, so in order to get some information on this dependence we will start by considering a very simple system. After this we will go to a more realistic system, consisting of a nitrogen molecule adsorbed on a ruthenium cluster.

A. Nitrogen on a fictitious surface

In this section we consider a very simple representation of a molecule adsorbed on a surface. As the adsorbed molecule we use the diatomic nitrogen molecule and instead of representing the surface with a lot of individual atoms, we use a simple external potential. One could just use a step function but in order to avoid any spurious effects due to the hard edges, we make a fit to the Kohn-Sham potential of a ruthenium slab density functional theory (DFT) calculation, which is shown in Fig. 1.

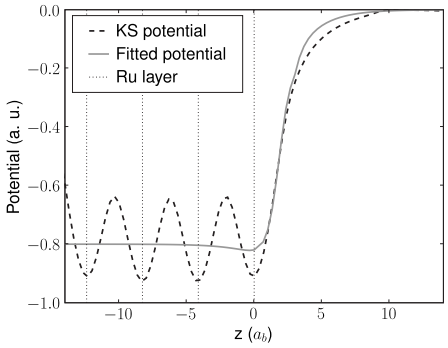

FIG. 1. A fit of the Kohn-Sham potential at a ruthenium surface. The dotted curve shows the self-consistent ground-state Kohn-Sham potential of a four-layer ruthenium (0001) slab averaged over the directions parallel to the surface. The solid curve shows our fit from Eq. (1). The vertical lines indicate the positions of the layers in the slab. The DFT calculation was made with the GPAW code (Refs. 24 and 25).

The slab consists of four atomic layers and the exposed surfaces are close-packed (0001) surfaces. The shown Kohn-Sham potential has been averaged over the directions parallel to the surface. The fitted potential is in atomic units[26] (a.u.) given by the expression

$$V_{\mathrm{fit}}(z) = -0.8\frac{1}{1+e^{4(z-1)}} - 0.16e^{-|z-1.55|}, \qquad (1)$$

where z is the coordinate perpendicular to the surface and $z=0$ corresponds to the position of the outermost layer of atoms in the surface. The expression of Eq. (1) only represents the surface, i.e., the entire system of a surface and a molecule is handled by applying an external potential of $V_{\mathrm{fit}}(z)+\Sigma_a V^a_{\mathrm{cent}}(\mathbf{r})$, where V^a_{cent} is the central potential of atom a in the molecule. Furthermore the valence electrons of the molecule are included in the calculations, whereas no electrons of the surface are included.

This simple representation of the surface has the advantage that it is easy to generate a starting orbital for the hot electron inside the surface, which is orthogonal to the other occupied orbitals since all other electrons are located on the molecule outside the surface. Furthermore the computational effort is significantly lowered by the fact that only a few electrons are included in the calculation. Figure 2 shows an example of how the orbital of a hot electron evolves over time, when it starts inside the surface with a momentum toward the surface.

Before the time-evolution calculation the states of the valence electrons of the nitrogen molecule was found by performing a ground-state calculation with just these electrons. The starting orbital of the hot electron is an unoccupied eigenfunction of this ground-state Hamiltonian multiplied by $e^{i0.8z}$, in order to give it a momentum of 0.8 a.u. toward the surface. This eigenfunction was chosen because it is almost entirely located inside the surface and it has the Π symmetry needed in order for it to interact with the $2\pi^*$ states of the molecule.

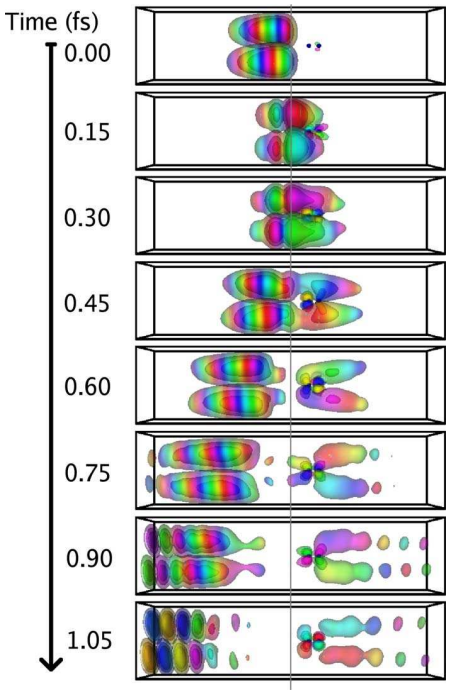

FIG. 2. (Color online) An example of the evolution over time of a hot electron with a momentum directed toward the molecule. The hot-electron orbital is shown at times: 0, 0.15, 0.30, 0.45, 0.60, 0.75, 0.90, and 1.05 fs. The gray scale (online: color grading) indicates the phase of the orbital. The two dots, which are visible at $t=0$ fs, indicate the positions of the nitrogen atoms and the gray line indicates the surface. The unit cell is cylindrical with a radius of 4 Å and a length of 40 Å and is exactly contained in the shown boxes.

Figure 2 shows several interesting features. When hitting the surface a large fraction of the electron is reflected due to the work function of the surface but some of the electron ends up in the $2\pi^*$ states of the molecule, indicating a nonzero probability of exciting the molecule. In this calculation some of the electron is apparently also transmitted by the molecule, which indicates that some of the electron has an energy above the vacuum level. From the figure it is also obvious that it does not make sense to continue the calculation much further since the reflections of the electron at the unphysical unit-cell edges start to interfere with the molecule after approximately 1 fs.

For the calculation displayed on Fig. 2 we chose the starting orbital of the hot electron rather randomly. In order to get an idea of how the obtained results vary with the starting orbital we have carried out calculations with the hot electron starting in a number of different starting orbitals as illustrated in Table I. Each of the orbitals shown in Table I has an average momentum in the z direction of 0.8 a.u. but we also made several calculations on the same orbitals but with different average momenta, i.e., multiplied with a different exponential factor ($e^{ip_{0z}}$). The unit cells have been made twice as long as the unit cell in Fig. 2 in order to prolong the time it takes before reflected waves reach the molecule.

The fraction of the electron that gets into the $2\pi^*$ orbitals of the molecule varies a lot from calculation to calculation.

TABLE I. (Color online) The five different types of wave functions we use as starting orbitals for the hot electron in Sec. III. The first order Bessel function used in the radial direction for wave functions 1–3 is scaled such that the first node coincides with the unit-cell boundary. The gray scale (online: color grading) indicates the phase of the wave functions. The unit cells are cylindrical with a radius of 6 Å and a length of 80 Å.

Wf. no.	Picture	Specifications
1		**Radial direction:** 1. order Bessel function **z direction:** Gaussian wavepacket with $p_0 = 0.8$, $\Delta p = 0.1$
2		**Radial direction:** 1. order Bessel function **z direction:** Gaussian wavepacket with $p_0 = 0.8$, $\Delta p = 0.2$
3		**Radial direction:** 1. order Bessel function **z direction:** Gaussian wavepacket with $p_0 = 0.8$, $\Delta p = 0.4$
4		Eigenfunction for the ground state Hamiltonian (eigenfunction no. 7) times $e^{ip_0 x}$, $p_0 = 0.8$
5		Eigenfunction for the ground state Hamiltonian (eigenfunction no. 13) times $e^{ip_0 x}$, $p_0 = 0.8$

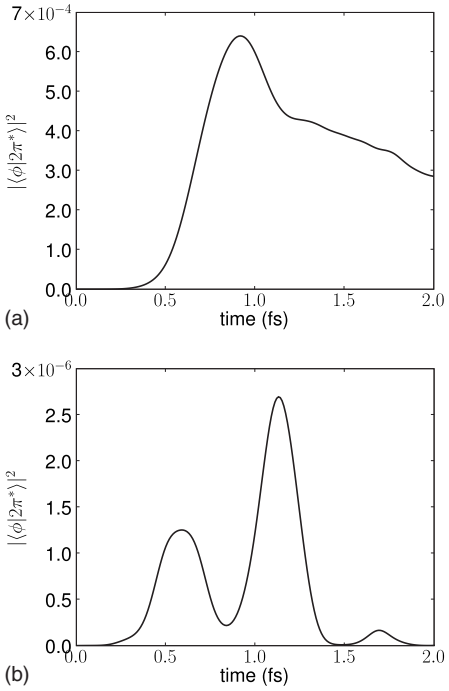

FIG. 3. The difference between an electron that hits resonance and one that does not. The y axes are the orbital of the hot electron, ϕ, projected to the subspace spanned by the two $2\pi^*$ orbitals of the molecule squared. The x axes show the time. Top panel is an example of an electron hitting resonance (Wf. No. 1 from Table I with p_0=0.8). Bottom panel is an example of an electron not hitting resonance (Wf. No. 1 from Table I with p_0=0.4). Please notice the more than 2 orders of magnitude difference in the y-axis scales.

The upper and lower panels in Fig. 3 illustrate the situations where a rather large part and a rather small part, respectively, of the electron goes into the $2\pi^*$ orbitals. The y axes show the projection of the orbital of the hot electron onto the subspace spanned by the two $2\pi^*$ orbitals of the molecule and the x axes are time. In the top panel the electron seems to hit resonance since a rather large part of it gets into the $2\pi^*$ orbital. Furthermore it is seen that the excitation is quite long lived compared to the small fluctuations in the off-resonance calculation shown on the lower panel.

The results of all the calculations have been collected in Fig. 4, which shows the maximum overlap between the hot-electron orbital and the $2\pi^*$ orbitals of the molecule squared, $|\langle\phi|2\pi^*\rangle|^2$, as a function of the average momentum for each of the five different starting orbitals from Table I. By maximum overlap we mean the maximum overlap within the first 2 fs, which is time enough for the wave function to fully hit the molecule but not enough time for the reflections at unit-cell boundaries to interfere with the results. For all the curves there is a large dependence on the momentum, i.e., there are certain values of p_0 which are at resonance and others which are off-resonance. The curves are, however, also quite different. Curves 1–3 all have the maximum at the same momentum but it is also clear that the more well-defined momentum the wave function has, the more well defined is the resonance peak. This indicates that the shape of the resonance peaks are reflected by the Fourier transforms of the wave functions.

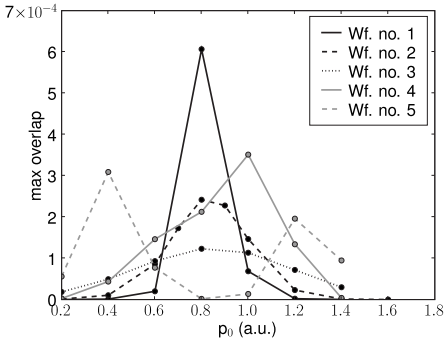

FIG. 4. The amount of electron that gets into the $2\pi^*$ orbitals of the molecule within the first two femtoseconds plotted as a function of the average momentum of the hot electron, p_0. The five different curves are for the five different orbitals given in Table I.

This is supported by Fig. 5, which shows the Fourier transforms of wave functions 4 and 5 integrated over the axes parallel to the surface. These curves resemble the resonance curves on Fig. 4 a lot. One interpretation of this is that the wave function, which is sent toward the molecule, is just probing the resonance. In an energy picture this means that the maximal overlap, MO, which we interpret as the excitation probability, can be written as

$$\mathrm{MO} = \int R(\epsilon) W(\epsilon) d\epsilon, \tag{2}$$

where $W(\epsilon)$ is the amount of the hot electron that has the energy ϵ, i.e.,

$$W(\epsilon) = \sum_i |\langle \phi | \psi^i_{\mathrm{KS}} \rangle|^2 \delta(\epsilon - \epsilon^i_{\mathrm{KS}}). \tag{3}$$

ϕ is the hot-electron orbital and ψ^i_{KS} is the ith Kohn-Sham orbital, which has the energy ϵ^i_{KS}. $R(\epsilon)$ is the energy representation of the resonance. The difference of the Kohn-Sham eigenvalues do not describe excitation energies, therefore in Eq. (3) we are neglecting the renormalizaton of the Kohn-Sham eigenvalues by the exchange-correlation kernel. For resonances as in the case of molecular systems in front of metallic surfaces this renormalization can be accounted for.[27]

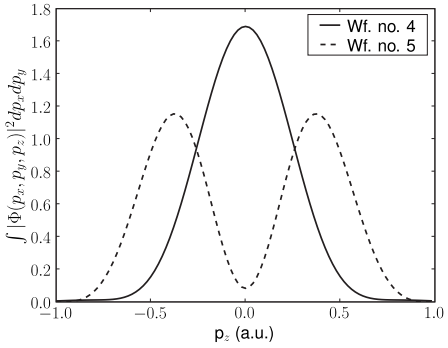

FIG. 5. The Fourier transform of wave functions 4 and 5 from Table I integrated over the momenta parallel to the surface. The horizontal axis indicates the momentum in the direction perpendicular to the surface, p_z.

For the resonance we will assume a Lorentzian shape,

$$R(\epsilon) = \alpha_{\mathrm{res}} \frac{(\Gamma/2)^2}{(\epsilon - \epsilon_{\mathrm{res}})^2 + (\Gamma/2)^2}, \tag{4}$$

which corresponds to an exponentially decaying excitation. Γ is the full width at half maximum of the resonance and is related to the lifetime of the resonance. ϵ_{res} is the mid point of the resonance, which we will refer to as the resonance energy. The excitation probability is proportional to α_{res}, so it is closely related to the resonance cross section.

We estimate the three parameters, Γ, ϵ_{res}, and α_{res}, in Eq. (4) by performing a least-squares fit of the maximum overlaps obtained by inserting Eqs. (4) and (3) in Eq. (2) to the maximum overlaps shown in Fig. 4. This gives the values of $\Gamma = 1.4$ eV and $\epsilon_{\mathrm{res}} = 9.8$ eV above the Fermi level and $\alpha_{\mathrm{res}} = 5.4 \times 10^{-3}$. The value of $\epsilon_{\mathrm{res}} = 9.8$ eV may seem high but one should keep in mind that for this system the Fermi level lies at the highest occupied molecular orbital of the nitrogen molecule and that the surface cannot create an image charge, which would lower the resonance energy. The 9.8 eV also seem reasonable, when comparing to the lowest excitation energies of the nitrogen molecule, which are at the same level. In Sec. III B we will calculate the equivalent number for a molecule sitting at a more realistic cluster surface. Here we do indeed find that the presence of electrons in the surface and the possibility of an image charge will lower this number.

The resulting Lorentz distribution is shown in Fig. 6, where $W(\epsilon)$ from Eq. (3) is also plotted for different momenta of the hot-electron orbital. From this it is evident that the resonance features from Fig. 4 arise because the energy distribution of the hot electron passes the resonance as the momentum of the hot electron is increased.

Figure 7 shows how close the true maximum overlaps fits with the ones obtained by inserting the optimal values of Γ, ϵ_{res}, and α_{res} into Eqs. (2)–(4). It is seen that they agree quite well, especially it should be noted that the double-peaked feature at Wf. No. 5 is reproduced. This indicates that the assumptions made in Eqs. (2)–(4) are reasonable and that Γ, ϵ_{res}, and α_{res} are truly properties of the system and not the arbitrarily chosen orbitals for the hot electrons.

B. Nitrogen on a ruthenium cluster

The system considered in Sec. III A is only a very crude approximation to a real system. First of all, in a real system the surface will be build from individual atoms and, perhaps more importantly, the other electrons in the surface will feel the hot electron, giving rise to a screening effect.

The intention of this section is to utilize the experiences gained in Sec. III A on a more realistic system, i.e., we want to probe the resonance with some wave function for the hot electron and then perform the fitting of Eqs. (2)–(4) in order to extract the values of Γ, ϵ_{res}, and α_{res}. We will consider the cluster shown in Fig. 8, which consists of 20 ruthenium atoms and a nitrogen molecule adsorbed on it.

The cluster is a simple model of a nitrogen molecule adsorbed on a close-packed (0001) ruthenium surface and includes the first three layers. We use a cluster instead of a slab

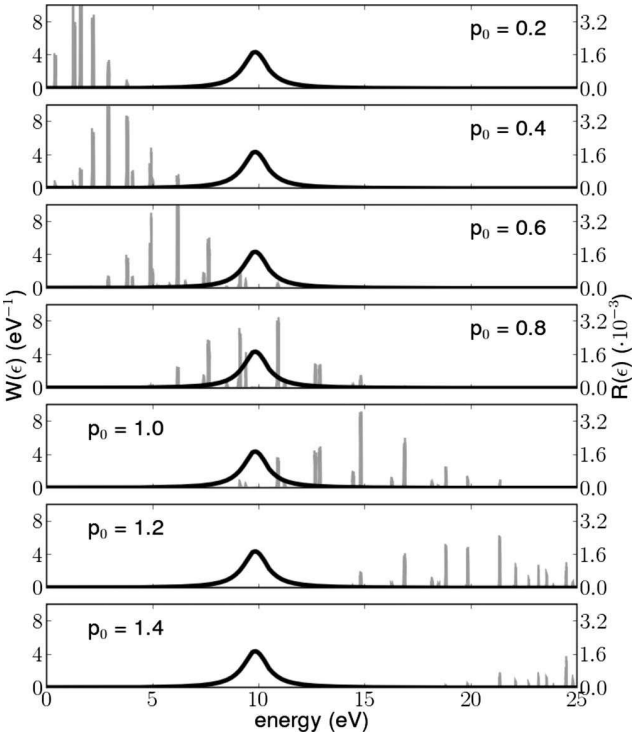

FIG. 6. The gray peaks show $W(\epsilon)$ from Eq. (3), where the delta functions have been replaced by Gaussians with a spread of 0.1 eV, for Wf. No. 1 in Table I. The different subplots are for different average momenta, p_0. The black curves show the fitted Lorentzian, $R(\epsilon)$, from Eq. (4) with the values $\Gamma=1.4$ eV and $\epsilon_{\text{res}}=9.8$ eV above the Fermi level and $\alpha_{\text{res}}=5.4\times10^{-3}$. The left y axes indicate $W(\epsilon)$ and the right $R(\epsilon)$.

in order to avoid all the difficulties that arise when applying periodic boundary conditions in a time-evolution TDDFT calculation.[16] A possible intermediate system to consider

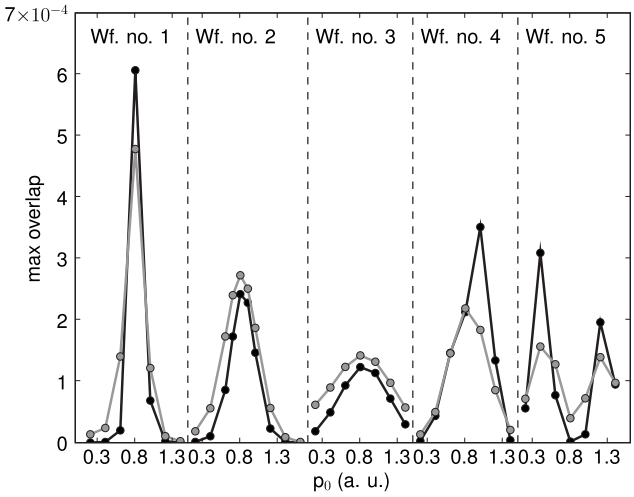

FIG. 7. The black lines show the same maximum overlaps depicted on Fig. 4. The gray lines are obtained by inserting Eqs. (3) and (4) in Eq. (2) and varying Γ, ϵ_{res}, and α_{res} until the best least-squares fit is obtained. We find this to be at $\Gamma=1.4$ eV and $\epsilon_{\text{res}}=9.8$ eV above the Fermi level and $\alpha_{\text{res}}=5.4\times10^{-3}$.

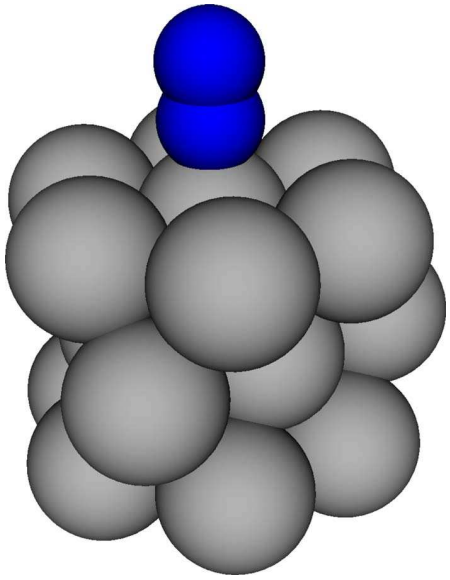

FIG. 8. (Color online) The ruthenium cluster with adsorbed nitrogen, on which we perform calculations in Sec. III B. The gray atoms are ruthenium and the dark (online: blue) nitrogen. The cluster has 20 ruthenium atoms.

would be a jellium surface, where the external step potential is made deeper and combined with extra electrons inside the surface. One would not gain much compared to the cluster calculation with respect to the calculational complexity and effort needed, so we have not done this here.

Some extra care has to put into finding a suitable starting orbital of the hot electron in this system because of the other electrons present in the cluster, which the orbital of the hot electron must be orthogonal to. Furthermore the Fourier transform of the hot-electron orbital should be quite simple, preferably with just one peak, such that we can expect that the fitting described in Sec. III A can be done easily. The procedure we choose is to first perform an ordinary ground-state DFT calculation on the 20 atoms ruthenium cluster without the nitrogen molecule. We then project the function,

$$\Psi(r,\theta,z) = J_1\left(\frac{r}{r_0}\right)e^{i\theta}e^{-(z+3.3)^2/3.3^2}, \tag{5}$$

onto the space spanned by the 116 lowest lying Kohn-Sham orbitals. $J_1(r)$ is a Bessel function of the first kind and r, θ, and z are the usual semipolar coordinates and the equation is in atomic units. r_0 is chosen such that the first node of $J_1(\frac{r}{r_0})$ lies at $r=8$ a_0. $z=0$ corresponds to the z value of the highest lying layer of atoms in the cluster. We normalize this projected version of $\Psi(r,\theta,z)$ and multiply it with $e^{ip_0 z}$, where p_0 is the average momentum and use it as the starting orbital for the hot electron. With this choice we ensure that the Fourier transform of the starting orbital only has one significant peak, as it can be seen from Fig. 9, and we ensure that the orbital is nicely localized within the cluster. The choice of $\Psi(r,\theta,z)$ in Eq. (5) is made because it only has a single peak in the Fourier representation and the $e^{i\theta}$ factor gives it the Π symmetry required in order for the electron to interact

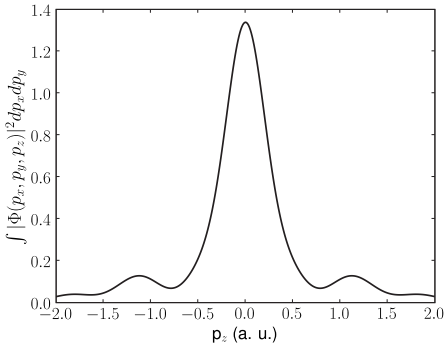

FIG. 9. The momentum space representation of the hot-electron wave function squared and integrated over the directions parallel to the surface.

with the $2\pi^*$ orbitals of the nitrogen molecule. Other than that the exact choice of $\Psi(r,\theta,z)$ is not so critical. We have tried both varying the number of included KS orbitals and the parameters of the Gaussian in Eq. (5).

Finally a ground-state DFT calculation is performed on the cluster with the nitrogen molecule attached and all the occupied Kohn-Sham orbitals are othogonalized to the starting orbital of the hot electron through an ordinary Gram-Schmidt orthogonalization procedure. Furthermore one spin-up electron is removed at the Fermi level and placed in the orbital of the hot electron, still with spin-up. This is then used as the starting point for the time-evolution TDDFT calculation. Spins are treated using an ordinary spin-polarization procedure.

As it was also done in Sec. III A the time-evolution calculations are performed for different values of the average momentum, p_0. Figure 10 shows the maximum projection of the hot-electron orbital onto the subspace spanned by the $2\pi^*$ orbitals of the nitrogen molecule within the first 3 fs as a

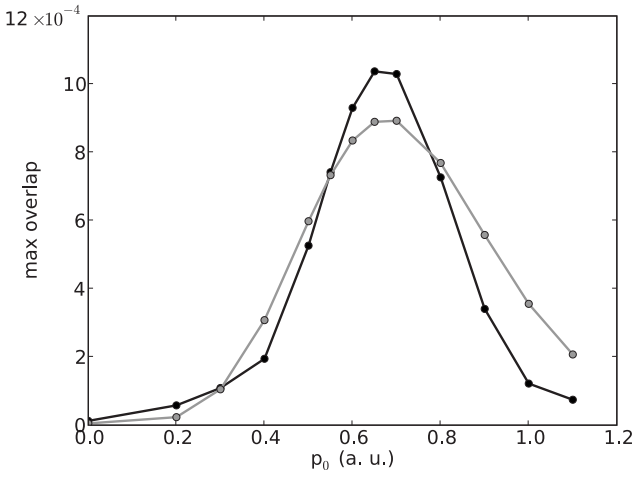

FIG. 10. The black curve shows the amount of electron that gets into the $2\pi^*$ orbital of the molecule within the first three fs plotted as a function of the average momentum of the hot electron, p_0. The gray lines are obtained by inserting Eqs. (3) and (4) in Eq. (2) and varying Γ, ϵ_{res}, and α_{res} until the best least-squares fit is obtained. We find this to be at $\Gamma=0.36$ eV, $\epsilon_{\mathrm{res}}=4.9$ eV, and $\alpha_{\mathrm{res}}=1.9\times10^{-3}$.

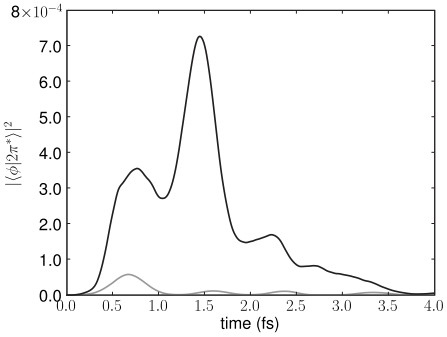

FIG. 11. The orbital of the hot electron, ϕ, projected to the plane spanned by the two $2\pi^*$ orbitals of the molecule squared as a function of time. The black curve is at a momentum of $p_0=0.8$ a.u. and the gray curve is at $p_0=0.2$.

function of p_0. Again a clear resonance peak is found. From Fig. 11 it is also seen that the difference between an electron hitting resonance and an off-resonance electron is not only the size of the overlap with the molecular orbital but also the time the electron stays there. An electron hitting resonance will stay on the molecule for some time before returning to the surface, which seems physically reasonable. This was also what we saw in Sec. III A.

Figure 10 shows also the least-squares fit we obtain by varying Γ, ϵ_{res}, and α_{res} in Eqs. (2)–(4). The optimal values we find are $\Gamma=0.36$ eV and $\epsilon_{\mathrm{res}}=4.9$ eV above the Fermi energy and $\alpha_{\mathrm{res}}=1.9\times10^{-2}$. The Γ value is quite uncertain because $R(\epsilon)$ is much more localized than $W(\epsilon)$ in Eq. (2); i.e., we try to determine the shape of a very thin function by probing it with a very wide. The 4.9 eV resonance energy is significant lower than the 9.8 eV found in Sec. III A, which was also expected as the Fermi level is now raised by the electrons in the surface and as the resonance energy is lowered by an image charge effect with the surface. Inverse photoemission experiments for N_2 on a nickel surface give an energy of approximately 4.4 eV.[28] When we perform ΔSCF calculations in the manner described in Ref. 11 we find that there is only a minor difference in energy between having a nickel and a ruthenium surface. This indicates that the value of 4.9 eV is quite reasonable. It is also worth noticing that the projected density of states for the 2π states has its maximum between 2 and 3 eV above the Fermi level as we will show in Sec. IV. This means that the optimal value of ϵ_{res} cannot be explained as a mere matching in energy between the hot electron and the 2π Kohn-Sham states. This is probably because the energy of the Kohn-Sham states will change as the density changes, which fits well with a ΔSCF picture of the situation. In Sec. IV we will consider the value of Γ.

We expect that the found α_{res} values will depend on the cross-section areas of the considered systems, i.e., the unit-cell cross section in Sec. III A and the cluster cross section in this section since the hot-electron orbital is spread over these areas. It will probably be reasonable to assume that α_{res} is inversely proportional to the cross-section area of the system, i.e.,

$$A_{\mathrm{res}} = \alpha_{\mathrm{res}} \times A_{\mathrm{system}}, \tag{6}$$

where A_{res} is the resonance cross section and A_{system} is the cross section of the system. With this crude approximation

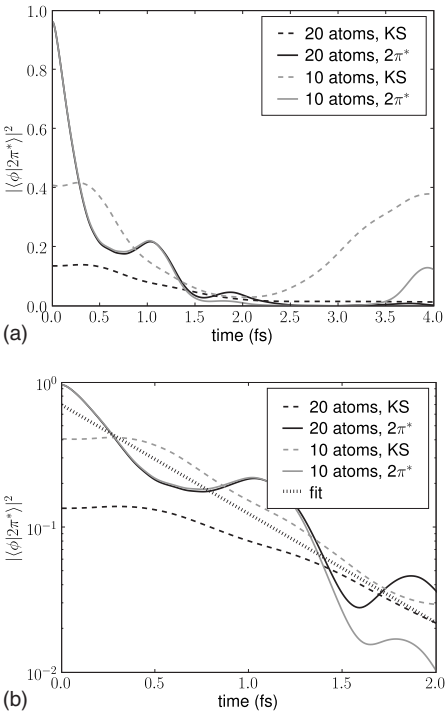

FIG. 12. The orbital of the excited electron projected plane spanned by the $2\pi^*$ orbitals of the nitrogen molecule squared as a function of time for four different calculations. The only difference between upper and lower panels is that they use a normal and a logarithmic scale, respectively, on the y axes. Two of the calculations are performed on the 20-atom cluster from Fig. 8 and the other two on the 10-atom cluster from Fig. 13. The difference between the two calculations on each cluster is the state of the excited electron. Either the Kohn-Sham orbital with the largest overlap with the $2\pi^*$ orbitals of the molecule is used or simply one of the $2\pi^*$ orbitals found from a gas phase calculation is used.

we can make a very rough estimate of the resonance cross section. As the system cross section we use the area that seven atoms fill in a ruthenium (0001) surface because there are seven atoms in the top layer of the cluster. We then get $A_{\mathrm{res}}=0.88$ Å^2. By performing calculations for different system cross sections it would be possible to test the assumption of Eq. (6). However, this is beyond the scope of this paper.

IV. DECAY OF AN EXCITATION

In Sec. III we simulated the entire event of an electron hitting a molecular resonance and then returning to the surface. It is, however, also interesting to just consider the decay of an excited molecule, in order to gain some information on the lifetime, which is a very important parameter when trying to calculate the probability that the electron will induce some chemistry.[12] Again we consider a nitrogen molecule adsorbed on a ruthenium cluster.

The decay is considered by exciting an electron to the nitrogen molecule and then monitoring the overlap between the electron and the molecular $2\pi^*$ orbitals as time passes. Figure 12 shows this overlap as a function of time for four different calculations.

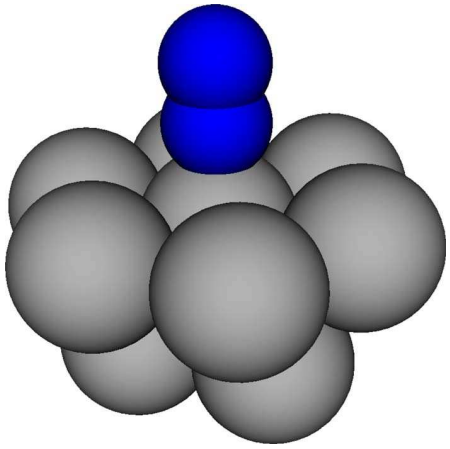

FIG. 13. (Color online) One of the ruthenium clusters used in Sec. IV. The gray atoms are ruthenium and the dark (online: blue) are an adsorbed nitrogen molecule. The cluster has 10 ruthenium atoms.

The difference between the calculations is the state the electron has started in and/or the size of the cluster considered. The electron is either started in the Kohn-Sham eigenfunction with the largest overlap with the $2\pi^*$ orbitals of the nitrogen molecule or simply in one of the $2\pi^*$ orbitals of the nitrogen molecule found from a gas phase calculation. The cluster is either the 20 atoms ruthenium cluster shown in Fig. 8 or the 10 atoms ruthenium cluster shown in Fig. 13.

From the semilogarithmic plot in the lower panel of Fig. 12 it is seen that the lifetime is quite similar for all four calculations, indicating that the arbitrary choice of a starting orbital for the excited electron and the size of the cluster is not too critical when estimating the lifetime. From the linear fit on the semilogarithmic plot we get a lifetime of $\tau=0.6$ fs. With the use of Heisenberg's uncertainty relation, $\Delta t\Delta E\approx\hbar$, we can associate this lifetime with an uncertainty in the resonance energy: $\Delta E\approx 1.1$ eV. By comparing this with the density of states projected onto the plane spanned by the $2\pi^*$ orbitals of the nitrogen molecule, as it is done in Fig. 14, we see that it fits quite well with the spread of the projected density of states. This indicates that estimating excitation lifetimes from the projected density of Kohn-Sham states is reasonable. In Sec. III B we found a value of $\Gamma=0.36$ eV, which is approximately a factor of 3 different from the ΔE found here. This difference is consistent with the large uncertainty attached to the Γ value determined in the fitting procedure.

From the upper panel of Fig. 12 it is also seen that the electron returns to the $2\pi^*$ orbitals after a few femtoseconds for the ten-atom cluster, when the electron is placed in a Kohn-Sham orbital. This looks like a two-level oscillation and in fact a more careful analysis reveals that the electron oscillates between two Kohn-Sham orbitals, i.e., the couplings to the other Kohn-Sham orbitals are very low. Similar effects can also be seen in the other calculations if they are continued and is a consequence of the fact that it does not make sense to continue the calculations too far because the system cannot dissipate the electronic energy as it would when connected to a large surface.

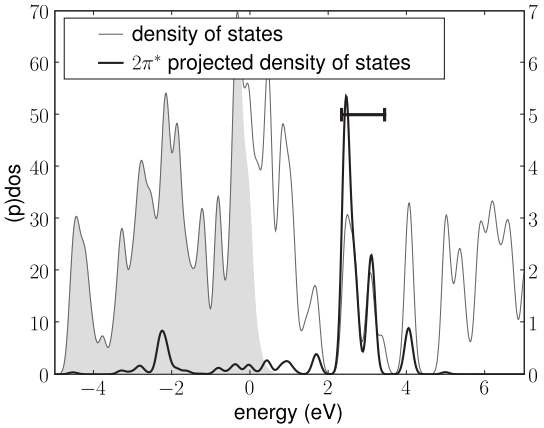

FIG. 14. The density of states for the 20 atoms cluster of Fig. 8 and the density of states projected onto the plane spanned by the $2\pi^*$ orbitals of the nitrogen molecule. The inserted bar has a length of 1.1 eV, which corresponds to the expected uncertainty in energy of the $2\pi^*$ resonance (see text). The light gray filling indicates the occupied states. Left axis is the density of states and the right the projected density of states.

V. SUMMARY

We have applied time-evolution TDDFT to model the interaction of electrons with molecular resonances at surfaces. More specifically we have considered systems consisting of a nitrogen molecule adsorbed either on a simple fictive surface or a more realistic ruthenium cluster. We found that this TDDFT approach can be used to extract several physical properties of the systems:

(1) when an electron collides with a molecule from inside the surface, some of the orbital is reflected, some places itself in a molecular state, and in some case some of it passes the molecule. This can be associated with the probabilities of reflection, excitation, and transmission.

(2) When the momentum (or energy) of the incoming electron is varied a resonance feature is observed.

(3) An electron hitting the resonance will stay on the molecule for some time in contrast to an electron hitting off-resonance.

(4) We obtain reasonable values for the resonance energies. As expected the resonance energy is lowered by the contact with a realistic surface.

(5) The decay of the electronic excitation fits an exponential quite well.

Furthermore we have established a picture where the incoming hot electron can be considered as a probe, which probes the resonance. Using a fitting procedure we have been able to extract resonance properties, which apparently are system specific and not dependent on the exact nature of the incoming electron orbital. We have shown how this picture can be applied to a more realistic system consisting of a molecule adsorbed on a cluster of atoms.

Finally we compared the lifetime observed in a time-evolution TDDFT calculation with a simple projected density-of-states analysis. We found that they agree quite well.

ACKNOWLEDGMENTS

The Center for Individual Nanoparticle Functionality CINF is sponsored by the Danish National Research Foundation. This work was supported by the Danish Center for Scientific Computing. A.R. acknowledges funding by the Spanish MEC (Grant No. FIS2007-65702-C02-01), "Grupos Consolidados UPV/EHU del Gobierno Vasco" (Grant No. IT-319-07), CSIC, and European Community through e-I3 ETSF project (Project No. INFRA-2007-1.2.2; Grant Agreement Number 211956). We acknowledge support by the Barcelona Supercomputing Center, "Red Espanola de Supercomputacion," and SGIker ARINA (UPV/EHU). The Center for Atomic-Scale Materials Design CAMD is sponsored by the Lundbeck Foundation.

*schiotz@fysik.dtu.dk

[1] *Laser Spectroscopy and Photochemistry on Metal Surfaces*, edited by H.-L. Dai, and W. Ho (World Scientific, Singapore, 1995).
[2] J. W. Gadzuk, Phys. Rev. B **44**, 13466 (1991).
[3] R. E. Palmer and P. J. Rous, Rev. Mod. Phys. **64**, 383 (1992).
[4] R. R. Cavanagh, D. S. King, J. C. Stephenson, and T. F. Heinz, J. Phys. Chem. **97**, 786 (1993).
[5] X.-Y. Zhu, Annu. Rev. Phys. Chem. **45**, 113 (1994).
[6] D. G. Busch and W. Ho, Phys. Rev. Lett. **77**, 1338 (1996).
[7] J. W. Gadzuk, Phys. Rev. Lett. **76**, 4234 (1996).
[8] M. Bonn, S. Funk, C. Hess, D. N. Denzler, C. Stampfl, M. Scheffler, M. Wolf, and G. Ertl, Science **285**, 1042 (1999).
[9] J. A. Misewich, T. F. Heinz, and D. M. Newns, Phys. Rev. Lett. **68**, 3737 (1992).
[10] L. B. Thomsen, G. Nielsen, S. B. Vendelbo, M. Johansson, O. Hansen, and I. Chorkendorff, Phys. Rev. B **76**, 155315 (2007).
[11] J. Gavnholt, T. Olsen, M. Engelund, and J. Schiøtz, Phys. Rev. B **78**, 075441 (2008).
[12] T. Olsen, J. Gavnholt, and J. Schiøtz, Phys. Rev. B **79**, 035403 (2009).
[13] T. Kreibich and E. K. U. Gross, Phys. Rev. Lett. **86**, 2984 (2001).
[14] R. Baer and N. Siam, J. Chem. Phys. **121**, 6341 (2004).
[15] OCTOPUS is a freely available real-space-time-dependent density functional theory code (see www.tddft.org/programs/octopus/).
[16] A. Castro, H. Appel, M. Oliveira, C. Rozzi, X. Andrade, F. Lorenzen, M. Marques, E. Gross, and A. Rubio, Phys. Status Solidi B **243**, 2465 (2006).
[17] A. Zangwill and P. Soven, Phys. Rev. A **21**, 1561 (1980).
[18] Pseudopotentials from the Fritz-Haber institute are available on the website www.abinit.org/Psps/?text=./Psps/LDA_FHI/fhi
[19] N. Troullier and J. L. Martins, Phys. Rev. B **43**, 1993 (1991).
[20] M. Hochbruck and C. Lubich, SIAM (Soc. Ind. Appl. Math.) J. Numer. Anal. **41**, 945 (2003).
[21] M. Hochbruck and C. Lubich, SIAM (Soc. Ind. Appl. Math.) J. Numer. Anal. **34**, 1911 (1997).
[22] D. M. Ceperley and B. J. Alder, Phys. Rev. Lett. **45**, 566 (1980).

[23] C. G. Broyden, Math. Comput. **19**, 577 (1965).
[24] The GPAW code including the implementation of ΔSCF is available as a part of the CAMPOS software: www.camp.dtu.dk/Software
[25] J. J. Mortensen, L. B. Hansen, and K. W. Jacobsen, Phys. Rev. B **71**, 035109 (2005).
[26] Lengths in Bohr radii and energies in Hartree.
[27] K. S. Thygesen, Phys. Rev. Lett. **100**, 166804 (2008).
[28] P. D. Johnson and S. L. Hulbert, Phys. Rev. B **35**, 9427 (1987).

Paper IV

T. Olsen
Inelastic scattering in a local polaron model with quadratic coupling to bosons
Phys. Rev. B **79**, 235414 (2009).

Inelastic scattering in a local polaron model with quadratic coupling to bosons

Thomas Olsen*
Department of Physics, Danish National Research Foundation's Center of Individual Nanoparticle Functionality (CINF), Technical University of Denmark, DK-2800 Kongens Lyngby, Denmark
(Received 10 March 2009; revised manuscript received 22 May 2009; published 12 June 2009)

We calculate the inelastic scattering probabilities in the wide band limit of a local polaron model with quadratic coupling to bosons. The central object is a two-particle Green's function which is calculated exactly using a purely algebraic approach. Compared with the usual linear interaction term a quadratic interaction term gives higher probabilities for inelastic scattering involving a large number of bosons. As an application we consider the problem hot-electron-mediated energy transfer at surfaces and use the delta self-consistent field extension of density-functional theory to calculate and compare coupling parameters and probabilities for exciting different vibrational modes of CO adsorbed on a Cu(100) surface.

DOI: 10.1103/PhysRevB.79.235414 PACS number(s): 71.38.−k, 71.45.−d, 31.15.xr, 71.15.Qe

I. INTRODUCTION

The local polaron model describes a localized electronic state which is coupled to a boson field. The local state is then assumed to be hybridized with a continuum of delocalized states and is thus not an eigenstate of the electronic part of the Hamiltonian.

One of the first applications of the model was the coupling of plasmons to core holes[1] and valence holes[2] in metals. The boson field then represents the plasmons which can be excited by the introduction of a structureless core hole or a valence hole which may be hybridized with metallic states. Plasmon excitation spectra are typically measured using electron-energy-loss spectroscopy (EELS) where the energy loss of highly energetic electrons is measured after transmission through a metallic film. A similar application is that of deep-level spectroscopy[3] where the boson field represents a phonon system which can be excited by the introduction of a core hole. Hybridization of the core hole is then introduced to capture the degeneracy of the core hole with a continuum of states with no core hole but a high-energy Auger electron present. A somewhat different line of application is that of certain rare-earth compounds which are known to give rise to mixed valence states.[4,5] These states are characterized by an alternating valence in an otherwise periodic lattice which can result in unusual thermodynamic properties. The reason is that the difference in valence results in a difference in ionic radii and the extra valence electron thus have a strong coupling to the phonon system. The model designed to capture the effect consists of a localized f state (the extra valence electron) coupled to a continuum of delocalized electrons and a phonon field coupled to the f state. Although, there are orders-of-magnitude differences between typical plasmon and phonon energies, the physics in the models is very similar and only the model parameters differ.

Finally the local polaron model has been applied to the problem of resonant tunneling[6] in the context of electronic transport and the very similar problem of hot-electron femtochemistry at surfaces (HEFatS).[7] The idea of HEFatS is that an adsorbate system on a metal surface can have unoccupied electronic states which obtain a broadening due to interaction with the metallic states. If a hot electron (an electron above the Fermi level) is generated in the metal, it may interact with the unoccupied state and induces a chemical reaction on the surface. As an example we can think of a single molecule on a metal surface with one unoccupied electronic state well above the Fermi level. A hot electron with an energy that matches the unoccupied orbital has the possibility of tunneling from the metal to the molecule resulting in a transient occupation of the orbital. If the molecule was initially in an equilibrium position, the electron will assert a force on the internal molecular degrees of freedom and can excite vibrational modes of the molecule before it tunnels back into the conductor. The molecule may acquire enough energy in this process to undergo a chemical reaction or a desorption event. A clever method to produce hot electrons is based on a metal-insulator-metal (MIM) heterostructure as suggested by Gadzuk.[8] With an ideal MIM device it is possible to tune hot electrons to any desired resonance of an adsorbate system and the approach thereby suggests the highly attractive possibility of performing selective chemistry at surfaces. Such devices have been constructed and characterized[9] and comprise a promising candidate for advanced HEFatS experiments.

Common to all these applications is that a linear bosonic coupling term has been assumed. It is by no means obvious that linear coupling captures the possibly complicated interaction of bosons and electrons although it is probably often a good approximation. To examine the local polaron model beyond linear coupling we calculate the consequences of substituting the linear coupling term with a quadratic coupling term. In principle we should add the quadratic coupling on top of the linear, but this renders the model somewhat tedious to work with and the physics of quadratic coupling becomes hidden in complicated expressions. In contrast, having only quadratic coupling allow us to obtain inelastic scattering amplitudes very similar to those with linear coupling and the comparison is very instructive. In terms of bosonic potentials, a linear coupling term corresponds to a shift in the potential minimum whereas a quadratic coupling term corresponds to a shift in the frequency of the potential.

This paper is organized as follows. In Sec. II we present the local polaron model with a general coupling function and no bosonic dispersion. The electronic part is briefly reviewed and the wide band limit which is imposed in the remainder of

the paper is defined. We then present the well-known spectral function and inelastic scattering probabilities of the model with linear coupling and compare with a quadratically coupled model calculated in the present work. It is shown that for inelastic scattering involving a large number of bosons, quadratic coupling can give rise to much larger scattering probabilities. In Sec. III we apply the theory to hot-electron-mediated excitation of the different modes of CO adsorbed on Cu(100). The model parameters are calculated using density-functional theory and the delta self-consistent field method and we find that linear coupling dominates desorption probabilities for the normal modes along the molecular axis, but vanishes for the frustrated rotations where quadratic coupling has to be taken into account. In Appendix A we derive a path-integral representation of the Newns-Anderson retarded Green's function and show that the special properties of the wide band limit allow us to decouple bosonic and electronic degrees of freedom. Appendixes B and C present the details of the calculations leading to the spectral functions and inelastic scattering probabilities associated with linear and quadratic coupling. In Appendix D, we show how a linear transformation of creation operators makes it possible to obtain the exact Green's functions including both linear and quadratic coupling.

II. MODEL

A. Newns-Anderson model with coupling to bosons

The general model we are concerned with is composed of a Newns-Anderson-type Hamiltonian[10,11] coupled to a dispersionless (single frequency) boson field through a single electronic state. A dispersionless boson field naturally corresponds to a single mode of oscillation in an adsorbate system, whereas we can think of the dispersionless model as describing an Einstein band if the boson field represents a phonon system. Thus it is a model of noninteracting metallic electrons $|k\rangle$, a localized resonant state $|a\rangle$, and a harmonic oscillator described by the coordinate x or equivalently the bosonic creation and annihilation operators $a^\dagger$ and a. The Hamiltonian is given by

$$H = \sum_k \epsilon_k c_k^\dagger c_k + \sum_k (V_{ak} c_a^\dagger c_k + V_{ak}^* c_k^\dagger c_a) + \hbar\omega_0 a^\dagger a + \varepsilon_a(x) c_a^\dagger c_a, \tag{1}$$

where c_a creates an electron in the state $|a\rangle$ and c_k creates an electron in the state $|k\rangle$. The function $\varepsilon_a(x)$ couples the resonant electron to the oscillator degrees of freedom. If one considers a hole coupled to the bosons instead of an electron, the order of c_a and $c_a^\dagger$ should be exchanged. We assume that the metallic electrons do not couple to the oscillator $(V_{ak}(x)=V_{ak})$, since we expect such a dependence to be small in comparison with that of the resonant electron. The Hamiltonian (1) can be viewed as a special case of a Frölich-type Hamiltonian which can be handled by variational methods base on a path-integral approach.[12,13] However, the present model describes a local polaron and as we will show, it can be solved exactly under certain assumptions.

It is natural to Taylor expand the coupling function in the vicinity of the ground-state minimum x_0. Including only the zeroth-order term $\varepsilon_a(x_0)=\varepsilon_0$ results in the Newns-Anderson model. Since it is quadratic in the electronic creation and annihilation operators, one could in principle formally diagonalize it. However, it is much more useful to investigate the resonant state $|a\rangle$ (which is not an eigenstate of the Hamiltonian) and we are thus led to consider the retarded Green's function

$$G_R^0(t) = -i\theta(t)\langle 0|c_a(t)c_a^\dagger(0)|0\rangle, \tag{2}$$

where $|0\rangle$ is an electronic vacuum state and

$$c(t) = e^{iHt/\hbar} c(0) e^{-iHt/\hbar}.$$

It is easily calculated in the energy domain using the Dyson equation and the result is

$$G_R^0(\omega) = \frac{1}{\hbar\omega - \varepsilon_0 - \Sigma(\omega) + i\Gamma(\omega)/2}, \tag{3}$$

with

$$\Gamma(\omega) = 2\pi \sum_k |V_{ak}|^2 \delta(\hbar\omega - \epsilon_k) \tag{4}$$

and

$$\Sigma(\omega) = \int \frac{d\omega'}{2\pi} \frac{\Gamma(\omega)}{\omega - \omega'}. \tag{5}$$

Assuming the hopping matrix elements V_{ak} to be constant, $\Gamma(\omega)$ becomes proportional to the metal density of states. If we furthermore assume the metal density of states to be wider than the resonance energy we can write $\Gamma(\omega)=\Gamma(\varepsilon_0)$ and $\Sigma=0$. This is the wide band limit which will be imposed in the present paper. It allows us to separate electronic and bosonic degrees of freedom in the general case and we can calculate Green's functions corresponding to linear and quadratic coupling exactly.

In the wide band limit the electronic retarded Green's function is

$$G_R^0(t) = -i\theta(t) e^{-(i\varepsilon_0 + \Gamma/2)t/\hbar}, \tag{6}$$

and the spectral function is a Lorentzian with full width at half maximum given by Γ. When boson coupling terms are included [first-order and second-order Taylor expansions of $\varepsilon_a(x)$ in Eq. (1)] the spectral function changes and inelastic scattering on the resonance becomes possible. Note that the inclusion of coupling between the oscillator and metallic electrons would naturally give rise to a position-dependent resonance width $\Gamma(x)$.[14]

Suppose the resonance is initially unoccupied and the oscillator is in the state n. The differential probability that an incoming particle (hole or electron) with energy ε will scatter through the resonance into a state of energy ε' is given by the inelastic scattering matrix which can be expressed in terms of a two-particle Green's function[6] as

$$R(n;\varepsilon',\varepsilon) = \Gamma^2 \int \frac{d\tau ds dt}{2\pi\hbar^3} e^{i(\varepsilon-\varepsilon')\tau/\hbar + i\varepsilon' t/\hbar - i\varepsilon s/\hbar} \times G(n;\tau,s,t), \tag{7}$$

where

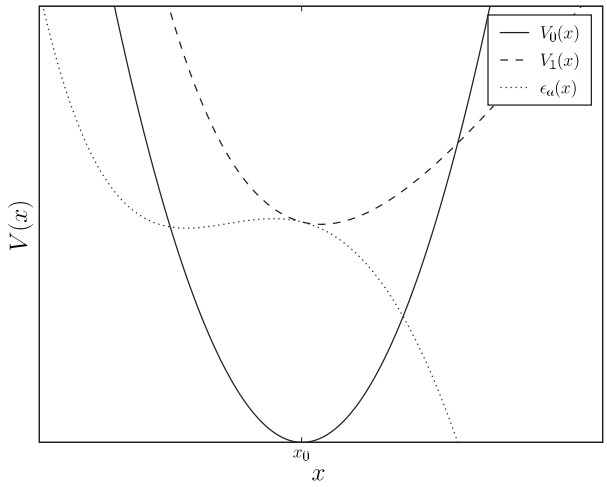

FIG. 1. A general example of adiabatic potentials $V_1(x)$ and $V_0(x)$ and the coupling function $\varepsilon_a(a)=V_1(x)-V_0(x)$. The vertical distance between the two potentials at the ground-state minimum is ε_0.

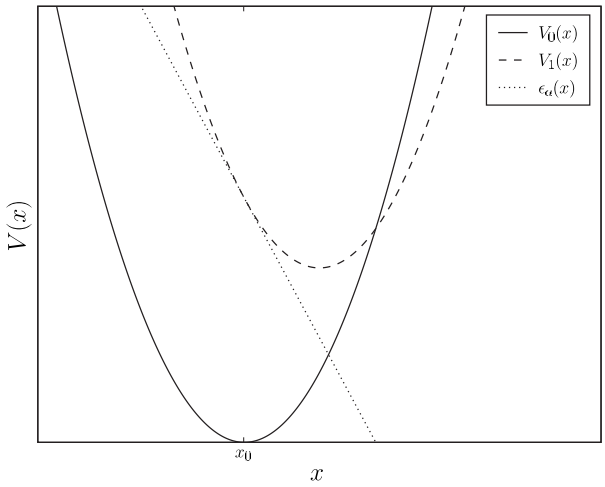

FIG. 2. A shifted excited state corresponds to a linear coupling function $\varepsilon_a(x)\sim x$. The strength of the coupling is proportional to the derivative of the excited state at x_0.

$$G(n;\tau,s,t) = \theta(s)\theta(t)\langle n|c_a(\tau-s)c_a^\dagger(\tau)c_a(t)c_a^\dagger(0)|n\rangle.$$

The probability of transferring a given amount of energy to the bosons can thus be obtained by integrating the inelastic scattering matrix over the relevant values of ε'. In this paper we focus on inelastic scattering by electrons since this is the relevant quantity in the context of HEFatS and EELS. However, the two-particle Green's function also appear in the calculation of optical transition amplitudes of an adsorbed molecule[15] and knowing $G(n;\tau,s,t)$ allows one to calculate a variety of observable quantities.

Finally, we note that the lifetime of the electron is independent of the boson coupling in the wide band limit. The probability that the state $|a\rangle$ is unoccupied and that the oscillator is in any state at time t given that the state was occupied and the oscillator was in the state $|n\rangle$ at $t=0$ is

$$p_a(n;t) = \sum_{m=0}^{\infty} |\langle m,a;t|n,a;0\rangle|^2 = e^{-\Gamma t/\hbar}, \tag{8}$$

which is proved in Appendix A.

B. Coupling function and adiabatic potentials

Consider the state $|x,a\rangle$ with the oscillator at x and an electron occupying the resonance. The expectation value of the Hamiltonian on such a state will depend on the value of x due to the coupling $\varepsilon_a(x)$ and if we could calculate the electronic energy for all values of x we would obtain an excited-state potential $V_1(x)=\langle x,a|H|x,a\rangle$. Doing the same for the state with no electron in the resonance $|x,0\rangle$ would result in a different potential $V_0(x)$ and the coupling function should then be given by $\varepsilon_a(x)=V_1(x)-V_0(x)$ which is illustrated in Fig. 1. In the model (1) we have implicitly assumed that the potential $V_0(x)$ is quadratic but in general it could have any form. The potentials $V_1(x)$ and $V_0(x)$ are called Born-Oppenheimer surfaces and are obtained by moving the oscillator adiabatically in the electronic environment.

C. Linear coupling

We now Taylor expand the coupling function $\varepsilon_a(x)$ to first order and express the boson coordinate in terms of creation and annihilation operators. This gives an interaction term

$$H_I = \lambda_1 c_a^\dagger c_a(a^\dagger + a), \tag{9}$$

with

$$\lambda_1 = \frac{l}{\sqrt{2}}\frac{\partial}{\partial x}V_1|_{x=x_0}, \quad l = \sqrt{\frac{\hbar}{m\omega_0}}, \tag{10}$$

where m and ω_0 are the mass and frequency of the oscillator. This model corresponds to the potentials and coupling function shown in Fig. 2.

As shown in Appendix A, the bosonic degrees of freedom decouple from electronic degrees of freedom in the wide band limit and the retarded Green's function thus becomes a product of an electronic part given by Eq. (6) and a bosonic part. Since the interacting term is linear in the oscillator coordinate the oscillator part of the Hamiltonian can be diagonalized by "completing the square" or equivalently, performing a canonical transformation which shifts the boson coordinate an amount proportional to $c_a^\dagger c_a$,

$$H \to e^{iP}He^{-iP}, \quad P = -i\frac{\lambda_1}{\hbar\omega_0}c_a^\dagger c_a(a^\dagger - a). \tag{11}$$

The retarded Green's function can then be calculated exactly for the nth excited state, giving

$$G_R^{(1)}(n;t) = -i\theta(t)e^{(-i\varepsilon_0-\Gamma/2)t/\hbar}e^{-g_1(1-i\omega_0 t-e^{-i\omega_0 t})} \times L_n[g_1|1-e^{i\omega_0 t}|^2], \tag{12}$$

where L_n is the nth Laguerre polynomial and $g_1 = \lambda_1^2/(\hbar\omega_0)^2$. In this paper g_n denotes a dimensionless effective coupling constant and $G^{(n)}$ denotes the *exact* Green's function corresponding to a coupling term $\varepsilon_a(x)\sim x^n$ and *not* the contribution from an nth-order perturbative calculation as is sometimes custom. The spectral function is given by

$A_n^{(1)}(\omega) = -2\ \mathrm{Im}\ G_R^{(1)}(n;\omega)$ and for the ground state we obtain

$$A_0^{(1)}(\omega) = \Gamma e^{-g_1} \times \sum_{m=0}^{\infty} \frac{g_1^m}{m!} \frac{1}{[\hbar\omega - \varepsilon_0 + (g_1 - m)\hbar\omega_0]^2 + (\Gamma/2)^2}. \tag{13}$$

The spectral function is thus a sum of Lorentzians of width Γ and an internal spacing of ω_0 and the amplitude of the mth peak follows a Poisson distribution. It should be noted that the peaks do not represent excited states of the oscillator. It is the spectral function of the resonant electron with the oscillator in the ground state and the different peaks show that the coupling term mixes the eigenstates of the isolated oscillator. The real part of the self-energy is always negative and given by $-\hbar\omega_0 g_1$, and all physical observables are invariant to $\lambda_1 \rightarrow -\lambda_1$ since linear coupling corresponds to a shifted harmonic oscillator and the direction of the shift is irrelevant.

The two-particle Green's function and inelastic scattering matrix can also be calculated exactly[6,16] and the probability that an incoming electron scatters on the resonance and excites the oscillator from the ground state to the nth-excited state is

$$P_n^{(1)}(\varepsilon) = \Gamma^2 e^{-2g_1} \frac{g_1^n}{n!} |F_n^{(1)}(\varepsilon)|^2, \tag{14}$$

with

$$F_n^{(1)}(\varepsilon) = \sum_{k=0}^{n} (-1)^j \binom{n}{j} \times \sum_{l=0}^{\infty} \frac{g_1^l}{l!} \frac{1}{\varepsilon - \varepsilon_0 + (g_1 - j - l)\hbar\omega_0 + i\Gamma/2}.$$

The probability of exciting the nth vibrational state thus essentially conserves the Poisson distribution but the Lorentzians are replaced by the interference factor $|F_n(\varepsilon)|^2$. The results in Eqs. (13) and (14) can also be obtained using a disentangling theorem[17] as shown in Appendix B.

D. Quadratic coupling

We will now consider a quadratic excited-state potential energy surface $V_1(x)$ which has a minimum that coincides with the ground-state minimum but has a different harmonic evolution. The potentials and coupling function corresponding to this is shown in Fig. 3. Alternatively we could regard this model as a second-order Taylor expansion of the phonon coupling function $\varepsilon_a(x)$ when the first-order contribution vanishes. The interaction term in the Hamiltonian becomes

$$H_I = \lambda_2 c_a^\dagger c_a (a^\dagger + a)^2, \tag{15}$$

with

$$\lambda_2 = \frac{\hbar}{2m\omega_0} \frac{1}{2} \left. \frac{\partial^2 (V_1 - V_0)}{\partial x^2} \right|_{x=x_0}. \tag{16}$$

In this work we will only consider bound excited-state potentials of the form $V_1(x) = m\omega_1^2 (x - x^0)^2/2$ and we can then write

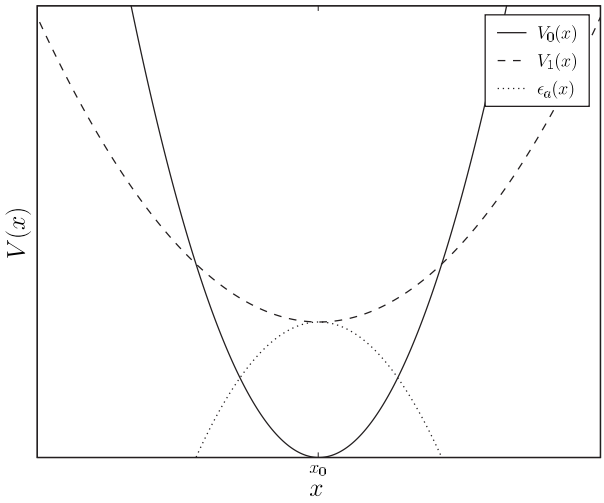

FIG. 3. A frequency shifted excited state gives rise to a quadratic coupling function: $\varepsilon_a(x) \sim x^2$.

$$\lambda_2 = \frac{(\hbar\omega_1)^2 - (\hbar\omega_0)^2}{4\hbar\omega_0}, \quad \omega_1 = \omega_0 \sqrt{1 + 4\lambda_2/\hbar\omega_0}. \tag{17}$$

In the wide band limit the electronic and bosonic degrees of freedom decouple and the boson propagator can be evaluated using a generalization of the Baker-Campbell-Hausdorff formula.[17] As a result the retarded Green's function and spectral function can be calculated exactly. The derivation is shown in Appendix C and gives for the ground state

$$A_0^{(2)}(\omega) = \Gamma \sqrt{1 - g_2} \times \sum_{m=0}^{\infty} \frac{b_m g_2^m}{(\hbar\omega - \varepsilon_0 + \hbar(\omega_0 - \omega_1)/2 - 2m\hbar\omega_1)^2 + (\Gamma/2)^2}, \tag{18}$$

where

$$g_2 = \left(\frac{\omega_0 - \omega_1}{\omega_0 + \omega_1} \right)^2, \quad b_m = \frac{1}{m!} \frac{\partial^m}{\partial x^m} (1 - x)^{-1/2}|_{x=0}.$$

This result is valid for $\omega_1 > 0$ which implies that $g_2 < 1$. Again, the spectral function is a sum of Lorentzians but with the mth peak damped by a factor of $b_m g_2^m$ instead of a Poisson's distribution. The real part of the self-energy is now given by half the frequency shift. The internal spacing between the peaks is $2\omega_1$ and we see that the quadratic coupling only mixes the oscillator ground state with the even excited states of $V_1(x)$. This is due to the mirror symmetry of $\varepsilon_a(x)$ which implies that only oscillator states with equal parity mix. In the quadratic case, the effective dimensionless coupling g_2 is not simply given by $\lambda_2^2/(\hbar\omega_0)^2$ as may have been anticipated, and thus the mth term in Eq. (18) does not correspond to a mth order perturbative calculation of $G_R^{(2)}(t)$ in λ_2. The calculation leading to the exact result (18) is very different from the perturbative approach and we have checked that the second-order Taylor expansion of Eq. (18) indeed gives the result obtained from second-order perturbation theory.

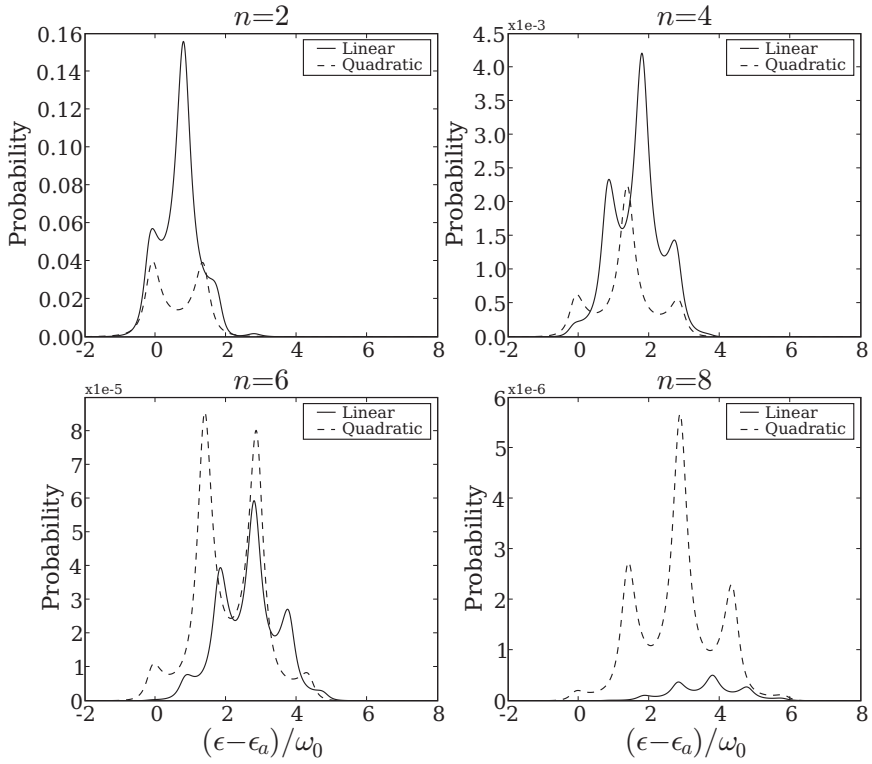

FIG. 4. Probabilities of making the transition $0\rightarrow n$ through resonant inelastic scattering with linear and quadratic coupling. The parameters are $\Gamma/\hbar\omega_0=0.5$, $g_1=0.2$, and $\omega_1=0.75\omega_0$ $(g_2=0.02)$. Even though $g_2<g_1^2$ the quadratic coupling becomes dominating for large n due to the slowly decaying expansion coefficients. One should also note the spacing between peaks which is ω_0 for linear coupling and $2\omega_1$ for quadratic coupling. The centers of the probability distributions are approximately shifted by $n\omega_0/2$ for the linear coupling and $n\omega_1/2$ for the quadratic coupling relative to the bare resonance energy ε_0, since this is where the binomial coefficients in Eqs. (14) and (19) have their maxima.

Although the spectral function (18) shows a series of peaks spaced by $2\omega_1$ it is only possible to excite an integer number of ω_0 through inelastic scattering. The reason is of course that the boson field is completely decoupled from the electronic states in the asymptotics of a scattering event and will thus be observed in a free oscillator eigenstate. Again, the symmetry of the quadratic coupling means that transitions involving an uneven number of bosons are forbidden. The two-particle Green's function and inelastic scattering matrix are calculated in Appendix A and the probability for an incoming hot electron to excite $2n$ quanta of oscillation when initially in the ground state is

$$P_{2n}^{(2)}(\varepsilon)=\Gamma^2(1-g_2)b_n g_2^n|F_n^{(2)}(\varepsilon)|^2 \tag{19}$$

with

$$F_n^{(2)}(\varepsilon)=\sum_{j=0}^{n}(-1)^j\binom{n}{j}\sum_{k=0}^{\infty}\sum_{l=0}^{\infty}\frac{b_l g_2^{k+l}(n+k-1)!}{k!\,(n-1)!}\times\frac{1}{\varepsilon-\varepsilon_0+(\hbar\omega_0-\hbar\omega_1)/2-2(j+k+l)\hbar\omega_1+i\Gamma/2}.$$

The structure is very similar to the case of linear coupling. With linear coupling the probability for an electron to create n bosons is proportional to the nth order Taylor expansion of e^{g_1} and normalized by e^{-2g_1} whereas in the quadratic case the probability to create $2n$ bosons is proportional to the nth order Taylor expansion of $(1-g_2)^{-1/2}$ and normalized by $(1-g_2)$. In the context of EELS and plasmon excitations one would now observe a series of peaks spaced by $2\omega_0$. If the plasma frequency is not known the spacing itself cannot give clues to whether linear or quadratic coupling governs the transitions, but one could use the relative amplitude between peaks since these follow a Poisson distribution if linear coupling dominates and the distribution $b_n g_2^n$ if quadratic coupling dominates. If both linear and quadratic coupling are present one would observe a coupling-dependent enhancement of every second peak.

In a model with linear coupling, the probability of exciting $2n$ vibrational quanta is proportional to g_1^{2n} whereas it is proportional to g_2^n in a quadratic coupled model. This implies that if $g_2>g_1^2$ a quadratic coupling term will give rise to larger inelastic scattering probabilities than a linear term. Even with $g_2<g_1^2$ a quadratic coupling term may have stronger effect for large n since the expansion coefficients of $(1-x)^{-1/2}$ decay slower than those of e^x. This is illustrated in Fig. 4, where the probability of transferring n vibrational quanta to the ground state is shown for linear and quadratic coupling.

III. APPLICATION TO HOT-ELECTRON-MEDIATED DESORPTION

As an example of a system where the dynamics can be approximated by a local polaron model, we consider the problem of hot-electron-mediated energy transfer on a metal surface. Such an energy transfer can lead to desorption of adsorbed molecules[18–25] or induce chemical reactions which cannot proceed by thermal heating.[26] The conceptual picture of the process is the following: hot electrons are generated in the metal by means of an MIM device or a femtosecond laser. The hot electrons may then interact with a chemisorped molecule by tunneling from the metal to an unoccupied molecular state and excite vibrational states in the molecule. If enough energy is transferred to the molecule either by a

single or multiple scattering events, the molecule may eventually desorp or break an internal chemical bond. As a particular example we will calculate transition probabilities for CO adsorbed on Cu(100).

To calculate inelastic scattering probabilities within the local polaron model we need to obtain the coupling function $\varepsilon_a(x)$. As described in Sec. II B, we can fix the molecule at different positions and calculate the potential-energy surfaces $V_1(x)$ and $V_0(x)$ at each point and $\varepsilon_a(x)=V_1(x)-V_0(x)$. Model (1) does not directly contain Coulomb interactions between electrons, but these are included in the calculation of $\varepsilon_a(x)$ which thus becomes an effective coupling that is supposed to contain all the electronic interactions associated with the excited state of the molecule.

The potential energies $V_1(x)$ and $V_0(x)$ have been obtained using the code GPAW[27,28] which is a real-space density-functional theory (DFT) code that uses the projector augmented wave method.[29,30] In all our calculations we used the revised Perdew-Burke-Ernzerhof (RPBE) exchange-correlation functional[31] since this has been designed to perform well for molecules adsorbed on surfaces, and has been shown to perform better than the original PBE functional[32] for adsorbed molecules.

We set up a Cu(100) surface consisting of three atomic layers with the top layer being relaxed. 10 Å of vacuum has then been introduced above the slab and 0.50 monolayer of adsorbate molecules relaxed at top sites which is the preferred adsorption site. Both molecules adsorb with their molecular axis perpendicular to the surface with O pointing away from the surface. We then did a normal mode analysis and mapped out the three ground-state potential-energy functions $V_0(x_i)$ corresponding to the two normal modes that involve the perpendicular degrees of freedom and a frustrated rotation. The perpendicular modes roughly correspond to an internal stretch $d=x_O-x_{C(N)}$ and center of mass $z=(m_O x_O+m_{C(N)}x_{C(N)})/(m_O+m_{C(N)})$. We do not include the three remaining molecular modes since one is another frustrated rotation with identical properties to the one considered, and the two frustrated translations are only weakly coupled to the resonant electron and are not expected to play a significant role in the femtochemistry. In all calculations we use a $p(2\times2)$ cell, sample 12 irreducible k points in the surface plane, and use a grid spacing of 0.2 Å.

To find the excited-state potential energies $V_1(x_i)$ corresponding to the three normal modes of interest, we have used the method of linear expansion ΔSCF which has been published in a previous work[33] and implemented in GPAW. In the previous publication we have tested the method against inverse photoemission spectroscopy, and found that it performed well for molecules chemisorped on surfaces.[33] In each step of the self-consistency cycle an electron is removed from the Fermi level, the density of an excited state is added to the total density and the band energy of this state is added to the total energy. To get the band energy right we need to expand the excited state on the Kohn-Sham orbitals found in each iteration. The method is thus a generalization of the usual ΔSCF where occupation numbers are changed. Instead of changing occupation numbers we occupy an orbital which is not an eigenstate of the Kohn-Sham Hamiltonian, but a superposition of eigenstates in such a way that the state is as close as possible to the original molecular state. In the present case the excited state is the antibonding 2π orbital of CO. In Fig. 5 we show the ground and excited-state potential-energy surfaces corresponding to the frustrated rotation along with $\varepsilon_a(x)$. It is clear that the excited-state potential is not exactly a quadratic potential and the parameter λ_2 which we need to calculate transition probabilities will depend on how we fit this potential to a quadratic form. However the width of the Gaussian ground-state vibrational wave function corresponds to $x=0.08$ Å and for low lying excitations we can thus use this region of the potential which is rather flat. In fact, a closer look at the excited-state potential reveals that the ground-state minimum geometry actually has an unstable extremum in the excited state, but since the curvature is rather small we will simply approximate it by a constant potential. For both perpendicular modes we find that $\varepsilon_a(x_i)\sim x_i$ and quadratic coupling can thus be neglected. In contrast, due to symmetry the excited-state potential energy of frustrated rotation is invariant to $x_i\rightarrow -x_i$ and the linear coupling term thus vanishes. We have calculated the excitation energy to $\varepsilon_a(x_0)=2.8$ eV and the resonance width is estimated from the Kohn-Sham projected density of states to $\Gamma\approx 1.0$ eV. In Table I, we display the calculated parameters corresponding to the three modes.

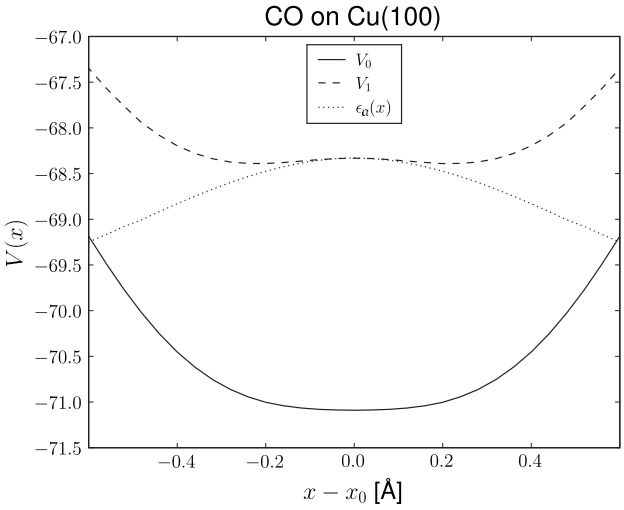

FIG. 5. Potential energy surfaces along the frustrated rotation mode of CO adsorbed on a Cu(100) surface. The coordinate x is a generalized coordinate representing the deviation from equilibrium. $x=0.4$ corresponds to a 24° angular deviation from the perpendicular position.

TABLE I. Parameters for CO adsorbed on Cu(100). All numbers are in eV. Note that while the quadratic coupling for the two perpendicular modes is very small and thus neglectable, the linear coupling of frustrated rotation vanishes exactly due to symmetry.

Mode	$\hbar\omega$	λ_1	λ_2
Frustrated rotation	0.037	0	−0.009
Center of mass	0.043	−0.006	∼0
Internal stretch	0.248	−0.170	∼0

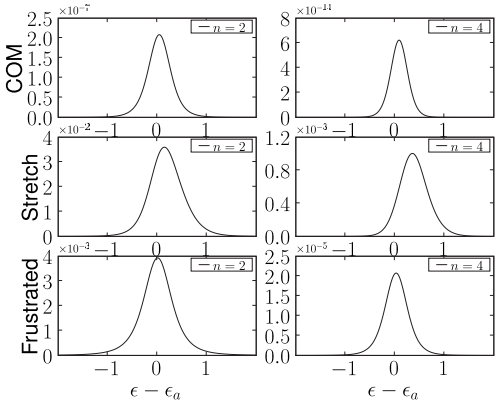

FIG. 6. Probabilities of exciting two and four quanta of vibrations to the center-of-mass, internal stretch and frustrated rotation modes CO adsorbed on Cu(100).

We note that when calculating transition probabilities we should include all modes in model (1), because even if the modes are not coupled directly they have an indirect coupling since they all interact with the resonance. It is possible to obtain expressions for the scattering matrix including more than one mode, but these are rather complicated to handle and for weakly coupled systems the physics can usually be extracted from three one-mode models.[16] In Fig. 6 we show the calculated probabilities for a hot electron to excite the different modes of CO adsorbed on Cu(100). The internal stretch and frustrated rotation show transition probabilities on the same order of magnitude whereas the center-of-mass vibrations are very unlikely to get excited. This is in accord with calculations of the electronic friction coefficients of this system[34,35] which is very closely related to the coupling function $\varepsilon_a(x)$.[14] The frequency of internal vibration is five times larger than both the center-of-mass and frustrated rotation frequencies and as previously shown[16] the stretch mode will completely dominate the total energy transfer. Thus, in a simple model where hot-electron-mediated desorption[22] is reduced to calculating the probability of transferring the chemisorption energy to the adsorbate, the internal mode governs the desorption probability. Nevertheless, our estimate of Γ is based on the Kohn-Sham density of states which may give a poor description of the electronic spectral function $A^0(\omega)$. If Γ is significantly smaller than our estimate, the quadratically coupled frustrated rotation will play an important role in hot-electron-mediated desorption for this system.

IV. SUMMARY AND DISCUSSION

We have calculated the spectral function and inelastic scattering amplitudes in a local polaron model with quadratic coupling to bosons. The probability of exciting n bosons is found to be damped by a distribution function given by the nth Taylor expansion of $1/\sqrt{1-g_2}$ which decays much slower than the Poisson distribution appearing in a linearly coupled model. Hence for comparable values of linear and quadratic coupling constants, a quadratic term will dominate inelastic scattering probabilities involving a large number of bosonic excitations.

As an application we have considered the problem of hot-electron-mediated vibrational excitations of molecules adsorbed on metal surfaces. The coupling constants were calculated from the excitation energy along the molecular normal modes using delta self-consistent field DFT. It was found that quadratic coupling is important for exciting the frustrated rotations since this mode does not couple linearly due to symmetry.

A major approximation in the model is the quadratic assumption for the ground-state potential. In our numerical example with HEFatS it is clear from Fig. 5 that the potentials is not exactly quadratic. For the center-of-mass mode the situation is even worse and a Morse potential is much better suited to describe this mode. The anharmonic deviations are likely to have a significant effect on high lying excited states but renders the model much more complicated. In fact, since the coupling to the internal stretch mode seems to govern the rate of energy transfer,[16] one has to assume that the energy is readily redistributed to other degrees of freedom and anharmonic coupling is thus expected to play a vital role in the actual desorption process.

The wide band limit has been essential in the derivation of scattering amplitudes, and we do not have the means to solve the model (with linear or quadratic coupling) exactly beyond this approximation. The limit is a good approximation for an adsorbate interacting with a metallic s-p band, but tend to fail when the dominating interaction is with a localized band such as the d band of the transition metals. Since, the Kohn-Sham projected density of states of CO on Cu(111) is well approximated with a Lorentzian we believe that the essential physics of that system can be modeled in the wide band limit. However, it would be very interesting to do perturbation theory with the general retarded Green's function (3) to examine the effect of energy dependence in the electronic self-energy.

ACKNOWLEDGMENTS

We are grateful to Karsten Jacobsen for his advice and help with the path-integral representation of the Newns-Anderson model and to Jakob Schiøtz for helpful comments and guidance into the exciting field of Hot-Electron Femtochemistry. The Center for Individual Nanoparticle Functionality (CINF) is sponsored by the Danish National Research Foundation. This work was supported by the Danish Center for Scientific Computing.

APPENDIX A: DECOUPLING OF ELECTRONIC AND BOSONIC DEGREES OF FREEDOM IN THE WIDE BAND LIMIT

1. Path-integral representation of the Newns-Anderson retarded Green's function

The path-integral representation of propagators often give a renewed insight into the underlying physics, although the mathematical complexity can be somewhat larger. By writing the Newns-Anderson retarded Green's function as a sum over paths, we see that each path can be understood as sequence of jumps from the resonance to the metallic band and

we then have to sum over all possible time intervals between each jump. In the wide band limit the time spend in the metal band goes to zero and the electron thus spends all the time of propagation in the resonant state. The Newns-Anderson model is given by Eq. (1) with $\varepsilon_a(x)=\varepsilon_a(x_0)=\varepsilon_0$,

$$H_0 = \epsilon_0 c_a^\dagger c_a + \sum_k \epsilon_k c_k^\dagger c_k + \sum_k (V_{ak} c_a^\dagger c_k + V_{ak}^* c_k^\dagger c_a) \quad \text{(A1)}$$

and

$$G_R^0(t) = -i\theta(t)\langle a|e^{-iHt}|a\rangle. \quad \text{(A2)}$$

The path-integral representation is derived by dividing the time interval t in N intervals of length $\Delta t=t/N$. When N becomes sufficiently large we can take $e^{-iHt}=(e^{-iH\Delta t})^N\approx(1-iH\Delta t)^N$. We then insert $N-1$ complete sets of states $|n\rangle$ such that the Green's function becomes a sum over N-fold products of matrix elements

$$G_R^0(t) \approx -i\theta(t) \sum_{n_1,n_2,\ldots,n_{N-1}} \langle a|1-iH_0\Delta t|n_1\rangle\langle n_1|1 - iH\Delta t|n_2\rangle \cdots \langle n_{N-1}|1-iH_0\Delta t|a\rangle. \quad \text{(A3)}$$

Assuming that $\langle a|k\rangle=0$ the states $|n\rangle$ can either be $|a\rangle$ or $|k\rangle$ and the matrix elements $\langle a|1-iH_0\Delta t|a\rangle=e^{-i\varepsilon_0\Delta t}$, $\langle k_1|1-iH_0\Delta t|k_2\rangle=\delta_{k_1k_2}e^{-i\varepsilon_k\Delta t}$, and $\langle a|1-iH_0\Delta t|k\rangle=-iV_{ak}\Delta t$ represent propagation in the resonance, propagation in the band and, a jump from band to the resonance, respectively. When we take the limit $N\to\infty$, Eq. (A3) becomes formally exact and the jumps between band and resonance become instantaneous. It is then most convenient to order the terms in Eq. (A3) according to the number of jumps. Since the end points of the time interval are at the resonance, a jump into the band has to be accompanied by a jump back into the resonance and each such "band excursion" comes with a factor of $-\Sigma_k|V_{ak}|^2e^{-i\varepsilon_k\tau_i}$, where τ_i is the time spend in the ith excursion into band. It is also clear that p excursions into the resonance have to be accompanied by $p+1$ resonant propagation factors $e^{-i\varepsilon_0\sigma_i}$, where σ_i is the ith time interval in the resonant state. Finally, for a given number of band excursion we have to integrate over all possible bands and resonance time intervals and the retarded Green's function becomes

$$G_R^0(t) = -i\int_0^\infty d\sigma_0 e^{-i\varepsilon_0\sigma_0}\sum_{p=0}^\infty \left(-\int_0^\infty\int_0^\infty d\sigma d\tau \times \sum_k |V_{ak}|^2 \exp -i\varepsilon_k\tau \exp -i\varepsilon_0\sigma\right)^p \times \delta\left(\sigma_0+\sum_j(\sigma_j+\tau_j)-t\right), \quad \text{(A4)}$$

where the delta function has been introduced to ensure that the time intervals sum to t and the theta function has become redundant. We can use the delta function to eliminate the σ_i integration variables and get

$$G_R^0(t) = \int \mathcal{D}\chi e^{iS_0(\chi)} = -ie^{-i\varepsilon_0 t}\int_0^\infty d\sigma_0 \sum_{p=0}^\infty \left[-\int_0^\infty\int_0^\infty d\sigma d\tau \Gamma(\tau)\right]^p \times \delta\left[\sigma_0+\sum_j(\sigma_j+\tau_j)-t\right], \quad \text{(A5)}$$

with

$$\Gamma(t) \equiv \sum_k |V_{ak}|^2 \exp -i(\varepsilon_k-\varepsilon_0)t = \int_{-\infty}^\infty \frac{d\omega}{2\pi}\Gamma(\omega)e^{-i(\omega-\varepsilon_0)t}. \quad \text{(A6)}$$

By using that $\delta(t)=(1/2\pi)\int d\omega e^{i\omega t}$ it is now possible to evaluate Eq. (A5) and recover Eq. (3). In the wide band limit, $\Gamma(t)=\Gamma\delta(t)$, which implies that the electron does not spend any time in the band and the retarded Green's function becomes a sum over paths which are composed of *instantaneous* excursions into the band. We use the notation χ to represent a position in state space and $\int\mathcal{D}\chi e^{iS_0(\chi)}$ as a formal expression representing the sum over all paths weighted by the Newns-Anderson action S_0.

2. Resonant electron in a bosonic environment

We now proceed with full Hamiltonian (1). Introducing the bosonic coordinate x the full retarded Green's function (with the boson field in the state x_0) can be written

$$G_R(x_0;t) = \int \mathcal{D}\chi\mathcal{D}x e^{iS_0(\chi)+iS_B(x)+iS_I(\chi,x)}, \quad \text{(A7)}$$

where $S_0(\chi)$ is the Newns-Anderson action, $S_B(x)$ is the free bosonic action corresponding to the Hamiltonian $H_B=\omega_0 a^\dagger a$, and S_I is the interaction part of the action corresponding to the Hamiltonian $H_I=c_a^\dagger c_a\varepsilon_a(x)$. However, there is a much nicer way to handle the coupling to the boson field. One can think of the bosons as an environment influencing the paths of the resonant electron and it can be shown that the Green's function can be written as[36,37]

$$G_R(x_0;t) = \int \mathcal{D}\chi e^{iS_0(\chi)}\langle x_0|\tilde{U}(\chi;t)|x_0\rangle, \quad \text{(A8)}$$

with the environment time evolution operator

$$\tilde{U}(\chi;t) = e^{iH_Bt}\mathcal{T}e^{-i\int_0^t dt'\tilde{H}_I(\chi(t'))}, \quad \text{(A9)}$$

where $\tilde{H}_I[\chi(t')]=H_B+H_I[\chi(t')]$ is the environment Hamiltonian evaluated on an electronic state fixed at χ and $\mathcal{T}$ denotes time ordering. Thus, the price we pay in separating bosonic and electronic degrees of freedom is an explicit path dependence in the environment part of the propagator. In general it is not possible to evaluate $\tilde{H}_I[\chi(t')]$ on all possible paths but in the wide band limit it is particularly simple. The reason is that the resonant electron stays on the resonance in all possible paths and the environment Hamiltonian is therefore *independent* of the electronic path. In fact, the environment propagator becomes $\tilde{U}(\chi;t)=e^{i\omega a^\dagger at}e^{-i\omega a^\dagger at-i\varepsilon_a(x)t}$ and

the electronic and bosonic degrees of freedom completely decouple in the retarded Green's function

$$G_R(n;t) = G_R^0(t)G_B(n;t), \quad G_B(n;t) = \langle n|e^{i\omega a^\dagger at}e^{-i\omega a^\dagger at - i\varepsilon_a(x)t}|n\rangle. \tag{A10}$$

The situation is very similar for the two-particle Green's function,

$$\begin{aligned} G(n;\tau,s,t) &= \theta(s)\theta(t)\langle n|c_a(\tau-s)c_a^\dagger(\tau)c_a(t)c_a^\dagger(0)|n\rangle \\ &= \theta(s)\theta(t)\langle n|\hat{c}_a(\tau-s)U(\tau-s,\tau)\hat{c}_a^\dagger(\tau)\hat{c}_a(t) \\ &\quad \times U(t,0)\hat{c}_a^\dagger(0)|n\rangle. \end{aligned}$$

The resonant electron is first propagated forward in time from 0 to t and then backward in time from τ to $\tau-s$. The interaction vanishes between the $c^\dagger(\tau)$ and $c(t)$ because the resonant state is unoccupied here. Again, the full Green's function can be written in terms of a bosonic influence propagator and in the wide band limit the electronic and bosonic degrees of freedom decouple so

$$G(n;\tau,s,t) = G_R^0(t)\bar{G}_R^0(s)G_B(n;\tau,s,t) \tag{A11}$$

with

$$G_B(n;\tau,s,t) = \langle n|e^{iH_0(\tau-s)}e^{i[H_0+\varepsilon_a(x)]s}e^{-iH_0\tau}e^{iH_0t}e^{-i[H_0+\varepsilon_a(x)]t}|n\rangle. \tag{A12}$$

This can be seen by applying the arguments above to both of the time evolution operators and the fact that $G^0(\tau,s,t) = G_R^0(t)\bar{G}_R^0(s)$.

We observe that for any coupling function $\varepsilon_a(x)$ the above form of the two-particle Green's function implies that $G(n;t,t,t) = |G_R^0(t)|^2$. This means that in the wide band limit, the resonant lifetime is unaffected by the phonon coupling since the probability of finding the electron in the state $|a\rangle$ at time t (and the oscillator in any state $|m\rangle$) given that it was there at $t=0$ (where the oscillator was in the state $|n\rangle$) is

$$\begin{aligned} p_a(n;t) &= \sum_{m=0}^{\infty} |\langle m,a;t|n,a;0\rangle|^2 \\ &= \sum_{m=0}^{\infty} |\langle m|c_a(t)c_a^\dagger|n\rangle|^2 = \langle n|c_a c_a^\dagger(t)c_a(t)c_a^\dagger|n\rangle \\ &= G(n;t,t,t) = |G_R^0(t)|^2 = e^{-\Gamma t}. \end{aligned} \tag{A13}$$

So, in the wide band limit the resonant state always has a well-defined lifetime given by $T_a = \hbar/\Gamma$

The problem of calculating the inelastic scattering matrix has now been reduced to evaluating the phonon propagator $G_B(n;\tau,s,t)$. In general this is not an easy task, but we will show that in the case of linear and quadratic coupling terms we can use a disentangling theorem[17] to write the exponential operators in a form that allows a direct evaluation of the expectation value. The theorem is a generalization of the Baker-Campbell-Hausdorff theorem and states that if A, B, and C are three operators with a closed commutator algebra then $e^{aA+bB+cC} = he^{\alpha A}e^{\beta B}e^{\gamma C}$, where h, α, β, and γ are known functions of a,b,c, and the commutation parameters.

APPENDIX B: GREEN'S FUNCTIONS WITH LINEAR COUPLING TO BOSONS

1. Single-particle Green's function

Model (1) with linear coupling function given by

$$\varepsilon_a(x) = \lambda_1(a^\dagger + a) \tag{B1}$$

is well known and the one-particle Green's functions can be obtained exactly in the wide band limit by a canonical transformation.[6,15] Here we derive it using the formalism above and the disentangling theorem.[17] To obtain the one-particle Green's function we need to evaluate the boson propagator

$$G_B^{(1)}(n;t) = \langle n|e^{i\omega_0 ta^\dagger a}e^{-i\omega_0 t[a^\dagger a + \lambda_1(a+a^\dagger)/\omega_0]}|n\rangle. \tag{B2}$$

Using the disentangling theorem on the second exponential operator leads directly to the expression

$$\begin{aligned} G_B^{(1)}(n;t) &= e^{in\omega_0 t}e^{-g_1(1-i\omega_0 t - e^{-i\omega_0 t})} \\ &\quad \times \langle n|e^{-\lambda_1/\omega_0(1-e^{-i\omega_0 t})a^\dagger}e^{\lambda_1/\omega_0(1-e^{i\omega_0 t})a}e^{-i\omega_0 ta^\dagger a}|n\rangle \\ &= e^{-g_1(1-i\omega_0 t - e^{-i\omega_0 t})}L_n[g_1|1-e^{i\omega_0 t}|^2], \quad g_1 = \left(\frac{\lambda_1}{\omega_0}\right)^2, \end{aligned} \tag{B3}$$

where $L_n(x)$ is the nth Laguerre polynomial. To obtain ground-state spectral function (13) we Taylor expand $\exp(g_1 e^{i\omega_0 t})$, perform a Fourier transformation, and take the imaginary part.

2. Two-particle Green's function

The procedure can also be used to obtain the two-particle Green's function. The object of interest is now the two-particle boson propagator which we write as

$$\begin{aligned} G_B^{(1)}(n;\tau,s,t) &= \langle n|e^{i\omega_0(\tau-s)a^\dagger a}e^{i\omega_0 s[a^\dagger a + \lambda_1(a+a^\dagger)/\omega_0]}e^{-i\omega_0\tau a^\dagger a}e^{i\omega_0 ta^\dagger a} \\ &\quad \times e^{-i\omega_0 t[a^\dagger a + \lambda_1(a+a^\dagger)/\omega_0]}|n\rangle \\ &= e^{in\omega_0(\tau-t)}e^{-g_1(1-i\omega_0 t - e^{-i\omega_0 t})}e^{-g_1(1+i\omega_0 s - e^{i\omega_0 s})} \\ &\quad \times \langle n|e^{\lambda_1/\omega_0(1-e^{-i\omega_0 s})a^\dagger}e^{-\lambda_1/\omega_0(1-e^{i\omega_0 s})a}e^{i\omega_0(t-\tau)a^\dagger a} \\ &\quad \times e^{-\lambda_1/\omega_0(1-e^{-i\omega_0 t})a^\dagger}e^{\lambda_1/\omega_0(1-e^{i\omega_0 t})a}|n\rangle, \end{aligned} \tag{B4}$$

where we used two different forms of the disentangling theorem to move $e^{i\omega_0 sa^\dagger a}$ and $e^{-i\omega_0 ta^\dagger a}$ to the left and right, respectively. We then use the theorem again to move $e^{i\omega_0(t-\tau)a^\dagger a}$ to the left and obtain

$$\begin{aligned} G_B^{(1)}(n;\tau,s,t) &= e^{-g_1[2-i\omega_0(t-s)-e^{-i\omega_0 t}-e^{i\omega_0 s}]} \\ &\quad \times \langle n|e^{\lambda_1/\omega_0(1-e^{-i\omega_0 s})e^{-i\omega_0(t-\tau)}a^\dagger} \\ &\quad \times e^{-\lambda_1/\omega_0(1-e^{i\omega_0 s})e^{i\omega_0(t-\tau)}a}e^{-\lambda_1/\omega_0(1-e^{-i\omega_0 t})a^\dagger} \\ &\quad \times e^{\lambda_1/\omega_0(1-e^{i\omega_0 t})a}|n\rangle. \end{aligned}$$

Finally, we can use the Baker-Campbell-Hausdorff theorem to collect all lowering operators at the right. The evaluation of the remainder gives a Laguerre polynomial and the result is

$$G_B^{(1)}(n;\tau,s,t) = e^{ig_1\omega_0(t-s)}e^{-g_1 f_{\omega_0}(\tau,s,t)}L_n([g_1(f_{\omega_0}+f_{\omega_0}^*)]\ , \tag{B5}$$

with

$$f_{\omega_0}(\tau,s,t) = 2 - e^{-i\omega_0 t} - e^{i\omega_0 s} + e^{-i\omega_0\tau}(1-e^{i\omega_0 t})(1-e^{i\omega_0 s}). \tag{B6}$$

The inelastic scattering matrix has previously been derived[6,16] and we will not repeat the calculation here.

APPENDIX C: GREEN'S FUNCTIONS WITH QUADRATIC COUPLING TO BOSONS

1. Single-particle Green's function

We now consider a quadratic coupling function of the form

$$\varepsilon_a(x) = \lambda_2(a^\dagger + a)^2. \tag{C1}$$

To obtain the retarded Green's function we would like to calculate the boson propagator

$$\begin{aligned} G_B^{(2)}(n;t) &= \langle n|e^{i\omega_0 t a^\dagger a}e^{-i\omega_0 a^\dagger a t - i\lambda_2(a^\dagger a + aa^\dagger + aa + a^\dagger a^\dagger)t}|n\rangle \\ &= e^{ni\omega_0 t}e^{-i\lambda_2 t}\langle n|e^{-i(\omega_0+2\lambda_2)a^\dagger a t - i\lambda_2(aa+a^\dagger a^\dagger)t}|n\rangle. \end{aligned} \tag{C2}$$

We proceed by disentangling the exponential operator

$$e^{-i(\omega_0+2\lambda_2)a^\dagger a t - \lambda_2(aa+a^\dagger a^\dagger)t} = e^{i\lambda_2 t}e^{i\omega_0/2 t}e^{g/2}e^{fa^\dagger a^\dagger}e^{fe^{-2g}aa}e^{ga^\dagger a}, \tag{C3}$$

where

$$f(t) = \frac{-\lambda_2\tanh(i\omega_1 t)}{\omega_1 + (\omega_0+2\lambda_2)\tanh(i\omega_1 t)},$$

$$g(t) = -\ln\left[\cosh(i\omega_1 t) + \frac{\omega_0+2\lambda_2}{\omega_1}\sinh(i\omega_1 t\ \right], \tag{C4}$$

and $\omega_1 = \omega_0(1+4\lambda_2/\omega_0)^{1/2}$. This is valid for a bound excited-state potential with positive second derivative in which case the argument of the square root is positive. In the case of an unbound excited-state potential, the functions f and g involve real hyperbolic functions and the spectral function acquires a qualitatively different structure. Acting with the operator $e^{\alpha aa}$ on a state $|n\rangle$ gives

$$e^{\alpha aa}|n\rangle = \sum_{l=0}^{[n/2]}\frac{\alpha^l}{l!}\left(\frac{n!}{(n-2l)!}\right)^{1/2}|n-2l\rangle, \tag{C5}$$

where $[n/2]$ means the integer part of $n/2$. Collecting it all and noting that $f(t)e^{-g(t)} = \frac{-\lambda_2}{\omega_1}\sinh(i\omega_1 t)$ gives the retarded Green's function in the wide band limit

$$\begin{aligned} G_R^{(2)}(n;t) = &-i\theta(t)e^{(-i\varepsilon_0-\Gamma/2)t}e^{i(n+1/2)\omega_0 t}(\cosh(i\omega_1 t\ ) \\ &+ \frac{\omega_0+2\lambda_2}{\omega_1}\sinh(i\omega_1 t)^{-n-1/2}\sum_{l=0}^{[n/2]}\frac{h^{2l}}{(l!)^2}\frac{n!}{(n-2l)!} \end{aligned}$$

with

$$h = \frac{\lambda_2}{\omega_1}\sinh(i\omega_1 t) \tag{C6}$$

To find the spectral function of the oscillator ground state we Taylor expand the square root and obtain

$$\begin{aligned} G_R^{(2)}(n=0;t) = &\\ &-i\theta(t)e^{(-i\varepsilon_0-\Gamma/2)t}e^{i\omega_0 t/2}e^{-i\omega_1 t/2}\left(\frac{\omega_1+\omega_0+2\lambda_2}{2\omega_1}\right)^{-1/2} \\ &\times\left(1-\frac{\omega_0-\omega_1+2\lambda_2}{\omega_0+\omega_1+2\lambda_2}e^{-2i\omega_1 t}\right)^{-1/2} \\ =&-i\theta(t)e^{(-i\varepsilon_0-\Gamma/2)t}e^{i\omega_0 t/2}\left(\frac{\omega_1+\omega_0+2\lambda_2}{2\omega_1}\right)^{-1/2} \\ &\times\sum_{m=0}^{\infty}b_m g_2^m\exp -i(2m+1/2)\omega_1 t, \quad \omega_1>0 \end{aligned} \tag{C7}$$

with

$$g_2 = \frac{\omega_0-\omega_1+2\lambda_2}{\omega_0+\omega_1+2\lambda_2} = \left(\frac{\omega_0-\omega_1}{\omega_0+\omega_1}\right)^2,$$

$$b_m = \frac{1}{m!}\frac{\partial^m}{\partial x^m}(1-x)^{-1/2}|_{x=0}. \tag{C8}$$

Fourier transforming and taking the imaginary part then give

$$\begin{aligned} A_0^{(2)}(\omega) = &\Gamma\sqrt{1-g_2} \\ &\times\sum_{m=0}^{\infty}\frac{b_m g_2^m}{[\omega-\varepsilon_0+(\omega_0-\omega_1)/2-2m\omega_1]^2+(\Gamma/2)^2}, \end{aligned}$$

$$\omega_1 > 0, \tag{C9}$$

where we also used that $2\omega_1/(\omega_1+\omega_0+2\lambda_2) = 1-g_2$. Note that the condition of $\omega_1>0$ implies that $g_2<1$.

2. Two-particle Green's function

We now need the propagator

$$\begin{aligned} G_B^{(2)}(n;\tau,s,t) = &\langle n|e^{i\omega_0 a^\dagger a(\tau-s)}e^{i(\omega_0+2\lambda_2)a^\dagger a s + i\lambda_2(aa+a^\dagger a^\dagger)s} \\ &\times e^{-i\omega_0 a^\dagger a\tau}e^{i\omega_0 a^\dagger a t}e^{-i(\omega_0+2\lambda_2)a^\dagger a t - i\lambda_2(aa+a^\dagger a^\dagger)t}|n\rangle \\ = &e^{in\omega_0(\tau-s)}\sum_{m=0}^{\infty}\exp im\omega_0(t-\tau)\langle n| \\ &\times\exp i(\omega_0+2\lambda_2)a^\dagger a s + i\lambda_2(aa+a^\dagger a^\dagger)s|m\rangle \\ &\times\langle m|\exp -i(\omega_0+2\lambda_2)a^\dagger a t \\ &-i\lambda_2(aa+a^\dagger a^\dagger)t|n\rangle. \end{aligned} \tag{C10}$$

We restrict the calculation to the ground-state two-particle Green's function which using disentangled expression (C3) becomes

$$G^{(2)}(n=0;\tau,s,t) = G_R^0(t)\bar{G}_R^0(s)e^{i\omega_0(t-s)/2}e^{g(t)/2+g(-s)/2} \times \sum_{m=0}^{\infty} \exp 2im\omega_0(t-\tau)\frac{f^m(t)f^m(-s)(2m)!}{(m!)^2}. \tag{C11}$$

It is also possible to obtain a closed expression that does not involve the infinite sum, since instead of inserting a complete set in Eq. (C10) we could have brought all lowering operators to the left by repeated use of the disentangling theorem. However, to calculate the inelastic scattering matrix Eq. (7) we need to integrate over τ which is more convenient in the present form. Performing the τ integral and using the resulting delta function to replace $2m\omega_0$ with $\varepsilon-\varepsilon'$ leaves the two remaining integrals as complex conjugates. We note that $b_m=(2m)!/4^m(m!)^2$ and write

$$R^{(2)}(\varepsilon',\varepsilon) = \Gamma^2\sum_{m=1}^{\infty} 4^m b_m \delta(\varepsilon-\varepsilon'-2m\omega_0)|D_m(\varepsilon)|^2, \tag{C12}$$

with

$$D_m = \int_0^{\infty} dt e^{-i(\varepsilon_0-\varepsilon-\omega_0/2-i\Gamma/2)t}\left(\cosh(i\omega_1 t) + \frac{\omega_0+2\lambda_2}{\omega_1}\sinh(i\omega_1 t)\right)^{-1/2} \times\left(\frac{-\lambda_2\tanh(i\omega_1 t)}{\omega_1+(\omega_0+2\lambda_2)\tanh(i\omega_1 t)}\right)^m.$$

The reason we have excluded the $m=0$ term is that it does not give rise to inelastic scattering and the elastic part of the scattering matrix have an additional term that we do not consider here.[6] This expression implies that quadratic coupling can only give rise to inelastic scattering events involving an even number of vibrational quanta. This is also true if the initial state is not the ground state since from Eq. (C10) we see that in general $(m-n)$ has to be even. To evaluate the inelastic scattering matrix we note that

$$\left(\frac{-\lambda_2\tanh(i\omega_1 t)}{\omega_1+(\omega_0+2\lambda_2)\tanh(i\omega_1 t)}\right)^m = \left(\frac{-\lambda_2}{\omega_1+\omega_0+2\lambda_2}\right)^m(1-e^{-2i\omega_1 t})^m\left(\frac{1}{1-g_2e^{-2i\omega_1 t}}\right)^m = \frac{g_2^{m/2}}{2^m}\sum_{j=0}^{m}(-1)^j\binom{m}{j}\exp -2ij\omega_1 t\sum_{k=0}^{\infty}\frac{(m+k-1)!}{k!\,(m-1)!}g_2^k \times\exp -2ik\omega_1 t, \quad \omega_1>0,$$

where we used that $-\lambda_2/(\omega_1+\omega_0+2\lambda_2)=\sqrt{g_2}/2$. The Taylor expansion of the square root gives

$$(\cosh(i\omega_1 t) + \frac{\omega_0+2\lambda_2}{\omega_1}\sinh(i\omega_1 t)^{-1/2} = \sqrt{1-g_2}\sum_{l=0}^{\infty} b_l g_2^l \exp -i(2l+1/2)\omega_1 t, \quad \omega_1>0. \tag{C13}$$

leading to

$$D_m = \frac{i\sqrt{1-g_2}g_2^{m/2}}{2^m}\sum_{j=0}^{m}(-1)^j\binom{m}{j}\sum_{k=0}^{\infty}\sum_{l=0}^{\infty}\frac{b_l g_2^{k+l}(m+k-1)!}{k!\,(m-1)!} \times\frac{1}{\varepsilon-\varepsilon_0+(\omega_0-\omega_1)/2-2(j+k+l)\omega_1+i\Gamma/2}, \tag{C14}$$

and

$$R^{(2)}(\varepsilon',\varepsilon) = \Gamma^2(1-g_2)\sum_{m=1}^{\infty} b_m g_2^m\delta(\varepsilon-\varepsilon'-2m\omega_0) \times\left|\sum_{j=0}^{m}(-1)^j\binom{m}{j}\sum_{k=0}^{\infty}\sum_{l=0}^{\infty}\frac{b_l g_2^{k+l}(m+k-1)!}{k!\,(m-1)!} \times\frac{1}{\varepsilon-\varepsilon_0+(\omega_0-\omega_1)/2-2(j+k+l)\omega_1+i\Gamma/2}\right|^2.$$

APPENDIX D: LINEAR AND QUADRATIC COUPLING COMBINED

It is in principle straightforward to generalize the expressions above to the case of a linear *and* a quadratic coupling term in the Hamiltonian. The linear term can be transformed away by noting that

$$\omega_0 a^\dagger a+\lambda_1(a^\dagger+a)+\lambda_2(a^\dagger+a)^2 = \omega_0\tilde{a}^\dagger\tilde{a}+\lambda_2(\tilde{a}^\dagger+\tilde{a})^2-\gamma\lambda_1, \tag{D1}$$

with

$$\tilde{a}=a+\gamma, \quad \tilde{a}^\dagger=a^\dagger+\gamma, \quad \gamma=\frac{\lambda_1}{\omega_0+4\lambda_2}, \quad [\tilde{a},\tilde{a}^\dagger]=1. \tag{D2}$$

Since the commutator algebra of $\tilde{a}$ and $\tilde{a}^\dagger$ is identical to that of a and $a^\dagger$ we can immediately write down the one-particle boson propagator in its disentangled form

$$G_B^{(1,2)}(n;t) = e^{i\gamma\lambda_1 t}e^{i(n+1/2)\omega_0 t}e^{g/2}\langle n|e^{f\tilde{a}^\dagger\tilde{a}^\dagger}e^{g\tilde{a}^\dagger\tilde{a}}e^{f\tilde{a}\tilde{a}}|n\rangle. \tag{D3}$$

Using that

$$e^{g\tilde{a}^\dagger\tilde{a}} = e^{-\gamma^2(1-e^g)}e^{\gamma(e^g-1)a^\dagger}e^{-\gamma(e^{-g}-1)a}e^{ga^\dagger a}, \tag{D4}$$

we can evaluate the propagator in the ground state and obtain

$$G_B^{(1,2)}(n=0;t) = e^{i\gamma\lambda_1 t}e^{i\omega_0 t/2}e^{g/2}e^{-\gamma^2(1-e^g-2f)}. \tag{D5}$$

The expression clearly reduces to $G_B^{(1)}(t)$ and $G_B^{(2)}(t)$ in the limits $\lambda_1 \to 0$ and $\lambda_2 \to 0$, respectively. It should be straightforward to obtain the spectral function by Fourier transforming this expression after a Taylor expansion of the exponentials. However, the result becomes rather involved and we will not attempt to do the calculation here.

*tolsen@fysik.dtu.dk

[1] D. C. Langreth, Phys. Rev. B **1**, 471 (1970).
[2] M. Cini, Phys. Rev. B **17**, 2486 (1978).
[3] C.-O. Almbladh and P. Minnhagen, Phys. Rev. B **17**, 929 (1978).
[4] A. C. Hewson and D. M. Newns, J. Phys. C **12**, 1665 (1979).
[5] A. C. Hewson and D. M. Newns, J. Phys. C **13**, 4477 (1980).
[6] N. S. Wingreen, K. W. Jacobsen, and J. W. Wilkins, Phys. Rev. B **40**, 11834 (1989).
[7] J. W. Gadzuk, Phys. Rev. B **44**, 13466 (1991).
[8] J. W. Gadzuk, Phys. Rev. Lett. **76**, 4234 (1996).
[9] L. B. Thomsen, G. Nielsen, S. B. Vendelbo, M. Johansson, O. Hansen, and I. Chorkendorff, Phys. Rev. B **76**, 155315 (2007).
[10] P. W. Anderson, Phys. Rev. **124**, 41 (1961).
[11] D. M. Newns, Phys. Rev. **178**, 1123 (1969).
[12] R. P. Feynman, Phys. Rev. **97**, 660 (1955).
[13] V. Sa-yakanit, V. D. Lakhno, and K. Hass, Phys. Rev. B **57**, 5772 (1998).
[14] M. Brandbyge, P. Hedegård, T. F. Heinz, J. A. Misewich, and D. M. Newns, Phys. Rev. B **52**, 6042 (1995).
[15] G. D. Mahan, *Many-Particle Physics* (Plenum, New York, 1981).
[16] T. Olsen, J. Gavnholt, and J. Schiøtz, Phys. Rev. B **79**, 035403 (2009).
[17] H. Mitter and K. Yamazaki, Lett. Math. Phys. **8**, 321 (1984).
[18] J. A. Prybyla, T. F. Heinz, J. A. Misewich, M. M. T. Loy, and J. H. Glownia, Phys. Rev. Lett. **64**, 1537 (1990).
[19] J. A. Prybyla, H. W. K. Tom, and G. D. Aumiller, Phys. Rev. Lett. **68**, 503 (1992).
[20] F. Budde, T. F. Heinz, M. M. T. Loy, J. A. Misewich, F. de Rougemont, and H. Zacharias, Phys. Rev. Lett. **66**, 3024 (1991).
[21] J. A. Misewich, A. Kalamarides, T. F. Heinz, U. Höfer, and D. M. Newns, J. Chem. Phys. **100**, 736 (1994).
[22] L. M. Struck, L. J. Richter, S. A. Buntin, R. R. Cavanagh, and J. C. Stephenson, Phys. Rev. Lett. **77**, 4576 (1996).
[23] P. T. Howe and H. L. Dai, Surf. Sci. **451**, 12 (2000).
[24] L. Cai, X. Xiao, and M. M. T. Loy, Surf. Sci. Lett. **464**, L727 (2000).
[25] F. Fournier, W. Zheng, S. Carrez, H. Dubost, and B. Bourguignon, Phys. Rev. Lett. **92**, 216102 (2004).
[26] M. Bonn, C. Hess, S. Funk, J. H. Miners, B. N. J. Persson, M. Wolf, and G. Ertl, Phys. Rev. Lett. **84**, 4653 (2000).
[27] The GPAW code is available as a part of the CAMPOS software (www.camd.dtu.dk/Software).
[28] J. J. Mortensen, L. B. Hansen, and K. W. Jacobsen, Phys. Rev. B **71**, 035109 (2005).
[29] P. E. Blöchl, Phys. Rev. B **50**, 17953 (1994).
[30] P. E. Blöchl, C. J. Först, and J. Schimpl, Bull. Mater. Sci. **26**, 33 (2003).
[31] B. Hammer, L. B. Hansen, and J. K. Nørskov, Phys. Rev. B **59**, 7413 (1999).
[32] J. P. Perdew, K. Burke, and M. Ernzerhof, Phys. Rev. Lett. **77**, 3865 (1996).
[33] J. Gavnholt, T. Olsen, M. Engelund, and J. Schiøtz, Phys. Rev. B **78**, 075441 (2008).
[34] M. Head-Gordon and J. C. Tully, Phys. Rev. B **46**, 1853 (1992).
[35] J. C. Tully, M. Gomez, and M. Head-Gordon, J. Vac. Sci. Technol. A **11**, 1914 (1993).
[36] P. Hedegård, Phys. Rev. B **35**, 533 (1987).
[37] P. Hedegård, Phys. Rev. B **35**, 6127 (1987).

Paper V

T. Olsen and J. Schiøtz
Origin of Power Laws for Reactions at Metal Surfaces Mediated by Hot Electrons
Phys. Rev. Lett. **103**, 238301 (2009).

Origin of Power Laws for Reactions at Metal Surfaces Mediated by Hot Electrons

Thomas Olsen and Jakob Schiøtz*

Danish National Research Foundation's Center of Individual Nanoparticle Functionality (CINF), Department of Physics, Technical University of Denmark, DK-2800 Kongens Lyngby, Denmark

(Received 4 June 2009; published 30 November 2009)

A wide range of experiments have established that certain chemical reactions at metal surfaces can be driven by multiple hot-electron-mediated excitations of adsorbates. A high transient density of hot electrons is obtained by means of femtosecond laser pulses and a characteristic feature of such experiments is the emergence of a power law dependence of the reaction yield on the laser fluence $Y \sim F^n$. We propose a model of multiple inelastic scattering by hot electrons which reproduces this power law and the observed exponents of several experiments. All parameters are calculated within density functional theory and the delta self-consistent field method. With a simplifying assumption, the power law becomes exact and we obtain a simple physical interpretation of the exponent n, which represents the number of adsorbate vibrational states participating in the reaction.

DOI: 10.1103/PhysRevLett.103.238301 PACS numbers: 82.53.St, 34.35.+a

Hot-electron-induced femtochemistry at surfaces (HEFatS) is a class of chemical reactions, where the energy to overcome the reaction barrier is provided by energetic (''hot'') electrons. These electrons are often photoelectrons emitted from the surface when struck by intense laser pulses, but other hot-electron sources are possible, such as scanning tunneling microscope tips and metal-insulator-metal nanodevices [1]. For these reactions, the reaction rate usually scales as a power law with the electron flux. For example, in a pioneering study of NO on Pd(111) [2], it was shown that femtosecond laser pulses could induce desorption of NO, and a mechanism by multiple electronic excitations was identified [3]. The yield depended on the fluence as $Y \propto F^n$ with $n \sim 3.3$. Subsequently, desorption induced by femtosecond lasers has been demonstrated for several other adsorbate systems [4–7] showing nonlinear yields, which can be fitted to power laws with exponents $3 < n < 8$. It has also been shown that femtosecond laser pulses can induce surface hopping [8] and oxidation reactions [9–11], all of which can be characterized by power laws.

A popular theoretical approach to the interaction of adsorbates with a high density of hot electrons is the electronic friction model [12] where the excited electrons are assumed to equilibrate rapidly to a thermal distribution with electronic temperature T_e. For sufficiently large time scales the propagation of the adsorbate is well approximated by semiclassical Langevin dynamics with an electronic friction η_e depending on T_e as well as the adsorbate coordinates. While the friction model has certainly been successful in reproducing various experimental observations, it cannot account for the physical origin of the power law exponent n. Furthermore, measurements on the distribution of hot electrons in gold excited by subpicosecond laser pulses implies thermalization times up to 1 ps [13], which is on the order of reaction times, and there are examples of laser induced surface chemistry where the assumption of a thermal distribution of hot electrons is in direct conflict with observations [5,11,14].

In this Letter we introduce a general model for first-principles calculations of the rates of HEFatS processes, regardless of the source of hot electrons. The central object of the model is a nonadiabatic Hamiltonian, which is used to calculate the hot-electron-induced vibrational transition probabilities of adsorbates. All parameters in the Hamiltonian are obtained from density-functional theory (DFT) and we show that the model reproduces experimentally observed power laws. Finally, we will make a simple approximation for the transition probabilities and show that the power law then becomes exact in the limit of large electron flux and that the exponent is given by $n = E_R/\hbar\omega$ where E_R is the energy barrier of the reaction and $\hbar\omega$ is the energy quantum of the vibrational mode dominating the energy transfer.

To analyze HEFatS rates involving multiple hot electrons, we consider a quadratic potential energy surface of an adsorbate with vibrational states $|n\rangle$ coupled to a localized electronic resonance $|a\rangle$. The probability for a hot electron with energy ε to inelastically scatter on the localized state and induce a vibrational transition $m \rightarrow n$ is denoted $P_{mn}(\varepsilon)$ and we assume a constant flux J_0 of hot electrons incident on the adsorbate. It is further assumed that each vibrational quantum has a fixed lifetime T_{vib} and that there exists a maximum quantum number n_R such that a reaction will proceed immediately if $n \geq n_R$. The probability that one vibrational quantum survives the time interval $\Delta t = 1/J_0$ between subsequent scattering events is then $e^{-\Delta t/T_{\text{vib}}}$. Each incoming electron will thus change the distribution of adsorbate vibrational states $Q(n)$ until an equilibrium is reached between decay and reexcitation.

If the adsorbate is initially in the ground state, the distribution of vibrational states induced by the first elec-

tron with energy ε_1 is

$$Q_1(n;\varepsilon_1) = P_{0n}(\varepsilon_1). \quad (1)$$

The probability of the adsorbate being in the nth vibrational state after the second electron has scattered is

$$Q_2(n;\varepsilon_1,\varepsilon_2) = \sum_{m=0}^{n_R-1} p_1(m;\varepsilon_1)P_{mn}(\varepsilon_2), \quad (2)$$

where $p_1(m)$ is the probability that the adsorbate is in the state m after the time interval Δt given by

$$p_1(m;\varepsilon_1) = \sum_{l=m}^{n_R-1} Q_1(l;\varepsilon_1)\binom{l}{m}(e^{-\Delta t/T_{\mathrm{vib}}})^m \times (1-e^{-\Delta t/T_{\mathrm{vib}}})^{l-m}. \quad (3)$$

We exclude terms with $m \geq n_R$ since such excitations would have led to a reaction by assumption. Proceeding like this, the probability $Q_3(n;\varepsilon_1,\varepsilon_2,\varepsilon_3)$ of being in the nth excited state after the third scattering event can be expressed in terms of $Q_2(n;\varepsilon_1,\varepsilon_2)$ and so forth. Since all vibrational states $n \geq n_R$ lead to a reaction, the reaction probability of the kth electron is

$$P_k^R = \sum_{n=n_R}^{\infty} Q_k(n). \quad (4)$$

For large k this will approach a limiting value, P_R.

To calculate the vibrational transition matrix $P_{mn}(\varepsilon)$ we consider a Newns-Anderson–type Hamiltonian with substrate states $|k\rangle$ and a resonant state $|a\rangle$ linearly coupled to a number of vibrational modes with creation operators for vibrational quanta $b_i^\dagger$ [15,16]:

$$H = \varepsilon_0 c_a^\dagger c_a + \sum_k \epsilon_k c_k^\dagger c_k + \sum_k (V_{ak} c_a^\dagger c_k + V_{ak}^* c_k^\dagger c_a) + \sum_i \hbar\omega_i\left(b_i^\dagger b_i + \frac{1}{2}\right) + \sum_i \lambda_i c_a^\dagger c_a (b_i^\dagger + b_i). \quad (5)$$

The model essentially describes a harmonic oscillator, which is displaced when the state $|a\rangle$ is occupied and the coupling V_{ak} to the metallic states introduces a finite lifetime of $|a\rangle$. As previously published [17], the transition probabilities $P_{mn}(\varepsilon)$ can be calculated exactly in the wide-band limit where the density of states projected on the localized state $|a\rangle$ is a Lorentzian centered at ε_0 with full width at half maximum given by $\Gamma = 2\pi\sum_k |V_{ak}|^2 \delta(\varepsilon_0 - \epsilon_k)$. The probabilities $P_{mn}(\varepsilon)$ depend on the dimensionless parameters, $\hbar\omega_i/\Gamma$ and $g_i = (\lambda_i/\hbar\omega)^2$, and the reaction probability P^R also depends on these parameters in addition to the reaction quantum number $n_R \sim E_R/\hbar\omega$. The quantities E_R and ω can be calculated within standard density-functional theory and Γ is estimated from the projected density of states. The resonance energies as well as the nonadiabatic coupling parameters λ_i are obtained from excited state potential energy surfaces which are calculated with the method of linear expansion delta self-consistent field (ΔSCF). The method is a generalization of standard delta self-consistent field designed to handle molecular orbitals hybridized with metallic states and calculates the expectation values of excited states which are not eigenstates of the Hamiltonian but involve an occupied resonance. Details on the method and comparison with experiment can be found in Refs. [17,18].

As an example we calculate the fluence dependent transfer of energy from hot electrons to a CO molecule adsorbed on Cu(111), mediated by excitation of an unoccupied π^* orbital. CO adsorbs with the molecular axis perpendicular to the surface and the symmetry of the adsorbed molecule thus only allows a linear coupling to the center of mass (c.m.) and internal stretch vibrations of CO. The parameters for CO chemisorbed at a Cu(111) bridge site were calculated with the code GPAW [19,20], which is a real-space density-functional theory code using the projector augmented wave method [21]. We modeled the surface by a three layer (4×4) supercell with the top layer relaxed, a grid spacing of 0.2 Å, and a 4×4 surface K-point sampling. With the revised Perdew-Burke-Ernzerhof [22] functional, we find $\varepsilon_0 = 2.4$ eV, $\hbar\omega = 231$ meV, and $\lambda = -118$ meV for the internal stretch vibration, and $\hbar\omega = 42$ meV and $\lambda = -4$ meV for the c.m. vibration. The internal mode completely dominates the transfer of energy from hot electrons to the molecule since it has a much larger coupling λ, and the quantum of energy is 5 times larger than for the c.m. mode. Figure 1 shows the density of an excited top site molecule obtained with ΔSCF DFT relative to the ground state density and one clearly sees the excited π^* orbital. In Fig. 2 we have used (1)–(5) with hot electrons at $\varepsilon = 2.0$ eV corresponding to the laser frequency used in [4] to calculate reaction rates, which require energies corresponding to 3, 4, 5, and 6 internal vibrational excitations. In the nonlinear regime corresponding to reactions induced by multiple scattering

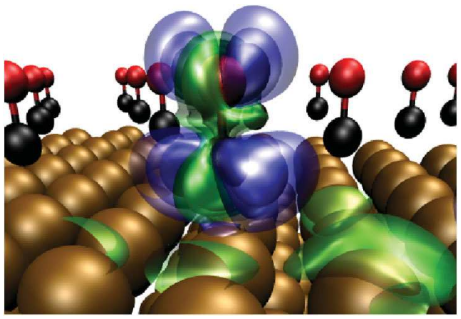

FIG. 1 (color). The difference between excited and ground state densities for CO adsorbed on Cu(111). Black balls are carbon atoms and red balls are oxygen atoms. Blue contours is excess density in excited state and green contours is excess density in ground state. The excited state is constructed by occupying a π^* orbital of CO. For clarity we only show the density difference in a single supercell.

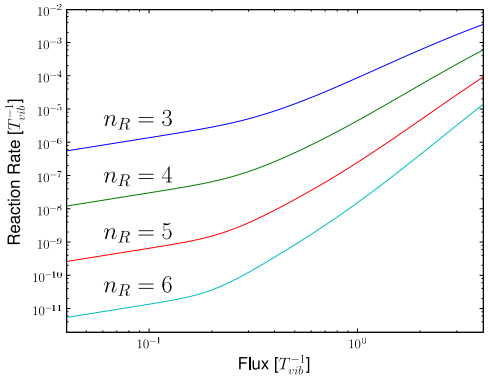

FIG. 2 (color online). The reaction yield of CO on Cu(111) as a function of hot-electron flux for four reaction energies. Note the initial linear dependence corresponding to single electron reactions.

events, the rates are very well approximated by power laws with $n = 2.8$, $n = 3.6$, $n = 4.3$, and $n = 5.1$. Varying the parameters in the model reveals that, in general, one always obtains very good power law fits with exponents $n \sim n_R$. Increasing the energy of the hot electrons above the resonant energy ε_0 tends to decrease n.

Table I shows the calculated power law exponents for five systems compared with corresponding experiments. The DFT parameters used were the same as for CO on Cu(111). We have assumed that a reaction occurs when an energy of 0.2 eV in excess of the reaction barrier has been transferred, which is consistent with measurements of the kinetic and internal energy distributions of desorbed molecules [7], and we have used hot-electron energies $\varepsilon = \varepsilon_f + \hbar\Omega$ where Ω is the laser frequency. The agreement is very good except for CO on Cu(100). This could be due to the role of frustrated rotations, which has previously been found to couple strongly to metallic electrons in this particular system [23]. In general, however, the frustrated rotations have a low energy compared with the internal stretch mode and we expect their effect to be neglectable. Because of symmetry the frustrated rotations cannot couple linearly to the resonant electron and one would need a quadratic term like $\lambda_2 c_a c_a^\dagger (b + b^\dagger)^2$ in (5) to include these in the model [24].

TABLE I. Power law exponents obtained from (1)–(5). The systems involving NO, CO, and O_2 are desorption experiments whereas O/Pt(111) is hot-electron-induced diffusion of atomic oxygen from a step to a terrace hollow site. For O_2/Pt(111), the exponent depends on the laser frequency.

System	Experimental n	Calculated n	E_R
NO/Pd(111) [2]	3.3	3.7	1.0 eV
CO/Cu(111) [4]	3.7	3.6	0.4 eV
CO/Cu(100) [7]	8.0 ± 1	3.7	0.5 eV
O_2/Pt(111) [5]	3.0/5.6	2.5/5.5	0.4 eV
O/Pt(111) [8]	15	12	0.8 eV

A particularly interesting case is the hot-electron-induced desorption of O_2 from Pt(111) where a power law with exponent $n \sim 5.6 \pm 0.7$ was observed using a photon energy of 2.0 eV and an exponent of $n \sim 3.0 \pm 0.5$ using a photon energy of 4.0 eV [5]. The fact that the power law exponent depends on the photon energy contradicts the picture of a thermalized hot-electron gas interacting with the molecule, which is the basic assumption in models based on electronic friction. In contrast, the model (1)–(5) naturally gives rise to a decrease in the power law exponent when the energy of hot electrons is increased.

The transition matrix $P_{mn}(\varepsilon)$ has a very complicated structure and it is hard to extract the physics of the power law using these probabilities and (1)–(4). However, the magnitude of $P_{mn}(\varepsilon)$ is largely governed by the prefactor $g^{n-m}/(n-m)!$ [17] and in the following we will examine the consequences of assuming transition probabilities of the form

$$P_{mn} = e^{-\alpha} \frac{\alpha^{n-m}}{(n-m)!}, \qquad n \geq m, \tag{6}$$

where α is a dimensionless coupling constant, which describes the coupling of hot electrons to the adsorbate vibrational states. Repeated use of the algorithm (1)–(4) with these probabilities then reveals that to leading order in α one has

$$Q_k(n) = \frac{\alpha^n}{n!} \left(\sum_{j=0}^{k-1} e^{-j\Delta t/T_{\mathrm{vib}}} \right)^n. \tag{7}$$

We then consider a large flux $e^{-\Delta t/T_{\mathrm{vib}}} \sim 1 - \Delta t/T_{\mathrm{vib}}$, sum up the geometric series, take the limit $k \to \infty$ corresponding to steady state, and get

$$Q(n) = \frac{\alpha^n}{n!} (T_{\mathrm{vib}} J_0)^n, \tag{8}$$

where $\Delta t = 1/J_0$. Thus, for small α the reaction probability (4) will be dominated by such a term with $n = n_R$.

The power law emerges from summing up the detailed combinatorics of all possible ways of rising through the vibrational states in the potential well. In Fig. 3(a) we show the reaction yields for three values of n_R and they are seen to approach power laws of the form $Y \propto J_0^{n_R}$ for large fluxes. Even if α is not small, Eqs. (1)–(4) tend to conserve the power law although the exponent becomes reduced from the value of n_R when terms beyond leading order are not vanishing. In Fig. 3(b) we show the yield when $n_R = 15$ for $\alpha = 0.2$, $\alpha = 0.5$, and $\alpha = 1.0$. At large fluxes the yields are well approximated by power laws with exponents 14, 12, and 10, respectively. One might worry that the fixed time interval Δt between scattering events is too crude an approximation for the random nature of hot electrons interacting with the adsorbate. However, a sequence of time intervals $\{t_k\}$ with an average of Δt would

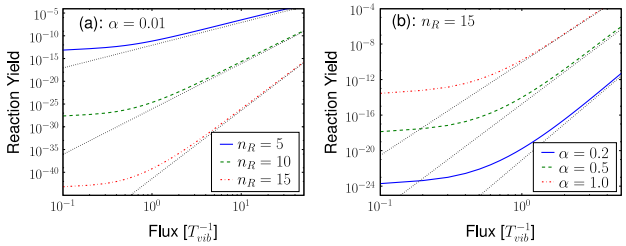

FIG. 3 (color online). The yield as a function of electron flux obtained using the transition probabilities in Eq. (6) for different parameters (see text).

lead to the replacement $j\Delta t \rightarrow \sum_{i=1}^{j} t_{k-i}$ in (7), which is well approximated by $j\Delta t$ for large j. We have repeated the calculations leading to Fig. 3 but with the time intervals randomly drawn from an exponential distribution $p(t) \sim e^{-t/\Delta t}$ and the power law is conserved on average.

The interpretation of the power law exponent as the number of contributing vibrational states can be used to identify the reaction channel of a given adsorbate system. For example, in the study of hot-electron-mediated desorption of NO from Pd(111) [2] a power law with exponent $n \simeq 3.3$ was found. The internal stretch vibration corresponds to an energy of $\hbar\omega \simeq 210$ meV whereas the other modes have vibrational energies $\hbar\omega \leq 70$ meV. Since the adsorption energy is $E_a \simeq 1.0$ eV we conclude that the power law exponent $n_R \sim E_a/\hbar\omega$ has to arise from sequential excitation of the internal stretch vibration and subsequent anharmonic energy transfer to the desorption coordinate. In contrast, the study of hot-electron-induced surface diffusion of atomic oxygen on Pt(111) [8] gave rise to a power law with exponent $n \simeq 15$, which fit very well with an experimental diffusion barrier of $E_d \simeq 0.8$ eV and vibrational modes on the order $\hbar\omega \sim 50$ meV.

In summary, we have presented a theory of multiple inelastic scattering with transition probabilities calculated in a nonadiabatic Newns-Anderson model, which lead to the ubiquitous power law of HEFatS and reproduce experimentally found exponents. The interpretation of the exponents as the number of contributing vibrational states is a very useful tool to identify the reaction channel of a given system and also indicates that a classical treatment of the adsorbate motion is insufficient. However, the model can only treat quadratic potentials and is thus not able to treat the anharmonic effects, which are expected to play an important role in the transfer of internal vibrational energy to the reaction coordinate. In the case of molecular desorption the model applies because the internal stretch mode, which is well approximated by a harmonic potential, dominates the energy transfer. Furthermore, while our assumption of constant hot-electron energy $\varepsilon = \varepsilon_f + \hbar\Omega$ gives the right dependence of the exponents on Ω, the hot electrons proceeding a laser pulse will undergo scattering and produce some distribution of electron energies. The true (time-dependent) distribution lies somewhere between the present assumption and a thermalized hot-electron gas and the model should thus be regarded as complementary to a statistical approach based on electronic friction and Langevin dynamics, which assumes a thermalized hot-electron gas.

This work was supported by the Danish Center for Scientific Computing. The Center for Individual Nanoparticle Functionality (CINF) is sponsored by the Danish National Research Foundation.

*schiotz@fysik.dtu.dk

[1] J. W. Gadzuk, Phys. Rev. Lett. **76**, 4234 (1996).
[2] J. A. Prybyla *et al.*, Phys. Rev. Lett. **64**, 1537 (1990).
[3] F. Budde *et al.*, Phys. Rev. Lett. **66**, 3024 (1991).
[4] J. A. Prybyla, H. W. K. Tom, and G. D. Aumiller, Phys. Rev. Lett. **68**, 503 (1992).
[5] F.-J. Kao, D. G. Busch, D. Cohen, D. Gomes da Costa, and W. Ho, Phys. Rev. Lett. **71**, 2094 (1993).
[6] W. Ho, Surf. Sci. **363**, 166 (1996).
[7] L. M. Struck *et al.*, Phys. Rev. Lett. **77**, 4576 (1996).
[8] K. Stépán, J. Güdde, and U. Höfer, Phys. Rev. Lett. **94**, 236103 (2005).
[9] M. Bonn, C. Hess, and M. Wolf, Science **285**, 1042 (1999).
[10] F.-J. Kao, D. G. Busch, D. Gomes da Costa, and W. Ho, Phys. Rev. Lett. **70**, 4098 (1993).
[11] S. Deliwala *et al.*, Chem. Phys. Lett. **242**, 617 (1995).
[12] M. Brandbyge *et al.*, Phys. Rev. B **52**, 6042 (1995).
[13] W. S. Fann *et al.*, Phys. Rev. Lett. **68**, 2834 (1992).
[14] D. G. Busch and W. Ho, Phys. Rev. Lett. **77**, 1338 (1996).
[15] N. S. Wingreen, K. W. Jacobsen, and J. W. Wilkins, Phys. Rev. B **40**, 11834 (1989).
[16] J. W. Gadzuk, Phys. Rev. B **44**, 13466 (1991).
[17] T. Olsen, J. Gavnholt, and J. Schiøtz, Phys. Rev. B **79**, 035403 (2009).
[18] J. Gavnholt, T. Olsen, M. Engelund, and J. Schiøtz, Phys. Rev. B **78**, 075441 (2008).
[19] The GPAW code is available as a part of the CAMPOS software, www.camd.dtu.dk/Software.
[20] J. J. Mortensen, L. B. Hansen, and K. W. Jacobsen, Phys. Rev. B **71**, 035109 (2005).
[21] P. E. Blöchl, Phys. Rev. B **50**, 17 953 (1994).
[22] B. Hammer, L. B. Hansen, and J. K. Nørskov, Phys. Rev. B **59**, 7413 (1999).
[23] J. C. Tully, M. Gomez, and M. Head-Gordon, J. Vac. Sci. Technol. A **11**, 1914 (1993).
[24] T. Olsen, Phys. Rev. B **79**, 235414 (2009).

Paper VI

T. Olsen and J. Schiøtz
Vibrationally mediated control of single-electron transmission in weakly coupled molecule-metal junctions
Phys. Rev. B **81**, 115443 (2010).'

Vibrationally mediated control of single-electron transmission in weakly coupled molecule-metal junctions

Thomas Olsen* and Jakob Schiøtz

Danish National Research Foundation's Center for Individual Nanoparticle Functionality (CINF), Department of Physics, Technical University of Denmark, DK-2800 Kongens Lyngby, Denmark

(Received 4 January 2010; revised manuscript received 4 March 2010; published 23 March 2010)

We propose a mechanism which allows one to control the transmission of single electrons through a molecular junction. The principle utilizes the emergence of transmission sidebands when molecular vibrational modes are coupled to the electronic state mediating the transmission. We will show that if a molecule-metal junction is biased just below a molecular resonance, one may induce the transmission of a single electron by externally exciting a vibrational mode of the molecule. The analysis is quite general but requires that the molecular orbital does not hybridize strongly with the metallic states. As an example we perform a density-functional theory analysis of a benzene molecule between two Au(111) contacts and show that exciting a particular vibrational mode can give rise to transmission of a single electron.

DOI: 10.1103/PhysRevB.81.115443 PACS number(s): 82.53.St, 34.35.+a, 73.23.Hk

Several experiments have established that vibrational excitations can have a significant effect on the *I-V* characteristics of single-molecule junctions.[1–5] In particular, the emergence of peaks in the differential conductance corresponding to vibrational frequencies, shows that tunneling electrons interact with certain vibrational states of the molecule, possibly providing a means for controlling the transmission of electrons. A considerable amount of theoretical work has been dedicated to elucidate the effect of phonons on electronic transport in mesoscopic systems. Analysis of model Hamiltonians[6–9] have given qualitative insight into the interaction of tunneling electrons with molecular vibrations while DFT-based studies in conjunction with a nonequilibrium Green's-function approach show quantitative agreement with experiments.[10–12] Most efforts so far have been directed toward the influence of vibrations on transmission functions and *I-V* characteristics. In the present paper, we will take a slightly different point of view and partition the electronic transmission function into pieces that involve different vibrational excitations. We then show that the molecular junction may be put in a configuration where the vibrationally excited molecule allows the transmission of a single electron while transmission is forbidden in the vibrational ground state. Controlling the vibrational state of the molecule, e.g., by means of a laser, then implies control of single-electron transmission.

The system under consideration is a molecule sandwiched between two metallic leads. We assume that there is a single unoccupied molecular state which obtains a finite lifetime due to hybridization with metallic states. This state will be referred to as the resonance and its position may be tuned by applying a gate voltage. If a bias voltage is applied to the contacts and the resonance is positioned in the bias window, electrons may tunnel through the resonance into the downstream contact and one will observe a current. If the molecule is weakly interacting with the metal such that the resonance is well localized in energy, one can apply a gate voltage which situates the resonance above the upstream chemical potential and no current will be observed. However, if the resonance couples to molecular vibrations, an off-resonant enhancement of transmission known as transmission sidebands may be observed.[6] In particular, if the molecule is initially vibrationally excited, off-resonant electrons below the resonance may tunnel though the molecule by absorbing a vibrational quantum of energy. This is illustrated in Fig. 1. Since transmission is only allowed combined with a downward vibrational transition, only one or a few electrons may tunnel through the contact and the transmission channel will be closed once the vibrational mode reaches the ground state.

Inspired by these considerations, we perform a quantitative analysis based on the model Hamiltonian,[6,13]

$$H = \varepsilon_0 c_a^\dagger c_a + \sum_i \hbar\omega_i b_i^\dagger b_i + \sum_i \lambda_i c_a^\dagger c_a (b_i^\dagger + b_i) + \sum_k \epsilon_{Lk} c_{Lk}^\dagger c_{Lk} + \sum_k (V_{Lk} c_a^\dagger c_{Lk} + V_{Lk}^* c_{Lk}^\dagger c_a) + \sum_k \epsilon_{Rk} c_{Rk}^\dagger c_{Rk} + \sum_k (V_{Rk} c_a^\dagger c_{Rk} + V_{Rk}^* c_{Rk}^\dagger c_a), \quad (1)$$

where $c_a^\dagger$ is the creation operator for the lowest unoccupied

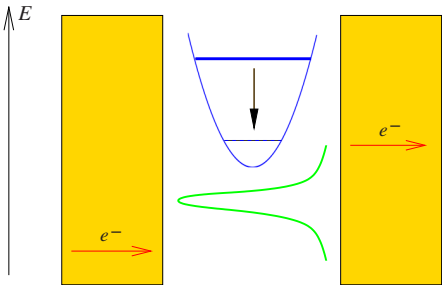

FIG. 1. (Color online) A molecule between two metal contacts is represented by a resonant state (for example, the lowest unoccupied molecular orbital) and a vibrational potential. If the molecule is initially vibrationally excited, an electron below the resonance may tunnel through the molecule by absorbing a quantum of vibration. When the molecule is initially in its vibrational ground state, transmission is not possible.

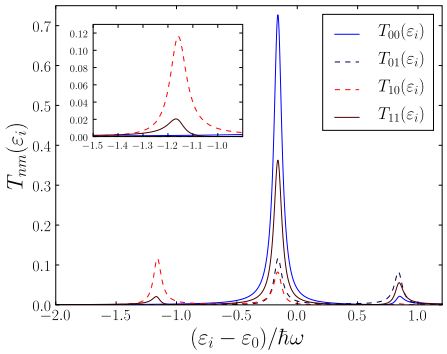

FIG. 2. (Color online) Transmission probabilities calculated from Eq. (1) as a function of incoming electron energy with $\Gamma_L = \Gamma_R = 0.04\hbar\omega$ and $\lambda = 0.4\hbar\omega$. Below the resonance energy ε_0, the ground-state transmission functions $T_{00}(\varepsilon_i)$ and $T_{01}(\varepsilon_i)$ essentially vanish. The inset shows the lower sideband, where stimulated emission of a vibrational quantum $T_{10}(\varepsilon_i)$ is the dominating transmission channel.

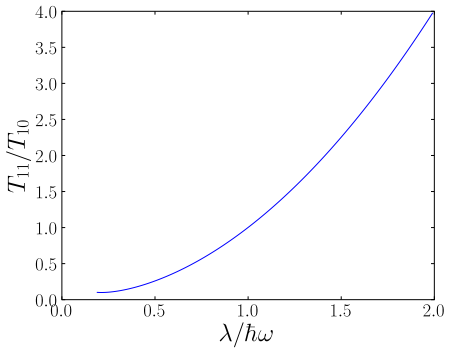

FIG. 3. (Color online) Ratio of elastic and inelastic transmission probabilities in the first vibrationally excited state. At weak coupling, the elastic transmission T_{11} goes to zero indicating that a vibrational excitation results in only a single electron being transmitted.

molecular orbital (LUMO), $c_{Lk}^\dagger$ and $c_{Rk}^\dagger$ are creation operators for metallic states in the left and the right lead, respectively, and $b_i^\dagger$ are creation operators for the vibrational normal modes of the molecule with frequencies ω_i. Thus, the electronic states of the left and the right contacts are coupled through the molecular resonance which is coupled to molecular vibrations with coupling strengths λ_i. We impose the wideband limit in which the contact density of states is constant in the region of the resonance and the resonance hybridization with metallic states is determined by the parameters,

$$\Gamma_L = 2\pi \sum_k |V_{Lk}|^2 \delta(\varepsilon_0 - \epsilon_{Lk}), \tag{2}$$

and a similar expression for the coupling to the right lead Γ_R. Without the vibrational coupling, the resonance spectral function would then be a Lorentzian with full width at half maximum given by $\Gamma = \Gamma_L + \Gamma_R$. We will be interested in the regime $\Gamma,\ k_BT \ll \hbar\omega_i$ but we will not restrict ourselves to the classical limit $\Gamma \ll k_BT$ where the contact current can be expressed in terms of rate equations.[8,9,14] Instead, we consider the transmission matrix $T_n(\varepsilon_i, \varepsilon_f)$ for an electron with initial-state energy ε_i and final-state energy ε_f. Within scattering theory, the transmission matrix can be expressed in terms of a two-particle Green's function[6] which can be evaluated exactly in the wideband limit.[15] The subscript n refers to the initial state of the oscillator and integrating out the final-state energy, one obtains the transmission probability $T_{nm}(\varepsilon_i)$ that an electron with initial-state energy ε_i is transmitted while the molecule makes the vibrational transition $n \to m$.

In the Appendix, we have calculated the transmission matrix in the ground and the first excited states and in Fig. 2, we show the transmission probability corresponding to four different vibrational transitions of the molecule. It shows that incoming electrons with energies below $\varepsilon_0 - \hbar\omega$ have a vanishing probability of transmission ($\Sigma_n T_{0n}$) when the molecule is in its vibrational ground state. This means that if a bias voltage is applied such that the Fermi level of the upstream contact is at $\varepsilon_F = \varepsilon_0 - \hbar\omega$, no current will be observed when the molecule is in its vibrational ground state. If the molecule is vibrationally excited, e.g., by means of a IR laser, transmission becomes possible through the low-lying vibrational sideband (T_{11} and T_{10}). However, the first electron which is transmitted through the T_{10} channel induces a transition to the vibrational ground state and thus closes the transmission channel completely. Hence, the net effect is that applying a short laser pulse to the molecular contact can induce the transmission of a few electrons.

The distribution of the number of electrons being transmitted as a result of a vibrational excitation depends on the ratio T_{11}/T_{10} shown in Fig. 3 as a function of the vibrational coupling. For small coupling parameters, the ratio approaches zero and the first electron to be transmitted is therefore highly likely to induce a vibrational decay and close the channel. For $\lambda \ll \hbar\omega$, we thus have $T_{11} \ll T_{10}$ which is needed for single-electron transmission. One might worry that the inelastic transmission amplitude may become too small for anything to happen in this case. However, the absolute amplitude of sideband transmission can easily be small if the vibrational lifetime of the molecule is long. For physisorbed molecules, the lifetime of a vibrational state is typically on the order of nanoseconds whereas, for example, with Au(111), we can use the density of states to estimate that ~ 40 electron hit each surface atom per picosecond within 0.1 eV of the Fermi level. Thus, as long as T_{10} is on the order of $\sim 1 \times 10^{-4}$, there will be plenty of attempts to result in a single transmission event.

The setup is illustrated in Fig. 4 where a small bias voltage $V_B \sim \Gamma/e$ has been applied and a gate voltage V_G has been tuned such that the position of the resonance is located $\hbar\omega$ above the bias window. It is crucial that the electronic resonance has a width much smaller than the quantum of vibration ($\Gamma \ll \hbar\omega$) since otherwise there will be a small but constant transmission probability when the molecule is in the vibrational ground state.

As an example we have performed a density-functional theory (DFT) study of a benzene molecule sandwiched between two Au(111) contacts. The calculations were performed with the code GPAW (Refs. 16 and 17) which is a

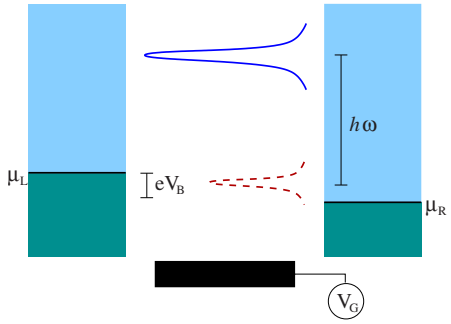

FIG. 4. (Color online) The principle of single-electron transmission. A small bias is applied such that the bias window just covers the resonance: $eV_B \sim \Gamma$ and a gate voltage is tuned such that the resonance is located at $\varepsilon_0 \sim \mu_L - eV_B/2 + \hbar\omega$. In the vibrational ground state, the transmission function T_{00} (solid line) is zero in the bias window. Exciting the first vibrational state changes the transmission function which is dominated by the inelastic part T_{10} (dashed line) in the bias window. A vibrational excitation of the molecule will thus result in a single electron being transmitted.

real-space DFT code using the projector-augmented wave method.[18] The contact were simulated by a three-layer Au(111) slab where the top layer has been relaxed. We used a supercell with 12 Au atoms in each slab layer which were sampled by a 4×4 grid of K points and 12.2 A of vacuum. Benzene was added with its plane parallel to the surface and the adsorption energy was calculated as a function of distance to the slab. This is shown in Fig. 5 for Perdew-Burke-Ernzerhof (PBE),[19] revised PBE (revPBE),[20] and van der Waals (vdW) (Ref. 21) functionals. The PBE and revPBE functional show weak and no bonding, respectively, whereas the vdW functional shows a 0.3 eV minimum at 3.6 A. The weak van der Waals bonding indicates that benzene is physisorbed on Au(111) which means that the molecular orbitals are weakly hybridized with metallic states as required by

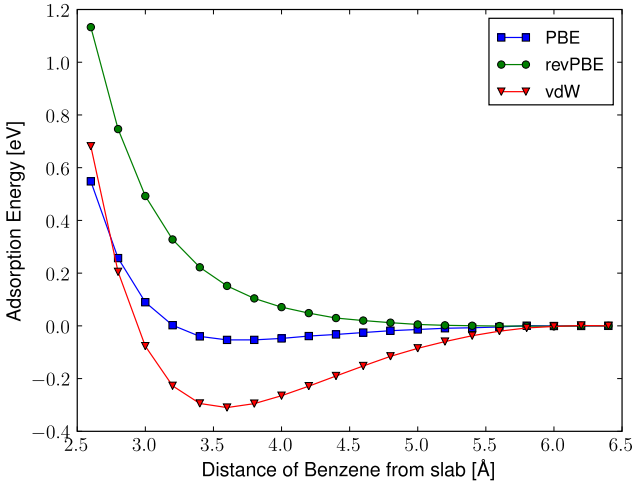

FIG. 5. (Color online) Adsorption energy of benzene on Au(111) as a function of distance to the surface, calculated with three different functionals. The molecular states are weakly hybridized with the metallic states and only the functional including the van der Waals interaction gives the correct adsorption well.

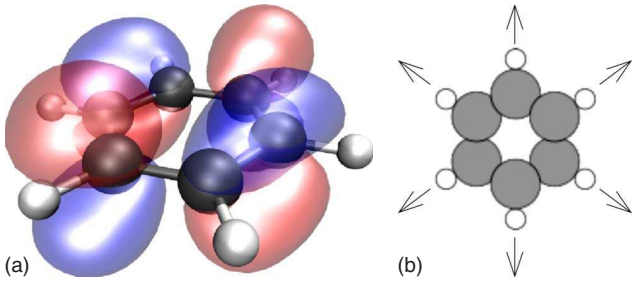

FIG. 6. (Color online) Left: the LUMO of benzene. Right: the vibrational mode of highest energy which can be excited by a transient occupation of the LUMO.

vibrationally mediated transmission of single electrons. This can also be seen explicitly from the Kohn-Sham projected density of states from which we estimate the width of highest occupied molecular orbital (HOMO) and LUMO resonances to be $\Gamma_L \sim 0.01$ eV. It should be noted that we assumed a LUMO state in Eq. (1) and Fig. 2 but the analysis is equally valid for transmission of hole states mediated by the HOMO and in the following, we will consider both types of resonance. Benzene has two degenerate HOMOs and two degenerate LUMOs which have the potential to mediate transmission of electrons through the molecule. One of the LUMOs is shown in Fig. 6 and it is expected that a transient occupation of the orbital may induce internal forces in the molecule and thus couple to the vibrational modes of the molecule. We have performed a DFT-based normal-mode analysis of the benzene molecule which has 36 vibrational modes. There are six degenerate highly energetic modes with $\hbar\omega_i \sim 0.39$ eV and the rest of the modes are evenly distributed in the interval $\hbar\omega_i \sim 0-0.20$ eV. The high-energy modes involve the hydrogen atoms oscillating in the plane of the molecule along the individual H-C bonds as shown in Fig. 6. The HOMO and LUMO states are expected to couple to several of the molecular vibrational states but we will focus on the high-energy modes which have highly separated vibrational sidebands in the weak-coupling limit. The coupling constants λ_i can be related to the excited-state potential-energy surface V_a associated with the LUMO being occupied or the HOMO being emptied,[22]

$$\lambda_i = \frac{l_i}{\sqrt{2}} \frac{\partial V_a}{\partial u_i}\bigg|_{u_i=u_i^0}, \quad l_i = \sqrt{\frac{\hbar}{m_i\omega_i}}, \tag{3}$$

where u_i is the coordinate of the ith normal mode, u_i^0 its equilibrium position in the electronic ground state, m_i its effective mass, and V_a the excited-state potential-energy surface associated with the resonance.[22,23] To obtain V_a, we have used the method of linear-expansion Δ self-consistent field DFT (Ref. 23) which allows us to calculate the excited-state energies while moving the atoms along the high-energy mode where the six hydrogen atoms move in phase (see Fig. 6). The results for this mode are $\lambda^{\mathrm{HOMO}}=27$ meV and $\lambda^{\mathrm{LUMO}}=9$ meV which should be compared with the quantum of oscillation $\hbar\omega_i \sim 0.39$ eV. The coupling is thus rather weak and we obtain maximum probabilities of inelastic transmission of 5×10^{-3} and 5×10^{-4}, respectively (with Γ

=0.01 eV), at the lower vibrational sideband. However, assuming the vibrational lifetime to be on the order of nanoseconds, the probabilities are most likely large enough that an elastic transmission event will occur. Furthermore, a small coupling constant means that the ratio T_{11}/T_{10} becomes very small and vibrational excitation will thus nearly always result in only a single electron being transmitted.

In summary, we have presented a method, which allows one to control the transmission of single electrons in weakly coupled molecule-metal junctions. The transmission is mediated by exciting a vibrational mode of the molecule while a gate voltage is tuned such that the resonant state is kept a quantum of vibrational energy above the bias window. It is assumed that such an excitation can be obtained with an external perturbation, for example, a short laser pulse. The requirement of weak metallic coupling ($\Gamma \ll \hbar\omega$) is essential since it excludes elastic transmission in the vibrational ground state. For small vibrational coupling ($\lambda \ll \hbar\omega$), the junction will then be highly reliable and always give rise to one electron being transmitted. For large vibrational coupling ($\lambda > \hbar\omega$), a vibrational excitation will typically result in a few electrons being transmitted due to a nonvanishing elastic transmission. To illustrate a quantitative approach to obtain the parameters of a real system, we have used DFT to calculate coupling parameters for a benzene molecule interacting with two gold contacts. Since benzene is bound by van der Waals forces and only show a weak hybridization with metallic states, it satisfies the minimum requirement for the principle to work. However, there may be others reasons why this system is not well suited for experiments of this kind and it would be very interesting to investigate the principle in systems where transmission through single molecules with significant vibrational coupling has been observed.[1–5]

We are grateful to K. S. Thygesen for advice and comments on the manuscript. This work was supported by the Danish Center for Scientific Computing. The Center for Individual Nanoparticle Functionality (CINF) is sponsored by the Danish National Research Foundation.

APPENDIX

In this appendix, we will show the details of the calculations leading to Fig. 2 for a single vibrational mode of frequency ω_0 and coupling λ_0. Within scattering theory, the transmission matrix $T_n(\varepsilon_i, \varepsilon_f)$ for a vibrationally excited state n can be expressed as[6]

$$T_n(\varepsilon_i, \varepsilon_f) = \Gamma_L \Gamma_R \int \frac{d\tau dt ds}{2\pi\hbar^3} e^{i[(\varepsilon_i - \varepsilon_f)\tau + \varepsilon_f t - \varepsilon_i s]/\hbar} G_n(\tau, s, t), \tag{A1}$$

where

$$G_n(\tau, s, t) = \theta(s)\theta(t)\langle n | c_a(\tau - s) c_a^\dagger(\tau) c_a(t) c_a^\dagger | n \rangle \tag{A2}$$

is the two-particle Green's function of the vibrational state n. The Green's function can be evaluated exactly in the wide-band limit and the result is[15]

$$G_n(\tau, s, t) = G_R^0(t) G_R^{0*}(t) e^{ig\omega_0(t-s)} e^{-g f_{\tau,s,t}} L_n[g(f_{\tau,s,t} + f^*_{\tau,s,t})], \tag{A3}$$

where L_n is the nth Laguerre polynomial, $g = \lambda_0^2/(\hbar\omega_0)^2$,

$$G_R^0(t) = -i\theta(t) e^{-i(\varepsilon_0 - i\Gamma/2)t/\hbar}$$

and

$$f_{\tau,s,t} = 2 - e^{-i\omega_0 t} - e^{i\omega_0 s} + e^{-i\omega_0 \tau}(1 - e^{i\omega_0 t})(1 - e^{i\omega_0 s}).$$

An explicit result for T_n can be obtained by performing the integrals in Eq. (A1) after a Taylor expansion of $e^{-g f_{\tau,s,t}}$.

The result for the vibrational ground state T_0 involves $L_0(x) = 1$ and has been calculated previously.[6] Here, we simply state the result which is

$$T_0(\varepsilon_i, \varepsilon_f) = \Gamma_L \Gamma_R e^{-2g} \sum_{m=0}^{\infty} \frac{g^m}{m!} \delta(\varepsilon_i - \varepsilon_f - m\hbar\omega_0) \left| \sum_{j=0}^{m} (-1)^j \binom{m}{j} \sum_{l=0}^{\infty} \frac{g^l}{l!} \left[\frac{1}{\varepsilon_i - \varepsilon_0 - (j + l - g)\hbar\omega_0 + i\Gamma/2} \right] \right|^2. \tag{A4}$$

It is clear that integrating over final-state energies simply produces a sum over vibrational transitions such that the nth term in Eq. (A4) represents T_{0n}. Calculating $T_1(\varepsilon_i, \varepsilon_f)$ is a bit more involved since the integrand in Eq. (A1) now includes the first Laguerre polynomial $L_1(x) = 1 - x$. We start by writing

$$T_1(\varepsilon_i, \varepsilon_f) = T_0(\varepsilon_i, \varepsilon_f) + \tilde{T}(\varepsilon_i, \varepsilon_f), \tag{A5}$$

where

$$\begin{aligned}
\tilde{T}(\varepsilon_i, \varepsilon_f) = \Gamma_L \Gamma_R e^{-2g} g & \int_0^\infty ds e^{i(\varepsilon_0 - \varepsilon_i - g\omega_0 + i\Gamma/2)s/\hbar} \exp(g e^{i\omega_0 s}) \\
& \times \int_0^\infty dt e^{-i(\varepsilon_0 - \varepsilon_i - g\omega_0 - i\Gamma/2)t/\hbar} \exp(g e^{-i\omega_0 t}) e^{-i(\varepsilon_i - \varepsilon_f)t/\hbar} \\
& \times \int_{-\infty}^\infty \frac{d\tau}{2\pi\hbar^3} e^{i(\varepsilon_i - \varepsilon_f)\tau/\hbar} \exp[g e^{-i\omega_0 \tau} e^{i\omega_0 t}(1 - e^{-i\omega_0 t})(1 - e^{i\omega_0 s})] \\
& \times [(1 - e^{i\omega_0 t})(e^{-i\omega_0 t} - 1) + (1 - e^{i\omega_0 s})(e^{-i\omega_0 s} - 1)
\end{aligned}$$

$$- e^{-i\omega_0\tau}(1-e^{i\omega_0 t})(1-e^{i\omega_0 s}) - e^{i\omega_0\tau}(1-e^{-i\omega_0 t})(1-e^{-i\omega_0 s})].$$

Taylor expanding the second exponential in the τ integral and performing the integration gives

$$\begin{aligned}\tilde{T}(\varepsilon_i,\varepsilon_f) = \Gamma_L\Gamma_R e^{-2g}\frac{g}{\hbar^2}\int_0^\infty ds e^{i(\varepsilon_0-\varepsilon_i-g\omega_0+i\Gamma/2)s/\hbar}\exp(ge^{i\omega_0 s})\\ \times\int_0^\infty dt e^{-i(\varepsilon_0-\varepsilon_i-g\omega_0-i\Gamma/2)t/\hbar}\exp(ge^{-i\omega_0 t})\\ \times\Bigg[\sum_{m=0}^\infty\frac{g^m}{m!}e^{i\omega_0 t}(1-e^{-i\omega_0 t})^{m+2}(1-e^{i\omega_0 s})^m\delta(\varepsilon_i-\varepsilon_f-m\hbar\omega_0)\\ +\sum_{m=0}^\infty\frac{g^m}{m!}e^{-i\omega_0 s}(1-e^{-i\omega_0 t})^m(1-e^{i\omega_0 s})^{m+2}\delta(\varepsilon_i-\varepsilon_f-m\hbar\omega_0)\\ +\sum_{m=0}^\infty\frac{g^m}{m!}(1-e^{-i\omega_0 t})^{m+1}(1-e^{i\omega_0 s})^{m+1}\delta(\varepsilon_i-\varepsilon_f-(m+1)\hbar\omega_0)\\ +\sum_{m=0}^\infty\frac{g^m}{m!}e^{-i\omega_0(s-t)}(1-e^{-i\omega_0 t})^{m+1}(1-e^{i\omega_0 s})^{m+1}\delta(\varepsilon_i-\varepsilon_f-(m-1)\hbar\omega_0)\Bigg].\end{aligned}$$

The first two terms are each others complex conjugated and the last two terms factorizes (s and t integrals) into complex conjugated and the integrals can then be performed. The final result is rather complicated but consists of an infinite number of terms, each of which involves a delta function $\delta(\varepsilon_i-\varepsilon_f-m\hbar\omega_0)$, where m runs from -1 to infinity. We can thus obtain T_{10} and T_{11} by collecting terms involving $m=-1$ and $m=0$, respectively. The results are

$$T_{10}(\varepsilon_i) = \Gamma_L\Gamma_R e^{-2g} g\left|\sum_{l=0}^\infty\frac{g^l}{l!}\frac{1}{\varepsilon_i-\varepsilon_0-(l-1-g)\hbar\omega_0+i\Gamma/2}-\sum_{l=0}^\infty\frac{g^l}{l!}\frac{1}{\varepsilon_i-\varepsilon_0-(l-g)\hbar\omega_0+i\Gamma/2}\right|^2$$

and

$$\begin{aligned}T_{11}(\varepsilon_i) = \Gamma_L\Gamma_R e^{-2g}\left|\sum_{l=0}^\infty\frac{g^l}{l!}\frac{1}{\varepsilon_i-\varepsilon_0-(l-g)\hbar\omega_0+i\Gamma/2}\right|^2\\ +2g\Gamma_L\Gamma_R e^{-2g}\,\mathrm{Re}\left(\sum_{j=0}^2(-1)^j\binom{2}{j}\sum_{l=0}^\infty\frac{g^l}{l!}\frac{1}{\varepsilon_i-\varepsilon_0-(j+l-1-g)\hbar\omega_0+i\Gamma/2}\sum_{l=0}^\infty\frac{g^l}{l!}\frac{1}{\varepsilon_i-\varepsilon_0-(l-g)\hbar\omega_0-i\Gamma/2}\right)\\ +g^2\Gamma_L\Gamma_R e^{-2g}\left|\sum_{j=0}^2(-1)^j\binom{2}{j}\sum_{l=0}^\infty\frac{g^l}{l!}\frac{1}{\varepsilon_i-\varepsilon_0-(j+l-1-g)\hbar\omega_0+i\Gamma/2}\right|^2.\end{aligned}$$

*tolsen@fysik.dtu.dk

[1] H. Park, J. Park, A. K. L. Lim, E. H. Anderson, A. P. Alivisatos, and P. L. McEuen, Nature (London) **407**, 57 (2000).
[2] L. H. Yu, Z. K. Keane, J. W. Ciszek, L. Cheng, M. P. Stewart, J. M. Tour, and D. Natelson, Phys. Rev. Lett. **93**, 266802 (2004).
[3] A. N. Pasupathy, J. Park, C. Chang, A. V. Soldatov, S. Lebedkin, R. C. Bialczak, J. E. Grose, L. A. K. Donev, J. P. Sethna, D. C. Ralph, and P. L. McEuen, Nano Lett. **5**, 203 (2005).
[4] S. Sapmaz, P. Jarillo-Herrero, Y. M. Blanter, C. Dekker, and H. S. J. van der Zant, Phys. Rev. Lett. **96**, 026801 (2006).
[5] R. Leturcq, C. Stamper, K. Inderbitzin, L. Durrer, C. Hierold, E. Mariani, M. G. Schultz, F. von Oppen, and K. Ensslin, Nat. Phys. **5**, 327 (2009).
[6] N. S. Wingreen, K. W. Jacobsen, and J. W. Wilkins, Phys. Rev. B **40**, 11834 (1989).
[7] T. Mii, S. G. Tikhodeev, and H. Ueba, Phys. Rev. B **68**, 205406 (2003).
[8] S. Braig and K. Flensberg, Phys. Rev. B **68**, 205324 (2003).
[9] A. Mitra, I. Aleiner, and A. J. Millis, Phys. Rev. Lett. **94**, 076404 (2005).
[10] M. Galperin and M. A. Ratner, Nano Lett. **4**, 1605 (2004).
[11] T. Frederiksen, M. Paulsson, M. Brandbyge, and A.-P. Jauho, Phys. Rev. B **75**, 205413 (2007).
[12] I. S. Kristensen, M. Paulsson, K. S. Thygesen, and K. W. Jacobsen, Phys. Rev. B **79**, 235411 (2009).
[13] M. Galperin, M. A. Ratner, and A. Nitzan, J. Phys.: Condens.

Matter **19**, 103201 (2007).
[14] A. Mitra, I. Aleiner, and A. J. Millis, Phys. Rev. B **69**, 245302 (2004).
[15] T. Olsen, Phys. Rev. B **79**, 235414 (2009).
[16] The GPAW code is available as a part of the CAMPOS software, www.camd.dtu.dk/Software
[17] J. J. Mortensen, L. B. Hansen, and K. W. Jacobsen, Phys. Rev. B **71**, 035109 (2005).
[18] P. E. Blöchl, Phys. Rev. B **50**, 17953 (1994).
[19] J. P. Perdew, K. Burke, and M. Ernzerhof, Phys. Rev. Lett. **77**, 3865 (1996).
[20] Y. Zhang and W. Yang, Phys. Rev. Lett. **80**, 890 (1998).
[21] M. Dion, H. Rydberg, E. Schröder, D. C. Langreth, and B. I. Lundqvist, Phys. Rev. Lett. **92**, 246401 (2004).
[22] T. Olsen, J. Gavnholt, and J. Schiøtz, Phys. Rev. B **79**, 035403 (2009).
[23] J. Gavnholt, T. Olsen, M. Engelund, and J. Schiøtz, Phys. Rev. B **78**, 075441 (2008).

Paper VII

R. Frigge, T. Hoger, B. Siemer, H. Witte, M. Silies, H. Zacharias, T. Olsen, and J. Schiøtz
Site Specificity in Femtosecond Laser Desorption of Neutral H Atoms from Graphite(0001)
Phys. Rev. Lett. **104**, 256102 (2010).

Site Specificity in Femtosecond Laser Desorption of Neutral H Atoms from Graphite(0001)

R. Frigge,[1,*] T. Hoger,[1] B. Siemer,[1] H. Witte,[1] M. Silies,[1] H. Zacharias,[1] T. Olsen,[2] and J. Schiøtz[2]

[1]*Physikalisches Institut and Center for Nanotechnology (CeNTech), Westfälische Wilhelms-Universität, 48149 Münster, Germany*

[2]*Danish National Research Foundation's Center of Individual Nanoparticle Functionality (CINF), Department of Physics, Technical University of Denmark, DK–2800 Kongens Lyngby, Denmark*

(Received 1 April 2010; published 25 June 2010)

Femtosecond laser excitation and density functional theory reveal site and vibrational state specificity in neutral atomic hydrogen desorption from graphite induced by multiple electronic transitions. Multimodal velocity distributions witness the participation of ortho and para pair states of chemisorbed hydrogen in the desorption process. Very slow velocities of 700 and 400 ms^{-1} for H and D atoms are associated with the desorption out of the highest vibrational state of a barrierless potential.

DOI: 10.1103/PhysRevLett.104.256102 PACS numbers: 68.43.Tj, 68.65.Pq, 82.20.Gk, 82.65.+r

The adsorption and desorption dynamics of hydrogen on graphite and graphene sheets has attracted considerable interest recently. In addition to the dramatic changes in the electronic properties of graphene, rendering it insulating [1,2], atomic hydrogen chemisorbed on carbon scaffolds has been considered for hydrogen storage [3,4], a sink in plasma fusion devices [5], and a precursor for the formation of molecular hydrogen in interstellar molecular clouds [6]. Recent scanning tunneling microscopy revealed preferential sticking sites [7] in the case of preadsorbed H atoms and preferred sites for thermal reaction and desorption [8]. Also a tip-induced desorption of H atoms from graphene has recently been observed [9]. Theoretical calculations show that atomic hydrogen binds on top of carbon atoms with an energy of about $E_b \sim 0.7$ eV. Thereby the sp^2 bound carbon scaffold is locally distorted and the now sp^3 binding C atoms pucker out of the graphite plane by about 0.3 Å. Because of this electronic change and atomic movement a barrier of about 0.25 eV appears in the reaction pathway to chemisorption [10,11]. Co-adsorption of a second H atom in the vicinity of an already adsorbed one is preferred on the next neighbor ortho position and in the so-called para position located on the opposite site of the carbon hexagons. In these two positions the binding energy increases to about 1.9 to 2.1 eV, while in the nearest next neighbor position the binding energy remains unchanged [7,11]. In addition, the adsorption barrier is reduced in the ortho position, and even vanishes for adsorption in the para position. Further, energetic correlations over more extended regions of the carbon scaffold exist [12]. Correspondingly, evidence has been found that thermal molecular hydrogen formation occurs predominantly from such preferred pairs of atomic hydrogen [8]. Temperature programmed desorption (TPD) experiments show the formation of molecular hydrogen from chemisorbed atoms at temperatures in the range from 400 to 600 K and a first order desorption kinetics [13]. The double peak structure observed in TPD results from the recombination of H atoms out of these preferred pair sites on the graphite surface. Surface diffusion is not important, because the diffusion barrier on graphite is higher than 1 eV thereby exceeding the binding energy of unpaired chemisorbed atoms and thus making diffusion unlikely [14].

Femtosecond laser excitation of graphite in the visible spectral range produces hot electrons which subsequently undergo various scattering processes, as electron-electron or electron-phonon scattering. Thereby a cloud of excited electrons is created which might scatter on adsorbates. Two-pulse time-correlated excitation experiments yield information about these electronic relaxations. Electron-electron scattering occurs on a time scale of a few tens of femtoseconds [15,16] followed by phonon-mediated intraband cooling in 100 to 500 fs and a corresponding population of the optical phonon mode in graphite [16–18]. This optical phonon shows a lifetime in the range of a few picoseconds and decays further into the phonon bath of the substrate [19].

In the present experiment a sample of highly oriented pyrolytic graphite with (0001) orientation is placed in an ultrahigh vacuum chamber at a base pressure in the low 10^{-10} mbar range. The sample is cleaned by cleaving the top layers just before placing it into the vacuum and then annealing it at temperatures of 1000 K for several minutes to remove any adsorbates. H and D atoms are produced by thermal dissociation in a tungsten capillary heated to about 2200 K. The graphite sample at a distance of 80 mm from the capillary is exposed to the hydrogen flux at a chamber pressure of 5×10^{-8} mbar for about 20 min to ensure saturation, which corresponds to a coverage of 0.4 ML [13]. After exposure to atomic hydrogen the surface is irradiated under $\theta = 67.5°$ by p-polarized pulses of a frequency doubled Ti:sapphire laser at a repetition rate of 10 Hz. Pulses with a duration of about 35 fs and energies up to 40 μJ are applied to an area of about 500×780 μm^2. Using known electron-phonon coupling constants, it is estimated that at these laser intensities the distribution of hot electrons reaches peak temperatures of about 18 000 K.

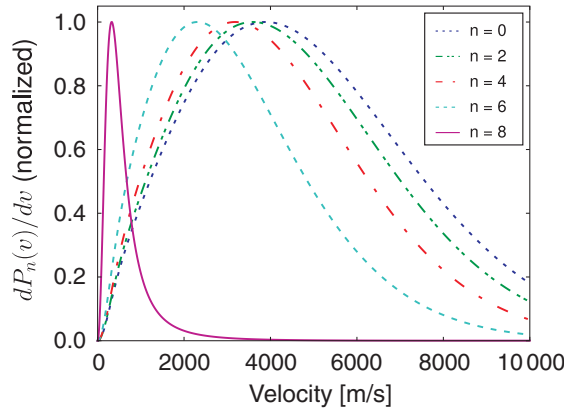

FIG. 1 (color online). Kinetic energy distribution for desorption out of five bound states for the para adsorption site, calculated from Eq. (2). The parameters are given in the text, and $\epsilon_i = \epsilon_0$. The probabilities have been normalized to fit the figure, in fact the maximum value of $P_n(v)$ increases by an order of magnitude for each n. The $n = 8$ state thus has a much larger desorption probability than the rest.

Each laser pulse desorbs about 2.2×10^{-5} ML of the adsorbed hydrogen at dilute coverage, see below.

The desorbing hydrogen atoms are detected in the gas phase after a defined flight path and time delay by pulses of a tunable, frequency doubled dye laser. This laser operates at $\lambda = 243$ nm, which excites the atoms via two-photon absorption in the $2\ s^2S_{1/2} \leftarrow 1\ s^2S_{1/2}$ transition. Absorption of a third photon ionizes only the electronically excited H atoms. The generated H^+ (D^+) ions are detected by a time-of-flight mass spectrometer. Since the distance from the surface to the detection volume is known, the velocity of the desorbing atoms can be derived from the arrival time at the detection volume.

To calculate the atomic kinetic energy spectrum we employ scattering theory in conjunction with density functional theory (DFT). We consider an adsorbed atom which is described by an adiabatic potential $V_0(z)$ with desorption coordinate z and a corresponding Hamiltonian H_0. The electronic system, which comprises both adsorbate and substrate, is described by a Newns-Anderson type Hamiltonian H_{NA} with a resonant electronic state $|a\rangle$ localized near the hydrogen atom and being unoccupied when the system is in the electronic ground state. When $|a\rangle$ becomes occupied the electronic structure changes and the Born-Oppenheimer potential of the adsorbate is altered to $V_1(z)$. The state $|a\rangle$ thus gives rise to a Hamiltonian term H_I which couples the pure electronic term H_{NA} and the pure atomic term H_0. Even though the resonant state is short-lived, a transient occupation will perturb the system and may induce transitions between the bound states of $V_0(z)$ or from a bound to a dissociative state. The Hamiltonian describing the system is then

$$H = H_{\mathrm{NA}} + H_0 + H_I \tag{1}$$

with

$$H_{\mathrm{NA}} = \varepsilon_0 c_a^\dagger c_a + \sum_q \epsilon_q c_q^\dagger c_q + \sum_q (V_{aq} c_a^\dagger c_q + V_{aq}^* c_q^\dagger c_a),$$

$$H_0 = \tfrac{1}{2} m \dot{z}^2 + V_0(z),$$

$$H_I = \varepsilon_a(z) c_a^\dagger c_a - \varepsilon_0 c_a^\dagger c_a.$$

Here, $\epsilon_a(z) = V_1(z) - V_0(z)$ denotes the vertical potential energy difference, $c_a^\dagger$ and $c_q^\dagger$ are creation operators for the resonant state $|a\rangle$ and metallic states $|q\rangle$, respectively, and $\epsilon_0 = \epsilon_a(0)$ [20,21]. Conceptually, the Hamiltonian describes an adsorbate with dynamics governed by $V_0(z)$ when the resonant state is unoccupied and $V_1(z)$ when the resonant state is occupied. To handle the model (1) we impose the wide band limit in which the resonance projected density of states is a Lorentzian with a full width at half maximum of Γ. Furthermore, we Taylor expand the interaction Hamiltonian to first order in the vicinity of the ground state minimum ($z = 0$) and get $H_I = -f_a z c_a^\dagger c_a$, where f_a is the force felt by the adsorbate when the resonance is occupied. We can then use second order perturbation theory to calculate the differential probability $dP_n(k)$ that an incoming hot electron of energy ϵ_i will induce a transition in the adsorbate from a bound state $|n\rangle$ to a free state $|k\rangle$ [22]. The free states become plane waves asymptotically and can thus be converted into velocities. The result for the scattering probability is

$$dP_n(k) = \frac{f_a^2 \Gamma^2}{(E_k - E_n)^2} |\langle k|z|n\rangle|^2 dk \left| \frac{1}{\varepsilon_i - \varepsilon_0 + i\Gamma/2} - \frac{1}{\varepsilon_i - \varepsilon_0 - (E_k - E_n) + i\Gamma/2} \right|^2, \tag{2}$$

where E_n and $E_k = \hbar^2 k^2 / 2m$ are eigenenergies of bound and free states, respectively.

The parameters and potential energy surfaces in the model (1) have been calculated with the code GPAW [23,24], which is a real-space density DFT code using the projector augmented wave method. The excited state potential energy surface was obtained with the linear expansion delta self-consistent field (ΔSCF) method [21,25], where the resonant state is taken to be a localized antibonding C-H orbital which is unoccupied without excitation. The resonance width Γ is obtained from the Kohn-Sham projected density of states. We will focus on the para and ortho dimer configurations which dominate at low coverage and are responsible for the two peaks observed in TPD spectra [8,13]. All calculations have been performed on a single graphene layer with a hydrogen dimer in a super cell containing 24 carbon atoms. We used a 4×4 K-point sampling, a grid spacing of 0.2 Å, and the PBE exchange-correlation functional [26]. The atomic adsorption potential for hydrogen in the para configuration has no barrier [7,11] and can be approximated by a Morse poten-

tial $V_0(z) = D(e^{-2\alpha z} - 2e^{-\alpha z})$ with $D = 2.0$ eV and $\alpha = 3.5$ Å^{-1} yielding 9 bound states. In addition we find $\Gamma = 1.5$ eV, $\epsilon_0 = 3.8$ eV, and $f_a = 0.27$ eV/Å. The eigenenergies E_n and matrix elements $\langle n|z|k\rangle$ of the Morse potential are well known.

Figure 1 shows the kinetic energy spectrum according to Eq. (2) of desorbing H atoms associated with different bound states within the H-graphene potential for the para pair site. The positions of the peaks is roughly related to the widths of the bound state wave functions. The highest vibrational state is thus well separated from the others due to the fact that the potential is very wide close to the desorption energy. Since a desorption event is the result of multiple hot electrons sequentially exciting the adsorbate, the distribution of vibrational states is not in equilibrium with the graphite temperature at the time of desorption. To calculate the vibrational distribution resulting from scattering of multiple hot electrons, we use the model (1) to obtain the transition probability that a hot electron induces a vibrational transition $n \rightarrow m$ and obtain an expression similar to (2). Each hot electron thus changes the distribution induced by the previous hot electron and we can obtain the total yield by summing all $P_n(k)$ weighted by a distribution resulting from a given number of hot electrons. The desorption of atoms in the ortho configuration is treated in the same way except that $f_a = 0.57$ eV/Å and there is an adsorption barrier of $E_B = 0.18$ eV, which is included by accelerating desorbed atoms accordingly.

Experimentally, we measure the desorption yield and the velocity distribution of the desorbed H and D atoms. The atomic desorption yield shows for both H and D atoms a nonlinear dependence on the absorbed laser fluence with exponents of $n = (2.42 \pm 0.12)$ and (1.85 ± 0.11), respectively. This power law dependence hints to the fact that multiple electron scattering events are responsible for this DIMET desorption process [27]. Irradiating the surface at constant fluence without redosing the hydrogen coverage yields an effective desorption cross section. As is often the case in laser desorption experiments a fast initial decay followed by a significantly slower one is observed. At a fluence of 10 mJ/cm^2 we arrive at initial cross sections of $(2.5 \pm 1.0) \times 10^{-20}$ cm^2 and $(4.9 \pm 1.0) \times 10^{-20}$ cm^2 for H and D atoms, respectively, up to a total absorbed fluence of 5×10^{19} photons/cm^2 or about 2500 pulses. After this initial irradiation coverages of about 0.13 ML and 0.07 ML of H and D atoms, respectively, remain on the graphite surface. For higher total fluences and thus lower remaining coverages lower cross sections of about $(5.6 \pm 0.2) \times 10^{-21}$ cm^2 and $(4.1 \pm 0.1) \times 10^{-21}$ cm^2 are, respectively, observed for H and D atoms. The initial desorption cross section at high surface coverage is thus significantly larger for the heavier isotopic species, while at more dilute coverages the cross sections are approximately equal for both isotopes. It should be kept in mind, however, that we measure in this way only a decrease in the hydrogen or deuterium coverage of graphite. It may be speculated that the larger cross section is associated with the desorption of molecular hydrogen. Experiments to proof this conjecture by selective laser detection of H_2 and D_2 are currently in progress.

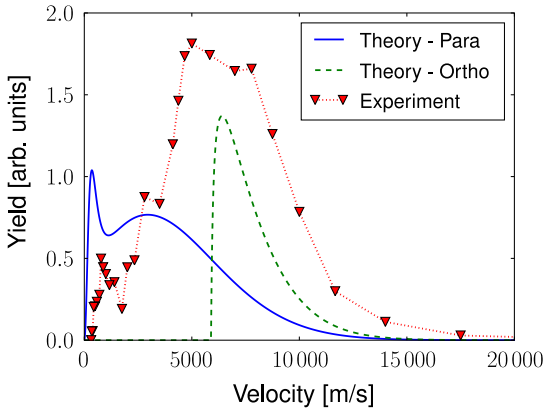

FIG. 2 (color online). Observed and calculated velocity distribution of H atoms from graphite. Triangles and dotted line denote the experimental data, the solid and dashed lines represent the theoretical results.

Velocity distributions have always been measured at dilute hydrogen coverages of the graphite surface of less than 0.1 ML by preirradiating the system accordingly. Figures 2 and 3 show the velocity distributions of H and D atoms, respectively, desorbing from graphite. Triangles and dotted lines denote the experimental data, and the solid and dashed lines represent results from the theoretical analysis. It is evident that multimodal velocity distributions are observed which can not be described by thermal distributions. For neutral hydrogen atoms a peak is observed around $v = 700$ m/s and one around $v = 5700$ m/s, while for D atoms three peaks, at $v = 400$ m/s, 1600 m/s, and about 4400 m/s can be discerned. Very intriguing are especially the peaks in the distributions at

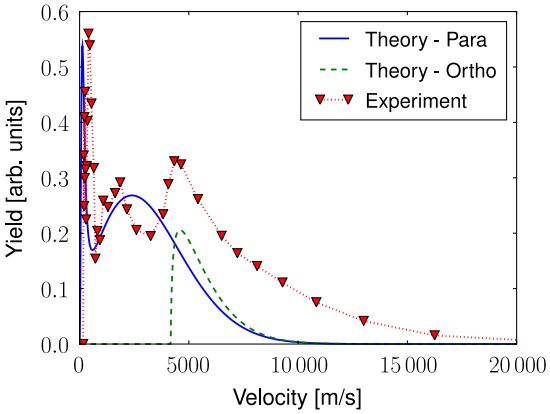

FIG. 3 (color online). Same as Fig. 2, but for D atoms. Note the distinct peak at very low velocities in both the experimental data and the theoretical results.

very slow velocities. For assumed thermal distributions these peaks would correspond to kinetic energies of about 3 to 4 meV, or corresponding temperatures around 15 to 20 K, which are not present in the system. On the other hand the peaks at high velocities correspond to average kinetic energies of about $\langle E_{\mathrm{kin}} \rangle = 224$ meV (H atoms) and 267 meV (D atoms). It should further be noted that after velocity integration the observed yields for H and D atoms reveal that the total yield of desorbing H atoms is about 3 times higher than for D atoms. To recall, the initial deuterium coverage of graphite is much faster depleted than the hydrogen coverage, and at the dilute coverage both isotopic coverages are depleted with about the same effective cross section.

In Figs. 2 and 3 we compare the observed velocity distributions of hydrogen and deuterium with those calculated in the model. The solid lines in both figures indicate a good agreement between the experimental observations and first principals or model calculations. We have assumed that the distribution of vibrational states is the result of five hot electrons at resonance and that the fraction of para dimers is 10 times that of ortho dimers which is consistent with the observations of ref. [8]. While the choice of five initial hot electrons is rather arbitrary we have checked that the qualitative results do not depend crucially on this number. The positions of the peaks are independent of the initial distribution of vibrational states and changing the number of initial hot electrons only changes the relative magnitude of the peaks slightly. The two initial peaks at lower velocities are due to hydrogen atoms which originate from para states, while the high velocity peak reflects desorption from ortho states at which hydrogen atoms are accelerated by the barrier. In particular, one should note the low velocity peaks which result from desorption out of para dimers with atoms being in the highest vibrational states of the adsorption potential. The ortho configuration only shows a single peak, since the potential with a barrier does not have very wide vibrational states. Very fast atoms might origine from desorption out of monomer states which show an even higher barrier than the ortho states and, moreover, show a tighter binding to the graphene plane. According to the Franck-Condon principle this results in an excitation of the repulsive state at a higher energy.

The model used to calculate the desorption yield contains no fitted parameters, but one has to make an assumption on the distribution of hot electrons. Here we have made the simplest possible approximation, namely, all electrons being at the resonant energy. Increasing the number of contributing electrons would increase the population of high-lying vibrational states and thus change the ratio of the two para state peaks as well as increase the absolute value of the total calculated yield. In conclusion, we addressed the dynamics of photodesorption of neutral atomic hydrogen from the chemisorbed states on graphite. A DIMET process as suggested by the nonlinear yield dependence and the theoretical calculation is responsible for the desorption process. The observed velocity distributions can be associated with desorption out of ortho and para pair adsorption sites. Very low velocities result from desorption out of the highest vibrational state of the para pairs. We expect that these mechanisms play an important role also for the association reaction and in other systems.

*r.f@wwu.de

[1] J. O. Sofo, A. S. Chaudhari, and G. D. Barber, Phys. Rev. B **75**, 153401 (2007).
[2] D. C. Elias *et al.*, Science **323**, 610 (2009).
[3] L. Schlapbach and A. Züttel, Nature (London) **414**, 353 (2001).
[4] A. C. Dillon *et al.*, Nature (London) **386**, 377 (1997).
[5] C. H. Skinner and A. Haasz, Fusion Sci. Technol. **54**, 891 (2008).
[6] D. Hollenbach and E. E. Salpeter, Astrophys. J. **163**, 155 (1971).
[7] L. Hornekær *et al.*, Phys. Rev. Lett. **97**, 186102 (2006).
[8] L. Hornekær *et al.*, Phys. Rev. Lett. **96**, 156104 (2006).
[9] P. Sessi *et al.*, Nano Lett. **9**, 4343 (2009).
[10] X. Sha and B. Jackson, Surf. Sci. **496**, 318 (2002).
[11] N. Rougeau, D. Teillet-Billy, and V. Sidis, Chem. Phys. Lett. **431**, 135 (2006).
[12] Ž. Šljivančanin *et al.*, J. Chem. Phys. **131**, 084706 (2009).
[13] T. Zecho *et al.*, J. Chem. Phys. **117**, 8486 (2002).
[14] Y. Ferro *et al.*, J. Chem. Phys. **120**, 11 882 (2004).
[15] S. Xu *et al.*, Phys. Rev. Lett. **76**, 483 (1996).
[16] M. Breusing, C. Ropers, and T. Elsaesser, Phys. Rev. Lett. **102**, 086809 (2009).
[17] G. Moos *et al.*, Phys. Rev. Lett. **87**, 267402 (2001).
[18] H. Wang *et al.*, Appl. Phys. Lett. **96**, 081917 (2010).
[19] T. Kampfrath *et al.*, Phys. Rev. Lett. **95**, 187403 (2005).
[20] N. S. Wingreen, K. W. Jacobsen, and J. W. Wilkins, Phys. Rev. B **40**, 11 834 (1989).
[21] T. Olsen, J. Gavnholt, and J. Schiøtz, Phys. Rev. B **79**, 035403 (2009).
[22] T. Olsen, Phys. Rev. B **79**, 235414 (2009).
[23] The GPAW code is available as a part of the CAMPOS software: www.camd.dtu.dk/Software.
[24] J. J. Mortensen, L. B. Hansen, and K. W. Jacobsen, Phys. Rev. B **71**, 035109 (2005).
[25] J. Gavnholt, T. Olsen, M. Engelund, and J. Schiøtz, Phys. Rev. B **78**, 075441 (2008).
[26] J. P. Perdew, K. Burke, and M. Ernzerhof, Phys. Rev. Lett. **77**, 3865 (1996).
[27] T. Olsen and J. Schiøtz, Phys. Rev. Lett. **103**, 238301 (2009).

Paper VIII

B. Siemer, T. Olsen, T. Hoger, M. Rutkowski, C. Thewes, S. Düsterer, J. Schiøtz, and H. Zacharias
Desorption of H atoms from graphite(0001) using XUV free electron laser pulses
Submitted to Chem. Phys. Lett.

Desorption of H atoms from graphite(0001) using XUV free electron laser pulses

B. Siemer[a], T. Olsen[b], T. Hoger[a], M. Rutkowski[a], C. Thewes[a], S. Düsterer[c], J. Schiøtz[b], H. Zacharias[a]

[a] *Physikalisches Institut, Westfälische Wilhelms-Universität Münster, Wilhelm Klemm Str. 10, 48149 Münster, Germany*

[b] *Danish National Research Foundation's Center of Individual Nanoparticle Functionality (CINF), Department of Physics, Technical University of Denmark, DK–2800 Kongens Lyngby, Denmark*

[c] *HASYLAB, Deutsches Elektronen Synchotron, Notkestr. 85, 22607 Hamburg, Germany*

Abstract

The desorption of neutral H atoms from graphite with femtosecond XUV pulses is reported. The velocity distribution of the atoms peaks at extremely low kinetic energies. A DFT-based electron scattering calculation traces this distribution to desorption out of specific adsorption sites on graphite, and identifies the highest vibrational state in the adsorbate potential as a major source for the slow atoms. It is evident that multiple electron scattering processes are required for this desorption. A direct electronic excitation of a repulsive hydrogen - carbon bond seems not to be important.

Keywords: desorption, XUV, hydrogen, FLASH,
PACS: 68.43.Tj, 68.65.Pq, 82.20.Gk, 82.65.+r

1. Introduction

Photochemically triggered reactions on dust grains are considered to be a major source of molecule formation in interstellar clouds. These grains typically consist of graphitic and silicate particles and conglomerates, in the central regions of the clouds often covered with icy layers. In warmer parts of the clouds which are irradiated by newly born stars and in the accretion discs of such stars most of the ice layers have evaporated, and bare grains are exposed [1]. The reaction dynamics of hydrogen constitutes then one of the more important reactions. Such reactions on graphite or graphene

sheets gained considerable interest recently, as they are accompanied with a considerable change in the local electronic structure.

Upon chemical binding of atomic hydrogen the generally sp^2 bound carbon scaffold of graphene is locally distorted. The now binding C atom develops an sp^3 hybridization, and puckers out of the graphite plane by about 0.3 Å. This electronic change and the atomic movement cause a barrier in the adsorption pathway of about 0.25 eV [2, 3]. The H atoms then bind with an energy of about $E_b \sim 0.7\,eV$. Co-adsorption of a second H atom in the vicinity of an already adsorbed one is preferred on the next-neighbor ortho position and on the so-called para position on the opposite site of the carbon hexagons, as was confirmed by scanning tunnelling microscopy [4]. In these two positions the binding energy increases to 1.9 to 2.1 eV, while in the nearest next neighbor (meta) position it remains unchanged. In both positions the adsorption barrier is reduced, for para adsorption even to zero energy. Correspondingly, preferential reaction sites exist for thermal molecular hydrogen formation out of these pre-paired H atoms [5, 6].

Recently, femtosecond laser induced desorption of atomic hydrogen from graphite has been observed with near-UV radiation of 3.1 eV photon energy [7]. Distinct features in the velocity distribution could be assigned to desorption out of the mentioned pre-paired preferential ortho and para adsorption sites. In this Letter we report on first results obtained after irradiation of the surface system with femtosecond extreme ultraviolet (XUV) pulses provided by the free-electron laser at Hamburg (FLASH) at DESY. The photon energy chosen ($h\nu = 38$ eV) is close to the HeII resonance line. This high photon energy in principle enables a direct electronic excitation of the hydrogen graphite bond, but also the creation of a hot electron gas in the graphite substrate.

2. Experimental

The experiment is carried out at the free-electron laser at Hamburg (FLASH) at DESY which provides radiation in the XUV and soft x-ray regime from about 20 eV to 206 eV in the fundamental on the unmonochromatized beamline BL1 [8]. The highly oriented pyrolytic graphite (HOPG) sample is placed on a manipulator mounted in a UHV chamber with a base pressure of 2×10^{-10} mbar. The sample is cleaned by cleaving the top layers just before placing it into the chamber and heading up to ~ 850 K for prolonged time to remove any adsorbates. For atomic hydrogen adsorption and

the experiment the sample is cooled to a temperature of $T_s = 300\,K$. Hydrogen atoms are produced by thermal dissociation in a tungsten capillary heated to more than 2200 K. The capillary has a distance of 80 mm from the sample. During H atom adsorption the chamber pressure rises up to 8 $\times 10^{-8}$ mbar for ca. 60 minutes, which corresponds to a coverage of 0.4 ML. As desorption laser FLASH operates at 5 Hz repetition rate in a single bunch mode at a photon energy of $h\nu = 38.8\,eV (\lambda = 32.0\,nm)$ with a temporal pulse width of about 30 fs [9]. The weakly focused $\hat{p}$-polarized XUV beam strikes the surface at an angle of incidence of 67.5^o relative to the surface normal, see Fig. 1. Due to the oblique incidence the 200 $\times$ 300 μm^2 ellipsoidal beam produces a 0.19 mm^2 ellipsoidal spot on the surface. An average pulse energy of 13 μJ resulting in a fluence of $6.9\,mJ/cm^2$ is thus applied. At this wavelength the reflectivity of graphite amounts to $R = 43.4\,\%$, and therefore a fluence of $3.9\,mJ/cm^2$ is absorbed by the sample. The penetration depth of the radiation is about 5.08 nm [10].

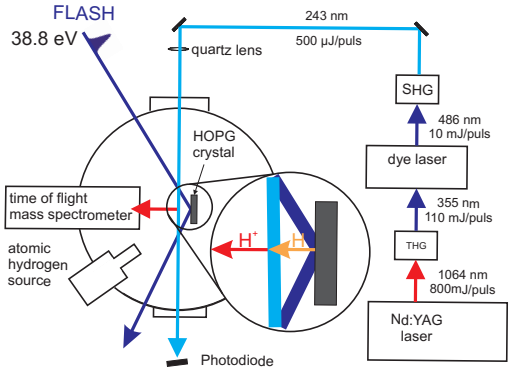

Figure 1: Scheme of the experimental set-up.

Desorbing hydrogen atoms are detected in the gas phase by (2+1) resonantly enhanced multi photon ionization (REMPI) via two-photon absorption in the $2s^2S_{1/2} \leftarrow 1s^2S_{1/2}$ transition. The detection laser system consists of a frequency tripled Nd:YAG laser (Quanta Ray, GCR-170) pumping a commercial dye laser system (Sirah, Cobra Stretch, $\Delta\tilde{\nu} = 0.06\,cm^{-1}$, $\lambda \sim 486\,nm$, 10 mJ/pulse). The output is frequency doubled in a BBO crystal to produce radiation around 243 nm for the two-photon excitation. The detection laser runs in a toggle mode with 10 Hz, recording signal and background separately. H^+ photoions are detected by a Wiley-McLaren type time-of-flight

mass spectrometer. This device is also capable to detect ions directly desorbed by the FLASH pulse [11]. The output of the micro channel plates is monitored on a digital oscilloscope, gated and forwarded to a computer. The ionization of the neutral H atoms occurs after a defined flight path of 7 mm and a defined time delay with respect to the desorbing XUV pulse. By changing the delay between FLASH and the detection laser the kinetic energy of neutral desorbing molecules can be inferred, under the assumption of a prompt desorption. At each time setting about 500 pulses are summed and averaged.

3. Results and discussion

Figure 2a shows the raw data of hydrogen atoms desorbing from the graphite surface as detected by changing the time delay between desorption and detection laser up to about 75 μs. In Fig.2b the resulting velocity distribution is shown, after converting the arrival time distribution of Fig.2a into a flight time and then by a Jacobi transformation into the velocity distribution. The solid circles represent the experimental data points. The distribution peaks at a comparatively low velocity of about 380 ms^{-1} with additional shoulders at even lower velocities of about 250 ms^{-1} and 120 ms^{-1}. A second distinct maximum at 1000 ms^{-1} and a third weak feature around 2200 ms^{-1} can be discerned. The solid curves represent Gaussian velocity distributions fitted to the experimental data. From these fitted distributions the average kinetic energies can easily be obtained, resulting in $\langle E_{kin} \rangle = 0.8$ meV, $\langle E_{kin} \rangle = 5.3$ meV, and $\langle E_{kin} \rangle = 25$ meV, evidently very low kinetic energies. Fast atoms as expected for a direct excitation of a repulsive H - graphite electronic state are not observed.

Without redosing the surface and desorbing always at the same surface spot an exponential decrease of the signal is observed. Since the fluence dependence of the signal depends linearly on the desorption laser pulse energy one can deduce an effective desorption cross section from such a measurement. Observing this signal for more than 500 pulses which results in a total applied/absorbed fluence of 1.95 J/cm^2 or 5.6×10^{17} photons per cm^2 one arrives at a desorption cross section of $\sigma = 1.3 \times 10^{-19} cm^2$. A desorption yield of about 3×10^{-5}ML per XUV pulse is observed. For the velocity distribution shown in Fig.2 only about 2000 pulses are accumulated at the same surface spot. Then another spot is chosen. Data for the same delay but different surface spots are averaged.

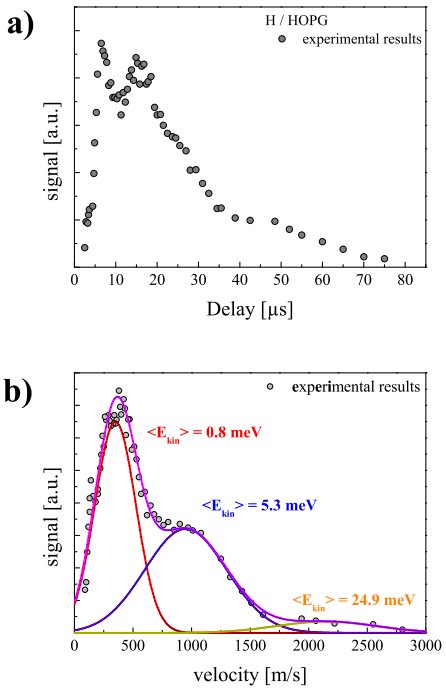

Figure 2: (a)Arrival time distribution of neutral H atoms desorbing from graphite (0001). Flight distance to detection ΔL = 7 mm, desorption wavelength λ_{des} = 32 nm, surface temperature T_s = 300 K. b) Converted velocity distribution of the neutral H atoms from graphite (hν = 38.8 eV).

For a theoretical description of the neutral atomic kinetic energy spectrum we employ electron scattering theory in conjunction with density functional theory (DFT). The adsorbed atom is described by an adiabatic potential $V_0(z)$, where z denotes the desorption coordinate, and the corresponding Hamiltonian H_0. This potential supports vibrations of the adsorbed hydrogen atoms. The electronic system comprising both the adsorbate and the substrate is described by a Newns-Anderson type Hamiltonian H_{NA} featuring a normally unoccupied resonant electronic state $|a\rangle$, localized near the hydrogen atom. When $|a\rangle$ becomes occupied by hot electron scattering the electronic structure changes and the Born-Oppenheimer potential of the adsorbate changes to an excited state potential $V_1(z)$ The state $|a\rangle$ is therefore connected with an interaction Hamiltonian H_I which couples the pure elec-

tronic term $\mathrm{H_{NA}}$ with the adsorbate Hamiltonian $\mathrm{H_0}$. Even when the state $|a\rangle$ is only short-lived, a transient population disturbs the system and may induce transitions between bound vibrational states within $\mathrm{V_0}$ or from a bound to a desorbed state. The total Hamiltonian of the system is then

$$H = H_{NA} + H_0 + H_I. \tag{1}$$

The adsorbate Hamiltonian in the electronic ground state is given by

$$H_0 = \frac{1}{2} m\dot{z}^2 + V_0(z), \tag{2}$$

The Newns-Anderson Hamiltonian of the electronic system is described by

$$H_{NA} = \varepsilon_0 c_a^\dagger c_a + \sum \epsilon_q c_q^\dagger c_q + \sum \left(V_{aq} c_a^\dagger c_q + V_{aq}^* c_q^\dagger c_a \right), \tag{3}$$

and the interaction term is

$$H_I = \varepsilon_a(z) c_a^\dagger c_a - \epsilon_0 c_a^\dagger c_a. \tag{4}$$

In these expressions $\epsilon_\mathrm{a}(\mathrm{z}) = \mathrm{V_1(z)} - \mathrm{V_0(z)}$ gives the vertical excitation energy between the ground and excited state potentials, $c_a^\dagger$ and $c_q^\dagger$ are creation operators for the resonant state $|a\rangle$ and the substrate states $|q\rangle$, respectively, and $\epsilon_0 = \epsilon_\mathrm{a}(\mathrm{z}=0)$ [12, 13]. The dynamics of the system is thus given by the motion on $V_0(z)$ when the state $|a\rangle$ is unoccupied, and on $V_1(z)$ when the electronically resonant state is occupied. In the next step the resonance is assigned a Lorentzian width Γ, and the interaction Hamiltonian is expanded around the ground state minimum yielding $\mathrm{H_I} = -\mathrm{f_a z c_a^\dagger c_a}$, where $\mathrm{f_a}$ denotes the force felt by the adsorbate when the resonance $|a\rangle$ is occupied.

The differential probability $\mathrm{dP_n(k)}$ that a hot electron with energy ϵ_i will induce a transition from a bound state $|n\rangle$ of the adsorbate to a free state $|k\rangle$ can be calculated in second order perturbation theory [14]. Asymptotically, the free states become plane waves and therefore can be converted into velocities.

The scattering probability into a free state $|k\rangle$ is calculated to be [7]

$$dP_n(k) = \frac{f_a^2\Gamma^2}{(E_k - E_n)^2}|\langle k|z|n\rangle|^2 dk \times\left|\frac{1}{\varepsilon_i - \varepsilon_0 + i\Gamma/2} - \frac{1}{\varepsilon_i - \varepsilon_0 - (E_k - E_n) + i\Gamma/2}\right|^2, \quad (5)$$

were $\mathrm{E_n}$ and $\mathrm{E_k} = \hbar^2\,\mathrm{k}^2/2\mathrm{m}$ are eigenenergies of bound and free states, respectively.

As has been shown previously [7], this expression allows one to calculate the contribution of each vibrational state in the bound potential to the kinetic energy distribution of the desorbed atoms. The parameters and potentials have been calculated with GPAW which is a grid-based DFT code using the projector augmented wave method. [15] The excited potential energy is obtained from a delta self-consistent field (ΔSCF) method, [16] where an anti-bonding C - H orbital is taken as the resonant state $|a\rangle$. The ground state atomic adsorption potential shows no barrier for the para, and one of $E_b = 180$ meV for the ortho configuration [4, 5]. These potentials are approximated by Morse potentials with $\mathrm{V_0(z) = D[e^{-2\alpha z} - 2e^{-\alpha z}]}$. For the para configuration D = 1.97 eV and $\alpha = 3.57$ Å^{-1} , for the ortho D = 2.1 eV and a = 3.5 Å^{-}1 are used. The coupling parameters f are obtained from the excited state potential energy $V_1(z)$ and gives f = 0.27 eV/Å for the para state and f = 0.57eV/Å for the ortho state. It turns out that at the high coverages of 0.1 ML used in the present experiment another adsorption configuration is of importance. When all adsorbed H atoms show a para configuration with respect to each other, a so-called uniform para configuration as shown in Fig.3, the individual binding energy increases to even $E_b = 2.7$ eV, again with no barrier for a further adsorption into (or desorption from) another para site. The corresponding Morse potential is then parameterized by D=2.7 eV, $\alpha = 3.5$ Å^{-1} and f = 0.37eV/Å.

To calculate the desorption yield at a given velocity, we need to sum up all $\mathrm{dP_n(k)}$ weighted by the probability that the adsorbate is in the vibrational state $|n\rangle$. The vibrational population distribution is the result of interactions with multiple hot electrons. We will assume that this distribution can be described by a vibrational temperature, which is taken as a fit parameter of the theoretical velocity distributions to the experimentally observed one. Figure 4 shows the calculated velocity distribution. The punctured dashed green

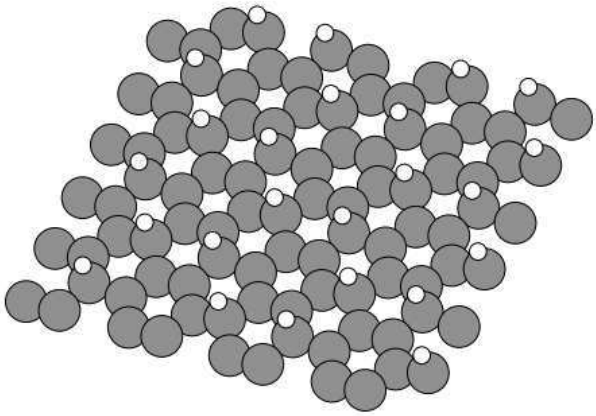

Figure 3: Model of the uniform para configuration of adsorbed hydrogen atoms on graphite. All nearest neighbor H atoms are in a para configuration with respect to each other. This yields an even larger binding energy of $E_b = 2.7$eV than the dimer para configuration of $E_b = 1.97$eV. Also in this case the adsorption into a free para state is barrier free.

curve describes the velocity distribution of H atoms expected for electron scattering on the last vibrational state of atoms in the para pair configuration. The distribution peaks at about 170 ms^{-1}. The dashed blue curve shows the velocity distribution expected from the uniform para distribution with a peak yield at about 1000 ms^{-1}. Desorption out of the ortho dimer configuration contributes only minor to the yield, barely visible in the inset of Fig. 4 at velocities above about 6000 ms^{-1}. These velocity distributions are obtained for high vibrational temperatures of the still bound H atom before a final electron scattering event excites them into the repulsive electronically excited state. For the uniform para configuration the vibrational temperature obtained amounts to T_{vib}(para, uniform) = 5500 K, that for the dimer para configuration to T_{vib}(para, dimer) = 2400 K, and for the ortho T_{vib}(ortho) = 3400 K. The relative yields for desorption out of different adsorption sites are $1 : 4.1 : 0.1$ for the para dimer, uniform para and ortho dimer states, respectively. The theoretical velocity distribution qualitatively

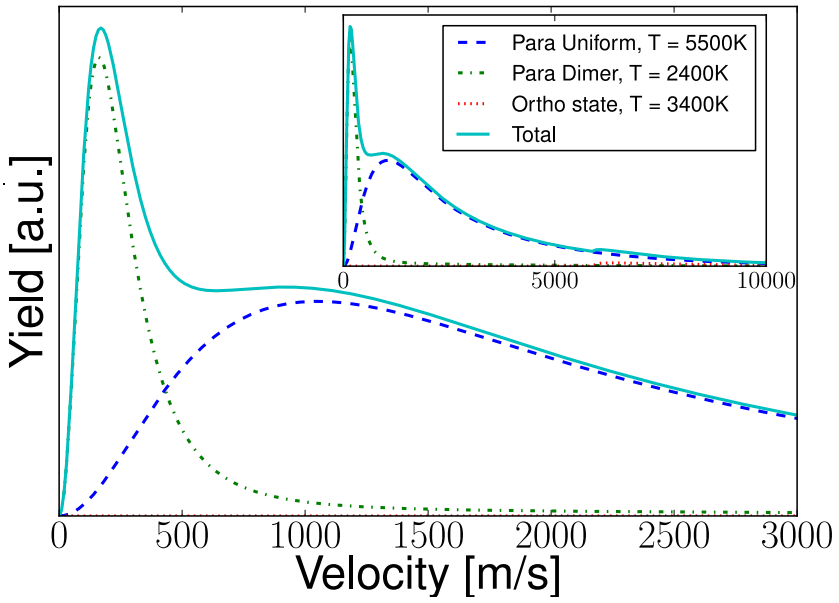

Figure 4: Theoretical velocity distribution of H atoms desorbing from graphite. The dashed green line is associated with desorption out of the dimer para state, the dashed blue line out of the uniform para configuration, and the dot-dashed red line out of the ortho state (inset) which appears above 6000 ms^{-1}.

fit the experimentally observed one.

The model calculation demonstrates that at the relatively high coverages chosen in the experiment large patches of uniform para configurations must be present on the graphite surface. Further, the required vibrational temperatures are significantly higher than in a previous experiment [7] where the desorption is initiated by near-UV excitation with a photon energy of about $h\nu = 3.1$ eV. This latter finding can be rationalized since the high XUV photon energy of about 38.8 eV results in a significantly hotter electron distribution which in turn excites the bound H - carbon vibration to a larger extent. Slightly different vibrational temperatures for the different adsorption configurations are also to be expected, because the electron scattering rate critically depends on the vibrational potential. Not only the overlap of the vibrational wavefunction enters via the Franck-Condon factor into the calculation, also the differences in the vibrational level spacing.

In summary, the experimental observation of a structured velocity distribution for desorbing neutral H atoms from graphite, initiated by XUV

pulses from a free-electron laser, can well be understood with the results from a model calculation based on first principles. The different velocity peaks are the result of desorption out of different adsorption sites with different potential energies. These energies are determined by the lateral hydrogen interactions on the surface. Patches of uniform para configurations contribute significantly to the total yield.

Acknowledgment

The authors gratefully acknowledge technical contributions by S. Eppenhoff and the mechanical workshop of the University Münster. For helpful collaboration we want to thank the FLASH-Team at HASYLAB and acknowledge partial financial support by the *Bundesministerium für Bildung und Forschung* via grant No. 05 KS4PMC/8.

[1] D. Williams, E. Herbst, It s a dusty universe: surface science in space, Surf. Sci. 500 (2002) 823.

[2] X. Sha, B. Jackson, First-principles study of the structural and energetic properties of h atoms on a graphite (0001) surface, Surf. Sci. 496 (2002) 318.

[3] N. Rougeau, D. Teillet-Billy, V. Sidis, Double h atom adsorption on a cluster model of a graphite surface, Chem. Phys. Lett. 431 (2006) 135.

[4] L. Hornekær, et al., Clustering of chemisorbed H(D) atoms on the graphite (0001) surface due to preferential sticking, Phys. Rev. Lett. 97 (2006) 186102.

[5] L. Hornekær, et al., Metastable structures and recombination pathways for atomic hydrogen on the graphite (0001) surface, Phys. Rev. Lett. 96 (2006) 156104.

[6] Ž. Šljivančanin, et al., Extended atomic hydrogen dimer configurations on the graphite(0001) surface, J. Chem. Phys. 131 (2009) 084706.

[7] R. Frigge, et al., Site specificity in femtosecond laser desorption of neutral h atoms from graphite(0001), Phys. Rev. Lett. in press.

[8] W. Ackermann, et al., Operation of a free-electron laser from the extreme ultraviolet to the water window, Nature Photonics 1 (6) (2007) 336 – 342.

[9] R. Mitzner, et al., Direct autocorrelation of soft-x-ray free-electron-laser pulses by time-resolved two-photon double ionisation of he, Phys. Rev. A 80 (2009) 025402.

[10] B. L. Henke, E. M. Gullikson, J. C. Davis, X-ray interactions: photoabsorption, scattering, transmission, and reflection at e= 50-30000 ev, z= 1-92, At. Data Nucl. Data Tables 54 (2) (1993) 181.

[11] B. Siemer, T. Hoger, M. Rutkowski, R. Treusch, H. Zacharias, Desorption of ionic species from ice/graphite by femtosecond xuv free-electron laser pulses, J. Phys.: Condens. Mat. 22 (2010) 084013.

[12] N. Wingreen, K. Jacobsen, J. Wilkins, Inelastic scattering in resonant tunneling, Phys. Rev. B 40 (1989) 11834.

[13] T. Olsen, J. Gavnholt, J. Schiøtz, Hot-electron-mediated desorption rates calculated from excited-state potential energy surfaces, Phys. Rev. B 79 (2009) 035403.

[14] T. Olsen, Inelastic scattering in a local polaron model with quadratic coupling to bosons, Physical Review B 79 (2009) 235414.

[15] J. J. Mortensen, L. B. Hansen, K. W. Jacobsen, Real-space grid implementation of the projector augmented wave method, Phys. Rev. B 71 (2005) 035109.

[16] J. Gavnholt, T. Olsen, M. Engelund, J. Schiøtz, Delta self-consistent field method to obtain potential energy surfaces of excited molecules on surfaces, Phys. Rev. B 78 (2008) 075441.

Paper IX

T. Olsen and J. Schiøtz
Quantum corrected Langevin dynamics for adsorbates on metal surfaces interacting with hot electrons
J. Chem. Phys. (2010).

Quantum corrected Langevin dynamics for adsorbates on metal surfaces interacting with hot electrons

Thomas Olsen[a] and Jakob Schiøtz
Danish National Research Foundation's Center for Individual Nanoparticle Functionality (CINF), Department of Physics, Technical University of Denmark, DK-2800 Kongens Lyngby, Denmark

(Received 11 March 2010; accepted 4 June 2010; published online 20 July 2010)

We investigate the importance of including quantized initial conditions in Langevin dynamics for adsorbates interacting with a thermal reservoir of electrons. For quadratic potentials the time evolution is exactly described by a classical Langevin equation and it is shown how to rigorously obtain quantum mechanical probabilities from the classical phase space distributions resulting from the dynamics. At short time scales, classical and quasiclassical initial conditions lead to wrong results and only correctly quantized initial conditions give a close agreement with an inherently quantum mechanical master equation approach. With CO on Cu(100) as an example, we demonstrate the effect for a system with *ab initio* frictional tensor and potential energy surfaces and show that quantizing the initial conditions can have a large impact on both the desorption probability and the distribution of molecular vibrational states. © *2010 American Institute of Physics*.
[doi:10.1063/1.3457947]

I. INTRODUCTION

Femtosecond lasers have proven to be a most valuable tool in the study of excited metallic electrons and their interactions with surface adsorbates. In Ref. 1 it was shown that a femtosecond laser pulse could be used to desorb NO from Pd(111) and a mechanism involving multiple electronic excitations of the adsorbate was identified.[2,3] Since then, it has been demonstrated that several other surface reactions can be induced by femtosecond laser pulses[4–10] and the mechanism is usually attributed to a direct interaction of excited (hot) metallic electrons interacting with adsorbate resonant states, although substrate heating may also contribute to reaction rates.[11]

A variety of theoretical models have been proposed to describe the interaction and resulting transfer of energy from hot electrons to adsorbates, but a common conceptual picture can be given in terms of the Born–Oppenheimer potential energy surfaces. It is then assumed that the adsorbate propagation is governed by a potential energy surface V_0 when the adsorbate is in its electronic ground state. If the adsorbate has a resonance (possibly partly occupied in the ground state), a hot metallic electron can transiently occupy the resonant state and the adsorbate dynamics will then be governed by a different potential energy surface V_1. Hot electrons can thus transfer energy to the adsorbate by inducing jumps between the two potential energy surfaces.[3] Although the lifetime of the excited electronic state on the adsorbate may be very short (<1 fs), several such events can eventually transfer enough energy for the adsorbate to overcome a reaction barrier.

The probability that a hot electron scatters inelastically on the adsorbate and transfers a given amount of energy can be calculated in a local polaron model[12–15] and may be generalized to reactions resulting from multiple electronic excitations.[16] However, since we are usually only interested in the adsorbate dynamics, it is often more convenient to apply open system density matrix theory. In this formalism, it is assumed that the femtosecond laser pulse gives rise to a hot thermalized distribution of electrons with a time dependent electronic temperature T_e. The time dependent density matrix of the full interacting system is then constructed and the electronic states are traced out resulting in a reduced density matrix with a diagonal that gives the probabilities that the adsorbate is in a particular state. Based on the Feynman–Vernon theory of influence functionals,[17–19] it is possible to calculate the reduced density matrix of a Newns–Anderson type Hamiltonian in either a coordinate basis[20] leading to Langevin dynamics or in a basis of vibrational eigenstates[21] leading to a master equation for the vibrational eigenstates. For a harmonic potential with frequency ω_0, the master equation reduces to a Fokker–Planck equation in the classical limit of $k_B T_e \gg \hbar\omega_0$ and desorption probabilities can be obtained from an Arrhenius type expression.[22] However, as shown explicitly in Refs. 23 and 21, the Fokker–Planck equation fails dramatically when the classical condition above is not satisfied and in general a quantum mechanical treatment of the adsorbate is needed. On the other hand, the coordinate representation of the reduced density matrix results in semiclassical dynamics for the adsorbate coordinates and the quantum nature of the problem only enters through the initial state.

Langevin dynamics have been applied with reasonable success to problems involving molecular collisions,[24,25] as well as hot electron induced surface reactions[26,27] and reac-

[a]Electronic mail: tolsen@fysik.dtu.dk.

tions involving non-adiabatic processes in general.[28–30] However, the initial quantum state is usually neglected or treated quasiclassically. The purpose of the present work is to investigate the role of quantum mechanical boundary conditions and compare the results to those obtained with classical and quasiclassical initial states where only the zero point energy is included. In particular, we will focus on the harmonic oscillator since, when the initial state is included correctly, Langevin dynamics with a quadratic potential is exact to second order in perturbation theory and we can thus compare with a quantum mechanical master equation.

The paper is organized as follows. In Sec. II we introduce the model Hamiltonian which constitutes the foundation of the calculations. The time dependent density matrix of the harmonic oscillator is then reviewed and is shown to give rise to classical dynamics with quantum corrections entering only through the initial state which must be included by a phase space sampling procedure. Generalizing this approach to our model Hamiltonian results in Langevin dynamics with explicit expressions for the electronic friction tensor and correlations between fluctuating forces. In Sec. III we start by analyzing the harmonic oscillator and show how to obtain the quantum mechanical probabilities from the classical phase space distribution resulting from a Langevin equation approach. It is demonstrated that, when the initial conditions is correctly taken into account, the results show excellent agreement with the master equation approach. The comparison is then repeated for the Morse potential where the Langevin dynamics does not provide an exact description of the quantum dynamics, but which has the advantage of having a well defined desorption energy. In Sec. IV we consider the example of hot electron induced desorption of CO from Cu(100) using *ab initio* potential energy surfaces and perform Langevin dynamics with classical, quasiclassical, and quantum mechanical initial conditions.

II. THEORY

A. Hamiltonian

The Langevin dynamics with local electronic friction can be derived from a Newns–Anderson[31,32] type Hamiltonian where a single adsorbate resonant state $|a\rangle$ is coupled to the adsorbate degrees of freedom x_i.[20] The resonant state is usually chosen as an eigenstate of the adsorbate far from the surface. Close to the surface, $|a\rangle$ becomes hybridized with metallic states and acquires a finite lifetime. In the electronic ground state, the resonant state has a partial (or zero) occupation and the adsorbate propagation is governed by a ground state Born–Oppenheimer potential energy surface $V_0(x_i)$ with a local minimum at x_i^0. However, the presence of hot metallic electrons may give rise to a transient full occupation of the resonant state and the adsorbate propagation will then be governed by the potential energy surface $V_1(x_i)$. Even though the resonant state is short lived, a transient occupation will perturb the system and may result in a transfer of energy to the adsorbate.[14] The Hamiltonian describing the system can then be modeled by[12–14]

$$
\begin{aligned}
H &= H_{el} + H_0 + H_I, \\
H_{el} &= \varepsilon_0 c_a^\dagger c_a + \sum_k \epsilon_k c_k^\dagger c_k + \sum_k V_{ak}^0 c_a^\dagger c_k + h.c., \\
H_0 &= \sum_i \frac{p_i^2}{2M_i} + V_0(x_i), \\
H_I &= (\varepsilon_a(x_i) - \varepsilon_0) c_a^\dagger c_a + \sum_k (V_{ak}(x_i) - V_{ak}^0) c_a^\dagger c_k + h.c., \\
\varepsilon_a(x_i) &= V_1(x_i) - V_0(x_i),
\end{aligned}
\tag{1}
$$

where $c_a^\dagger$ and $c_k^\dagger$ are creation operators for the resonant state $|a\rangle$ and metallic states $|k\rangle$, respectively, and $\varepsilon_0 = \varepsilon_a(x_i^0)$, $V_{ak}^0 = V_{ak}(x_i^0)$. Conceptually, the Hamiltonian describes an adsorbate with dynamics governed by $V_0(x_i)$ in the electronic ground state and $V_1(x_i)$ when the resonant state is occupied, and the reservoir of metallic electrons can exchange energy with the adsorbate via the resonant state. The hybridization depends on the position of the adsorbate through $V_{ak}(x_i)$ which become zero when the adsorbate is far from the surface. It should be noted that if V_{ak} are constant and the ground and excited state potentials are quadratic with displaced minima, one obtains $H_I = -c_a^\dagger c_a \Sigma_i f_i x_i$. The coupling constants are then given by $f_i = m_i \omega_i^2 \tilde{x}_i$ where $\tilde{x}_i$ is the shift in the minimum of the excited state potential with respect to the ground state minimum.

We will impose the wide band limit in which the metallic band coupled to the adsorbate is assumed to be much wider than the resonance width. For a fixed position of the adsorbate, the density of states projected onto the resonance is then a Lorentzian,

$$
\rho_a(\varepsilon) = \frac{1}{\pi} \frac{\Gamma/2}{(\varepsilon - \varepsilon_a)^2 + (\Gamma/2)^2}, \tag{2}
$$

with the full width at half maximum given by

$$
\Gamma = 2\pi \sum_k |V_{ak}|^2 \delta(\varepsilon_a - \epsilon_k). \tag{3}
$$

In these expressions both V_{ak} and ε_a and therefore ρ_a and Γ depend parametrically on the instantaneous position of the adsorbate.

B. The density matrix

The advantage of the density matrix formalism is twofold. First of all, for complicated systems one may trace out all irrelevant degrees of freedom from the density matrix and the resulting "reduced" density matrix then describes a system which can exchange energy with the environment. Second, the density matrix formalism allows one to treat a statistical ensemble of states in a natural way. In the case of an adsorbate interacting with electrons in a metal, as described by the Hamiltonian (1), the full density matrix can be reduced by tracing out the electronic degrees of freedom and the diagonal elements of the resulting reduced density matrix then gives the probabilities of finding the adsorbate in a particular state as a function of time.

The time dependent density matrix is

$$\rho(t) = e^{-iHt/\hbar}\rho_0 e^{iHt/\hbar}, \tag{4}$$

where ρ_0 is the density matrix at $t=0$. As always it is instructive to consider a harmonic oscillator and we thus start by considering H_0 of Eq. (1) with a single degree of freedom and a quadratic potential. In the coordinate basis the density matrix can be written as a product of propagators which for the harmonic oscillator are well known[33] and the result for the diagonal elements is

$$\rho(u;t) = \int du_0 dp_0 \mathcal{P}(u_0,p_0) \times \delta\left(u(t) - \left[u_0 \cos\,\omega t + p_0 \frac{\sin\,\omega t}{m\omega}\right]\right), \tag{5}$$

where

$$\mathcal{P}(x,p) = \frac{1}{2\pi\hbar}\int dy \langle x - y/2|\rho_0|x + y/2\rangle e^{ipy/\hbar} \tag{6}$$

is the Wigner distribution of an initial state described by the density matrix ρ_0. The Wigner distribution is often referred to as a quasiprobability distribution and can be interpreted as the quantum mechanical probability of finding a particle in the small phase space area $dxdp$.[34] This means that expression (5) can be thought of as a sum over all initial phase space configurations weighted by their probabilities and subject to the constraint dictated by the delta function. However, the constraint is equivalent to the Newtonian equations of motion and we can thus regard the time evolution as purely classical. In particular, given an initial state we could calculate $\rho(u;t)$ by sampling all phase space and adding $\mathcal{P}(u_0,p_0)$ if u_0 and p_0 are classically connected to $u(t)$. Furthermore, since each such classical trajectory will result in a well defined momentum at time t we interpret the probability of being at a given phase space point $u(t)$, $p(t)$ as being equal to $\mathcal{P}(u_0,p_0)$ where (u_0,p_0) is the unique point which is classically connected to $(u(t),p(t))$. The quantum nature of the particle propagating in a harmonic oscillator potential thus solely enters through the initial state specified by ρ_0. This is of course closely related to the well known fact that for a harmonic potential, the time evolution of the Wigner distribution is equal to the time evolution of a classical phase space distribution.[34]

The Langevin equations emerge when the electronic degrees of freedom are traced out from the time dependent density matrix corresponding to the full Hamiltonian (1). With a quadratic potential the result is very similar to Eq. (5) the only difference being that the coupling to a thermal reservoir of electrons introduces a broadening in the delta function. Thus the time evolution can be thought of as classical with fluctuations that has a magnitude determined by the broadening. It has previously been shown that these fluctuations can be handled in a statistical sense[18,19,35,36] and the full dynamics can be written in terms of classical equations of motion with a stochastic force $\xi_i(t)$. The stochastic force is specified by its statistical properties which is related to the broadening of the delta function. The result is the Langevin equation

$$M_i\ddot{u}_i + \frac{d}{du_i}V_0(u) + \sum_j \eta_{ij}(u)\dot{u}_j = \xi_i(t), \tag{7}$$

where the local temperature dependent friction tensor is given by

$$\eta_{ij}(u) = \frac{-\hbar}{\pi}\int_{-\infty}^{\infty} d\varepsilon \left(\frac{\Gamma(u)/2}{(\varepsilon - \varepsilon_a(u))^2 + (\Gamma(u)/2)^2}\right)^2 \times f_i(\varepsilon;u) f_j(\varepsilon;u)\frac{dn_F(T;\varepsilon)}{d\varepsilon}, \tag{8}$$

with

$$f_i(\varepsilon;u) = \frac{\varepsilon_a(u) - \varepsilon}{\Gamma(u)}\cdot\frac{\partial\Gamma(u)}{\partial u_i} - \frac{\partial\varepsilon_a(u)}{\partial u_i} \tag{9}$$

being the (dynamical) frictional force on the mode u_i. This result was derived in Ref. 20 for a single adsorbate mode and has been generalized to more than one modes here. It is also straightforward to extend the derivation to include N resonant states and the resulting friction is simply the sum of the N partial frictions resulting from each resonance. The diagonal elements of the friction tensor are strictly positive and the main contribution from η_{ij} in Eq. (7) will be a frictional force in a direction opposite the velocity. In the presence of hot metallic electrons, the ground state potential appearing in Eq. (7) should actually be replaced by a temperature dependent renormalized potential $V_0(u_i) \to V_0(u_i) + F(T;u_i)$.[20] However, the correction is usually so small that it can be neglected and we have explicitly verified this for the systems considered in the present work.

In the present work we will make the Markov approximation where there is no temporal correlation of the fluctuating forces. The approximation is valid when the thermal correlation time $t_c \sim \hbar/k_B T$ is much smaller than the timescale of adsorbate motion, and the fluctuating force $\xi_i(t)$ is a Gaussian distributed stochastic variable with a correlation function given by

$$\langle \xi_i(t_1)\xi_j(t_2)\rangle = 2\eta_{ij}k_B T\delta(t_1 - t_2). \tag{10}$$

To summarize, the Langevin Eq. (7) can be thought of as describing classical dynamics with stochastic fluctuations. Quantum effects enter through the initial state of the adsorbate and can be included by running classical trajectories with initial conditions sampled from a Wigner distribution of the initial state. For nonquadratic potentials the Langevin equation should be regarded as a semiclassical approximation to the true dynamics. The derivation leading to Eqs. (7)–(9) is based on a path integral representation of the reduced density matrix.[20,35–37]

C. Master equation

If one is interested in the time dependent probability for the adsorbate to be in a particular energy eigenstate rather than at certain position, it is more convenient to consider the reduced density matrix in a basis of Hamiltonian eigenstates. Taking the electronic trace of the Liouville equation leads to

$$\frac{d\rho_{\mathrm{red}}}{dt}+\frac{i}{\hbar}[H_0,\rho_{\mathrm{red}}]=\frac{-i}{\hbar}\mathrm{Tr}_{\mathrm{el}}[H_I,\rho], \tag{11}$$

where $\rho_{\mathrm{red}}=\mathrm{Tr}_{\mathrm{el}}(\rho)$ is the reduced density matrix and $\mathrm{Tr}_{\mathrm{el}}$ is the trace over electronic states. In a basis of eigenstates of H_0, the diagonal elements of the reduced density matrix are the time dependent probabilities of finding the adsorbate in a particular state. The right hand side is a complicated functional which depends on the complete history of the density matrix. However, making the self-consistent Born approximation, the Markov approximation and neglecting the off-diagonal elements of ρ_{red} leads to the master equation[21]

$$\frac{dp_n}{dt}=\sum_{m=0}^{\infty}(p_m W_{m\to n}-p_n W_{n\to m}), \tag{12}$$

where $p_n=(\rho_{\mathrm{red}})_{nn}$ and $W_{m\to n}$ are the transition rates given by

$$W_{m\to n}=\frac{2\pi}{\hbar}\sum_{q,q'}n_F(\varepsilon_q)(1-n_F(\varepsilon_{q'}))|\langle q;m|H_I|q';n\rangle|^2 \times\delta(\varepsilon_q-\varepsilon_{q'}+\varepsilon_n-\varepsilon_m), \tag{13}$$

where $|q\rangle$ is the eigenstates of H_{el} with eigenenergies ε_q and $n_F(\varepsilon)$ is the Fermi–Dirac distribution.

III. MODEL POTENTIALS

As shown above, zero point motion (or any other initial quantum state) can be included in the molecular dynamics by sampling all phase space and weighing each point according to the Wigner distribution of the initial state. For Langevin dynamics this can be tedious work since one has to run a large number of trajectories for each initial point in phase space to get reasonable statistics. An often used approximation to avoid phase space sampling is to use the classical initial conditions which reproduces the energy of the initial quantum state E_n. When the friction is small compared to the period of oscillation, one can then use a single initial phase space point with $E_{\mathrm{clas}}(x_0,p_0)=E_n$. We will refer to this as the quasiclassical approximation. However, as will be shown below, this method can give rise to seriously misleading results for Langevin dynamics when the timescale of the hot electron pulse is sufficiently short.

A. Quadratic potential

For a quadratic potential the Langevin equation is exact within second order perturbation theory provided we include the initial quantum state properly. We can thus compare results obtained by integrating the Langevin equation with those obtained from a master equation approach (12) and transition rates calculated from the Fermi golden rule expression (13). In principle, the two approaches should be equivalent since the level of approximation is the same (Markov approximation and second order perturbation theory) and we can investigate the importance of using quasiclassical initial conditions compared to true quantum initial conditions.

It may be surprising that the classical Langevin equation should give the same result as the master equation which is inherently quantum mechanical. Furthermore, it may not be obvious how the probabilities p_n, which is the basic quantity calculated within the master equation approach, can be extracted from Langevin dynamics. However, if one has access to the Wigner distribution $\mathcal{P}(x,p)$ at a given time, it is indeed possible to calculate p_n since

$$\begin{aligned}p_n=\langle n|\rho|n\rangle&=\int dxdy\rho(x,y)\varphi_n^*(x)\varphi_n(y)\\&=\int dudv\rho(u+v/2,u-v/2)\\&\quad\times\int d\tilde{v}\varphi_n^*(u+\tilde{v}/2)\varphi_n(u-\tilde{v}/2)\delta(v-\tilde{v})\\&=\int dudv\rho(u+v/2,u-v/2)\\&\quad\times\frac{1}{2\pi\hbar}\int d\tilde{v}dp\varphi_n^*(u+\tilde{v}/2)\varphi_n(u-\tilde{v}/2)e^{ip(v-\tilde{v})/\hbar}\\&=2\pi\hbar\int dudp\mathcal{P}_n(u,p)\mathcal{P}(u,p),\end{aligned} \tag{14}$$

where $\mathcal{P}_n(u,p)$ is the Wigner distribution of the pure state density matrix $\rho_n=|n\rangle\langle n|$. Integrating the Langevin equation gives rise to a final state classical phase space distribution, but since the equation of motion for a classical phase space distribution is identical to that of a Wigner distribution in a harmonic potential,[34] we can identify the final state classical phase space distribution with the final state Wigner distribution.

The pure state Wigner distributions in a quadratic potential are given by[34]

$$\mathcal{P}_n(x,p)=\frac{(-1)^n}{\pi\hbar}e^{-\mathcal{H}(x,p)/E_0}L_n(2\mathcal{H}(x,p)/E_0), \tag{15}$$

where $\mathcal{H}(x,p)=p^2/2m+m\omega^2x^2/2$ is the classical Hamiltonian, $E_0=\hbar\omega/2$, and L_n is the nth Laguerre polynomial. Since $\mathcal{P}_n$ is only a function of the Hamiltonian energy we can write

$$\begin{aligned}p_n&=2\pi\hbar\int_0^{\infty}dE\mathcal{P}_n(E)\frac{dP}{dE}\\&=2(-1)^n\int_0^{\infty}dEe^{-E/E_0}L_n(2E/E_0)\frac{dP}{dE},\end{aligned} \tag{16}$$

with

$$\frac{dP}{dE}=\int dxdp\mathcal{P}(x,p)\delta(E-\mathcal{H}(x,p)). \tag{17}$$

Note that the distribution dP/dE is not a true probability distribution since it is not strictly positive, but it can be rigorously translated into the quantum mechanical probabilities p_n. On the other hand, we can obtain the distribution dP_n/dE associated with a particular vibrational state $|n\rangle$ by replacing $\mathcal{P}(x,p)$ in Eq. (17) with $\mathcal{P}_n(x,p)$. Using that $dxdp=\hbar d\varphi d\mathcal{H}/2E_0$ with φ being a phase space angle, the integral can then be evaluated to

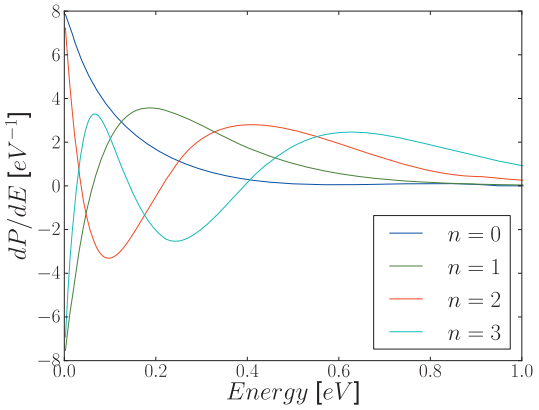

FIG. 1. The energy distributions given by Eq. (18) for the lowest four vibrational states of a harmonic oscillator with zero point energy $E_0=0.125$ eV. The corresponding quasiclassical distributions are delta functions centered at $E_0(2n+1)$.

$$\frac{dP_n}{dE}=\frac{(-1)^n}{E_0}e^{-E/E_0}L_n(2E/E_0). \tag{18}$$

The distributions Eq. (18) are shown in Fig. 1 for the first four vibrational states with $E_0=0.125$ eV. The structure of the distributions is in sharp contrast with that obtained in the quasiclassical (QC) approach where the energy is fixed at E_n and the energy distribution of the nth state is $dP_n^{(\mathrm{QC})}/dE=\delta(E-E_n)$ with $E_n=\hbar\omega(n+1/2)$. This gives rise to completely different and even negative probabilities. For example, using $dP_0^{(\mathrm{QC})}/dE=\delta(E-E_0)$ immediately yields $p_0=p_1=-p_2=0.74$ from Eq. (16).

We have performed Langevin dynamics using Eqs. (7) and (8) with a single mode and a linear interaction Hamiltonian: $H_I=-fc_a^\dagger c_a x$ using the parameters $m=6.86$ amu, $\hbar\omega=0.25$ eV, $\varepsilon_0=2.6$ eV, $\Gamma=2.0$ eV, and $f=8.7$ eV/Å. These parameters were chosen to mimic the internal vibrational mode of CO adsorbed on Cu(100) considered below, but presently we will just think of them as a realistic set of parameters which we use to compare different model calculations. The adsorbate is initially in its ground state described by the Wigner distribution

$$\mathcal{P}_0(x_0,p_0)=\frac{1}{\pi\hbar}e^{-x_0^2/x_Q^2-p_0^2/p_Q^2}, \tag{19}$$

with the quantum length and momentum given by

$$x_Q=\sqrt{\hbar/m\omega},\quad p_Q=\sqrt{\hbar m\omega}. \tag{20}$$

The distribution is even in both momentum and position and since the frictional decay is much slower than the vibrational time of oscillation, the final state phase space distribution can be assumed to be even in the initial phase space point. For simplicity we assume a constant electronic temperature at $T_e=4000$ K and integrate the Langevin equation for $t=1$ ps. For each point on an initial (6×6) positive phase space grid with a spacing $0.5x_Q\times0.5p_Q$, we run a large number of Langevin trajectories ($\sim$30 000) and record the final state energy. The final state energy distribution is then obtained by summing the distributions resulting from each initial phase space point $dP/dE(E;x_0,p_0)$ weighted by the initial state Wigner distribution $\mathcal{P}(x_0,p_0)$:

$$\frac{dP(E)}{dE}=\int dx_0dp_0\mathcal{P}(x_0,p_0)\frac{dP(E;x_0,p_0)}{dE}. \tag{21}$$

In Fig. 2 we show this distribution at $t=0.1$ ps and $t=0.5$ ps along with the distributions resulting from quasiclassical [initial phase space points with $\mathcal{H}(x_0,p_0)=E_0$] and classical initial condition (initial phase space point $x_0=p_0=0$). On long time scales the distributions will forget the initial conditions and approach a Boltzmann distribution at the appropriate temperature. However, on timescales less than a picosecond there is still plenty of memory of the initial state and the classical and quasiclassical distributions, which start as delta functions at $E=0$ and $E=E_0$, respectively, are completely wrong at timescales on the order of 0.1 ps. The quasiclassical initial conditions approach the correct distribution faster than the classical one since the initial state contains the right amount of energy which just needs to be redistributed.

With the interaction Hamiltonian $H_I=-fc_a^\dagger c_a x$ it is easy to calculate the transition rates Eq. (13) with the result

$$\begin{aligned}W_{m\to n}=&\,m\delta_{m,n+1}\frac{\pi f^2}{M\omega}\int d\varepsilon\rho_a(\varepsilon)\rho_a(\varepsilon+\hbar\omega)\\&\times n_F(\varepsilon)(1-n_F(\varepsilon+\hbar\omega))\\&+(m+1)\delta_{m,n-1}\frac{\pi f^2}{M\omega}\int d\varepsilon\rho_a(\varepsilon)\rho_a(\varepsilon-\hbar\omega)\\&\times n_F(\varepsilon)(1-n_F(\varepsilon-\hbar\omega)).\end{aligned} \tag{22}$$

Using the parameters above we can then integrate the master equation Eq. (12) and compare the probabilities p_n with those obtained from the Langevin equation, Eqs. (16) and

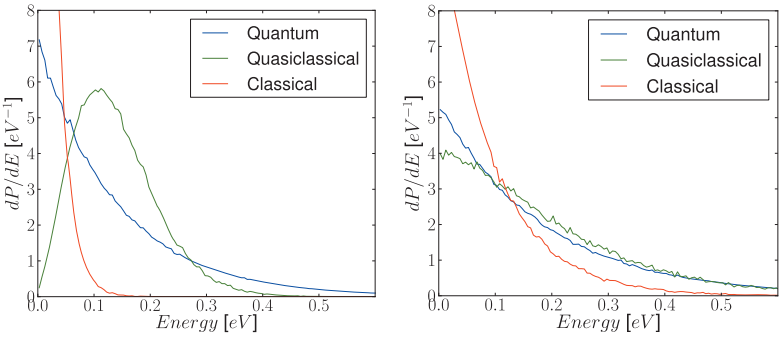

FIG. 2. The continuous energy distributions dP/dE obtained from Langevin dynamics with a constant $T_e=4000$; using quantum, quasiclassical, and classical boundary conditions. The initial quantum state is the vibrational ground state. Left: $t=0.1$ ps. Right: $t=0.5$ ps. After a while both the quasiclassical and classical distributions approach the quantum distribution.

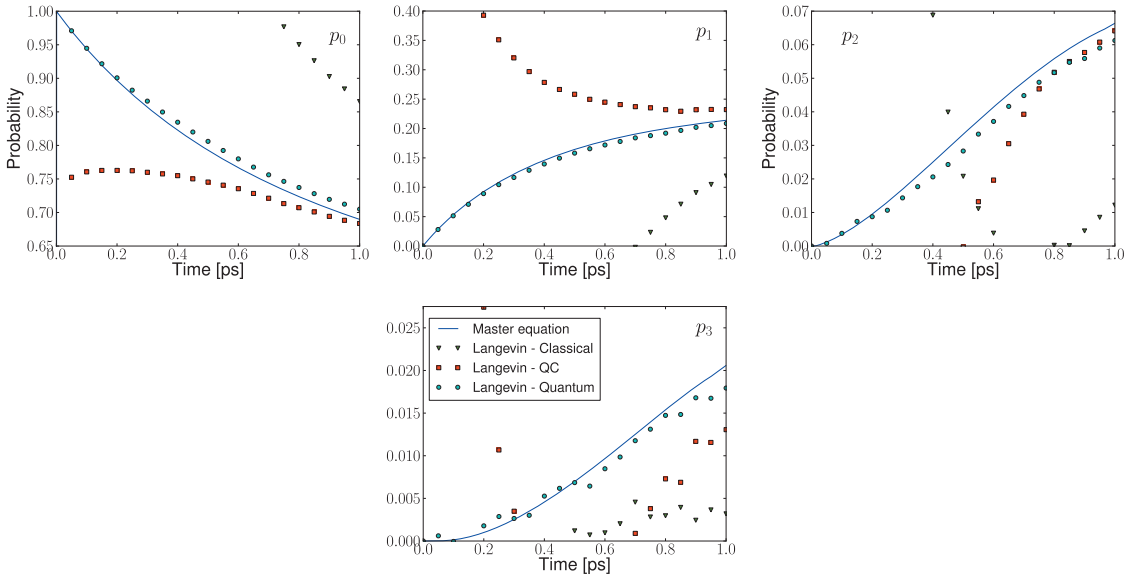

FIG. 3. The time dependent probabilities p_n for being in the vibrational state $|n\rangle$ obtained with the master equation and Langevin dynamics with three kinds of initial conditions. The correct quantum initial conditions are seen to give results nearly identical to the master equation, whereas the classical and quasiclassical initial conditions give wrong results. For small time scales the classical and quasiclassical initial conditions are not shown since the are not consistent with the harmonic oscillator Wigner distribution in the sense that they give rise to probabilities which are negative or larger than one.

(21). This is shown in Fig. 3 for the four lowest vibrational states. As expected we see a close correspondence between the master equation approach and Langevin dynamics with correct phase space sampling. In contrast, the classical initial conditions result in completely wrong probabilities and the quasiclassical initial conditions only result in sensible probabilities after ~0.5 ps.

It should be noted that the quasiclassical initial conditions gives a good description of average quantities and the average energy $\langle E\rangle=\Sigma_n p_n E_n$ is very well approximated by the quasiclassical approach, even at short timescales. However, if one was to model a surface reaction with a barrier by a truncated harmonic potential the quasiclassical approach is likely to fail. For example, the adsorption energy of CO on Cu(100) is ~0.6 eV and as a simple model for hot electron induced desorption one could use the present oscillator truncated above the desorption energy. This means that p_2+p_3 would be a measure of the desorption probability and from Fig. 3 it is clear that for times <0.5 ps one would severely miscalculate the desorption probability.

B. Morse potential

Although the quadratic potential comprises a nice toy model for comparing Langevin dynamics with the master equation approach, it is not particularly well suited to simulate surface reactions such as desorption or dissociation. We will make a simple model for a desorption potential and modify the quadratic potential considered above to a one-dimensional Morse potential $V_M(x)=D(1-e^{-ax})^2$ with $D=0.57$ eV. The parameter a is determined by requiring that the second derivative at the minimum of the well match the frequency of the harmonic potential considered above. A quantization of this potential yields five bound states with energies E_n and a continuum of free states with energies $E_k=\hbar^2k^2/2m$.

Under the influence of a thermal pulse of electrons, a bound state $|m\rangle$ can make transitions to other bound states $|n\rangle$ or to free states $|k\rangle$. The transition rates can be calculated within second order perturbation theory and the result is

$$W_{m\to n}=\frac{2\pi f^2|\langle m|x|n\rangle|^2}{\hbar}\int d\varepsilon\rho_a(\varepsilon)\rho_a(\varepsilon+\hbar\omega_{mn}) \times n_F(\varepsilon)(1-n_F(\varepsilon+\hbar\omega_{mn})) \quad (23)$$

for bound state transitions and

$$W_{m\to k}=\frac{2\pi f^2|\langle m|x|k\rangle|^2}{\hbar}\int d\varepsilon\rho_a(\varepsilon)\rho_a(\varepsilon+\hbar\omega_{mk}) \times n_F(\varepsilon)(1-n_F(\varepsilon+\hbar\omega_{mk})) \quad (24)$$

for transitions to free states. Here we have defined $\hbar\omega_{mi}=E_m-E_i$. The matrix elements have been calculated previously[38] and it is now straightforward to integrate the master Eq. (12). We will interpret the probability of being in a free state $|k\rangle$ at time t as the desorption probability.

For a nonquadratic potential the Langevin equation is based on a semiclassical approximation. However, since the master Eq. (12) is still correct within second order perturbation theory we can explicitly examine the validity of the semiclassical approximation by comparing the two approaches. Due to the lack of a classical/quantum correspondence for the Morse potential, it is not possible to convert the classical energy distribution resulting from Langevin dynamics into probabilities of being in eigenstates of the Morse potential. Nevertheless, it is natural to associate the probability of being in a continuum state $|k\rangle$ with the probability that a classical trajectory results in a final state energy E_k. The initial quantum state is included as described above by sampling phase space and integrate weighting by the Wigner distribution. The Wigner distribution of the Morse potential

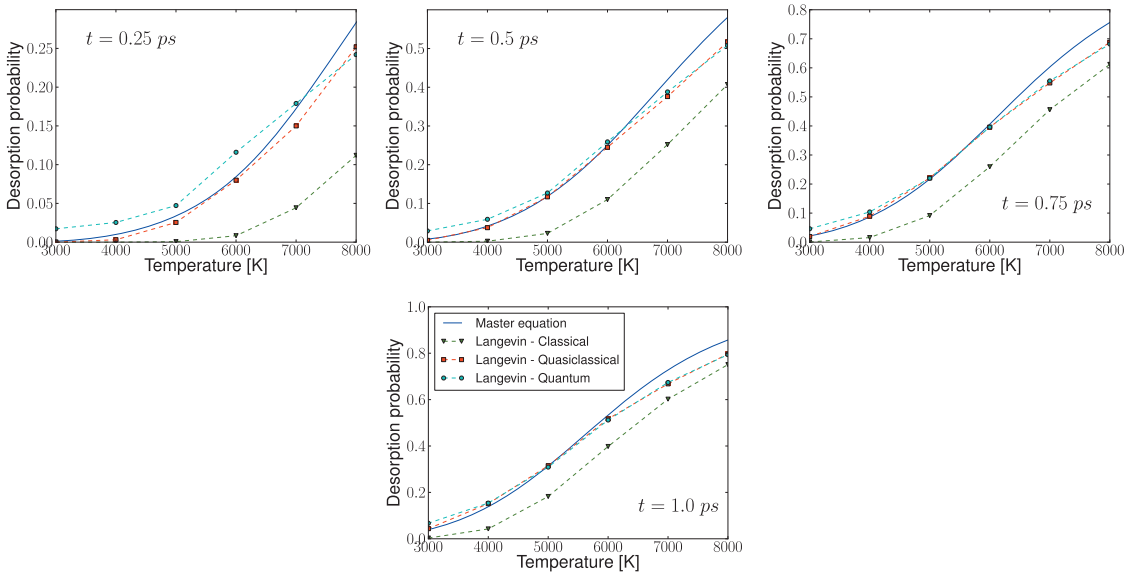

FIG. 4. Desorption probabilities as a function of the electronic temperature T_e calculated from the master equation approach and Langevin dynamics with classical quasiclassical and quantum initial conditions. The four figures show the desorption probability after interaction times of 0.25s, 0.5, 0.75, and 1.0 ps, respectively.

ground state is well known,[39] but since it is not even in the position coordinate we need to sample twice the phase space compared with the harmonic oscillator.

The desorption probabilities calculated with the master equation and Langevin dynamics are shown in Fig. 4. For $t=0.25$ ps, the probabilities show significant deviation signaling a breakdown of classical time evolution at small time scales which is expected. It is a bit more surprising that the high temperature limit deviates from the quantum probabilities even at $t=1$ ps. This could be due a breakdown of perturbation theory at such high temperatures, since the effective perturbation of the system becomes large when the electronic temperature is increased. We also show the probabilities resulting from Langevin dynamics with classical and quasiclassical initial conditions and it is again seen that the classical initial conditions severely underestimate the probabilities. In contrast with the harmonic oscillator, the quasiclassical approach is in very good approximation for the quantum initial conditions when calculating desorption probabilities. This is due to the fact that the quasiclassical approach is a good approximation for average quantities and the desorption probability in the present case is an integral over a continuum of excited states $|k\rangle$. This will be extremely useful since the quasiclassical approximation allows us to circumvent phase space sampling.

IV. *AB INITIO* POTENTIAL

As an example illustrating quantum effects in Langevin dynamics using *ab initio* potentials, we consider CO adsorbed on Cu(100). This system has previously been investigated in the context of electronic friction and the closely connected vibrational linewidth broadening induced by electron hole pair excitations.[26,40,41] All parameters in the model Hamiltonian (1) was obtained within density functional theory (DFT) using the code GPAW,[42,43] which is a real-space DFT code that uses the projector augmented wave method.[44,45] We used a grid spacing of 0.2 Å and the calculations were performed in a (2×2) supercell sampled by a (4×6) grid of k-points using the RPBE (Ref. 46) exchange correlation functional. The system was modeled by a three layer Cu(100) slab with the top layer relaxed and CO adsorbed in a $c(2\times2)$ structure (0.5 coverage at top sites). For this system the electronic friction is dominated by the unoccupied 2π orbitals which we assume to represent the resonant state $|a\rangle$.

We have calculated the potential energy surfaces in terms of the center of mass (COM) and bond length coordinates which are denoted by z and d, respectively. We restrict the analysis to these modes since in a first order Taylor expansion of $\varepsilon_a(x_i)$; the frustrated rotations and translations do not couple to the resonant state due to symmetry. The desorption energy is determined to be $E_{\mathrm{des}}\sim0.57$ eV in excellent agreement with the experimental value.[7] The excited state potential energy surface $V_1(d,z)$ was calculated using a generalization of the Δ-self-consistent field method where the resonant state is expanded in a basis of Kohn–Sham orbitals and the resulting resonant density is added to the density in each iteration step. Thus for each adsorbate position we calculate the energy resulting from forcing an electron into a 2π orbital which is then not an eigenstate of the full electronic system. The excited state thus has a finite lifetime which in the wide band limit can be related to the resonance width as $\tau=\hbar/\Gamma$.[15] For details on the method and comparison with experiments we refer to Ref. 47. Since electrostatic interactions may arise between an excited molecule and its periodic image we have checked that the excited state calculations do not change significantly when the supercell is changed to (4×4).

The ground and excited state potential energy surfaces are shown in Fig. 5. The ground state is well approximated by a quadratic potential in the internal mode and a Morse potential in the center of mass mode. The two modes are

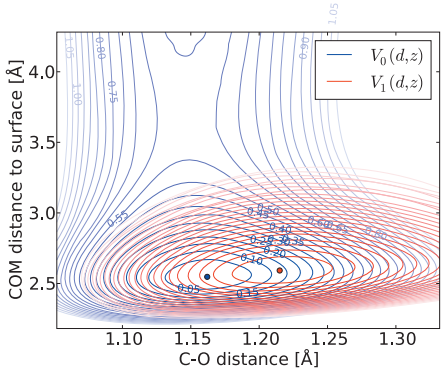

FIG. 5. Potential energy surfaces for the ground and excited state of CO adsorbed at a Cu(100) top site. The contours are at 0.05 eV intervals and the desorption barrier is at 0.57 eV. The extra electron in the antibonding 2π orbital is seen to stretch th C–O bond. The center of mass is moved slightly out from the surface in spite of the attraction to the image charge.

nearly decoupled and in Table I we display the parameters associated with the two modes at the ground state minimum. The resonance width Γ was obtained from the projected density of states shown in Fig. 6. At the ground state equilibrium position the width is approximately $\Gamma_0 \approx 2$ eV and varying the adsorbate position shows that the coordinate dependence is well approximated by $\Gamma = \Gamma_0 e^{-z/z_\Gamma}$ with $z_\Gamma \approx 0.7$ Å. Since the friction tensor is additive in contributing orbitals, we can simply multiply expression (8) by a factor of 4 to account for the degeneracy of the 2π orbital and spin, or equivalently, multiply the frictional force by a factor of 2 which for the internal mode reproduces the parameters used in Sec. III. The excitation energy at the ground state minimum is $\varepsilon_0 = 2.6$ eV. The diagonal elements of the friction tensor Eq. (8) at the equilibrium position and zero temperature can be roughly related to the vibrational lifetimes of the modes: $\tau_i = M_i / \eta_{ii}$. In Fig. 7 we show the two diagonal components as a function of distance to the surface. The two components have the same order of magnitude near the equilibrium position ($z - z_0 = 0$), but the friction in the internal mode (η_{dd}) is seen to decay much faster far from surface than the COM friction. Furthermore, the COM friction has a local maximum beyond the equilibrium position and the molecule is thus likely to dissipate energy on the path leading to desorption which decreases the desorption probability. It should be noted that although the frictional force parameters f_i have the same order of magnitude, they originate from different terms in Eq. (9). The center of mass minimum is nearly unaffected

TABLE I. Parameters for the internal vibration and center of mass mode for CO adsorbed on a Cu(100) top site.

	$\hbar\omega_i$ (eV)	$f_i(\varepsilon_F)$ (eV/Å)	$M_i/\eta_{ii}(0;0)$ (ps)
Internal	0.248	4.3	2.7
COM	0.043	−3.6	16

by a transition to the excited state as seen in Fig. 5 and the frictional force arises only from the COM dependence of the resonance width. On the other hand, the resonance width is nearly independent of the internal stretch mode and the internal frictional force originates in the large displacement of the excited state minimum position. The vibrational lifetimes are in good agreement with previous calculations using a different method.[26,40,41]

To model a particular surface experiment where a femtosecond laser pulse induces a surface reaction, one would need a detailed model for the time dependent distribution of hot electrons resulting from the laser pulse. In the present paper we do not aim at a precise quantitative calculation of reaction rates, but rather wish to examine the qualitative impact of including quantum initial states in the dynamics. Therefore, we will take a very simple model for the hot electrons and assume a thermal pulse with a Gaussian temporal shape $T_e(t) = T_{\max} e^{-t^2/2\Delta t^2}$ with $T_{\max} = 4000$ K and $\Delta t = 0.5$ ps. Under the influence of this pulse we have performed Langevin dynamics with classical quasiclassical and quantized initial conditions in both the internal and center of mass mode using the potentials shown in Fig. 5. The Langevin equation is integrated from 2 ps prior to the center of the pulse to 4 ps after the center of the pulse. Due to the very weak coupling between the two modes the initial condition of the internal mode has almost no influence on desorption probabilities. With fully quantized initial conditions (vibrational ground state) of the COM mode we find a desorption probability of $P_{\text{Quan}} = 3.7 \times 10^{-6}$, whereas we find $P_{\text{QC}} < 10^{-6}$ and $P_{\text{Clas}} < 10^{-6}$ when using quasiclassical and classical initial conditions, respectively (10^6 trajectories did not result in a single desorption event). We note that when calculating the fluctuating forces Eq. (10), it is most important to take into account the correlation between the two modes determined by the off-diagonal elements of the friction tensor.

Although a quantization of the internal mode does not

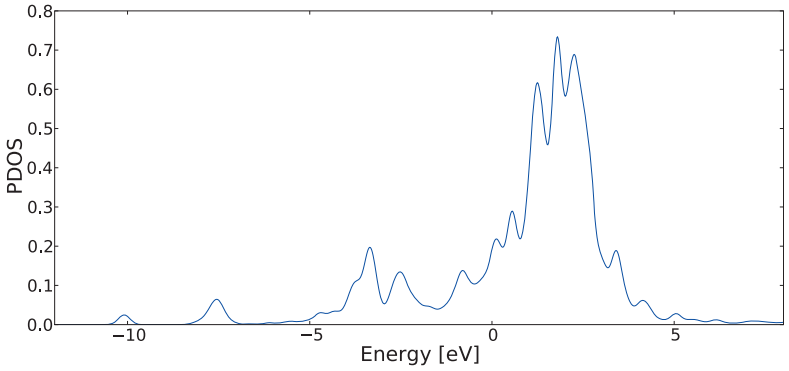

FIG. 6. Density of states projected onto the 2π orbital of CO adsorbed on Cu(100) top site. The full width at half maximum is estimated to be $\Gamma = 2.0$ eV. The Fermi level is at $E = 0$ eV and the resonance is seen to be mostly unoccupied in the electronic ground state.

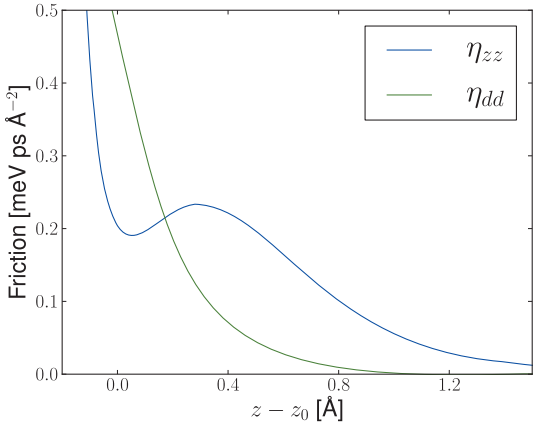

FIG. 7. Diagonal components of the friction tensor as a function of COM distance to surface evaluated at $T=6000$ K. Both components decrease exponentially far from the surface but have very different behavior near the minimum position.

influence the desorption probability it may have a large impact on the distribution of vibrational states of the desorbed molecules. This is illustrated in Fig. 8 where the distribution of energy is shown for desorbed molecules using the classical, quasiclassical, and quantum initial conditions. Due to the low desorption probabilities we had to start the molecule with a COM momentum of $p=3p_Q$ corresponding to 0.19 eV, since otherwise we were not able to get good statistics for the energy distribution of desorbed molecules. However, because of the very weak coupling between the two modes, we do not expect this to have a large influence on the internal energy distribution. The COM energy is not influenced by the initial conditions in the internal mode and the difference in total energy distributions is solely due to differences in the internal mode distributions. It is seen that the quasiclassical initial conditions yield a distribution which is similar to the quantized initial conditions, but with slightly more weight at high lying energies. The classical initial conditions yield a distribution which is inconsistent with a quantized picture, since from Eq. (18) it follows that $dP/dE(E=0)<E_0^{-1}\sim 8$ eV^{-1}.

To see this in more detail we calculate the probabilities of the desorbed molecules being in a particular vibrational state using the method of Sec. III and Eq. (16). The classical initial conditions lead to $p_0>1$ and $p_1<0$ whereas quasiclassical initial conditions give $p_1/p_0=0.22$ and quantized initial conditions give $p_1/p_0=0.092$ which is in agreement with Ref. 7. In general, quasiclassical initial conditions tend to overestimate p_1 and underestimate p_0 and p_2 as is seen in Fig. 3. In the present case the error on p_1/p_0 is more than a factor of 2. For long interaction times and high temperatures the quasiclassical approximation becomes better and we repeated the above analysis with $T_{\max}=6000$ K, which yields close agreement between the vibrational probabilities resulting from quasiclassical and quantized initial conditions.

V. DISCUSSION

In Sec. III it was shown that in order to obtain the correct vibrational probabilities for a harmonic oscillator, it is crucial to use quantized initial conditions. However, quasiclassical initial conditions yield good results for the average energy of the harmonic oscillator as well as for the desorption probability of the Morse potential. Naturally, the quasiclassical approximation is highly attractive since it only requires a single initial phase space point, whereas the correctly quantized initial conditions requires a full phase space sampling. In the present work we needed a 6×6 grid and 10×6 grid of initial phase space points to represent the relevant part of phase space of the harmonic and Morse potentials, respectively, and quantized initial conditions thus required a factor of 36–60 more calculations than the quasiclassical approach. In general we expect that average quantities are well described by the quasiclassical initial conditions. Similarly, high temperatures (compared to the quantum of oscillation) and long timescales tend to justify the quasiclassical approach.

With CO on Cu(100) as a generic example of a two-dimensional problem with *ab initio* potentials, we found that quantization of the internal mode had almost no effect on desorption probabilities. However, this is most likely due to the weak coupling between the two modes in the present example, but for reactions with very strong coupling between modes such as associative desorption processes,[27,28] quantization of the internal mode is likely to be important. Furthermore, if one is interested in the final state distribution of vibrational states, it will be crucial to take into account the initial zero point motion of the adsorbate. For example, the fact that hot electron induced associative desorption yields of hydrogen from Ru(0001) are well described by Langevin dynamics except for too low values of desorbate translational energies[27,48] may very well be due to initial zero point motion.

It should be mentioned that it is also possible to calculate the friction tensor directly from density functional theory using a basis of Kohn–Sham orbitals.[27–29] While that method is probably more accurate, the present approach based on the reduced density matrix and Newns–Anderson-like Hamil-

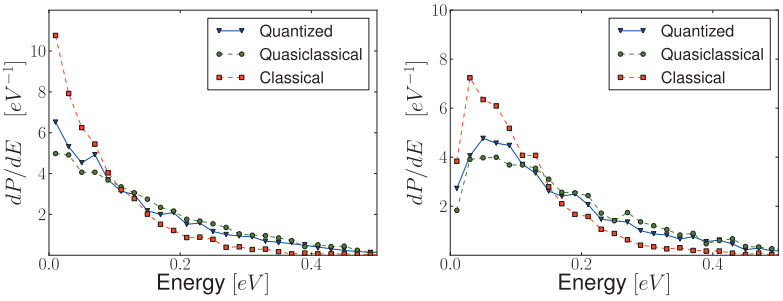

FIG. 8. The differential probability of desorbed molecule having a given amount of energy as a result of a Gaussian pulse of hot electrons with $T_{\max}=4000$ K obtained with classical, quasiclassical, and quantized initial conditions. On the left is the vibrational energy and on the right is the total energy.

tonian Eq. (1) gives better access to the physics involved. For example, in the Newns–Anderson framework it is evident that the frictional forces on the center of mass mode and the internal mode have very different physical origins. On the other hand, since the Kohn–Sham approach does not make any assumption about the physical nature of the friction, it will automatically include all contributing states and thus give better results when multiple adsorbate states contribute to the friction. The method applied in the present paper only takes into account a single resonance which we assume to have a Lorentzian shape, but the excitation energy is calculated using ΔSCF which gives a much better description than the Kohn–Sham eigenvalues.[47] At low temperatures, however, the friction is dominated by the projected density of states at the Fermi level which is unlikely to be well described within the wide band limit imposed here.

We have investigated the importance of including the quantized initial state in Langevin dynamics where the friction and stochastic force originate from a thermal bath of hot electrons. In the title we have referred to this as quantum corrected Langevin dynamics, but other quantum corrections may also be important. In particular, for nonquadratic potentials the time evolution is not classical and the Langevin equation should be thought of as a semiclassical approximation to the true dynamics. In principle, the validity of this approximation should always be analyzed in detail for a given potential and time of propagation, but very often one can use a quick "large n" or similar argument to justify the approximation. For example, in the case of CO on Cu(100) we expect the semiclassical approximation to work well, since the Morse potential describing the desorption coordinate has 27 bound states within the 0.57 eV potential well, which gives an energy spacing much smaller than the average adsorbate energy.

Another quantum effect is that of memory in the fluctuating forces. The Markov approximation leading to Eq. (10) completely neglects any correlation between forces at different times and essentially only contains thermal fluctuations. That the Markov approximation has a classical flavor can be seen in the low temperature limit where the fluctuating forces vanish. The Langevin equation with a harmonic potential then gives rise to a decaying average energy: $E(t)=E_0e^{-\eta t/M}$ which is not allowed quantum mechanically, since the average energy cannot become less than the zero point energy. This paradox is solved by going beyond the Markov approximation where a small fluctuating force exactly cancels the frictional decay. To get an idea of the range of temperatures where the Markov approximation works, we can estimate the correlation time by $t_c=\hbar/k_BT$.[19] The timestep used in the molecular dynamics in this work was 1 fs which corresponds to $T=2900$ K and this gives an estimate on the lower temperature limit to the Markov approximation. Memory effects in nonadiabatic dynamics will be explored further in a future paper.

In summary, we have analyzed the effect of including zero point motion properly in Langevin dynamics with a temperature dependent friction tensor. The method which involves initial phase space sampling has been compared to a quasiclassical approach where classical initial conditions matching the zero point energy are used. For a harmonic oscillator, the initial conditions are the only quantum mechanical correction since the quantum dynamics becomes classical and we have shown how to obtain vibrational probabilities from the classical energy distribution resulting from Langevin dynamics with phase space sampling. As expected, the result agrees extremely well with an inherently quantum mechanical master equation approach when the initial conditions is included correctly, whereas the quasiclassical approach only tends to a reasonable result after ~1 ps of interaction. With CO on Cu(100) as a generic example, we have demonstrated the effect for an adsorbate system with *ab initio* potentials and electronic friction. For a model pulse of hot electrons we showed that, compared to the quasiclassical approach, quantized initial conditions both increase the desorption probability and change the distribution of vibrational states.

ACKNOWLEDGMENTS

This work was supported by the Danish Center for Scientific Computing. The Center for Individual Nanoparticle Functionality (CINF) is sponsored by the Danish National Research Foundation.

[1] J. A. Prybyla, T. F. Heinz, J. A. Misewich, M. M. T. Loy, and J. H. Glownia, Phys. Rev. Lett. **64**, 1537 (1990).
[2] F. Budde, T. F. Heinz, M. M. T. Loy, J. A. Misewich, F. de Rougemont, and H. Zacharias, Phys. Rev. Lett. **66**, 3024 (1991).
[3] J. A. Misewich, T. F. Heinz, and D. M. Newns, Phys. Rev. Lett. **68**, 3737 (1992).
[4] J. A. Prybyla, H. W. K. Tom, and G. D. Aumiller, Phys. Rev. Lett. **68**, 503 (1992).
[5] F.-J. Kao, D. G. Busch, D. G. da Costa, and W. Ho, Phys. Rev. Lett. **70**, 4098 (1993).
[6] F.-J. Kao, D. G. Busch, D. Cohen, D. G. da Costa, and W. Ho, Phys. Rev. Lett. **71**, 2094 (1993).
[7] L. M. Struck, L. J. Richter, S. A. Buntin, R. R. Cavanagh, and J. C. Stephenson, Phys. Rev. Lett. **77**, 4576 (1996).
[8] W. Ho, Surf. Sci. **363**, 166 (1996).
[9] K. Stépán, J. Gűdde, and U. Hőfer, Phys. Rev. Lett. **94**, 236103 (2005).
[10] M. Bonn, C. Hess, and M. Wolf, Science **285**, 1042 (1999).
[11] S. Wagner, H. Ostrom, A. Kaebe, M. Krenz, M. Wolf, A. C. Luntz, and C. Frischkorn, New J. Phys. **10**, 125031 (2008).
[12] N. S. Wingreen, K. W. Jacobsen, and J. W. Wilkins, Phys. Rev. B **40**, 11834 (1989).
[13] J. W. Gadzuk, Phys. Rev. B **44**, 13466 (1991).
[14] T. Olsen, J. Gavnholt, and J. Schiøtz, Phys. Rev. B **79**, 035403 (2009).
[15] T. Olsen, Phys. Rev. B **79**, 235414 (2009).
[16] T. Olsen and J. Schiøtz, Phys. Rev. Lett. **103**, 238301 (2009).
[17] R. P. Feynman and F. L. Vernon, Ann. Phys. (N.Y.) **24**, 118 (1963).
[18] A. O. Caldeira and A. J. Leggett, Physica A **121**, 587 (1983).
[19] A. Schmid, J. Low Temp. Phys. **49**, 609 (1982).
[20] M. Brandbyge, P. Hedegård, T. F. Heinz, J. A. Misewich, and D. M. Newns, Phys. Rev. B **52**, 6042 (1995).
[21] S. Gao, Phys. Rev. B **55**, 1876 (1997).
[22] J. A. Misewich, A. Kalamarides, T. F. Heinz, U. Höfer, and D. M. Newns, J. Chem. Phys. **100**, 736 (1994).
[23] S. Gao, B. I. Lundqvist, and W. Ho, Surf. Sci. **341**, L1031 (1995).
[24] S. A. Adelman and J. C. Doll, J. Chem. Phys. **64**, 2375 (1976).
[25] E. Vilallonga and D. A. Micha, Phys. Rep. **212**, 329 (1992).
[26] J. C. Tully, M. Gomez, and M. Head-Gordon, J. Vac. Sci. Technol. A **11**, 1914 (1993).
[27] A. C. Luntz, M. Persson, S. Wagner, C. Frischkorn, and M. Wolf, J. Chem. Phys. **124**, 244702 (2006).
[28] A. C. Luntz and M. Persson, J. Chem. Phys. **123**, 074704 (2005).
[29] J. R. Trail, D. M. Bird, M. Persson, and S. Holloway, J. Chem. Phys. **119**, 4539 (2003).
[30] J. C. Tully, Annu. Rev. Phys. Chem. **51**, 153 (2000).

[31] P. W. Anderson, Phys. Rev. **124**, 41 (1961).
[32] D. M. Newns, Phys. Rev. **178**, 1123 (1969).
[33] J. J. Sakurai, *Modern Quantum Mechanics* (Addison-Wesley, New York, 1994).
[34] M. Hillery, R. F. O'Connell, M. O. Scully, and E. P. Wigner, Phys. Rep. **106**, 121 (1984).
[35] H. Metiu and G. Schön, Phys. Rev. Lett. **53**, 13 (1984).
[36] E. Vilallonga and H. Rabitz, J. Chem. Phys. **97**, 1562 (1992).
[37] G. A. Voth, D. Chandler, and W. H. Miller, J. Phys. Chem. **93**, 7009 (1989).
[38] E. F. de Lima and J. E. M. Hornos, J. Phys. B **38**, 815 (2005).
[39] G. W. Bund and M. T. Tijero, J. Phys. A **37**, 3687 (2004).
[40] B. N. J. Persson and M. Persson, Solid State Commun. **36**, 175 (1980).
[41] M. Head-Gordon and J. C. Tully, Phys. Rev. B **46**, 1853 (1992).
[42] The GPAW code is available as a part of the CAMPOS software, www.camd.dtu.dk/software.
[43] J. J. Mortensen, L. B. Hansen, and K. W. Jacobsen, Phys. Rev. B **71**, 035109 (2005).
[44] P. E. Blöchl, Phys. Rev. B **50**, 17953 (1994).
[45] P. E. Blöchl, C. J. Först, and J. Schimpl, Bull. Mater. Sci. **26**, 33 (2003).
[46] B. Hammer, L. B. Hansen, and J. K. Nørskov, Phys. Rev. B **59**, 7413 (1999).
[47] J. Gavnholt, T. Olsen, M. Engelund, and J. Schiøtz, Phys. Rev. B **78**, 075441 (2008).
[48] S. Wagner, C. Frischkorn, M. Wolf, M. Rutkowski, H. Zacharias, and A. C. Luntz, Phys. Rev. B **72**, 205404 (2005).

Paper X

T. Olsen and J. Schiøtz
Memory effects in non-adiabatic molecular dynamics at metal surfaces
Submitted to J. Chem. Phys. arXiv:1006.2264.

Memory effects in non-adiabatic molecular dynamics at metal surfaces

Thomas Olsen[a)] and Jakob Schiøtz
Danish National Research Foundation's Center for Individual Nanoparticle Functionality (CINF), Department of Physics, Technical University of Denmark, DK–2800 Kongens Lyngby, Denmark

(Dated: 11 June 2010)

We study the effect of temporal correlation in a Langevin equation describing non-adiabatic dynamics at metal surfaces. For a harmonic oscillator the Langevin equation preserves the quantum dynamics exactly and it is demonstrated that memory effects are needed in order to conserve the ground state energy of the oscillator. We then compare the result of Langevin dynamics in a harmonic potential with a perturbative master equation approach and show that the Langevin equation gives a better description in the non-perturbative range of high temperatures and large friction. Unlike the master equation, this approach is readily extended to anharmonic potentials. Using density functional theory we calculate representative Langevin trajectories for associative desorption of N_2 from Ru(0001) and find that memory effects lowers the dissipation of energy. Finally, we propose an ab-initio scheme to calculate the temporal correlation function and dynamical friction within density functional theory.

I. INTRODUCTION

Modern computational surface chemistry, as e.g. applied to heterogeneous catalysis, is largely based on the Born-Oppenheimer approximation and potential energy surfaces which are typically obtained using density functional theory (DFT).[1] In the adiabatic approximation the electrons are assumed to follow the motion of the nuclei instantaneously and the dynamics thus becomes confined to the ground state potential energy surface. While the adiabatic approximation has certainly been successful in giving a detailed quantitative account of a range of chemical reactions on metal surfaces, it is still not clear under which general circumstances the approximation is reliable.[2–5] In particular, the role of non-adiabatic effects is often difficult to asses due to the inadequacy of low dimensional models of surface dynamics. For example, unusual sticking coefficients in the measured dissociative adsorption of N_2 on Ru(0001) hints at strong non-adiabatic energy loss,[6] but has been accounted for by multi-dimensional adiabatic dynamics.[7,8] For other reactions, such as associative desorption of N_2 from Ru(0001), non-adiabatic effects still seem to be very important[2,9,10] and multi-dimensional adiabatic simulations have not been able to account for large energy losses during desorption.[11] Another example where adiabatic dynamics have failed is the dissociation of O_2 on Al(111) where spin selection rules gives rise to highly non-adiabatic behavior.[12]

Non-adiabatic dynamics for isolated molecules is usually handled by including the first few excited adiabatic potential energy surfaces and imposing some surface hopping scheme. When distinct adsorbate diabatic states are present there may be physical arguments why the adsorbate should remain in such a state during a reaction and the non-adiabatic dynamics can be evaluated by constraining the adsorbate to such a diabat.[13] This picture may then be improved by introducing surface hopping between diabats. However, for molecules adsorbed on metal surfaces there is an infinity of electronic excited states in the immediate vicinity of the ground state and surface hopping may not be the most practical scheme. Another popular and rather general method to handle non-adiabatic effects is through Langevin dynamics where electronic friction and stochastic forces account for dissipation and fluctuation as a result of coupling to excited electronic states.[14–17] Usually, the so-called Markov approximation is employed where the fluctuating forces are not temporally correlated but can be related to the electronic friction through the fluctuation-dissipation theorem.[18] At high electronic temperatures, thermal excitations dominate the electronic system and the Markov approximation is good for describing chemical reactions mediated by hot electrons.[19,20] However, for non-adiabatic dynamics in general, the Markov approximation may fail and it then becomes important to take into account the 'memory' of the system.

In the present paper we explore the consequences of Langevin dynamics with and without the Markov approximation at various temperatures. We follow the approach of Brandbyge et al.[17] and base the analysis on a model Hamiltonian from which the electronic friction and correlation function can be derived explicitly. We start by modelling the internal stretch mode of CO adsorbed on Cu(100) by a considering a harmonic oscillator coupled to a thermal reservoir of electrons and compare the results to those obtained with a master equation approach. The general trend we see is that at low temperatures the Markov approximation overestimates the effect of dissipation. This is because the fluctuating forces are of thermal origin in the Markov approximation while the dissipative terms originate from non-thermal excitations and the relative effect of dissipation compared to fluctuations is thus increased. We also show that non-Markovian dynamics is needed in order to ensure energy

[a)] Electronic mail: tolsen@fysik.dtu.dk

conservation at low temperatures and thus maintains detailed balance between fluctuations and dissipation. Associative desorption of N_2 from Ru(0001) is then studied using the Langevin equation on representative trajectories and again, memory effects are shown to reduce the dissipation of energy. Finally, we comment on a possible method to obtain the full correlation function and thus include memory effects in an ab-initio setting based on DFT.[21] In appendix A, we review the connection between the reduced density matrix and the Langevin equation and emphasize the probabilistic interpretation of the correlation function. In appendix B, we review how correlated stochastic forces can be randomly sampled given a discretized version of the correlation function.

II. MODEL

A commonly used electronic Hamiltonian describing of atoms or molecules adsorbed on metals surfaces is the Newns-Anderson model,[22,23] where the adsorbate is described by a single adsorbate state $|a\rangle$ which hybridizes with metallic states $|k\rangle$ and thus acquires a broadening in energy. A very simple non-adiabatic extension of this model is obtained by coupling the resonant states $|a\rangle$ to an adsorbate degree of freedom x and extending the Hamiltonian with a nuclear kinetic energy and adiabatic potential. Assuming a quadratic nuclear potential and linear coupling to the resonance, the Hamiltonian becomes

$$\begin{aligned} H &= H_{el} + H_0 + H_I, \qquad (1)\\ H_0 &= \frac{p^2}{2M} + \frac{1}{2}M\omega_0^2 x^2,\\ H_{el} &= \varepsilon_0 c_a^\dagger c_a + \sum_k \epsilon_k c_k^\dagger c_k + \sum_k (V_{ak} c_a^\dagger c_k + V_{ak}^* c_k^\dagger c_a),\\ H_I &= -f c_a^\dagger c_a x, \end{aligned}$$

where p is the nuclear momentum, M the adsorbate effective mass, and $c_a^\dagger$ and $c_k^\dagger$ are creation operators for adsorbate and metallic electronic states respectively. The Hamiltonian $H_0 + H_I$ can be thought of as a harmonic oscillator which is shifted when the resonance becomes occupied and the coupling constant f is the force felt by adsorbate in this state. We will furthermore restrict ourselves to the wide band approximation in which the metallic band of electrons is assumed to be much wider than the width of the resonant state. The resonance projected density of states is then a Lorentzian:

$$\rho_a(\varepsilon) = \frac{1}{\pi}\frac{\Gamma/2}{(\varepsilon-\varepsilon_0)^2 + (\Gamma/2)^2}, \qquad (2)$$

with full width at half maximum given by

$$\Gamma = 2\pi \sum_k |V_{ak}|^2 \delta(\varepsilon_0 - \epsilon_k). \qquad (3)$$

Due to the non-adiabatic coupling in Eq. 1, the adsorbate may exchange energy with the electronic system via the resonant state $|a\rangle$. However, usually we are only interested in the nuclear degrees of freedom and it is then convenient to trace out the electronic degrees of freedom from the full dynamics. This is accomplished by the reduced time dependent density matrix:

$$\rho_{red}(t) = \mathrm{Tr}_{el}\Big(e^{-iHt/\hbar}\rho_0 e^{iHt/\hbar}\Big), \qquad (4)$$

where Tr_{el} means the trace over electronic states and ρ_0 is the full density matrix at $t = t_0$. Choosing an adsorbate basis $|\nu\rangle$, the diagonal elements of the reduced density matrix give the probabilities that the adsorbate is in a particular state at time t.

A. Non-Markovian master equation

We will consider the time-dependent probability of being in a particular energy eigenstate $|n\rangle$. The equation governing these probabilities is known as a master equation and can be derived by taking the trace of the Liouville equation for the full density matrix. The result is

$$\frac{d\rho_{red}}{dt} + \frac{i}{\hbar}[H_0, \rho_{red}] = -i\mathcal{F}[\rho], \qquad (5)$$

where the influence functional $\mathcal{F}[\rho] = \mathrm{Tr}_{el}[H_I, \rho]/\hbar$ depends on the complete history of the full density matrix. Gao[24] has shown how to evaluate $\mathcal{F}[\rho]$ using the Hamiltonian (1) within the self-consistent Born approximation. Furthermore, imposing the Markov approximation, where it is assumed that the influence functional only depends on the instantaneous value of the density matrix, and taking the diagonal elements of Eq. (5) led to an explicit expression for the master equation. However, using the formalism of Gao[24], it is straightforward to generalize the results to a non-Markovian master equation. For completeness we state the result here which is

$$\begin{aligned} \dot{p}_m(t) = 2f^2 \sum_n |x_{mn}|^2 \int_{t_0}^{t} dt' \Big[&\widetilde{W}_{n\to m}(t-t')p_n(t') \qquad (6)\\ &- \widetilde{W}_{m\to n}(t-t')p_m(t')\Big], \end{aligned}$$

with the differential rates given by

$$\begin{aligned} \widetilde{W}_{n\to m}(t) = \int_{-\infty}^{\infty} d\omega_1 \int_{-\infty}^{\infty} d\omega_2 \rho_a(\omega_2)\big(1 - n_F(\omega_2)\big) \qquad (7)\\ \times \rho_a(\omega_1) n_F(\omega_1) \cos[(\omega_1 - \omega_2 + \omega_{nm})t], \end{aligned}$$

where $p_m(t) = \langle m|\rho_{red}(t)|m\rangle$, $|m\rangle$ is an eigenstate of H_0 with eigenvalue ε_m, $x_{mn} = \langle m|x|n\rangle$, $n_F(\varepsilon)$ is the Fermi-Dirac distribution, $\rho_a(\varepsilon)$ is the projected density of states (2) and $\omega_{nm} = (\varepsilon_n - \varepsilon_m)/\hbar$.

The Markov approximation is obtained by extending the temporal integration to infinity which is justified

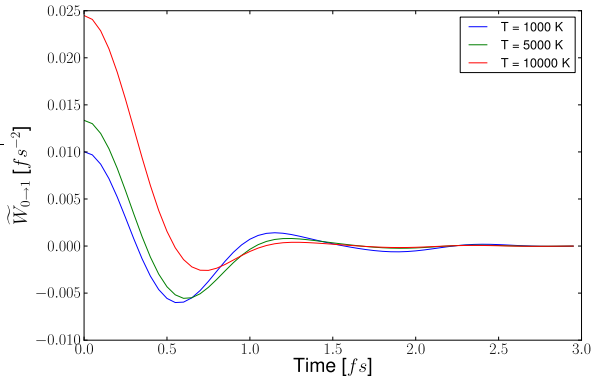

FIG. 1. The differential transition rate $W_{0\to1}(t)$ given in Eq. (7) using three different temperatures and $\Gamma = 2.0\ eV$, $\varepsilon_0 = 2.6\ eV$, $\hbar\omega_0 = 0.250\ eV$ and $f = 8.7\ eV/\text{Å}$. The figure shows that the time dependence vanishes after a few femtoseconds and since the typical timescale of change in $p_n(t)$ is $\sim 100\ fs$, the Markov approximation is expected to work well for the master equation.

when t is much larger than some electronic correlation time t_c. The probabilities p_m are then assumed to depend on t rather than t' and integrating over t' yields the usual golden rule type expression for the transition rates.[24] The master equation was derived assuming that off-diagonal elements of the density matrix are not important. Allthough it is straightforward to generalize the result (6) to a coherent master equation which takes off-diagonal elements into account, it has been shown that, if the initial state is not coherent, the off-diagonal elements will have very little influence on the diagonal elements.[24] In terms of multiple inelastic scattering events, neglecting coherency corresponds to associating a probability distribution to each scattering event.[25,26]

In Fig. 1 we show the differential transition rate $\widetilde{W}_{0\to1}(t)$ at three different temperatures. The time dependence only depends on the properties of the electronic system at the given temperature and the non-adiabatic coupling f simply gives an overall scaling. Since the probabilities $p_n(t)$ typically change on timescales of $\sim 100\ fs$ and the $\widetilde{W}_{n\to m}(t)$ approach zero within a few femtoseconds, the Markov approximation is expected to be very good for the master equation in a large range of temperatures.

B. Non-Markovian Langevin dynamics

If we calculate the diagonal of the reduced density matrix in a basis of position eigenstates, a Langevin equation emerges. This is achieved by writing Eq. (4) as a path integral and using the Feynman-Vernon formalism of influence functionals to obtain an effective action to second order in the frictional coupling f.[15,16,27] The result is given in Eq. (A6). This approach is not perturbative in the same sense as the master equation where the derivation is based on a direct second order expansion of the reduced density matrix. Rather, the second order expansion of the action leads to a density matrix which contains all orders of the frictional coupling. As explained in appendix A, the result can be interpreted as a sum over classical Langevin trajectories with initial conditions sampled from the Wigner distribution of the initial state and the equation of motion is

$$M\ddot{x}(t) + M\omega^2 x(t) + \int_{t_0}^{t} dt' \eta(t-t')\dot{x}(t') = \xi(t), \qquad (8)$$

where $\eta(t)$ the dynamical electronic friction and $\xi(t)$ is a Gaussian distributed stochastic force specified by its correlation function:

$$\langle \xi(t)\xi(t')\rangle = K(t-t'). \qquad (9)$$

With the model Hamiltonian (1) it is possible to evaluate the friction and correlation function explicitly. The result is:[17]

$$\eta(t) = \int_{-\infty}^{\infty} \frac{d\omega}{2\pi} \Lambda(\omega)\cos(\omega t), \qquad (10)$$

with

$$\Lambda(\omega) = \frac{\hbar}{\omega}\int_{-\infty}^{\infty}\frac{d\omega_1}{2\pi}\int_{-\infty}^{\infty} d\omega_2 G(\omega_1,\omega_2) \times \delta\Big(\omega - (\omega_2-\omega_1)\Big)\Big(n_F(\omega_1) - n_F(\omega_2)\Big), \qquad (11)$$

$$G(\omega_1,\omega_2) = 4\pi^2 f^2 \rho_a(\omega_1)\rho_a(\omega_2), \qquad (12)$$

and $\rho_a(\omega)$ is the projected density of states Eq. (2). The correlation function is

$$K(t) = \frac{\hbar}{2}\int_{-\infty}^{\infty}\frac{d\omega}{2\pi}\omega\Lambda(\omega)\coth\left(\frac{\hbar\omega}{2k_BT}\right)\cos(\omega t). \qquad (13)$$

In Fig. 2 we show the correlation function for three different temperature. The structure and typical correlation time is very similar to the differential rate shown in Fig. 1. However, in contrast to the master equation the timescale of motion in the Langevin equation is on the order of $\Delta t \sim 1\ fs$ and correlation effects may be very important at low temperatures. In general the stochastic forces at a given time depends on the state of the electronic system which again depends on the path taken by the adsorbate. This gives rise to correlation between forces at different times and this "memory" is the price one pays for tracing out the electronic degrees of freedom. The range of memory in the system depends strongly on temperature since high temperatures tend to rapidly destroy coherence in the state of the electronic system. In the high temperature limit where $k_BT \gg \hbar/\Delta t$, one obtains the well known expression

$$K(t) = 2k_BT\eta_0\delta(t), \qquad (14)$$

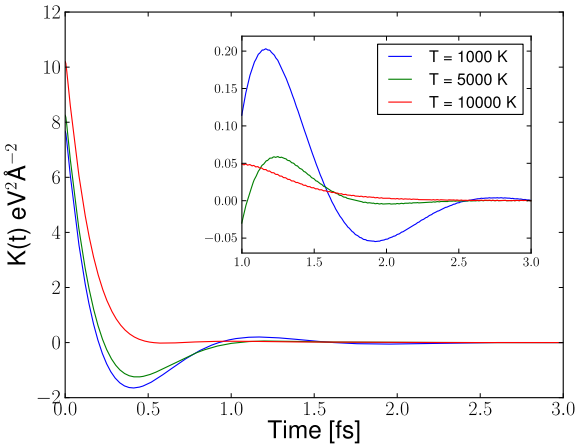

FIG. 2. The correlation function $K(t)$ given in Eq. (13) using three different temperatures with $\Gamma = 2.0\ eV$, $\varepsilon_0 = 2.6\ eV$, $\hbar\omega_0 = 0.250\ eV$ and $f = 8.7\ eV/\text{Å}$. At low temperatures correlation can persists for several femtoseconds.

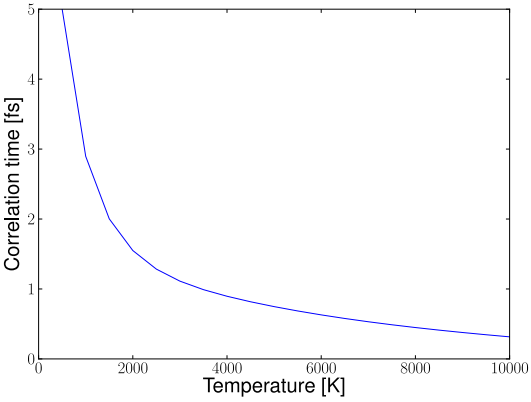

FIG. 3. The correlation time Eq. (15) as a function of temperature with. Below 3500 K the correlation time becomes larger than2 a femtosecond which is the largest time step we can use in the molecular dynamics and non-Markovian processes therefore begins to influence the dynamics below this temperature.

where $\eta_0 = \Lambda(0)/2$. This is the Markov approximation in which there is no correlation between forces at different times. Taking CO on Cu(100) as an example, the smallest timescale is the period of vibrational motion which is $\sim 16\ fs$. With a standard Verlet integration one needs a timestep of $\Delta t \sim 1 fs$ to describe ground state vibrations and a first estimate of the validity of the Markov approximation is obtained as: $T \gg \hbar/(\Delta t k_B) \sim 2900\ K$. To get a better quantitative estimate of the validity of the Markov approximation we can consider the correlation time t_c given by

$$t_c^2 = \frac{\int dt t^2 K(t)}{\int dt K(t)}. \qquad (15)$$

It should be noted that the correlation time is only a function of the electronic system and does not depend on the non-adiabatic coupling f. We have calculated t_c as a function of temperature and the result is shown in Fig. 3. For molecular dynamics requiring a time step no larger than $\sim 1\ fs$, we see that the correlation time becomes larger than this when the temperature comes below 3500 K. Thus below this temperature non-Markovian processes play an important role in the dynamics.

III. RESULTS

Before we test the role of non-Markovian effects on a generic non-adiabatic surface reaction, we will compare Markovian and non-Markovian Langevin dynamics for a harmonic oscillator potential with results obtained from a master equations approach.

A. Quadratic potential

It is easy to see that the fluctuating force in the Langevin equation has to vanish within the Markov approximation Eq. (14) when $T_{el} \to 0$. With a quadratic potential and $\eta(t) = \Lambda(0)/2\delta(t)$ it is then possible to solve the Langevin equation analytically which gives the time-dependent energy

$$E_{Markov}(t) = E_0 e^{-t/\tau}, \qquad \tau = 2M/\Lambda(0), \qquad (16)$$

where E_0 is the initial energy. However, as shown in Ref. 20, the Langevin equation is quantum mechanically exact for a harmonic potential if the initial conditions are accounted for correctly and the total energy should thus not be allowed to decay below $\hbar\omega/2$. The problem is that the Markov approximation neglects all non-thermal excitations of the electronic system and leads to pure dissipation at $T_{el} \to 0$. In reality, an oscillating adsorbate will induce (non-thermal) excitations of the electron gas which may then influence the propagation of the adsorbate. In general, it is therefore expected that the Markov approximation tends to underestimate the influence of the electronic system on the adsorbate. This non-Markovian effect should vanish at high temperature where the thermal excitations of the electronic system dominate. In Fig. 4 we show the time evolution of the average energy of a harmonic oscillator interaction with a thermal reservoir of electrons at six different temperatures. The average energy is calculated using the full non-Markovian correlation function as described in appendix B and within the Markov approximation. The initial state was chosen as the vibrational ground state and included exactly by phase space sampling the Wigner distribution.[20] The parameters used were chosen to match the internal vibrational mode of CO adsorbed on Cu(100)[20,28] and we have thus taken $\Gamma = 2.0\ eV$,

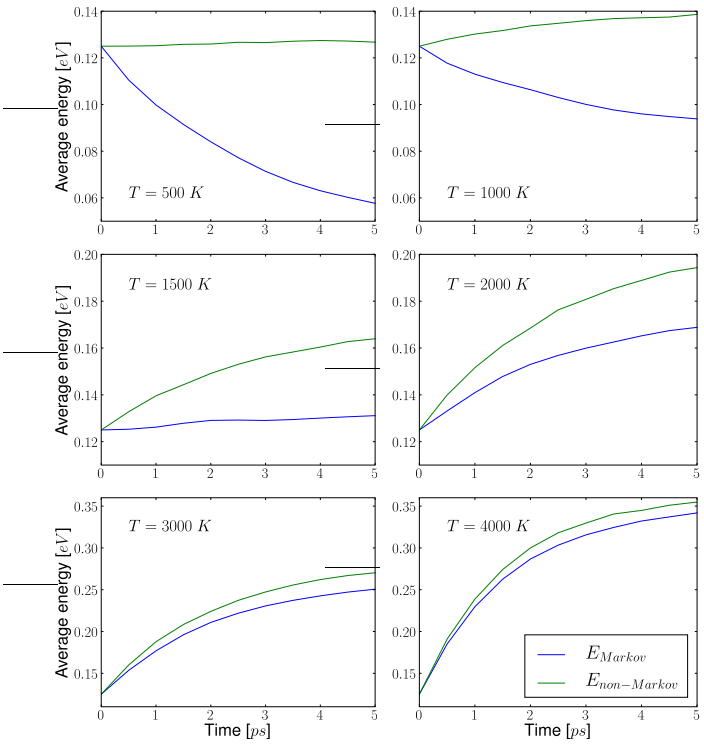

FIG. 4. Average energy of a harmonic oscillator interacting with a thermal reservoir of electrons at six different temperatures evaluated using Langevin dynamics with memory and with the Markov approximation. The Markov approximation fails below $T = 3000\ K$ where quantum fluctuations are important.

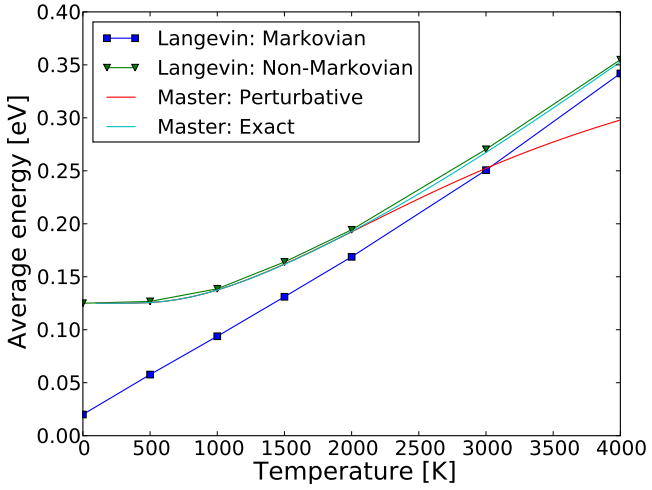

FIG. 5. Average energy of a harmonic oscillator after 5 ps of interaction with a thermal reservoir of hot electrons. The non-Markovian Langevin equation and the non-perturbative master equation both give the correct dependence, whereas the Markovian Langevin equation fails at low temperatures and the perturbative master equation fails at high temperatures.

$\varepsilon_0 = 2.6\ eV$, $\hbar\omega = 0.25\ eV$, and $f = -8.7\ eV/\text{Å}$. The failure of the Markov approximation and resulting decay of the average energy is clearly seen at low temperatures. In particular, at $T = 500\ K$ the Markov approximation gives rise to exponentially decaying energy whereas the energy remains nearly fixed at $E \approx E_0$ when memory effects are included. For high temperatures ($T > 3000\ K$) thermal excitations dominate and the Markov approximation becomes reliable. In all calculations we have converged the results by decreasing the time steps.

In Fig. 5 we show the average energy of the harmonic oscillator after 5 ps of interaction with a thermal reservoir of electrons. The energy is calculated with non-Markovian Langevin dynamics, Markovian Langevin dynamics, the master equation with rates obtained from perturbation theory and the master equation with exact (non-perturbative) rates.[24] Using the full non-Markovian master equation Eqs. (6)-(7) does not change the results. The non-Markovian Langevin approach matches the exact non-perturbative Master equation approach, whereas the perturbative Master equation fails at high temperatures and the Markovian Langevin approach fails at low temperatures. It may be surprising that the non-Markovian Langevin equation reproduces the exact and not the perturbative master equation. However, as mentioned above, the perturbative derivation of the master equation is based on a direct evaluation of the reduced density matrix to second order in the non-adiabatic coupling,[24] while the Langevin equation is derived by constructing an effective action to second order in the non-adiabatic coupling.[17] Thus, while the reduced density matrix calculated from the effective action only becomes exact in the small friction limit, it does contain terms to all orders in the non-adiabatic coupling and is a much better approximation for large frictional coupling and high temperatures than the direct perturbative derivation leading to the master equation Eqs. (6)-(7).

It may seem like a complete overkill to apply a non-adiabatic Langevin dynamics to a harmonic potential when the results are readily obtainable from the master equation approach. However, for anharmonic potentials it is not possible to derive transition rates for the master equation exactly and the best approximation is then the non-Markovian Langevin equation. This was also concluded in Ref. 20 where a perturbative master equation approach underestimated transition rates in a Morse potential compared to a Markovian Langevin approach.

B. Associative desorption of N_2 from Ru(0001)

As an example of a potential where the master equation approach is not readily applicable, we consider the well-known example of associative desorption of N_2 from Ru(0001). This system has been subject to extensive experimental[6,9,10] and theoretical[2,7–9,11] studies and much evidence points to a non-adiabatic dissipation of energy during associative desorption.

The Langevin equation can be generalized to an arbitrary potential $V_0(x)$ by a semiclassical expansion of the potential and the excited state forces acting on the adsorbate.[17] The potential is included by making the substitution $M\omega_0^2 x^2/2 \rightarrow V_0(x)$ in the Hamiltonian Eq. (1) and the friction arises from an excited resonant state with potential energy $V_1(x)$ and is included by the generalizations $-fx \rightarrow \varepsilon_a(x) = V_1(x) - V_0(x)$ and $V_{ak} \rightarrow V_{ak}(x)$ which in the wide band limit leads to a position dependent resonance width $\Gamma(x)$. When multiple coordinates $\{x_i\}$ are considered η, Λ, and $K(t)$ in Eqs. (10)-(13) become tensors and the Langevin equations for each coordinate become coupled through terms like $\sum_j \eta_{ij}(x)\dot{x}_j$. In addition to temporal correlation, the stochastic forces acting on different coordinates become correlated through the off-diagonal terms in the correlated function:

$$\langle \xi_i(t)\xi_j(0)\rangle = K_{ij}(t). \tag{17}$$

In fact, since the friction tensor is well approximated by $\Lambda_{ij}(\omega) \propto f_i f_j$ with $f_i = \partial\varepsilon_a(x)/\partial x_i$, $K_{ij}(t)$ has only one non-zero eigenvalue. This implies that there is a single (coordinate dependent) mode on which the stochastic force acts and the random forces can thus be regarded as completely spatially correlated at any given time.

We have studied associative desorption of N_2 from Ru(0001) using the code `gpaw`,[29,30] which is a real-space Density Functional Theory (DFT) code that uses the projector augmented wave method.[31,32] The Ru(0001) substrate was modelled by a three layer slab where the top layer was relaxed. We used a grid spacing of 0.2 Å and the calculations were performed in a (2x4) supercell sampled by a (4x6) grid of k-points using the RPBE[33] exchange-correlation functional. The friction is assumed to be dominated by the 2π orbital which is only partly occupied in the ground state. To calculate the excited state potential energy $V_1(x)$ we applied a generalization of the Δ-self-consistent field method where the resonant state is expanded in a basis of Kohn-Sham orbitals and the resulting resonant density is added to the density in each iteration step. Thus for each adsorbate position we calculate the energy resulting from forcing an electron into a 2π orbital. For details on the method and comparison with experiments we refer to Ref. 34 We have restricted the analysis to the two-dimensional desorption process considered in Ref. 9 where the two N atoms are adsorbed at adjacent hcp hollow sites and desorbs by moving perpendicular to the bridge towards the fcc hollow while changing the center of mass coordinate. While a two-dimensional analysis is almost certainly not sufficient to obtain quantitative results,[2,8,11] we do expect to draw some qualitative conclusions about the validity of the Markov approximation for this system. The calculated ground and excited state potential energy surfaces are shown in Fig. 6. To obtain $\Gamma(d,z)$ we have fitted the width of the projected density of states of the 2π orbital along the minimum reaction to an exponential $\Gamma(z) = \Gamma_0 e^{-(z-z_t)/z_d}$ and obtained $\Gamma_0 = 3.0\ eV$,

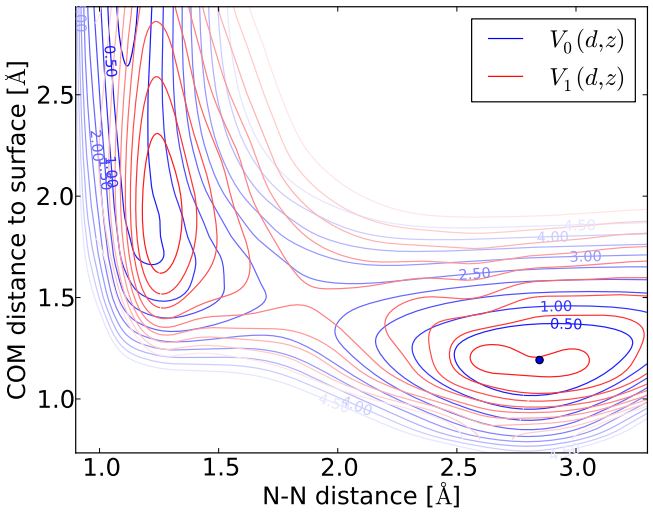

FIG. 6. Ground and excited state potential energy surfaces of N_2 adsorbed on Ru(0001). The excited state was obtained by occupying the 2π orbital of N_2.

$z_d = 0.5$ Å and z_t is the center of mass position at the transition state. The frictional force $\partial\varepsilon_a(d,z)/\partial d$ in the internal mode become large in the exit channel and gives rise to large dissipation of the internal energy while the molecule desorbs. However due to the rapid decay of $\Gamma(z)$ the friction tensor essentially vanishes at $z = 3$ Å. The amount of dissipated energy thus largely depends on the time spend in the exit channel in the immediate vicinity of the transition state.

To examine the impact of non-adiabatic dissipation of energy and, in particular, the validity of the Markov approximation, we have considered four representative initial conditions leading to desorption. All four are initially at the transition state with a kinetic energy of 0.1 eV. The kinetic energy is then concentrated in positive or negative center of mass momentum or positive or negative internal momentum. We have taken the surface and thus the electronic temperature to be $T = 900\ K$.[2,9]. Table I displays the average energy loss in a desorption event of the four initial conditions with and without the Markov approximation. The reason for the large difference is due to the average time spend in the exit channel which for initial negative internal momentum is $\sim 125\ fs$ and for initial positive center of mass momentum is $\sim 250\ fs$. The shift to lower dissipation in non-Markovian dynamics is what we would expect from the conclusions in Sec. III A and Fig 4. In general, memory effects tends to increase the importance of fluctuating forces and thus decrease the overall dissipation of energy.

The present analysis should in no way be taken as a quantitative study of non-adiabatic effect in associative desorption of N_2 from Ru(0001). In such a study one would need to sample a thermal distribution of initial configurations at the transition state and include all 6 molecular degrees of freedom.[11] Furthermore, the present study assumes that the electronic friction origi-

Mode	z-	z+	d-	d+
Markovian	0.31	0.49	0.079	0.10
non-Markovian	0.13	0.42	0.053	0.10

TABLE I. Average energy loss (all numbers in eV) of trajectories leading to desorption for four different initial conditions with and without the Markov approximation at $T = 900\ K$. The initial conditions were all at the transition state with a kinetic energy of 0.1 eV. d and z denotes initial momentum in the internal vibrational mode and the center of mass mode respectively and - and + denotes the sign of the initial momentum. In general, the Markov approximation tends to underestimate the effect of fluctuating forces which results in too much dissipation.

nates from a single resonance (2π) and it is well described by the wide band approximation. That this is not the case has already been established[2] and a complete ab-initio scheme for the electronic friction is needed. Such a scheme based on DFT has already been suggested and put to use within the Markov approximation[2,19,21], but need to be generalized slightly to take memory effects into account. In section IV we will propose such a generalization.

For anharmonic potentials where the friction tensor acquires a position dependence, non-Markovian Langevin dynamics is rather time consuming, since one has to calculate and diagonalize the correlation function in each time step. In the present simulation, the time required for a single time step in the dynamics was increased by a factor of 10^3 compared to Markovian dynamics, but the computational time is, however, vanishing compared to that required for a full DFT calculation at a given position. For N_2 on Ru(0001) the memory effects are clearly seen but probably not important compared to neglecting four degrees of freedom. The calculated energy dissipation is not large enough to account for the vibrational damping observed in Ref. 10, but it is very likely that inclusion of more degrees of freedom would result in a larger amount of time spend in the exit channel and thus a much larger dissipation of internal energy.

IV. NON-MARKOVIAN FRICTION AND FLUCTUATING FORCES FROM DENSITY FUNCTIONAL THEORY

Within linear response theory, it is possible to derive an expression for the electronic friction for a general non-adiabatic Hamiltonian if one assumes classical adsorbate motion.[21] The result depends on the response function of the electronic system as well as the derivative of the electron-vibron coupling with respect to adsorbate coordinates. Replacing the true response function with a Kohn-Sham response function and the coupling Hamiltonian by a Kohn-Sham potential, give the result for the electronic friction

$$\eta = -\pi\hbar \sum_{ij} \left|\langle\psi_i|\frac{dV_{KS}}{dx}|\psi_j\rangle\right|^2 \times \int d\varepsilon \frac{dn_F(\varepsilon)}{d\varepsilon}\delta(\varepsilon_i-\varepsilon)\delta(\varepsilon_j-\varepsilon), \tag{18}$$

where ψ_i are Kohn-Sham orbitals with eigenenergies ε_i. The result is valid within the Markov approximation, since the memory in the Kohn-Sham potential has been neglected. Generalizing this result to include non-Markovian dynamics would require a non-adiabatic exchange-correlation potential, which is presently out of reach. However, since the result is equivalent to that obtained within the reduced density matrix formalism and the Hamiltonian (1) we can impose a very simple generalization which reduces to the adiabatic result (18) in the Markov approximation and to (10)-(13) in the case of non-interacting electrons. Indeed, it is easy to verify that (18) reduces to the Markovian limit of (10)-(13) if V_{KS} is replaced with the Hamiltonian (1) and one is led to a non-Markovian Langevin equation based on DFT which is given by (8)-(11) and (13), but with

$$G(x;\omega_1,\omega_2) = 4\pi^2 \sum_{ij} \left|\langle\psi_i|\frac{dV_{KS}}{dx}|\psi_j\rangle\right|^2 \times \delta(\omega_1-\varepsilon_i/\hbar)\delta(\omega_2-\varepsilon_j/\hbar). \tag{19}$$

This result for the dynamical friction was also derived in Ref. 21, however, the dominating non-Markovian effect is the correlation function (13) which follows from the reduced density matrix formalism in conjunction with (19).

V. SUMMARY

From a fundamental point of view it is important to realize that the Langevin equation gives an exact description of a harmonic oscillator interacting with a reservoir of electrons if the initial quantum state is taken correctly into account.[20] However, it is easy to see that the fluctuating forces vanish at low temperatures in the Markov approximation, which then results in a exponentially decaying energy of the oscillator. This of course contradicts the quantum description of the oscillator and the problem can be traced to the Markov approximation which does not take non-thermal electronic excitations into account. In Fig. 4, we have shown explicitly how memory effects 'saves' the quantum behavior of the oscillator and conserves the energy of the vibrational ground state at low electronic temperatures.

Another way of handling dissipative systems is using the master equation. This approach is based on a perturbative calculation of the reduced density matrix in basis of energy eigenstates. While this approach is fast and intuitively appealing, the method breaks down at high

temperature or large friction due to the perturbative nature of the method. In contrast, the Langevin equation is based on an effective action Eq. (A2)-(A3) giving a non-perturbative flavor. Furthermore, the master equation requires quantization of the potential energy surface and becomes impractical for complicated potentials with many bound states.

As an example of such a potential we have considered the associative desorption of N_2 from Ru(0001). We have not tried to perform a quantitative two-dimensional study of this system as done by Luntz et al.[2], but rather examined the effect of temporal correlation in two representative trajectories. As expected, the effect is an increased significance of the fluctuating forces leading to lower dissipation when memory is included. While this is may be of qualitative interest, the effect of including all degrees of freedom and performing an ab-initio calculation of the friction tensor, would almost certainly lead to corrections which are quantitatively much more important.[11]

Finally, we have provided an expression for the correlation function within an ab-initio DFT scheme. The result follows naturally by combining the usual DFT based friction tensor[21] with the relationship between the friction and fluctuating forces in a non-adiabatic Newns-Anderson Model.[17] In principle, this scheme allows one to model non-adiabatic dynamics at metal surfaces by Langevin dynamics with ab-initio non-Markovian friction and fluctuating forces.

ACKNOWLEDGMENTS

This work was supported by the Danish Center for Scientific Computing. The Center for Individual Nanoparticle Functionality (CINF) is sponsored by the Danish National Research Foundation.

Appendix A: Path integral representation of the reduced density matrix

In this appendix we give a path integral representation of the reduced density matrix Eq. (4) in a coordinate basis. We will focus on the probabilistic interpretation of the path integral which leads to a Gaussian distributed classical Langevin equation.

In a coordinate representation the reduced density matrix is

$$\rho_{red}(x,y;t) = \langle x|Tr_{el}[\rho(t)]|y\rangle. \tag{A1}$$

and the diagonal elements give the probabilities of finding the adsorbate at a particular position regardless of the state of the electronic system. As shown in Ref. [17] the reduced density matrix of the Hamiltonian (1) can

$$\rho_{red}(x,y;t) = \int dx_0 dy_0 \langle x_0|\rho_0|y_0\rangle \int \mathcal{D}[x(t')]\mathcal{D}[y(t')] e^{iS_{eff}[x(t'),y(t')]/\hbar}, \tag{A2}$$

with the effective action given by

$$\begin{aligned} S_{eff}[x(t'),y(t')] = S_0[x(t')] - S_0[y(t')] - \int_0^t dt' \int_0^{t'} dt'' v(t')\eta(t'-t'')\dot{u}(t'') \\ + \frac{i}{2\hbar}\int_0^t dt' \int_0^t dt'' v(t')K(t'-t'')v(t''), \end{aligned} \tag{A3}$$

where $u(t) = x(t)/2 + y(t)/2$, $v(t) = x(t) - y(t)$ and $\eta(t)$ and $K(t)$ are given by Eqs. (10) and (13) respectively. With a quadratic potential the non-interacting action is given by $S_0[x(t')] = M\int_{t_0}^t dt'(\dot{x}^2 - \omega_0^2 x^2)/2$. Changing to coordinates u and v and performing a partial integration on the kinetic term then gives for the diagonal part of the density matrix:

$$\rho_{red}(u;t) = \int du_0 dp_0 \mathcal{P}(u_0,p_0) \int \mathcal{D}[u(t')]\mathcal{D}[v(t')] e^{-\frac{i}{\hbar}\int_0^t dt' \xi(t')v(t') - \frac{1}{2\hbar^2}\int_0^t dt' dt'' v(t')K(t'-t'')v(t'')}, \tag{A4}$$

where $\mathcal{P}(x_0,p_0)$ is the Wigner distribution of ρ_0,

$$\xi(t) = M\ddot{u}(t) + M\omega_0^2 u^2(t) + \int_{t_0}^t dt' \eta(t-t')\dot{u}(t'), \tag{A5}$$

and $u(t')$ have the additional constraint that $\dot{u}_0 = p_0/m$. For a non-quadratic potential $V(x)$, one is forced to make a semiclassical expansion of the potential to second order and the exponential in Eq. (A4) would contain additional

terms of order $\mathcal{O}(v^3V''')$. Similarly, with a nonlinear interaction H_I in (1) one can perform a semiclassical expansion of the frictional terms which leads to a position dependence in Eq. (12).

Without the quadratic term in $v(t')$, the density matrix (A4) would give a delta functional in $\xi(t)$ and the dynamics would be governed by a classical equation of motion with dynamical friction function $\eta(t)$. However the last term in the exponential of (A4) gives rise to a Gaussian broadening of the classical path. To see this explicitly we "complete" the square in the exponential and perform the path integral in $v(t')$ which gives

$$\rho_{red}(u;t) \propto \int du_0 dp_0 \mathcal{P}(u_0,p_0) \int \mathcal{D}[u(t')] e^{-\frac{1}{2}\int_0^t dt'dt''\xi(t')K^{-1}(t'-t'')\xi(t'')}, \tag{A6}$$

where K^{-1} solves

$$\int_0^t dt'' K^{-1}(t'-t'')K(t''-t''') = \delta(t'-t'''). \tag{A7}$$

The exponential in (A6) can be interpreted as the probability density of taking the path $u(t')$ given the endpoints u_0 and $u(t)$ and the initial velocity $\dot{u}_0 = p_0/m$. It has a maximum at $\xi(t) = 0$ corresponding to the classical dynamics and the classical path is broadened by K^{-1}. However, it will be more convenient to consider the probability density of $\xi(t)$ which obviously has dimensions of a force. It is then necessary to change the path integral measure from $\mathcal{D}[u(t')]$ to $\mathcal{D}[\xi(t')]$ and it can be shown that the Jacobian of this transformation is independent of $u(t')$.[15] The two-point correlation function of $\xi(t)$ can then be calculated by

$$\begin{aligned}
\langle \xi(t_1)\xi(t_2)\rangle &= \frac{\int \mathcal{D}[\xi(t')]\xi(t_1)\xi(t_2)e^{-\frac{1}{2}\int_0^t dt'dt''\xi(t')K^{-1}(t'-t'')\xi(t'')}}{\int \mathcal{D}[\xi(t')]e^{-\frac{1}{2}\int_0^t dt'dt''\xi(t')K^{-1}(t'-t'')\xi(t'')}} \\
&= \frac{\frac{\delta^2}{\delta J(t_1)\delta J(t_2)}\int \mathcal{D}[\xi(t')]e^{-\frac{1}{2}\int_0^t dt'dt''\xi(t')K^{-1}(t'-t'')\xi(t'')-\int_0^t dt' J(t')\xi(t')}\Big|_{J=0}}{\int \mathcal{D}[\xi(t')]e^{-\frac{1}{2}\int_0^t dt'dt''\xi(t')K^{-1}(t'-t'')\xi(t'')}} \\
&= \frac{\delta^2}{\delta J(t_1)\delta J(t_2)} e^{\frac{1}{2}\int_0^t dt'dt'' J(t')K(t'-t'')J(t'')}\Big|_{J=0} = K(t_1-t_2).
\end{aligned} \tag{A8}$$

This is the most compact way of specifying the statistical properties of $\xi(t)$ and Eq. (A5) can be regarded as a classical equation motion with a stochastic Gaussian distributed force $\xi(t)$.

Appendix B: Discretization of the correlation function

To sample a correlated "force path" $\xi(t)$ we need to discretize the correlation function and diagonalize the resulting correlation matrix. For a set of Gaussian distributed stochastic variables $\{\xi_i\}$ with probability distribution

$$P(\{\xi_i\}) \sim \exp\Big(-\frac{1}{2}\sum_{ij}\xi_i C_{ij}^{-1}\xi_j\Big). \tag{B1}$$

The correlation matrix C_{ij} can be assumed symmetric without loss of generality. Hence, there exist a diagonal basis of uncorrelated variables $\{\xi_i'\}$ which can be sampled from independent normalized Gaussians. The transformation can be obtained by a Cholesky decomposition of C_{ij} such that $\xi_i = \sum_j L_{ij}\xi_j'$, where $\sum_j L_{ij}L_{kj} = C_{ik}$.

The stochastic force appearing in the Langevin equation can be regarded as an infinite number of stochastic variables; one for each point in time from t_0 to t. Thus, to obtain an expression for the fluctuation force in a time interval Δt, we need the statistical properties of the integrals

$$\xi_i = \frac{1}{\Delta t}\int_{i\Delta t}^{(i+1)\Delta t}\xi(t')dt'. \tag{B2}$$

From the theory of multivariate Gaussian distributions it is readily shown that the set of these integrals are Gaussian distributed with the correlation matrix:

$$C_{ij} = \frac{1}{\Delta t^2}\int_{i\Delta t}^{(i+1)\Delta t}dt'\int_{j\Delta t}^{(j+1)\Delta t}dt'' K(t'-t''), \tag{B3}$$

and this is the expression used when calculating molecular trajectories using non-Markovian Langevin dynamics.

[1] C. H. Christensen and J. K. Nørskov, J. Chem. Phys. **128**, 182503 (2008).
[2] A. C. Luntz and M. Persson, J. Chem. Phys. **123**, 074704 (2005).
[3] J. I. Juaristi, M. Alducin, R. D. Muiño, H. F. Busnengo, and A. Salin, Phys. Rev. Lett. **100**, 116102 (Mar 2008).
[4] A. C. Luntz, I. Makkonen, M. Persson, S. Holloway, D. M. Bird, and M. S. Mizielinski, Phys. Rev. Lett. **102**, 109601 (Mar 2009).
[5] J. I. Juaristi, M. Alducin, R. D. Muiño, H. F. Busnengo, and A. Salin, Phys. Rev. Lett. **102**, 109602 (Mar 2009).

[6] L. Diekhöner, H. Mortensen, A. Baurichter, and A. C. Luntz, J. Chem. Phys. **115**, 3356 (2001).
[7] C. Díaz, J. K. Vincent, G. P. Krishnamohan, R. A. Olsen, G. J. Kroes, K. Honkala, and J. K. Nørskov, Phys. Rev. Lett. **96**, 096102 (2006).
[8] C. Díaz, J. K. Vincent, G. P. Krishnamohan, R. A. Olsen, G. J. Kroes, K. Honkala, and J. K. Nørskov, J. Chem. Phys. **125**, 114706 (2006).
[9] M. J. Murphy, J. F. Skelly, A. Hodgson, and B. Hammer, J. Chem. Phys. **110**, 6954 (1999).
[10] L. Diekhöner, L. Horneær, H. Mortensen, E. Jensen, A. Baurichter, V. V. Petrunin, and A. C. Luntz, J. Chem. Phys. **117**, 5018 (2002).
[11] C. Díaz, A. Perrier, and G. J. Kroes, Chem. Phys. Lett. **434**, 231 (2007).
[12] J. Behler, B. Delley, S. Lorenz, K. Reuter, and M. Scheffler, Phys. Rev. Lett. **94**, 036104 (Jan 2005).
[13] J. Behler, K. Reuter, and M. Scheffler, Phys. Rev. B **77**, 115421 (Mar 2008).
[14] H. Metiu and G. Schön, Phys. Rev. Lett. **53**, 13 (1984).
[15] A. Schmid, J. Low Temp. Phys. **49**, 609 (1982).
[16] A. O. Caldeira and A. J. Leggett, Physica A. **121**, 587 (1983).
[17] M. Brandbyge, P. Hedegård, T. F. Heinz, J. A. Misewich, and D. M. Newns, Phys. Rev. B **52**, 6042 (1995).
[18] J. C. Tully, M. Gomez, and M. Head-Gordon, J. Vac. Sci. Technol. A **11**, 1914 (1993).
[19] A. C. Luntz, M. Persson, S. Wagner, C. Frischkorn, and M. Wolf, J. Chem. Phys. **124**, 244702 (2006).
[20] T. Olsen and J. Schiøtz, Submitted , arxiv:1003.2318.
[21] J. R. Trail, D. M. Bird, M. Persson, and S. Holloway, J. Chem. Phys. **119**, 4539 (2003).
[22] P. W. Anderson, Phys. Rev. **124**, 41 (1961).
[23] D. M. Newns, Phys. Rev. **178**, 1123 (1969).
[24] S. Gao, Phys. Rev. B **55**, 1876 (1997).
[25] T. Olsen, J. Gavnholt, and J. Schiøtz, Phys. Rev. B **79**, 035403 (2009).
[26] T. Olsen and J. Schiøtz, Phys. Rev. Lett. **103**, 238301 (2009).
[27] R. P. Feynman and F. L. Vernon, Ann. Phys. (N.Y.) **24**, 118 (1963).
[28] T. Olsen, Phys. Rev. B **79**, 235414 (2009).
[29] The `gpaw` code is available as a part of the CAMPOS software: `www.camd.dtu.dk/Software`.
[30] J. J. Mortensen, L. B. Hansen, and K. W. Jacobsen, Phys. Rev. B **71**, 035109 (2005).
[31] P. E. Blöchl, Phys. Rev. B **50**, 17953 (1994).
[32] P. E. Blöchl, C. J. Först, and J. Schimpl, Bull. Mat. Sci. **26**, 33 (2003).
[33] B. Hammer, L. B. Hansen, and J. K. Nørskov, Phys. Rev. B **59**, 7413 (1999).
[34] J. Gavnholt, T. Olsen, M. Engelund, and J. Schiøtz, Phys. Rev. B **78**, 075441 (2008).